Czech University of Life Sciences in Prague

Faculty of Forestry and Wood Science

Department of Wood Processing and Biomaterials

Bending solutions for symmetrical and non-symmetrical generally orthotropic panels (CLT)

Diploma thesis

Bc. Ondřej Fiedler

Ing. Adam Sikora, Ph.D.

2023

CZECH UNIVERSITY OF LIFE SCIENCES PRAGUE

Faculty of Forestry and Wood Sciences

DIPLOMA THESIS ASSIGNMENT

Bc. Ondřej Fiedler

Timber Constructures and Structures Based on Wood

Thesis title

Bending solutions for symmetrical and non-symmetrical generally orthotropic panels (CLT)

Objectives of thesis

Cross-laminated timber (CLT) elements, consisting of several layers of lumber stacked crosswise and glued together, are becoming increasingly popular in civil engineering. The work aims at a theoretical and experimental analysis of the reaction of a layered composite material represented as (CLT) element to stress analysis induced by force. The theoretical study will concentrate on the numerical solution of a system of physical equations by applying various numerical methods describing the observed process – the movement of the force field in the material. The solution will implement the analytical or Finite Element Method (FEM) for linear elastic problems in this work. The experimental analysis will verify the theoretical model in specific selected boundary conditions. The result of the work is the application and comparison of various theoretical and experimental analyzes. The work will also analyze the influence of material constants on the resulting behavior of the structural element.

Methodology

Develop a numerical model based on at least two plate theories and apply it to a selected configuration of CLT panels or other laminated timber-based materials.

1. Search for relevant scientific literature

2. Define the numerical model

a. Define displacement field by chosen theories

b. Define stress field by chosen theories

c. By applying the fundamental equations of linear elasticity, define stress
resultants

d. Define governing equations in terms of displacement for orthotropic plates

3. Define the mechanical load cases and boundary conditions for each theory

4. Specify the material used in the numerical model

---

5. Apply the model to geometrical variation of CLT panels (or similar material)

6. Validate the numerical model by experimenting with a selected plate in laboratory conditions

7. Compare and evaluate the results of all theories.

8. Propose extension of stress resultants to hygro-thermal loading cases.

Schedule of work:

1. Processing the work's conceptual solution (until October 2022).

2. Analysis of the issue with an emphasis on the topic of the work (until November 2022).

3. Methodological processing of the work (until November 2022).

4. Experimental measurements and evaluation of the obtained data (until December 2022).

5. Processing of results and discussion (until January 2023).

6. Processing of work conclusions (until March 2023).

The proposed extent of the thesis

80 stran

Keywords

analytical method, numerical method, plate theories, cross-laminated timber (CLT), layered composite material

Recommended information sources

BHAGWAN, D. A., LAWRENCE, J. Analaysis and performance of fiber composites, Second Ed., Wiley, New York, 1990

BODIG, J., JAYNE, B. A. Mechanics of wood and wood composities. Malabar: Krieger Publishing Company, 1993, ISBN 0-89464-777-6

BUCALEM, M. L., BATHE, K. J. The mechanics of solids and structures-hierarchical modeling and the finite element solution. Springer Science & Business Media, 2011

NETTLES, A.T. Basic Mechanics of Laminated Composites Plates. MSFC, Alabama: NASA, 1994, NASA Ref. Pub. 1351

POŽGAJ, A. Náuka o dreve. : Metódy zisťovania mechanických vlastností dreva a drevných veľkoplošných kompozitných materiálov. ZVOLEN: VŠLD, 1987

SZILARD, R. Theories and applications of plate analysis: classical numerical and engineering methods, Appl. Mech., Rev 56.6, 2004, B32-B33

TIMOSHENKO, S. Advanced strengh of Materials – Elementary theory and problems, Van Nostrand, 1940

TROITSKY, M. S., HUPPMANN, W. H. Stiffened plates, bending, stability and vibrations, Journal of Applied Mechanics, 1977, ASME International, Volume 44

Expected date of thesis defence

2022/23 SS – FFWS

The Diploma Thesis Supervisor

Ing. Adam Sikora, Ph.D.

Supervising department

Department of Wood Processing and Biomaterials

Electronic approval: 12. 1. 2023

doc. Ing. Roman Fojtík, Ph.D.

Head of Institute

Electronic approval: 10. 3. 2023

prof. Ing. Róbert Marušák, PhD.

Dean

Prague on 11. 03. 2023

Affirmation:

I declare that I have prepared my thesis "Bending solutions for symmetrical and non-symmetrical generally orthotropic panels (CLT)" on my own, under the supervision of Ing. Adam Sikora, Ph.D. and using the literature and other sources of information cited in the thesis and listed in the reference list at the end of the thesis. As the author of the said thesis, I further declare that I have not violated the copyrights of third parties in connection with its creation.

In Prague, March 25. _____

Acknowledgement

Bending solutions for symmetrical and non-symmetrical generally orthotropic panels (CLT)

Abstract

This diploma thesis is focused on the development and verification of numerical models for the solution of bending of generally orthotropic plates based on the assumptions of CPT, FSDT, SSDT and TSDT theories. The thesis investigates the effect of material and axial asymmetry on the laminate stiffness parameters and mechanical response in the form of deflection and internal forces. A numerical non-stationary moisture diffusion model has been constructed to evaluate the effect of moisture on the wetting time of the CLT panel when exposed to rainwater. Subsequently, the effect of such moisture on the distribution of internal forces along the thickness of the panel was evaluated. The case of a moisture-loaded CLT panel, a panel without moisture loading and experiment measurements were compared. The results indicate a significant influence of material asymmetry of CLT ceiling panels caused by moisture loading of the panel lamellas in contact with pooled rainwater.

Keywords: analytical method, numerical method, plate theories, cross-laminated timber (CLT), layered composite material

Řešení ohybu symetrických a nesymetrických obecně ortotropních desek (CLT)

Abstrakt

Tato diplomová práce se zabývá na sestavení a ověření numerických modelů pro řešení ohybu vrstvených obecně ortotropních desek na základě předpokladů teorií CPT, FSDT, SSDT a TSDT. Práce zkoumá vliv materiálové a osové nesymetrie na parametry tuhosti laminátu a mechanickou odezvu v podobě průhybu a vnitřních sil. Pro zhodnocení vlivu vlhkosti byl sestaven nestacionární model vlhkostní difúze, kterým byla zhodnocena doba navlhání CLT panelu při vystavení dešťové vodě. Následně byl zhodnocen vliv takové vlhkosti na podobu průběhu vnitřních sil po tloušťce desky. Byl porovnán případ vlhkostně zatíženého CLT panelu a panelu bez vlhkostního zatížení. Výsledky ukazují na významný vliv materiálové asymetrie stropních panelů CLT způsobené vlhkostním zatížením lamel panelů při kontaktu se shromážděnou dešťovou vodou.

Klíčová slova: analytická metoda, numerická metoda, teorie desek, křížem lepené dřevo (CLT), vrstvený kompozitní materiál.

Table of Contents

Table of Figures, Graphs and Tables

Table of figures

Table of Graphs

Table of Table

1 Introduction

The scale of timber construction and its structural technological forms in our climatic conditions still do not correspond to European and global trends. There are certainly more reasons for this dismal situation, but one of them is certainly the lack of knowledge and experience of architects and designers with the aforementioned material base. New possibilities of wood application in current construction are clearly linked to the development of innovative wood processing technologies that support the development of contemporary wood structures (Pavlas, 2016). Timber is a material offering an answer to the currently discussed issue of renewable resources and energy efficiency of building production. Life cycle assessment (LCA) of timber buildings shows significantly lower CO_2 emissions than concrete buildings, after including stored biogenic carbon. The long-term trend towards low-energy buildings, linked to the process of technological innovation and the arrangement of the monitored parameters in accordance with the principles of sustainability, may be one of the most important factors (Pavlas, 2016; Shaobo Liang et al., 2020). Multi-storey wooden buildings made of CLT panels could be the answer to the problem of energy efficiency of building production. For these buildings, fire resistance, rigidity and acoustics are crucial issues. In terms of production, there is already a product standard, but technical standards need to be developed to give designers a basis for designing structures at normal temperatures and under fire conditions. In the Czech Republic, there is a significant increase in the number of wood-based building projects, as well as in multi-storey residential and office buildings. The Czech Republic can afford such an increase. Forests cover 34% of the entire territory and the wood reserves in these forests have been increasing for a long time. The very interest in wooden buildings can be seen in the example of family houses, where wooden buildings already account for 15% of the total. (ČSÚ, 2018), (Kuklík, [online]). In order to use timber as one of the main construction materials, it is necessary to verify all the properties of building products made from solid timber, such as cross-laminated timber or CLT panels. One of the performance categories of buildings is durability, which in the case of timber can be strongly affected by prolonged exposure to moisture. Because wood is a hygroscopic material, it exchanges moisture with the surrounding environment.

In the design of CTL made buildings, the stiffness and strength of the panels are adjusted by modification factors that take on values depending on the moisture content of the CLT panels in the structure. However, this modification of the material values is only done in relation to the relative humidity and situations where the material is exposed to moisture in the liquid state are not considered (With proper construction and maintenance of the building, such a situation will not really occur and if it does, it will only occur for a short period of time). During the construction process, CLT ceiling panels in particular are more exposed to weather conditions, especially rain and snow. Rainwater can therefore remain on CLT panels for up to several weeks. CLT panel lamellas exposed to liquid moisture for long periods of time may swell and degrade, and their modulus of elasticity

and strength may decrease. A ceiling panel with such degraded surface lamellae does not behave as a specially orthotropic panel due to the shifting neutral mid-plane, and the essence of the special orthotropy for which the panel was designed is temporarily lost. At the same time, stresses and strains may arise in the panel that are not considered in the final structural design. This can have a significant effect on the overall spatial stiffness of the structure or on the stiffness of connections that are not designed for such stresses.

When investigating the possibility of designing such moisture-loaded floor slabs, no design tool was found that could be used to perform an analysis of strain and internal stresses. Design tools for timber structures such as Dlubal, AxisVM or Stora Enso's CLT panel design tool Calculatis are based on the design and assessment of timber structures based on Eurocodes and for instance do not allow for the integration of swelling into the calculation. More complex and general finite element tools such as Abaqus or Ansys allow working with temperature and its effect on material properties, but do not work with the effect of moisture. In this regard, my work aims to develop a tool based on a numerical solution to analyse the effect of moisture on laminated panels (which can be CLT ceiling panels) in any configuration.

2 Objectives

The aim of my thesis is to develop a numerical model which allows for the analysis of deflection, deformation and internal stresses of timber panels intended for load-bearing structural purposes (CLT). The models are built on the basis of at least two selected shell elasticity plate theories. These theories are the most used for the analysis of isotropic sheet materials. One of the sub-objectives will be to define these theories so that they are applicable to any generally orthotropic panels in the models. The numerical model must be defined in the following terms:

- Displacement field
- Stress field
- Stress resultants
- Governing equations

Each of the models will be modified for possible symmetric and non-symmetric plate types and compared with each other. The model results for the chosen type of symmetry or asymmetry will be verified by experiment.

Sub-objectives of the thesis:
1. Development of a numerical model for deflection calculation according to the selected theories.
2. Defining of relations for calculation of internal stresses according to the mathematical theory of elasticity,
3. Experimental verification of numerical models
4. Defining relationships for integrating moisture or thermal deformations into the numerical models,
5. Defining possible compositions of symmetric and non-symmetric plates,
6. Comparison and evaluation of the results provided by each numerical model and the difference between them,
7. Proposed practical application of the results.

3   Elastic properties of wood

Wood, like any other material, is made up of atoms and molecules that are randomly or lawfully arranged in a given space. The degree of homogeneity of the arrangement of atoms and molecules in the volume of wood and the orientation of especially covalent and hydrogen bonds determines the magnitude and orientation of mechanical properties at the microstructural and macrostructural level. The variation of mechanical properties in the volume of wood and their dependence on direction is called anisotropy of mechanical properties (Požgaj et al., 1997). Parallel to the fibers, i.e. in the direction of the trunk, the strength of the material is particularly high, while perpendicular to the fibers the strength properties are low (Horáček, 2010).

Poisson's ratio

Poisson's numbers are an important characteristic of the elasticity of wood and are mainly used for volume changes due to mechanical tension. When a solid is subjected to compression or tension, the solid is elongated or shortened and deformed perpendicular to the direction of the tensile/compressive force. Such deformations are called transverse deformations. Poisson numbers express the ratio of transverse deformation to longitudinal deformation. We assign a positive sign to tensile deformations and a negative sign to compressive deformations (Požgaj *et al.,* 1997). According to Nettles (1994) Poisson number μ_{21} can be derived as:

$$\mu_{21} = \frac{E_{22}}{E_{11}} \mu_{12} \tag{1}$$

Modulus of elasticity

The modulus of elasticity expresses the internal resistance of the material to elastic deformation. The greater the modulus of elasticity, the greater the stress required to induce deformation. Of the basic ones, we distinguish between the elastic moduli E for normal stresses such as tension, compression and bending and the elastic moduli G for tangential stresses such as torsion or shear. According to Horáček (2010) the relationship for calculating the modulus of elasticity under normal stresses is.

$$E = \frac{d\sigma}{d\varepsilon} \tag{2}$$

where σ is the normal stress and ε is the normal strain. The relationship for calculating the shear modulus is.

$$G = \frac{d\tau}{d\gamma} \tag{3}$$

Where τ is the shear stress and γ is the shear strain (Horáček, 2010).

Mechanical stress is a defined as a process in which mechanical forces or other stress factors interact with the wood. This process results in temporary or permanent changes in the shape of the wood. The response of wood to mechanical stresses depends not only on the bonds of the chemical components of the wood and their interconnection (cellulose, lignin, hemicellulose), but often to a decisive extent on the geometry of the body itself. Therefore, each mechanical property of wood must be considered in terms of the geometry of the test body itself, inhomogeneity, structure, and chemical composition, as well as the resulting anisotropy of properties. The basic types of mechanical stresses are distinguished according to the type of stress that occurs in the body as a result of an external force. The stress in wood represents the intensity of the internal forces that occur in the body in response to external mechanical forces. These forces acting on the body can be oriented in different directions in space and can act on up to six mutually perpendicular planes. An example of mechanical stress is axial tension, which acts in only one plane of the body (Požgaj et. al., 1997). The stress σ is defined as the magnitude of the internal force, which is related per unit area of the body according to the relation.

$$\sigma = \frac{F}{S} \tag{4}$$

where F is the external force, S is the area of the body.

Compression, tension and shear

If the force pulls the cross-section and the internal forces act perpendicularly to it, we refer to tensile stress. Stress and strain is expressed positively. If an external force is pushing on the cross-section, compressive stresses are generated. Stress and strain is expressed negatively. In the first case the wood fibers are stretched and in the second case compressed. When the tensile strength is reached, the wood fibers break and are compressed. In tension and compression, the forces act perpendicular to the cross-section. If the resultant of external forces mutually displace fibers in their planes, tangential stresses are generated. The cross-section shifts. The wood ruptures on shear (Požgaj *et al.*, 1997).

4 Moisture properties of wood

4.1 Wood moisture content

The presence of water in wood is called the moisture content of the wood. It is expressed as the ratio of the weight of water to the weight of the wood in its dry state - absolute moisture content w_{abs}, or as the ratio of the weight of water to the weight of wet wood - relative moisture content w_{rel}. The absolute moisture content of wood is used to characterize the physical and mechanical properties of wood. Relative moisture content is used where it is necessary to know the percentage of water in the total wet weight of the timber, e.g., when selling or buying timber (Horáček, 2008). According to Horáček (2008), three different threshold values can be distinguished depending on the water content of the wood in relation to the dry weight of the wood:

- **Moisture content of dry wood** - the steady-state ratio of the weight of water to the weight of dry matter when the wood is dried at 103+-2 °C, i.e., there is no bound or free water in the wood. This moisture content is expressed in absolute dry wood ($w_0 = 0\%$).
- **Moisture at cell wall saturation** - the microcapillary system in the cell wall is filled with water. This moisture is expressed between the cell wall saturation Cell wall saturation limit or hygroscopicity limit (Cell wall saturation limit = Hygroscopicity limit = 22-35%).
- **Moisture saturation of the wood** - the micro and macro-capillary system is fully saturated with water; the wood contains the maximum amount of water. This moisture content is expressed by the maximum moisture content of the wood ($w_{max} = 80 - 400\%$).

4.2 Equilibrium wood moisture content

Wood is a hygroscopic material that has the ability to change its moisture content according to the humidity of the surrounding environment through adsorption. Wood is also a capillary-porous material. The average porosity of wood, depending on its density, is around 50-60%. Adsorption of wood is then understood as the binding of a gaseous or liquid substance on the specific internal surface of the wood. The specific internal surface of wood is formed by the fibrillar structure of the submicroscopic cell wall. The consequence of the considerable porosity is a large internal surface, which, depending on the density of the wood, is around 100-300 $m^2.g^{-1}$ dry weight or 20-300 $m.cm^{-3}$ for dry wood. Like most porous substances, this substantial internal surface can adsorb water vapour contained in the surrounding air and, thanks to capillary transport processes, can take up liquids (e.g., water, impregnating agents, adhesives) with which it is in direct contact. The internal surface of the wood is determined from the idea that the water in the wood is evenly distributed over the entire internal surface of the wood when the sorption

sites are hypothetically filled. According to the nature of the forces that cause adsorption, we divide adsorption into physical and chemical. In both cases, thermodynamic equilibrium must hold in the wood-adsorbent system. The amount of adsorbed substance in wood depends on its chemical and physical properties (molecular weight and volume, surface tension) and on environmental factors (pressure, temperature, relative humidity, air velocity). The dependence of the amount of adsorbed substance on environmental factors is expressed by adsorption isotherms. These are mathematical expressions of sorption theories that attempt to explain adsorption in terms of its physical or chemical nature. The moisture content of wood that will stabilize under given environmental conditions (relative humidity and temperature) is called the equilibrium moisture content of wood, equilibrium moisture content. The state that is reached is then called the equilibrium moisture content. With each change in relative humidity and air temperature, the equilibrium moisture content of the wood changes. If the moisture content of the wood is lower than the State of moisture balance, the wood takes up (adsorption) water in the form of water vapour from the surrounding air until it reaches the State of moisture balance. If the moisture content of the wood is higher than the State of moisture balance, the opposite process occurs, and the wood loses water (desorption). This process of wood moisture content change as a function of relative humidity and ambient temperature is reversible, but not along the same curve. For the same relative humidity and air temperature, the wood moisture content is higher in desorption than in adsorption, by 2.5 to 3.5 % over a range of relative humidity φ= 30-90 %. The dependence of Equilibrium wood moisture content on relative humidity at constant temperature is called the sorption isotherm (Horáček, 2008).
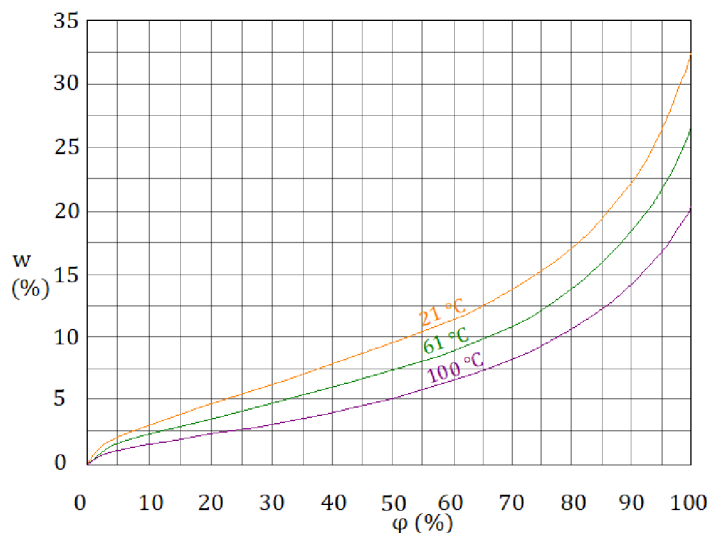
Figure 1 – Sorption isotherm at different temperatures (Horáček, 2008)

4.3 Dimensional changes due to changes in moisture content

If the moisture content of the wood changes within the range of bound water, the wood undergoes dimensional changes - dimensional hygroexpansion. A reduction in the

16

moisture content of wet wood to between hygroscopicity (evaporation of free water) has no significant effect on the dimensional change. The shrinking and swelling is localized in the cell wall, where the fibrillar structure moves away or closer. This changes the dimensions of the individual elements and the wood as a whole. The orientation of the fibrils in the cell wall has a major influence on the amount of shrinkage and swelling. The longitudinal shrinkage and swelling caused by the inclination of the fibrils is insignificant. The small dimensional changes in the longitudinal direction are explained by the fact that molecules cannot arise between fibrils to form a valence chain in the longitudinal junction, so there is no spacing in this direction. Hygroexpansion of dimensions can be described as a reversible process that follows the same trajectory. The different values of swelling and shrinkage result only from the definition and mathematical expression of the process, not from the nature of the process itself. Desiccation and swelling are processes in which the linear, planar or volumetric dimensions of a solid change as a result of a change in moisture content. They are defined as the ratio of the relevant dimensional change to the original value of the dimension (Horáček, 2008).

4.4 Swelling

Swelling α refers to the ability of wood to increase its dimensions by taking up bound water in the moisture content range of 0% - Hygroscopicity limit (Cell wall saturation limit). We distinguish between linear swelling (in each anatomical direction - longitudinal, radial, and tangential), surface swelling (change in solid surface area) and volumetric swelling (change in solid volume). The swelling of wood from the absolute dry state to the hygroscopic limit is called total swelling (maximum). Swelling of wood in any smaller interval is called partial swelling. Swelling is expressed as a percentage of the change in dimension to the original value and is most often given in %. For practical purposes, it is useful to know the percentage change in dimensions, area or volume if the humidity changes by 1%. The calculation and use of the swelling coefficient assumes that changes in the dimensions of solids below the hygroscopicity limit are linearly proportional to changes in moisture content. This assumption is not entirely accurate, but its use is sufficient for practical purposes. Swelling also has an anisotropic character. Along the fibers the swelling is very small and does not exceed 1%. The average value of total longitudinal swelling for our species is 0.1-0.4%. In the transverse direction the wood swells much more, 3-6 % in the radial direction and 6-12 % in the tangential direction. Swelling in each anatomical direction is often expressed by the ratio $\alpha\_t : \alpha\_r : \alpha\_l = 20 : 10 : 1$ (Horáček, 2008).

4.5 Moisture stress

During drying - evaporation of water from the wood - internal stresses are created in the wood during uneven drying, which consist of two components - moisture and residual stress. Moisture stresses are due to the existence of a moisture gradient. The hygroexpansion of wood is considered to be continuous and the resulting deformations

are directly proportional to the stresses due to Hooke's law. Moisture stresses and deformations are considered elastic, having a temporary character and disappearing after moisture equilibration (Horáček, 2008).

A change in moisture content is always associated with significant swelling or shrinking of the wood. Moisture deformation is therefore only dependent on the change in moisture inside the wood. This deformation can be defined as follows (Kollmann and Coté, 1968).

$$\alpha = \begin{bmatrix} \alpha_l & \alpha_r & \alpha_t & 0 & 0 & 0 \end{bmatrix}^T \qquad (5)$$

Where $\alpha_l, \alpha_r, \alpha_t$ - material swelling coefficients in individual directions (Ormarsson, 1998).

4.6   Effect of moisture on the mechanical properties of wood

The laws of the influence of bound water on mechanical properties are investigated in terms of the use of wood for structural purposes and also in terms of technological processes in the manufacture of wood products. Structural timber can reach an equilibrium moisture content in the range of 9-22% under our conditions. When the moisture content changes by 1% in the water-bound range, the strength of the wood changes by an average of 3-4%. This already shows that moisture has a great influence on the strength of wood. The change in wood strength has a non-linear pattern depending on the change in water content. If we take into account that a change in moisture content of 1% in the range of bound water causes a change in wood strength of 2.5% to 3.5%, the total decrease will be 30 to 70%. The elastic modulus of wood changes linearly due to bound water. A 1% change in moisture content within the range of bound water causes a change in the modulus of elasticity E of 1.5 to 2%. This means that the modulus of elasticity E drops by 35 to 50% when the moisture content changes from, for example, 8% to cell wall saturation limit. The shear elastic moduli of wood (G_{LR}, G_{LT}, G_{RT}) in the water-bonded range are closely related to moisture content. A 1% change in moisture content represents a 1.5 to 2% change in shear modulus (Požgaj *et al*., 1977).
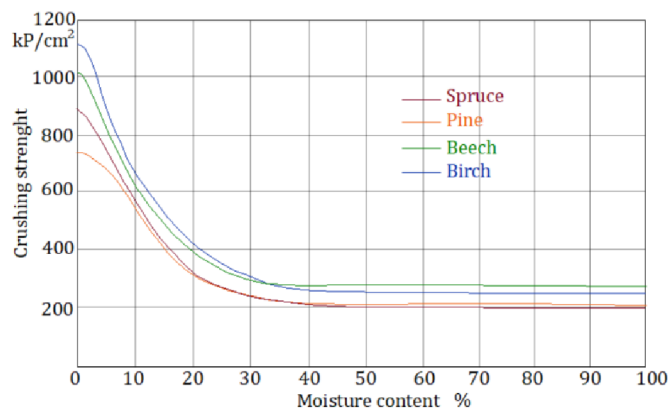
Figure 2 - Effect of moisture on wood strength in some wood species, Crushing strength = bending strenght (Kollman, 1968)

Conversion of the wood strength determined at any moisture content in the interval 5-25% to the property at 12% moisture content is carried out according to the following relation:

$$\sigma_{12} = \sigma_w(1 + \alpha(w - 12)) \qquad (6)$$

where w - wood moisture content (%), σ_w - wood strength (MPa), α - correction factor (Horáček, 2008)

Table 1 - Correction coefficients expressing the effect of moisture on a given property (Horáček, 2010)

Method of loading	Correction coefficients α
Compression in the direction of the fibers	0,04
Compression perpendicular to fibers	0,035
Tension in the direction of the fibers	0,01
Tension perpendicular to fibers (R)	0,01
Tension perpendicular to fibers (T)	0,025
Static bending	0,04
Shear in fiber direction	0,04
Modulus of elasticity	0,01-0,02

4.7 Water movement in wood

Fluids (liquids and gases) move through wood in two basic ways - volume flow and molecular flow. Volumetric flow takes place in meso- and macrocapillaries under the influence of a static or capillary pressure gradient. Molecular flow involves the movement of gases in the cell lumen across cell wall thinning and the movement of water bound in the cell wall microcapillaries. The magnitude of volume flow through wood is determined by its permeability. The application of molecular flux is the drying of the wood and the movement of the moisture field through the wood element to reach equilibrium moisture content. The molecular flow of substances is described by diffusion.

4.7.1 Mechanism of water movement in the cell wall

The explanation of the mechanism of movement of water bound in the cell wall is based on the theory of sorption and the actual mechanism will be further used to describe the diffusion of fluids in wood. The sorption theory assumes that:

- Water molecules are absorbed at sorption sites (hydroxyl groups) or due to the polar nature of water in their proximity by chemical bonds through hydrogen bridges and Van der Waals forces,
- Polymolecular sorption assumes the ability of an isolated sorption site to attract 1-5 water molecules depending on the equilibrium moisture content of the wood,
- The range between monomolecular and polymolecular sorption is around 6-8% moisture content.
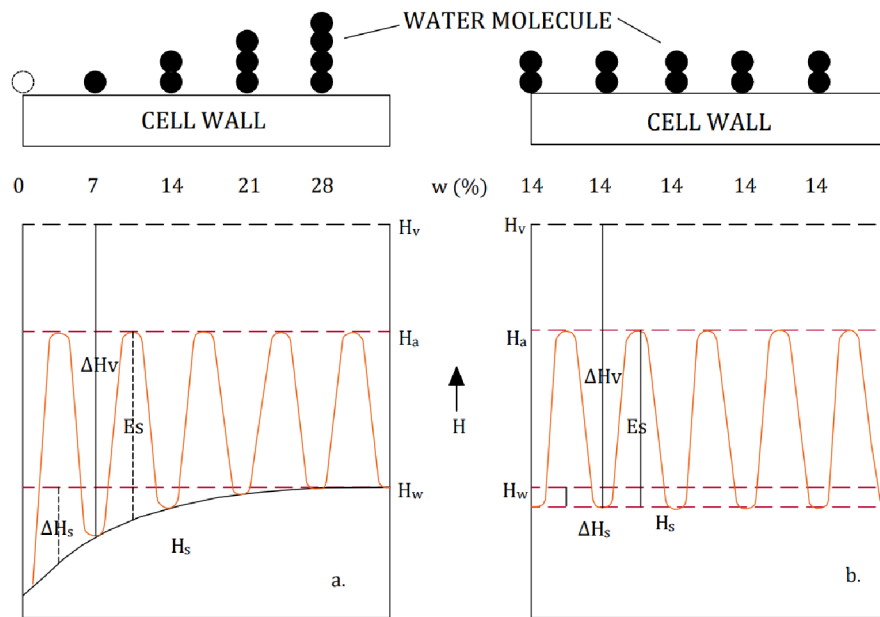
Figure 3 – Hypothetical model of the effect of moisture in the cell wall on the thermodynamics of bound water - a non-uniform moisture distribution, b uniform moisture distribution - Hv enthalpy of water vapour, Ha enthalpy of activated bound water, Hs enthalpy of bound water, delta Hs differential heat of sorption, delta Hv evaporative heat of water, Es activation energy of bound water (Siau 1995)

Assume that we know the number of sorption sites in a given mass or volume unit of wood and the number of water molecules (number of water layers) bound per sorption site at a given moisture content of the wood. In reality, we only have some idea of the magnitude of the binding energy of water in wood from the thermodynamics of sorption (e.g., differential heat of sorption, heat of wetting). Let us assume, then, that there is a moisture gradient in wood, i.e., that different numbers of water molecules are bound at different sorption sites, as shown in Figure 3. The different sorption sites are then separated according to the theory of isolated sorption sites via potential pits. We know from thermodynamics that water in different states has different enthalpies. The potential pit is then an energy barrier between two adjacent sorption sites that must be overcome if the water molecule is to move in the direction of the moisture gradient. The size of the potential pit varies with humidity and is already constant above hygroscopicity limit. The size of the potential pit is expressed in terms of the activation energy E_a, which determines the necessary magnitude of energy supplied to the water molecule to overcome the energy barrier and move into the adjacent potential pit. The activation energy depends on the moisture content of the wood (Horáček, 2008).

4.7.2 Diffusion of water and gases in wood

Diffusion characterizes the movement of bound water in wood. If there is an uneven distribution of moisture in the wood, water movement - diffusion - is induced to compensate for these differences. Diffusion refers to the molecular flux caused by a non-zero concentration gradient where a substance tries to find an equilibrium concentration.

No external static pressure is required for this movement, but only the concentration gradient is the driving force. The concentration gradient can be thought of as a non-uniformly distributed moisture in the wood, but also as a non-uniformly distributed temperature field or chemical potential of water. Let us consider only the movement of water bound across the fibers, e.g. in the radial direction. Water can then move in different states through the wood in three ways - (1) across the tangential cell wall as liquid g_1, (2) across the lumen in the radial direction as water vapor g_2, and (3) across the radial cell wall as liquid g_3. In the tangential direction, the movement of water can be described by analogy to the radial flow. The conductivity of path (3) is negligible due to the need to travel large distances and the considerable activation energy of the bound water, and the general transverse diffusion model is based only on the conductive paths (1) and (2)

$$\frac{1}{g_T} = \frac{1}{g_1} + \frac{1}{g_2} \tag{7}$$

where g_T is the conductivity of water bound in the transverse direction, g_1 is the conductivity of water through the cell wall, g_2 is the conductivity of water vapour through the lumen and $g_i \approx K_{wi}$ (the moisture conductivity coefficient $kg.m^{-1}.s^{-1}$). From the perspective of water in wood, it is necessary to consider wet wood as a continuum - an environment with continuously changing properties. All parameters of such an environment are then continuous functions of spatial coordinates and time. According to its nature, diffusion is divided into isothermal and non-isothermal, stationary and non-stationary (Horáček, 2008). The general physical notation of water diffusion in wood is:

$$\vec{j} = -D\nabla c \tag{8}$$

where $\vec{j}$ – flux density $(kg.m^{-2}.s^{-1})$, D – coefficient of diffusion $(m^2.s^{-1})$ a c – water concentration in wood $(kg.m^{-3})$.

4.7.2.1 Stationary diffusion

Under stationary (steady) conditions, i.e. if the diffusion is constant in time and varies only with distance, the process can be described according to Fick's law I:

$$\frac{m}{t\,S} = D\frac{\Delta c}{\Delta x} \tag{9}$$

where D – coefficient of diffusion $(m^2.s^{-1})$, m – weight of the diffused liquid (kg), t – time (s), S – diffusion area (m^2), Δx distance of different concentrations (m) a Δc difference in concentration $(kg.m^{-3})$ (Dushman, 1962).

4.7.2.2 Non-stationary diffusion

In non-stationary diffusion, the fluid flow and its concentration are variables in time and space, unlike in stationary diffusion, where both variables are considered constant.

Nonstationary fluid flow occurs during heating, impingement, or drying of wood; therefore, diffusion of water in wood is often described as a nonstationary process, which is derived from a stationary relationship of derivatives by time and distance with a simplification to a 1-dimensional Cartesian coordinate system. According to Horáček (2008):

$$\frac{dm}{dt} = K_w S \left(\frac{dw}{dx}\right)_{t,x} \tag{10}$$

By applying 1. Law of Thermodynamics

$$\dot{E}_1 - \dot{E}_2 = \dot{E}_3 \tag{11}$$

where $\dot{E}_1$ – energy flow into the system, $\dot{E}_2$ – energy flow from the system and $\dot{E}_3$ – energy balance in the system. The equation can be written as:

$$\dot{E}_1 \approx \left(\frac{dm}{dt}\right)_{in} = K_w S \left(\frac{dw}{dx}\right)_x \tag{12}$$

$$\dot{E}_2 \approx \left(\frac{dm}{dt}\right)_{out} = K_w S \left(\frac{dw}{dx}\right)_{x+\Delta x} \tag{13}$$

$$\dot{E}_3 \approx \left(\frac{dm}{dt}\right)_{gain} = S \rho_{r\bar{w}} \left(\frac{dw}{dt}\right)_{\Delta x} \tag{14}$$

Substituting (12) – (14) into equation (11) and rearranging, we get:

$$\frac{dw}{dt} = \frac{K_w}{\rho_{r\bar{w}}} \frac{d^2 w}{dx^2} \tag{15}$$

Substituting relation into equation (15) gives an equation for the approximate determination of the average diffusion coefficient of water in wood, which is assumed to be constant:

$$\frac{dw}{dt} = \bar{D} \frac{d^2 w}{dx^2} \tag{16}$$

A more accurate solution can be obtained by differentiating the coefficient D by the moisture content of the wood and equation (16) in the form:

$$\frac{dw}{dt} = \frac{d}{dx}\left(D \frac{dw}{dx}\right) \tag{17}$$

The partial differential equations (16) and (17) are called II. Fick's law, and by solving them partially we obtain the distribution of moisture (or concentration, osmotic pressure,

free energy of bound water) as a function of position and time, i.e. w=f(x,t). The general form of Fick's law II in the Cartesian coordinate system has the form:

$$\frac{dw}{dt} = \frac{d}{dx}\left(D_x \frac{dw}{dx}\right) + \frac{d}{dy}\left(D_y \frac{dw}{dy}\right) + \frac{d}{dz}\left(D_z \frac{dw}{dz}\right) \qquad (18)$$

When solving these equations, it is necessary to know the boundary conditions for the equilibrium moisture content on the surface of the solid, the moisture distribution at the initial moment and the target moisture content of the wood (Siau, 1995).

5 Thermal properties of wood

The thermal properties of wood are most often of interest to us when solving practical problems related to drying wood and using the thermal insulation properties of wood. For example, we are interested in how much heat must be supplied to a wood-water system to warm it to the desired temperature, and what is the temperature at a given point in the body and at a given time. We are less concerned with questions of changes in the dimensions of the solid associated with temperature change (Horáček, 2008).

5.1 Thermal expansion

Increasing the temperature of a body causes the energy of its molecules to increase, and ultimately the size of the body to increase. Thermal expansion is characterized by the coefficient of thermal expansion α_i, which is defined, similarly to the coefficient of swelling and slumping, by the ratio of the change in dimension and the dimension of the soil body with a linear dependence on temperature:

$$\alpha_i = \frac{l_T - l_0}{l_0 \Delta T} \qquad (19)$$

where α_i - coefficient of thermal expansion in i-direction (mm^{-1}.K^{-1}), l_0 - initial dimension (m) and l_T - dimension after temperature change ΔT (K).

The coefficient of thermal expansion α_i, expresses the change in the unit length of wood when heated by 1K. Due to the anisotropy of the wood, the ratios of α_i in each direction are similar to those of swelling or shrinking, $\alpha_T : \alpha_R : \alpha_L = 15 : 10 : 1$, but the values are about 4 orders smaller. Given these low values of the thermal expansion coefficient α_i, we can neglect the thermal dimensional changes in wood compared to moisture content. The linear dimension of the body when the temperature changes by ΔT can be calculated according to Eq (Horáček, 2008):

$$l_T = l_0 + \alpha_i \, \Delta T = l_0(1 + \alpha_i \, \Delta T) \qquad (20)$$

5.1.1 Effect of temperature on the mechanical properties of wood

Wood is subjected to the effects of temperature in different time modifications during different technological processes. Taking into account these heat treatments, it is desirable to investigate the changes in the structure of wood in order to influence its further use. In addition to temperature, the effect of moisture content must also be taken into account in the process of converting wood into a product. The interaction of temperature and moisture content of the wood has a more pronounced effect on the change in mechanical properties due to the individual action of these factors. The torsional modulus G is sensitive to temperature change. A significant decrease in elastic modulus due to temperature is generally described by physical and chemical changes in

lignin, hemicelluloses or amorphous cellulose. Similar results were found when the effect of temperature on the elastic moduli of wood E was also observed. The relationship between temperature and tensile modulus E is linear. When observing the effect of temperature on the shear strength of wood, there is a more pronounced decrease in strength observed at moisture contents around cell wall saturation limit than in the dry state. Even at this strength, moisture-temperature interactions are more pronounced. The relationship between temperature and strength in the humidity range from 20 to 100°C is linear. If the moisture content is greater than cell wall saturation limit, the modulus of elasticity no longer changes. The dependence of the elastic modulus on moisture content and temperature can be expressed according to the following relationships (Požgaj *et al.*, 1997):

$$E_l = E_{l0}\big(1 + E_{lT}(T_0 - T)\big) + E_{lw}(w_f - w_a) \tag{21}$$

$$E_r = E_{r0}\big(1 + E_{rT}(T_0 - T)\big) + E_{rw}(w_f - w_a) \tag{22}$$

$$E_t = E_{t0}\big(1 + E_{tT}(T_0 - T)\big) + E_{tw}(w_f - w_a) \tag{23}$$

$$G_{lr} = G_{lr0}\big(1 + G_{lrT}(T_0 - T)\big) + G_{lrw}(w_f - w_a) \tag{24}$$

$$G_{lt} = G_{lt0}\big(1 + G_{ltT}(T_0 - T)\big) + G_{ltw}(w_f - w_a) \tag{25}$$

$$G_{rt} = G_{rt0}\big(1 + G_{rtT}(T_0 - T)\big) + G_{rtw}(w_f - w_a) \tag{26}$$

where:

$$w_a = w \quad if \quad w \le w_f \tag{27}$$

$$w_a = w_f \quad if \quad w > w_f \tag{28}$$

$E_{l0}, E_{r0}, E_{t0}, G_{lr0}, G_{lt0}, G_{rt0}$ – modulus of elasticity at 20°C (MPa; %); $E_{lw}, E_{rw}. E_{tw}. G_{lrw}, G_{ltw}. G_{rtw}$ – coefficients describing the effect of humidity and temperature (MPa) (Ormarsson, 1998).
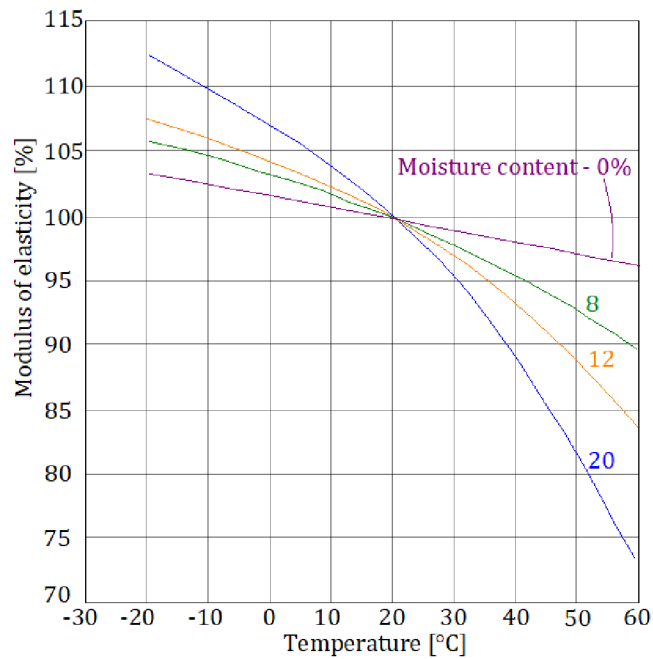
Figure 4 – Average values of the modulus of elasticity with changes in moisture content and temperature (Sulzberger, 1953)

It is therefore obvious that temperature also has an obvious effect on the mechanical properties, namely that the strength of the wood and its elasticity decrease with temperature. The smallest effect of temperature can be observed in tension parallel to the grain. On the other hand, mechanical properties perpendicular to the grain are more sensitive to temperature changes than in the direction of the grain. This can be explained by the fact that covalent bonds are less involved in the strength of wood than hydrogen bonds when stressed perpendicular to the fibers (Požgaj *et al.*, 1997).

6   Mechanics of plates and fiber-composite materials

Wood is a natural anisotropic material consisting of fibers of individual cells. Due to its fibrous structure, it is considered an orthotropic material in terms of mechanical behavior. Such materials lie between isotropic and anisotropic materials, where the degree of isotropy depends on the number and orientation of the planes of symmetry.

The variation in these materials can be observed most clearly in their response to different types of loads such as tensile and shear. When a rectangular material sample made of isotropic, anisotropic, and orthotropic materials is subjected to uniaxial tensile loading, the response will differ among them. The isotropic material sample under uniaxial tensile loading will stretch in the loading direction and compress in the transverse direction (as shown in the Figure 5), while the angles between the sides of the rectangle remain unchanged. However, under pure shear, the angles between the sides will change but there will be no elongation or compression. The deformations of an isotropic material are thus "direction-independent," meaning that normal deformations are determined by normal stresses and are not affected by shear stresses, while shear deformations are determined by shear stresses and are not affected by normal stresses. For anisotropic materials, we can observe a correlation between the normal load components and shear deformations and vice versa. When subjected to normal loads, the material will experience both shortening and a change in the angle of the sides. In addition to shear deformation, the material will elongate and shorten when subjected to pure shear (Agarwal, 2015).
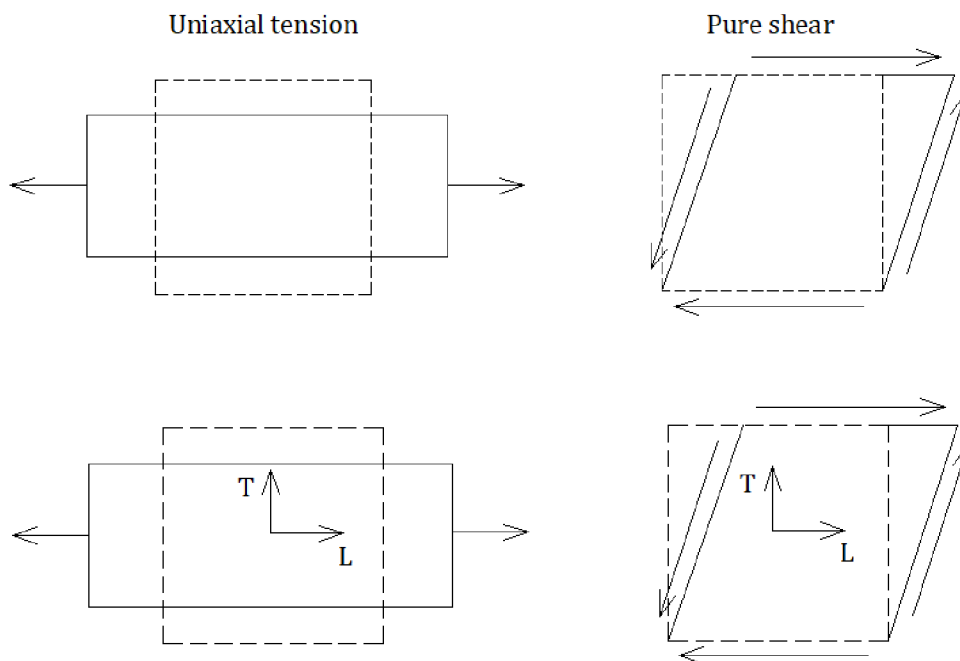
Figure 5 – Uniaxial tension, pure shear (Agarwal, 2015)

6.1 Hooke's law for anisotropic and orthotropic materials

Normal stress is a measure of force per unit area applied perpendicular to the surface. The corresponding displacement is defined as the elongation (or shortening) per unit length of material in the direction of loading. In isotropic materials, the relationship between stress and strain is direction-independent, requiring only one elastic constant to describe the elastic behavior of the material under uniaxial loading. However, in anisotropic materials, at least two elastic constants are required to describe the elastic behavior due to the dependence of stress and strain on the direction of the applied force (Nettles, 1994). When an isotropic material is subjected to normal stress σ in a particular direction, only the dimensions change, but not the shape. As a result, $\varepsilon = 0$ and $\gamma = 0$. However, in the case of shear stress, only the shape changes, not the dimensions, so $\varepsilon = 0$ and $\gamma \neq 0$. On the other hand, when an anisotropic material is subjected to normal stress σ in a particular direction, there is a change in both the dimensions and the shape, resulting in $\varepsilon \neq 0$ and $\gamma \neq 0$. The same is true when an anisotropic material is subjected to shear stress τ (Vrbka, 2008).
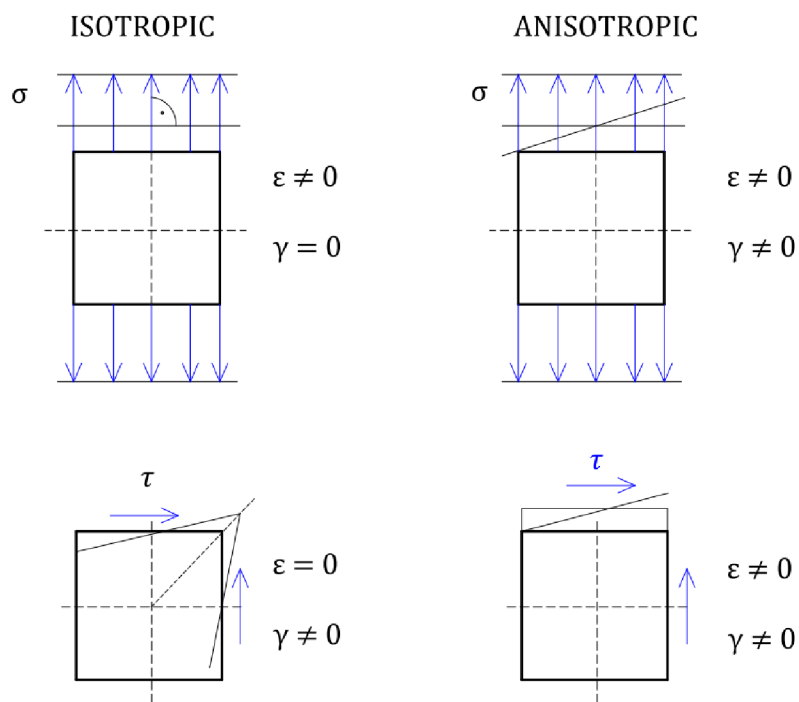
Figure 6 – Mechanical behavior of isotropic and anisotropic material (Vrbka, 2008)

The schematic shown Figure 6 illustrates a solid isotropic material. The material's strength is characterized by a single value, the modulus E, which is independent of the direction of the load. In contrast, the stiffness of an orthotropic (or anisotropic) material requires at least two material constants to describe its properties - one for the fibers' direction and another for the direction perpendicular to the fibers. Typically, these are E_L

(the elastic modulus of the material in the direction of the fibers) and E_T (the elastic modulus of the material perpendicular to the fibers) (Vrbka, 2008).

For ease of notation and definition, the subscripts 1 and 2 can be used, where E_1 represents the elastic modulus in the direction of the fibers (or equivalent) and E_2 represents the elastic modulus perpendicular to the fibers (or equivalent). Subscripts can also be used to indicate stresses, strains, and other elastic moduli. In contrast, for orthotropic materials, the directions or orientations must be explicitly specified. If external stresses are applied perpendicular or transverse to the fibers of a material, it is considered to be orthotropic in a specific way (Nettles, 1994).

Isotropic Plate   Orthotropic Plate

1   1
                                       Reinforcing fibers
                                       aligned in 1-direction

2   2

stiffness in 1-direction =   stiffness in 1-direction >> stiffness in
= stiffness in 2-direction =   2-direction ≠ stiffness in any direction
= stiffness in any direction
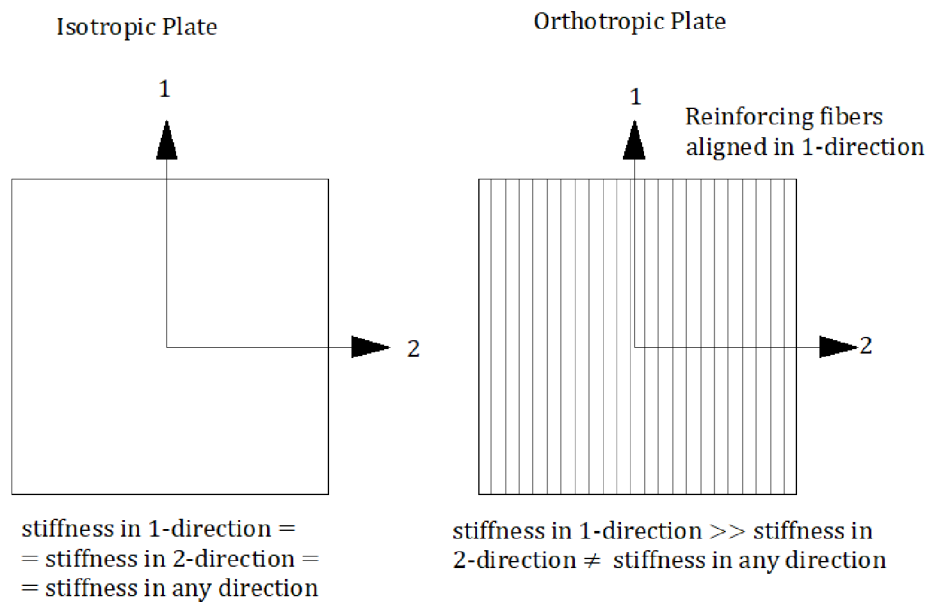
Figure 7 – Difference between isotropic and orthotropic material (Nettles, 1994)

6.1.1   General anisotropic material

It is the most general material model. Hooke's law can be according to Vrbka (2008) written in the following tensor form.

$$\sigma_{ij} = C_{ijkl}\varepsilon_{kl} \qquad i,j,k,l = 1,2,3 \tag{29}$$

possibly in a narrowed form, which we will use hereafter.

$$\sigma_i = C_{ij}\varepsilon_j \tag{30}$$

For reasons of formal simplicity, Einstein's summation symbolism was used to sum over all indices i, j, k, l and I, j, respectively. The relation above can be expressed as a matrix.

$$\begin{bmatrix} \sigma_1 \\ \sigma_2 \\ \sigma_3 \\ \tau_{23} \\ \tau_{31} \\ \tau_{12} \end{bmatrix} = \begin{bmatrix} C_{11} & C_{12} & C_{13} & C_{14} & C_{15} & C_{16} \\ C_{21} & C_{22} & C_{23} & C_{24} & C_{25} & C_{26} \\ C_{31} & C_{32} & C_{33} & C_{34} & C_{35} & C_{36} \\ C_{41} & C_{42} & C_{43} & C_{44} & C_{45} & C_{46} \\ C_{51} & C_{52} & C_{53} & C_{54} & C_{55} & C_{56} \\ C_{61} & C_{62} & C_{63} & C_{64} & C_{65} & C_{66} \end{bmatrix} \begin{bmatrix} \varepsilon_1 \\ \varepsilon_2 \\ \varepsilon_3 \\ \gamma_{23} \\ \gamma_{31} \\ \gamma_{12} \end{bmatrix} \tag{31}$$

The shear stresses and slope were included in the previous matrix relationship as part of the assignment to provide a clear physical interpretation.

$$\sigma_4 = \tau_{23} \; ; \; \sigma_5 = \tau_{31} \; ; \; \sigma_6 = \tau_{12} \tag{32}$$

$$\varepsilon_4 = \gamma_{23} \; ; \; \varepsilon_5 = \gamma_{31} \; ; \; \varepsilon_6 = \gamma_{12} \tag{33}$$

In simplified matrix form, we express the relationship in symbolic form.

$$\sigma = C\varepsilon \tag{34}$$

In expanded matrix form for plane 12 (xy):

$$\begin{bmatrix} \sigma_x \\ \sigma_y \\ \tau_{xy} \end{bmatrix} = \begin{bmatrix} C_{11} & C_{12} & C_{16} \\ C_{12} & C_{22} & C_{26} \\ C_{16} & C_{26} & C_{66} \end{bmatrix} \begin{bmatrix} \varepsilon_x \\ \varepsilon_y \\ \gamma_{xy} \end{bmatrix} \tag{35}$$

For the case of transverse stresses τ_{yz} and τ_{xz} in expanded matrix form:

$$\begin{bmatrix} \tau_{yz} \\ \tau_{xz} \end{bmatrix} = \begin{bmatrix} C_{44} & C_{45} \\ C_{45} & C_{55} \end{bmatrix} \begin{bmatrix} \gamma_{xz} \\ \gamma_{yz} \end{bmatrix} \tag{36}$$

where $[\sigma]$ is the stress tensor, C is the stiffness matrix, or the matrix of stiffness material constants, and $[\varepsilon]$ is the deformation vector. The matrix of stiffness material constants C is therefore a symmetric matrix, which contains a total of 21 independent material constants in the case of a general anisotropic material (Vrbka, 2008). According to Nettles (1994) some of the matrix's C, can be defined by known material constants:

$$C_{11} = \frac{E_{11}}{(1 - \mu_{12}\mu_{21})} \; ; \; C_{22} = \frac{E_{22}}{(1 - \mu_{12}\mu_{21})} \tag{37}$$

$$C_{66} = G_{12} \; ; \; C_{44} = G_{23} \; ; \; C_{55} = G_{13} \; ; \; C_{12} = C_{11}\mu_{21} \tag{38}$$

In some cases, Hooke's law is used in inverse form, which expresses the elements of the transformation vector ε as a linear combination of the elements of the stress vector σ. The corresponding relations are obtained by multiplying Hooke's law in its basic form by the internal stiffness matrix [C]-1 from the left, i.e. (Vrbka, 2008).

$$C - 1\sigma = C - 1C\varepsilon \qquad (39)$$

The inverse of the stiffness matrix [C]$^{-1}$ is called the material yield matrix with the designation [S], written mathematically (Vrbka, 2008).

$$[S] = [C]^{-1} \qquad (40)$$

After proper mathematical modifications, we obtain the relation for determining the deformations, i.e.

$$\begin{bmatrix} \varepsilon_1 \\ \varepsilon_2 \\ \varepsilon_6 \\ \gamma_{23} \\ \gamma_{31} \\ \gamma_{12} \end{bmatrix} = \begin{bmatrix} S_{11} & S_{12} & S_{13} & S_{14} & S_{15} & S_{16} \\ S_{21} & S_{22} & S_{23} & S_{24} & S_{25} & S_{26} \\ S_{31} & S_{32} & S_{33} & S_{34} & S_{35} & S_{36} \\ S_{41} & S_{42} & S_{43} & S_{44} & S_{45} & S_{46} \\ S_{51} & S_{52} & S_{53} & S_{54} & S_{55} & S_{56} \\ S_{61} & S_{62} & S_{63} & S_{64} & S_{65} & S_{66} \end{bmatrix} \begin{bmatrix} \sigma_1 \\ \sigma_2 \\ \sigma_3 \\ \tau_{23} \\ \tau_{31} \\ \tau_{12} \end{bmatrix} \qquad (41)$$

The material yield matrix [S] is, like the material stiffness matrix C, a symmetric matrix, where the following holds

$$S_{ij} = S_{ji} \qquad (42)$$

6.1.2 Generally orthotropic material

In general, an orthotropic material must satisfy the condition where the load is oriented at an angle to the material other than 0° or 90°. The body is considered generally orthotropic, also because the load is not considered in the anatomical directions of the material (Nettles, 1994).
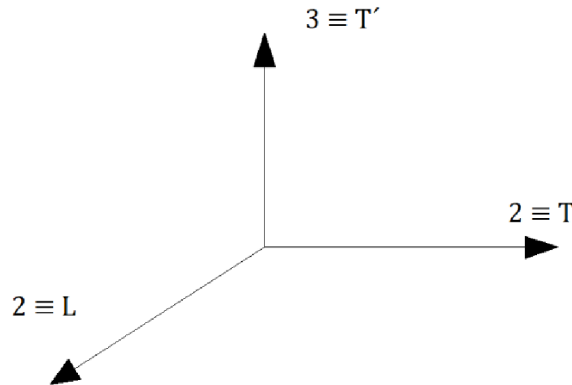
Figure 8 – Main orthotropic coordinate system (Nettles, 1994)

Stresses and strains in orthotropic material must be transformed into coordinates corresponding to the orientation of the fibers in the body, i.e., into anatomical directions. The orientations are illustrated in Figure 9 for the case where the forces act in the 1-direction (Nettles, 1994):
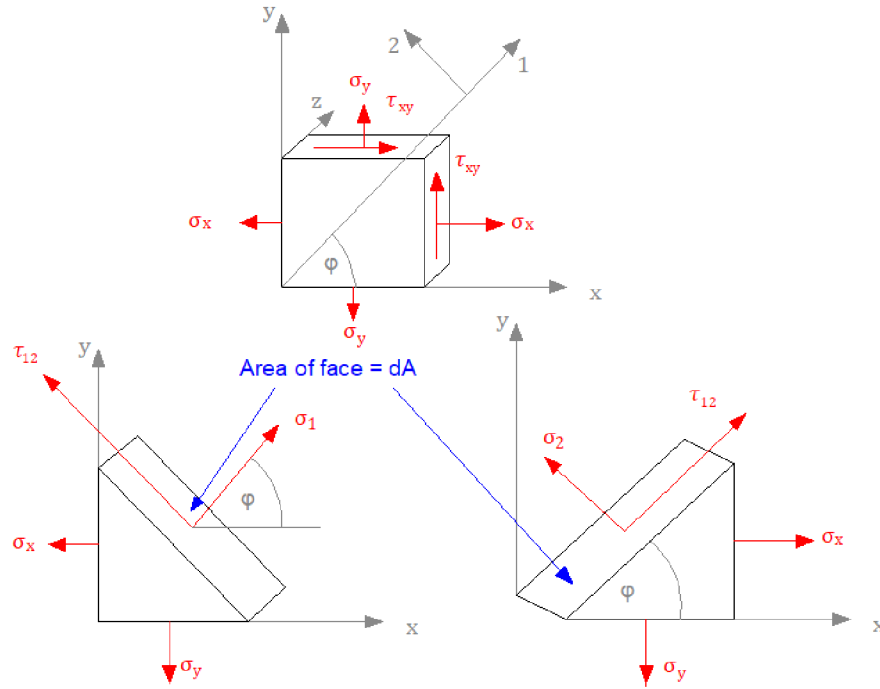
Figure 9 - Generally orthotropic body (Nettles, 1994)

We derive Hooke's law of general orthotropic material in the main orthotropic coordinate system from Hooke's law of general anisotropic material considering the characteristics of orthotropic axes (Ventsel, 2001):

$$
\begin{bmatrix} \sigma_1 \\ \sigma_2 \\ \sigma_3 \\ \tau_{23} \\ \tau_{31} \\ \tau_{12} \end{bmatrix} = \begin{bmatrix} C_{11} & C_{12} & C_{13} & 0 & 0 & 0 \\ C_{21} & C_{22} & C_{23} & 0 & 0 & 0 \\ C_{31} & C_{32} & C_{33} & 0 & 0 & 0 \\ 0 & 0 & 0 & C_{44} & 0 & 0 \\ 0 & 0 & 0 & 0 & C_{55} & 0 \\ 0 & 0 & 0 & 0 & 0 & C_{66} \end{bmatrix} \begin{bmatrix} \varepsilon_1 \\ \varepsilon_2 \\ \varepsilon_3 \\ \gamma_{23} \\ \gamma_{31} \\ \gamma_{12} \end{bmatrix} \qquad (43)
$$

Taking symmetry into account, a general orthotropic material's stiffness matrix [C] comprises 9 independent material constants. Hooke's law for a general orthotropic material can be obtained by modifying Hooke's law in inverse form in a similar manner as for a general anisotropic material.

$$
\begin{bmatrix} \varepsilon_1 \\ \varepsilon_2 \\ \varepsilon_3 \\ \gamma_{23} \\ \gamma_{31} \\ \gamma_{12} \end{bmatrix} = \begin{bmatrix} S_{11} & S_{12} & S_{13} & 0 & 0 & 0 \\ S_{21} & S_{22} & S_{23} & 0 & 0 & 0 \\ S_{31} & S_{32} & S_{33} & 0 & 0 & 0 \\ 0 & 0 & 0 & S_{44} & 0 & 0 \\ 0 & 0 & 0 & 0 & S_{55} & 0 \\ 0 & 0 & 0 & 0 & 0 & S_{66} \end{bmatrix} \begin{bmatrix} \sigma_1 \\ \sigma_2 \\ \sigma_3 \\ \tau_{23} \\ \tau_{31} \\ \tau_{12} \end{bmatrix} \qquad (44)
$$

Applying the superposition principle for loading stresses in the main orthotropic directions 1, 2 and 3, we obtain relations for the relative strains and slope. The procedure is similar to that for isotropic material.
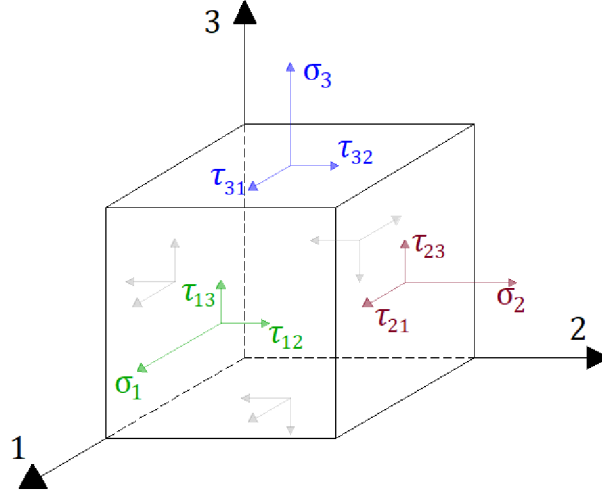
Figure 10 – Loading of an element of a general orthotropic material in the main orthotropic direction

For relative deformations and slope in the main orthotropic directions we get

$$\varepsilon_1 = \frac{\sigma_1}{E_1} - \mu_{21}\frac{\sigma_2}{E_2} - \mu_{31}\frac{\sigma_3}{E_3} \tag{45}$$

$$\varepsilon_2 = -\mu_{12}\frac{\sigma_1}{E_1} + \frac{\sigma_2}{E_2} - \mu_{32}\frac{\sigma_3}{E_3} \tag{46}$$

$$\varepsilon_3 = -\mu_{13}\frac{\sigma_1}{E_1} - \mu_{23}\frac{\sigma_2}{E_2} + \frac{\sigma_3}{E_3} \tag{47}$$

$$\gamma_{23} = \frac{\tau_{23}}{G_{23}} \quad ; \quad \gamma_{31} = \frac{\tau_{31}}{G_{31}} \quad ; \quad \gamma_{12} = \frac{\tau_{12}}{G_{12}} \tag{48}$$

The main orthotropic directions are indicated by the subscripts of the stress components, while the direction of the respective stress is denoted by the first subscript of the Poisson numbers and the direction of contraction is indicated by the second subscript. Previous equation written in matrix form.

$$\begin{bmatrix} \varepsilon_1 \\ \varepsilon_2 \\ \varepsilon_3 \\ \gamma_{23} \\ \gamma_{31} \\ \gamma_{12} \end{bmatrix} = \begin{bmatrix} \dfrac{1}{E_1} & -\dfrac{\mu_{21}}{E_2} & -\dfrac{\mu_{31}}{E_3} & 0 & 0 & 0 \\ -\dfrac{\mu_{12}}{E_1} & \dfrac{1}{E_2} & -\dfrac{\mu_{32}}{E_3} & 0 & 0 & 0 \\ -\dfrac{\mu_{13}}{E_1} & -\dfrac{\mu_{23}}{E_2} & \dfrac{1}{E_3} & 0 & 0 & 0 \\ 0 & 0 & 0 & \dfrac{1}{G_{23}} & 0 & 0 \\ 0 & 0 & 0 & 0 & \dfrac{1}{G_{31}} & 0 \\ 0 & 0 & 0 & 0 & 0 & \dfrac{1}{G_{31}} \end{bmatrix} \begin{bmatrix} \sigma_1 \\ \sigma_2 \\ \sigma_3 \\ \tau_{23} \\ \tau_{31} \\ \tau_{12} \end{bmatrix} \qquad (49)$$

Written in contracted form.

$$[\varepsilon] = [S][\sigma] \qquad (50)$$

There are a total of 12 material parameters contained within the S yield matrix. The material parameters are very significantly related through the symmetry condition of the material compliance matrix S.

$$\frac{\mu_{21}}{E_2} = \frac{\mu_{12}}{2} \quad ; \quad \frac{\mu_{31}}{E_3} = \frac{\mu_{13}}{E_3} \quad ; \quad \frac{\mu_{32}}{E_3} = \frac{\mu_{23}}{E_3} \qquad (51)$$

Therefore, according to material properties described in Vrbka (2008), a general orthotropic material is characterized by 9 independent parameters, namely E_1, E_2, E_3, μ_{12}, μ_{23}, μ_{31}, G_{12}, G_{23}, and G_{32}, as well as three Poisson's ratios: μ_{12}, μ_{32}, and μ_{13}.

6.1.3 Planar orthotropic material

For a planar orthotropic material where the principal orthotropic axes are the coordinate axes 1 and 2, the matrix relation for a general orthotropic material gives rise to the following basic form of Hooke's law Vrbka (2008).

$$\begin{bmatrix} \sigma_1 \\ \sigma_2 \\ \tau_{12} \end{bmatrix} = \begin{bmatrix} C_{11} & C_{12} & 0 \\ C_{21} & C_{22} & 0 \\ 0 & 0 & C_{66} \end{bmatrix} \begin{bmatrix} \varepsilon_1 \\ \varepsilon_2 \\ \gamma_{12} \end{bmatrix} \qquad (52)$$

As a result, a planar orthotropic material is characterized by four independent material constants within its stiffness matrix [C]. According to the previous relations, the inverse expression of Hooke's law can be given as follows:

$$\begin{bmatrix} \varepsilon_1 \\ \varepsilon_2 \\ \gamma_{12} \end{bmatrix} = \begin{bmatrix} S_{11} & S_{12} & 0 \\ S_{21} & S_{22} & 0 \\ 0 & 0 & S_{66} \end{bmatrix} \begin{bmatrix} \sigma_1 \\ \sigma_2 \\ \tau_{12} \end{bmatrix} \qquad (53)$$

Likewise, in this case, the compliance matrix S consists of four independent elements. When the independent elements of S are defined using material constants, the inverse Hooke's law can be expressed in the following form:

$$
\begin{bmatrix} \varepsilon_1 \\ \varepsilon_2 \\ \gamma_{12} \end{bmatrix} = \begin{bmatrix} \dfrac{1}{E_1} & -\dfrac{\mu_{21}}{E_2} & 0 \\ -\dfrac{\mu_{12}}{E_1} & \dfrac{1}{E_2} & 0 \\ 0 & 0 & \dfrac{1}{G_{12}} \end{bmatrix} \begin{bmatrix} \sigma_1 \\ \sigma_2 \\ \tau_{12} \end{bmatrix}
\tag{54}
$$

This expression involves four independent material constants, namely E_1, E_2, μ_{21}, and G_{12}, as described in Vrbka (2008).

6.2 Stress and strain transformations

When using wood and wood composites, situations often arise where the orientation of the fibers in the body does not correspond to a suitable coordinate system. The orientation of the fibers in the wood is represented by the anatomical coordinate system. This may ideally correspond to the global coordinate system, but in a non-ideal case the fiber deflection will be non-zero. In such cases, the directions in which the deformations due to stresses occur do not correspond to us and we have to use a transformation. The stress-strain properties of materials are generally discussed in relation to their non-isotropic nature (Bodig & Jayne, 1993).

In the transformation we will denote two coordinate systems:
- Global coordinate system (global axes) ...$x_{\bar{\iota}}$
- Anatomical coordinate system (anatomical axes) ... x_i

6.2.1 Stress transformation

The transformation matrix T is utilized in the form of a stress transformation. According to Bodig&Jayne (1993):

$$
T_\sigma = \begin{bmatrix} \cos^2\theta & \sin^2\theta & +2(\sin\theta\cos\theta) \\ \sin^2\theta & \cos^2\theta & -2(\sin\theta\cos\theta) \\ -(\sin\theta\cos\theta) & +(\sin\theta\cos\theta) & (\cos^2\theta - \sin^2\theta) \end{bmatrix}
\tag{55}
$$

In this case, the goniometric functions of sine and cosine that correspond to the deflection of fibers in anatomical axes from global axes are expressed using C and S, respectively. θ represents the angle of fiber deflection from global axes. The equation for stress transformation is expressed as follows:

$$
[\sigma] = [T\sigma][\bar{\sigma}]
\tag{56}
$$

35

where $|\sigma|$ is the stress matrix acting in the anatomical axes and $|\bar{\sigma}|$ is the stress matrix acting in the geometrical axes. Then θ is the angle of deflection of the fibers from the global axes. An alternative to this notation may look like the following:

$$\begin{bmatrix} \sigma_1 \\ \sigma_2 \\ \sigma_{12} \end{bmatrix} = [T_\sigma] \begin{bmatrix} \sigma_x \\ \sigma_y \\ \sigma_{xy} \end{bmatrix} \tag{57}$$

where σ_x, σ_y and σ_{xy} correspond to the global axes and σ_1, σ_2 and σ_{12} correspond to the anatomical axes. For example, for a material with a fiber offset of $60°$ from the geometric coordinate axes, the notation would be as follows

$$\begin{bmatrix} \sigma_1 \\ \sigma_2 \\ \sigma_{12} \end{bmatrix} = \begin{bmatrix} \cos^2\theta & \sin^2\theta & +2(\sin\theta\cos\theta) \\ \sin^2\theta & \cos^2\theta & -2(\sin\theta\cos\theta) \\ -(\sin\theta\cos\theta) & +(\sin\theta\cos\theta) & (\cos^2\theta - \sin^2\theta) \end{bmatrix} \begin{bmatrix} \sigma_x \\ \sigma_y \\ \sigma_{xy} \end{bmatrix} \tag{58}$$

Assumptions for stress transformation (Bodig & Jayne, 1993):
- Invariant,
- Equilibrium method,
- The goniometric relations apply,
- The general form of stress transformation is derived by incorporating goniometric relations into the equilibrium method, particularly when all stress components act in geometric axes,
- The components of transformation rotate in a circle (known as Mohr's circle),
- The transformation involves the appearance of the trigonometric functions $\sin(2\varphi)$ and $\cos(2\varphi)$.

6.2.2 Transformation of deformations

To perform stress transformation, we utilize the transformation matrix T, which according to Bodig&Jayne (1993) takes the following form:

$$T_\varepsilon = \begin{bmatrix} \cos^2\theta & \sin^2\theta & +(\sin\theta\cos\theta) \\ \sin^2\theta & \cos^2\theta & -(\sin\theta\cos\theta) \\ -2(\sin\theta\cos\theta) & +2(\sin\theta\cos\theta) & (\cos^2\theta - \sin^2\theta) \end{bmatrix} \tag{59}$$

Here, C and S represent the trigonometric functions of the sine and cosine of the angle between the fibers in the anatomical axes and the global axes. The equation for deformation transformation is expressed in the following form:

$$[\varepsilon] = [T\varepsilon][\bar{\varepsilon}]$$

Here, $|\varepsilon|$ refers to the deformation matrix operating in the anatomical axes, while $|\bar{\varepsilon}|$ refers to the deformation matrix operating in the geometric axes. An alternative to this notation may appear as follows.

$$
\begin{bmatrix} \varepsilon_1 \\ \varepsilon_2 \\ \varepsilon_{12} \end{bmatrix} = [T_\varepsilon] \begin{bmatrix} \varepsilon_x \\ \varepsilon_y \\ \varepsilon_{xy} \end{bmatrix}
$$

where ε_x, ε_y and ε_{xy} correspond to the global axes and ε_1, ε_2 and ε_{12} correspond to the anatomical axes (Bodig & Jayne, 1993).

6.2.3 Transformation of stiffness matrix

The relation for the stiffness matrix transformation is written in the forms.

$$
\begin{aligned}
\bar{C}_{11_i} &= C_{11}\cos^4\theta + 2(C_{12} + 2C_{66})\cos^2\theta\sin^2\theta + C_{22}\sin^4\theta \\
\bar{C}_{12_i} &= (C_{11} + C_{22} - 4C_{66})cos^2\theta sin^2\theta + C_{12}(cos^4\theta + sin^4\theta) \\
\bar{C}_{22_i} &= C_{11}sin^4\theta + 2(C_{12} + 2C_{66})cos^2\theta sin^2\theta + C_{22}cos^4\theta \\
\bar{C}_{16_i} &= C_{11} - C_{12} - 2C_{66})\,cos^3\theta sin\theta + (C_{12} - C_{22} + 2C_{66})cos\theta sin^3\theta \\
\bar{C}_{26_i} &= (C_{11} - C_{12} - 2C_{66})sin^3\theta cos\theta + (C_{12} - C_{22} + 2C_{66})sin\theta cos^3\theta \qquad (60) \\
\bar{C}_{66_i} &= (C_{11} + C_{22} - 2C_{12} - 2C_{66})cos^2\theta sin^2\theta + C_{66}(cos^4\theta + sin^4\theta) \\
\bar{C}_{44_i} &= C_{44} * cos^2\theta + C_{55} * \sin^2\theta \\
\bar{C}_{45_i} &= (C_{55} - C_{44})sin\theta cos\theta \\
\bar{C}_{55_i} &= C_{55}cos^2\theta + C_{44}sin^2\theta
\end{aligned}
$$

Where $\bar{C}_{ij_i}$ is the transformed stiffness matrix, C_{55} is the non-transformed stiffness matrix, θ is the angle expressing the fiber deflection from the longitudinal direction in the transformed laminate layer (Bodig & Jayne, 1993).

7 Plate theories

7.1 Kirchhoff-Love Plate Theory

Also known as Classical Plate Theory (CPT). The main assumption of Kirchhoff-Love Plate Theory is the perpendicularity and straightness of normals to the deformed central plane of the plate. The theory neglects shear along the thickness of the plate and works only with shear stress in the plane of the plate. Such neglect can lead to a relatively high error when applied to thick plates. To adopt this theory, two boundary conditions must be satisfied. Given the fact that (as in other cases) this is a shell theory, i.e., a theory that does not require a three-dimensional analysis, several assumptions according to Szilard (2004) must be satisfied:

- The plate is thin in the sense that the thickness is small compared to the main dimensions, but not so thin that the lateral buckling is comparable to the deflection w,
- The thickness of the plate is uniform or varies to such an extent that three-dimensional stresses are neglected,
- The applied transverse load is distributed over an area greater than the thickness of the plate,
- The support conditions are such that there are no significant extensions of the median plane.

Displacement field

The displacement of the plate in the x-axis direction is denoted by u. For the displacement of the plate in the y-axis direction, we denote v and for the displacement in the z-axis, w. The Figure 11 shows these displacements.
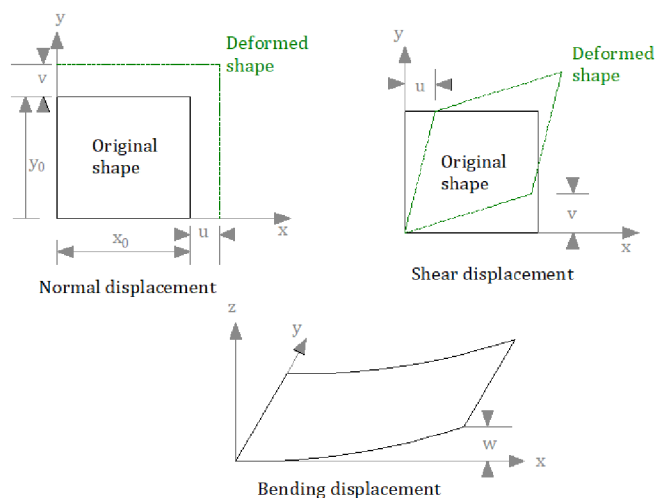
Figure 11 - CPT displacement field (Nettles, 1994)

The CPT is according to Nettles (1994) based on the following representation of the displacement field:

$$u(x, y, z) = u_0(x, y) + z\kappa_x(x, y) \qquad (61)$$

$$v(x, y, z) = v_0(x, y) + z\kappa_y(x, y) \qquad (62)$$

$$w(x, y, z) = w_0(x, y) \qquad (63)$$

Where u, v and w are the designations for the displacement components in the x, y and z directions, respectively. The displacements in the midplane are denoted by u_0, v_0, w_0. The displacement components u and v are functions in the x,y plane. The overall displacement in the plate's plane at a particular point is a combination of the normal displacements and the displacement caused by bending. Assuming the displacements in the midplane are denoted as u_0 and v_0 along the x and y axes, respectively, the total displacement can be expressed as shown in the Figure 12:

$$u = u_0 - z\frac{dw}{dx} \quad ; \quad v = v_0 - z\frac{dw}{dy} \qquad (64)$$

It is assumed that there is no strain in the direction of thickness, only displacement.
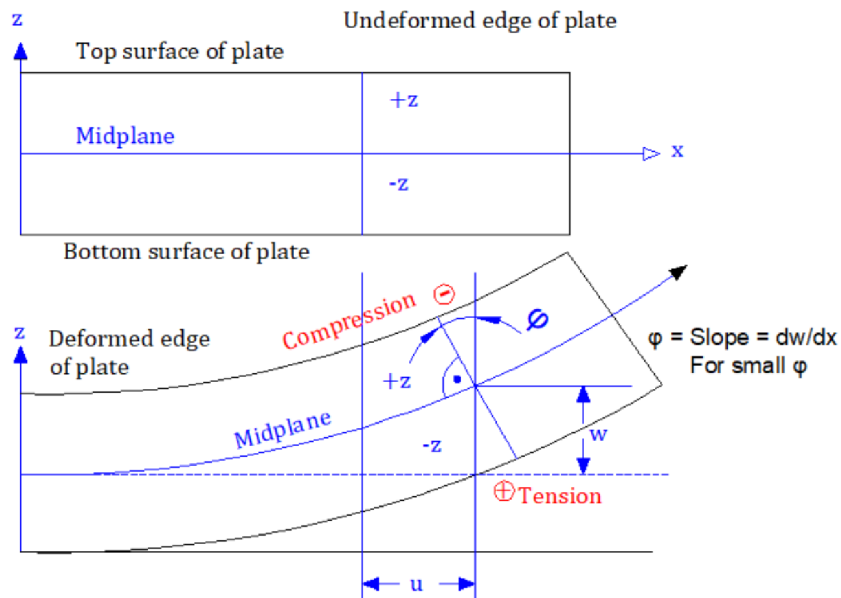
Figure 12 – Total displacements in a plate (Nettles, 1994)

The full derivation of the relations resulting from the definition of the displacement field are presented in the appendix 13.1.

7.2 Mindlin-Reissner Plate Theory

Also known as "First-Order Shear deformation theory" (FSDT). Mindlin-Reissner plate theory is a mathematical model utilized for analyzing the behavior of thin and thick plates, which are structural components that are typically much thinner in one direction than the others. It is a more advanced and precise model than classical plate theory, which assumes that plates are infinitely thin. Mindlin-Reissner plate theory considers the plate's thickness and material properties, such as its elastic modulus and Poisson's ratio, allowing for more accurate predictions of deformation and stress within the plate under external loads. Reissner and Mindlin developed a theory that considers shear deformation along the thickness of a plate, overcoming the limitations of the Kirchhoff-Love Plate theory and enabling analysis of thicker plates (Szilard, 2004). The Kirchhoff-Love Plate theory (CPT) disregards the influence of shear deformation across the thickness of the plate, which may lead to inaccurate results when dealing with plates of larger thicknesses. The definition of thin and thick plates is still a matter of debate and depends on several factors, including the stiffness of the individual laminates. Generally, plates considered as thin under CPT are those whose length/thickness ratio falls between <5-100>, while plates considered as thick have a ratio between <5-10>. The first-order shear deformation theory (FSDT) considers shear deformation in the plate thickness by assuming constant shear deformation throughout the plate's thickness, requiring the utilization of a shear correction factor to satisfy the assumption of zero shear stress on the top and bottom planes of the plate (Panyatong, 2015).

For this theory to be applicable, three boundary conditions must be satisfied. One of these involves the deflection, while the other two relate to normal and tangential rotations, respectively (Szilard, 2004).

Mindlin-Reissner Plate theory is according to Bittnar&Šejnoha (1992) based on the following assumptions:
- The difference in displacement of the edge points of the plate in the z-axis direction (plate compression) is negligible with respect to the absolute value of the displacement w,
- The normals to the midplane remain straight after deformation but are no longer perpendicular to the midplane surface of the plate. They are therefore called pseudonormals of the plate. The Mindlin-Reissner plate theory neglects the collapse of the transverse sections, as can be seen in the Figure 13,
- The normal stress of σ_z is small compared to the stresses of σ_x, σ_y.
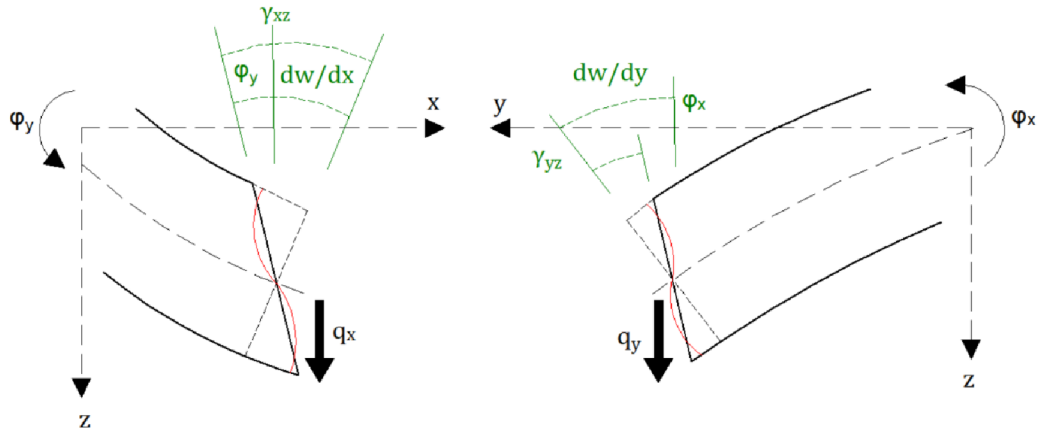
Figure 13 – Assumptions about plate reshaping (Bittnar&Šejnoha, 1992)

Displacement field

The FSDT is based on the following representation of the displacement field:

$$u(x, y, z) = u_0(x, y) + z\phi_x(x, y) \tag{65}$$

$$v(x, y, z) = v_0(x, y) + z\phi_y(x, y) \tag{66}$$

$$w(x, y, z) = w_0(x, y) \tag{67}$$

Where u, v and w are the designations for the displacement components in the x, y and z directions, respectively. The displacements of points in the midplane are denoted by u_0, v_0, w_0. All displacement components (u, v, ϕ_x, ϕ_y) are functions in the x,y plane. Compared to Kirchhoff-Love Plate theory, the assumption that there is no strain in the thickness direction, only displacement, no longer holds. The displacement in the thickness direction is now defined by the rotation of the perpendicular to the centerline of the neutral axis of the plate, as shown in the Figure 14 (Kolvik, 2012).
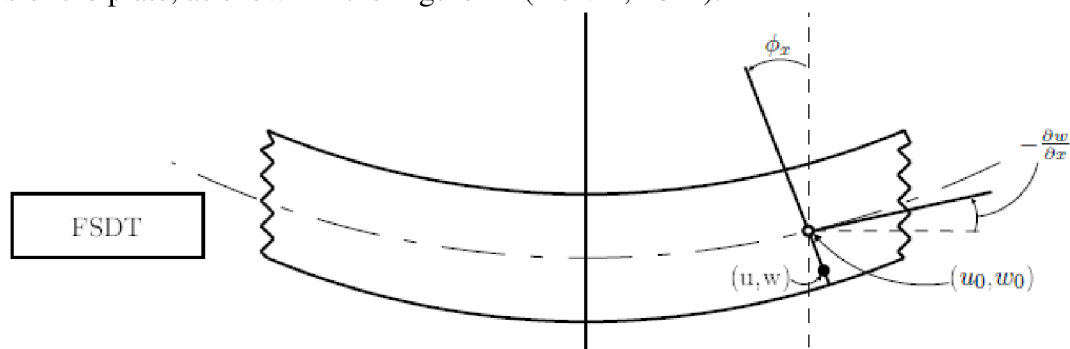
Figure 14 - Displacement of pseudonormals (Abbas, 2013)

The full derivation of the relations resulting from the definition of the displacement field are presented in the appendix 13.2.

41

7.3 Second-Order Shear Deformation Theory

Second-order shear deformation theory is a mathematical model that is used to describe the behavior of thin-walled beams and plates under loading. It is an extension of first-order shear deformation theory, which only accounts for linear deformations of a beam or plate. In contrast, second-order shear deformation theory takes into account the nonlinear deformations that can occur in a beam or plate, such as shear and rotation, and is therefore more accurate in predicting the behavior of these structures under various loads. The theory is typically used in the design of beams and plates in engineering applications, such as bridges, buildings, and aircraft.

Displacement field

The SSDT is based on the following representation of the displacement field:

$$u(x, y, z) = u_0(x, y) + z\phi_1 + z^2\phi_2 \tag{68}$$

$$v(x, y, z) = v_0(x, y) + z\psi_1 + z^2\psi_2 \tag{69}$$

$$w(x, y, z) = w_0(x, y) \tag{70}$$

Where u, v and w are the designations for the displacement components in the x, y and z directions, respectively. The displacements of points in the midplane are denoted by u_0, $v0$, w_0. All the displacement components u_0, v_0, w_0, ϕ_1, ϕ_2, ψ_1, ψ_2 are functions in the xy-plane (Shahrjerdi & Mustapha, 2011).
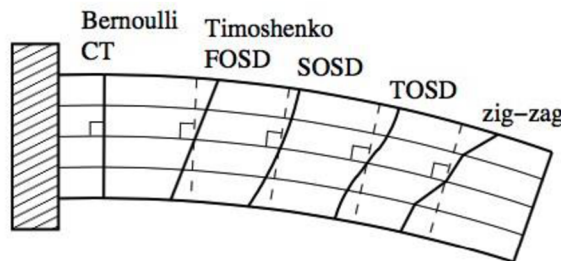
Figure 15 - Various shear deformation hypotheses (Zhang, 2014)

The full derivation of the relations resulting from the definition of the displacement field are presented in the appendix 13.3.

7.4 Third-Order Shear Deformation Theory

Third order shear deformation theory (TODT) is a mathematical model used in structural mechanics to analyze the behavior of plates and other structural elements subject to external loads. The theory accounts for the nonlinear shear deformations that occur in beams due to large deflections, which can cause the plates to twist and bend out of its original shape. This is in contrast to traditional plate theory, which assumes that the plate remains straight and only experiences small deflections. By taking into account the

nonlinear deformations, third order shear deformation theory can provide more accurate predictions of a plate behavior under load, which is important for designing safe and effective structures.

The main difference between the SODT and TODT is the level of accuracy they provide in predicting the behavior of the beam. Second order shear deformation theory is a simpler and less accurate model than third order shear deformation theory. It assumes that the plate remains straight and only experiences small deflections, and therefore it does not account for the nonlinear shear deformations that occur in the plate due to large deflections. This means that second order shear deformation theory is only suitable for analyzing plates that are not subject to significant loads or deformations. In contrast, third order shear deformation theory takes into account the nonlinear shear deformations that occur in the plate due to large deflections, which allows it to provide more accurate predictions of the plate 's behavior under load. This is important for designing safe and effective structures that are subject to large loads or deformations.

Displacement field

The TSDT is according to Shokrieh (2017) based on the following representation of the displacement field:

$$u(x, y, z) = u_0(x, y) + z\psi_x(x, y) + z^2\phi_x(x, y) + z^3\lambda_x(x, y) \qquad (71)$$

$$v(x, y, z) = v_0(x, y) + z\psi_y(x, y) + z^2\phi_y(x, y) + z^3\lambda_y(x, y) \qquad (72)$$

$$w(x, y, z) = w_0(x, y) \qquad (73)$$

Where u, v and w are the designations for the displacement components in the x, y and z directions, respectively. The displacements in the midplane are denoted by u_0, v_0, w_0. All the displacement components u_0, v_0, w_0, ϕ_x, ϕ_y, ψ_x, ψ_y, λ_x, λ_y are functions in the xy plane.
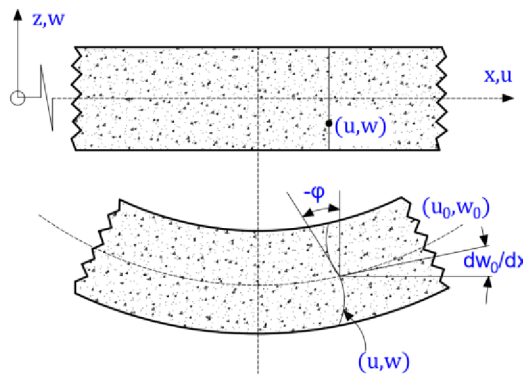
Figure 16 – Transfer displacement of plate according to TSDT (Ghiamy, 2022)

The full derivation of the relations resulting from the definition of the displacement field are presented in the *appendix 13.4.*

8 Methodology

8.1 CLT panel swelling

One of the problems faced in this work is the possible damage to laminated cross-laminated timber boards by the effects of rain and snow, respectively by the direct exposure to rainwater that is in direct contact with the top lamella of the board. Damage to the lamellas in terms of reduction in modulus of elasticity due to increased humidity should also be investigated in terms of time. Therefore, it was decided to verify numerically the rate of wetting of the top lamella of the plate by continuous water exposure. The objective of the verification is to determine for how long the top lamella of the plate must be exposed to water in order for the material used to reach the saturation limit of the cell wall. The script that has been developed for this purpose is based on the knowledge and relationships described in the chapter on water movement in wood.
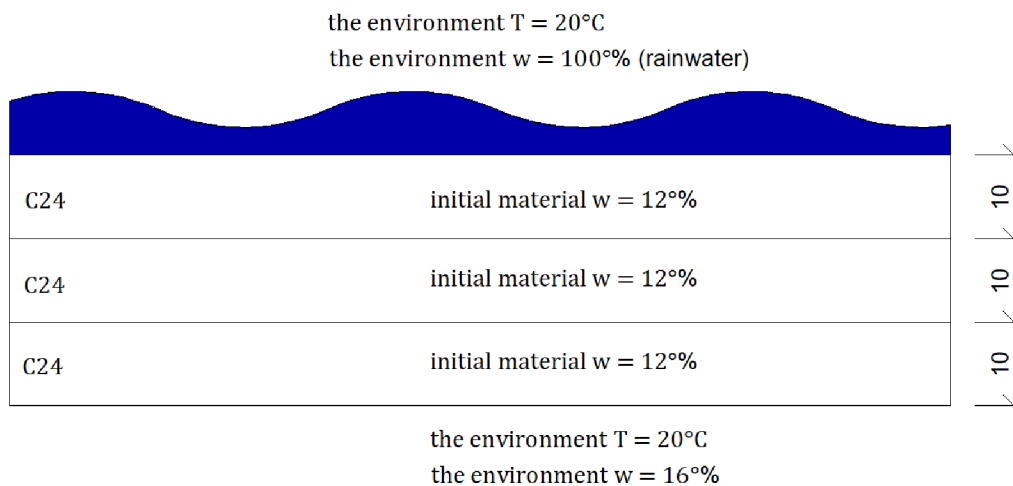
Figure 17 - Model boundary conditions

The model is based on the equation of non-stationary moisture diffusion (chapter Non-stationary diffusion), i.e.:

$$\frac{dw}{dt} = \frac{d}{dx}\left(D_x \frac{dw}{dx}\right) + \frac{d}{dy}\left(D_y \frac{dw}{dy}\right) + \frac{d}{dz}\left(D_z \frac{dw}{dz}\right) \qquad (74)$$

The complete numerical script is part of the appendix 13.6.

8.2 Extension to hygrothermal stresses in laminates

We know from the chapters *Moisture properties of wood* and *Thermal properties of wood* that a change in temperature and moisture of a material causes a change in the dimensions of the material in the form of swelling/drying or thermal expansion. In other words, changes in moisture content and temperature result in strains. These strains are not the

result of an external force acting on the body and are not accompanied by a response of the body in the form of the presence of internal forces. This is the case if the body is not constrained in any way and can change its dimensions in the radial, tangential and longitudinal direction, or its entire volume without limitation. Internal forces will be present in a body which is subjected to changes in temperature or moisture content and is restricted in any way in the directions of temperature and moisture deformations. The reasoning in relation to laminated materials is well illustrated in Figure 18 by a simple material consisting of two different materials with different moisture content and temperature properties. When the environmental moisture or temperature increases, one of the materials will react with dimensional changes before the other material. If the two materials are not bonded together, each will deform separately with respect to the environmental temperature and moisture conditions and no internal forces will occur in either material.
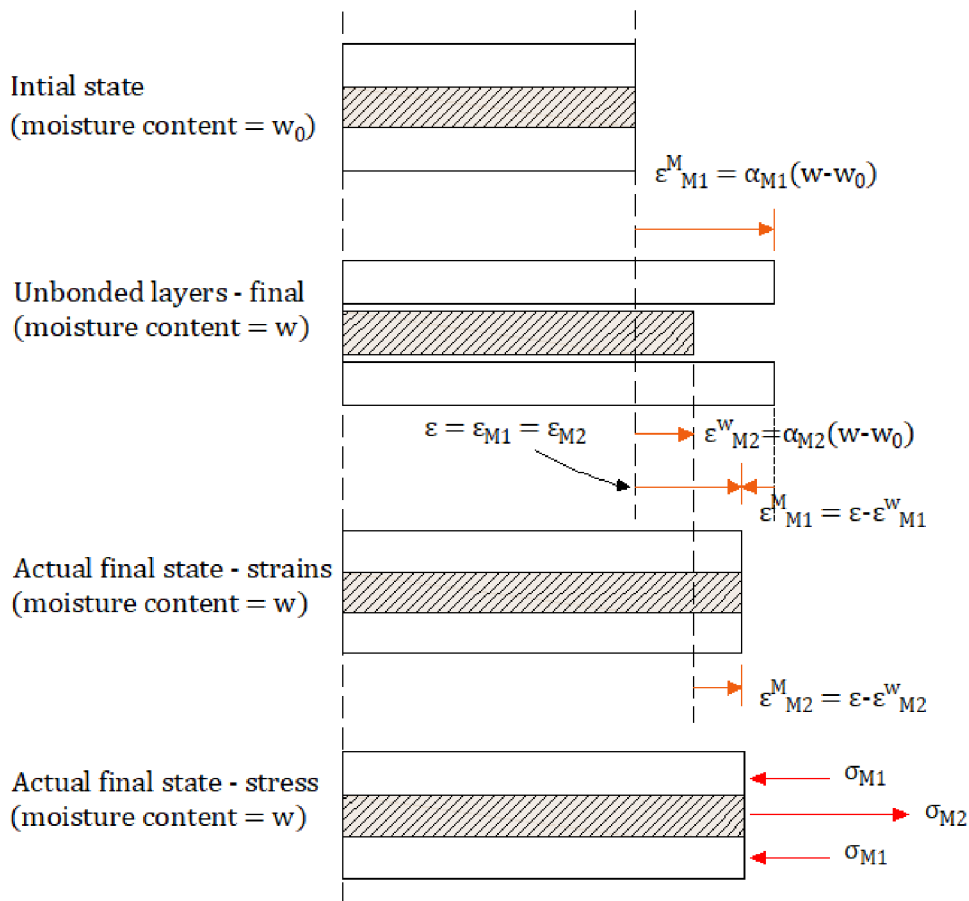
Figure 18 – Moisture change of bounded and unbounded laminate layers (Agarwal, 2015)

Since the two layers of materials form a single unit (are rigidly bonded), the actual deformations in both layers are the same. The magnitude of this deformation will be less than that of loose material 1 and greater than that of loose material 2 (if the modulus of elasticity $E_{material-1} > E_{materia-l2}$). The resulting deformation therefore depends on the elastic moduli of each material. If there is no external force acting on the body, the internal forces

from the hygrothermal loads balance each other - the net internal force is zero. Since hygrothermal changes are linear and reversible, the relationship between dimensional changes and moisture or temperature change can be written in the following form:

$$\varepsilon^T = \alpha \Delta T \tag{75}$$

$$\varepsilon^H = \beta \Delta C \tag{76}$$

where ΔT – temperature change, ΔC – change in moisture content, ε^T thermal deformation, ε^H moisture deformation, α, β – coefficients of temperature and moisture changes. In the case of an orthotropic material, the coefficients of thermal and moisture expansion, like other material properties, depend on the orientation of the fibers. The moisture and thermal deformations in the longitudinal and transverse directions are then written as follows:

$$\varepsilon_L^T = \alpha_L \Delta T \tag{77}$$

$$\varepsilon_T^T = \alpha_T \Delta T \tag{78}$$

$$\varepsilon_L^H = \beta_L \Delta C \tag{79}$$

$$\varepsilon_T^H = \beta_T \Delta C \tag{80}$$

Where α_L, α_T, β_L, β_T are the coefficients of thermal and moisture expansion in the longitudinal and transverse directions. These coefficients, like strain and stress, can be transformed arbitrarily in the x and y axes as in the case of strains.

$$\begin{bmatrix} \alpha_x \\ \alpha_y \\ \alpha_{xy} \end{bmatrix} = [T_\varepsilon]^{-1} \begin{bmatrix} \alpha_L \\ \alpha_T \\ 0 \end{bmatrix} \tag{81}$$

$$\begin{bmatrix} \beta_x \\ \beta_y \\ \beta_{xy} \end{bmatrix} = [T_\varepsilon]^{-1} \begin{bmatrix} \beta_L \\ \beta_T \\ 0 \end{bmatrix} \tag{82}$$

Where $[T_\varepsilon]$ is the transformation matrix, which is the same as the transformation matrix given in equation (59) for the strain transformation. Therefore, hygrothermal strains can be written in terms of strains:

$$\begin{bmatrix} \varepsilon_x^T \\ \varepsilon_y^T \\ \gamma_{xy}^T \end{bmatrix} = \begin{bmatrix} \alpha_x \Delta T \\ \alpha_y \Delta T \\ \alpha_{xy} \Delta T \end{bmatrix} \tag{83}$$

$$\begin{bmatrix} \varepsilon_x^H \\ \varepsilon_y^H \\ \gamma_{xy}^H \end{bmatrix} = \begin{bmatrix} \beta_x \Delta C \\ \beta_y \Delta C \\ \beta_{xy} \Delta C \end{bmatrix} \tag{84}$$

Hygrothermals strains themselves do not produce internal forces or moments when the body is not restrained against displacement, torsion or bending. When considering the laminate as a whole, thermal and moisture changes do not affect the resulting internal force and moment. However, the separate laminas are not free and are constrained by the remaining laminas. The deformation of each laminate is affected by the deformation of the other laminates. Since the hygrothermal deformations of the laminate are of the same nature as the deformations induced by external loading, they can be written as the resulting mechanical deformations:

$$
\begin{bmatrix} \varepsilon_x^M \\ \varepsilon_y^M \\ \gamma_{xy}^M \end{bmatrix}_k = \begin{bmatrix} \varepsilon_x \\ \varepsilon_y \\ \gamma_{xy} \end{bmatrix}_k - \begin{bmatrix} \varepsilon_x^T \\ \varepsilon_y^T \\ \gamma_{xy}^T \end{bmatrix}_k - \begin{bmatrix} \varepsilon_x^C \\ \varepsilon_y^C \\ \gamma_{xy}^C \end{bmatrix}_k
\tag{85}
$$

Mechanical stress in k^{th} ply is then calculated by:

$$
\begin{bmatrix} \sigma_x \\ \sigma_y \\ \tau_{xy} \end{bmatrix}_k = \begin{bmatrix} \bar{Q}_{11} & \bar{Q}_{12} & \bar{Q}_{16} \\ \bar{Q}_{12} & \bar{Q}_{22} & \bar{Q}_{26} \\ \bar{Q}_{16} & \bar{Q}_{26} & \bar{Q}_{66} \end{bmatrix}_k \begin{bmatrix} \varepsilon_x^M \\ \varepsilon_y^M \\ \gamma_{xy}^M \end{bmatrix}_k
\tag{86}
$$

The relationship (86) represents the solution to the combination of mechanical stresses combined with moisture and temperature stresses.

8.3   Effect of moisture and fiber orientation on material constants

As already mentioned in the chapter dealing with moisture properties of wood and the chapter dealing with the transformation of stiffness metric matrices, both fiber orientation and moisture have a significant effect on the material constants of wood. It is clear from the chapter *Moisture properties of wood* that a change in moisture content of wood results in a change in dimensions, or deformation. This deformation must be included in the calculation together with the change in material constants due to moisture.

The elastic moduli have a major dependence on the change in fiber orientation. The modulus of elasticity in the direction of the fibers decreases by more than 90% when the orientation of the fibers is changed by 45°, and by up to 96% when the orientation is changed by 90°. The shear modulus decreases by approximately 50% with a 45° change in fiber orientation. The stiffness matrix parameters C, which are defined by the elastic moduli, are similarly dependent. Similarly, a change in wood moisture content from 12% to 30% will reduce the stiffness matrix element C11 by more than 35%.

Graphic representations of the dependence of wood material parameters on moisture content and grain orientation are included in the appendix 13.5.

8.4 Compiling a numeric models

In this chapter, the principle (workflow) of defining numerical models according to the chosen plate theories is described in the *Figure 19,* This principle is the basis for the development of the numerical models, but the models themselves may differ slightly. The full form of the numerical models is included in the appendix 13.7 – 13.10.

INPUT

Laminate construction

Laminae elastic constants

Applied loads

Laminae stiffness matrices [Q]

[Q] for different orientations

Laminate stiffness matrices [A], [B], [D], [E], ...

Midplane strains (ε^0) and plate curvatures (κ)

Laminae strains (ε_x, ε_y, γ_{xy})

Laminae hygro(thermal) strains (ε^w_x, ε^w_y, γ^w_{xy})

Laminae stresses (σ_x, σ_y, σ_{xy})

Laminae stresses (σ_L, σ_T, σ_{LT})
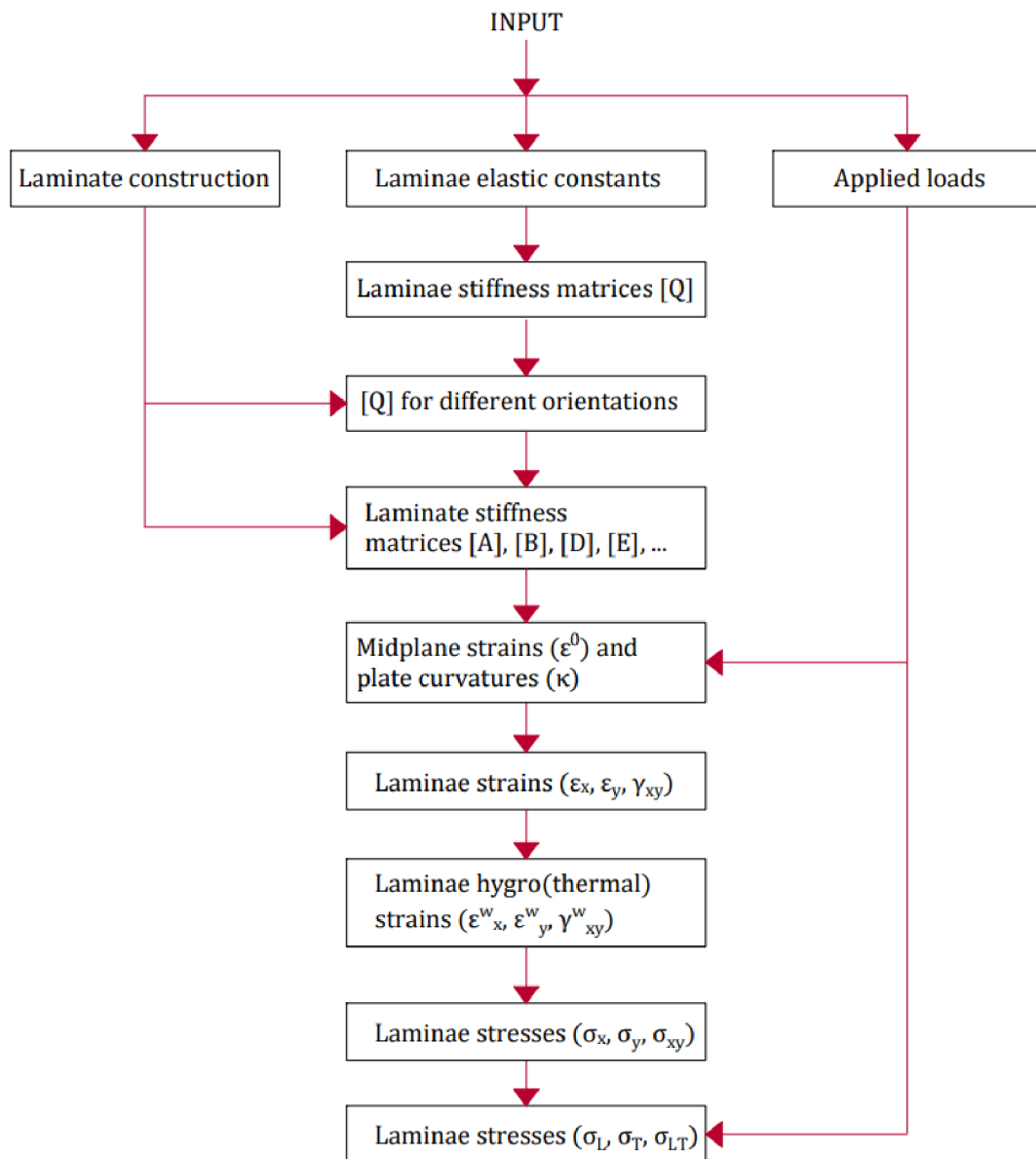
Figure 19 – Flowchart for laminate stress analysis

8.5 Experiment

8.5.1 Thin plate

The experiment was performed to verify the numerical model. Since it is well known and verified by research that the Kirchhoff-Love Plate Theory is not reliable when applied to thick plates and the remaining theories are based on CPT, several thin plates of 19 mm thickness, 300 mm width and 1500 mm length (*Figure 21*) were constructed to verify the numerical models. It was constructed of three layers of 6-7-6 mm of C22 strength, with the surface layers having an orientation in the direction of the plate length L1. The plates were placed on supports 1300 mm apart and loaded with the load-bearing arm of a loading machine.
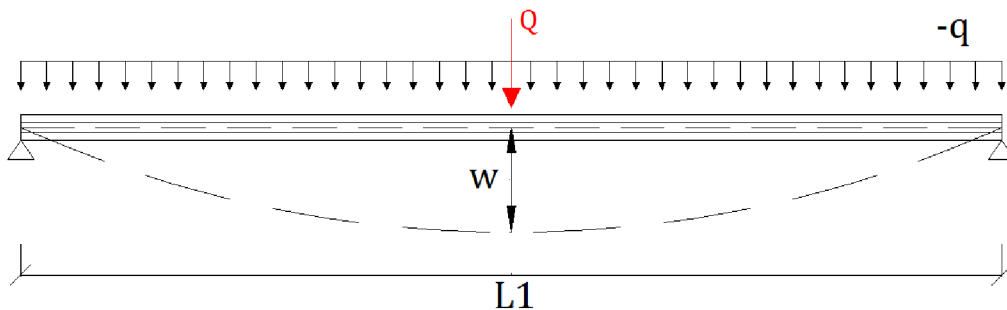
Figure 20 – Thin plate loading model

The plate was placed on the supports and gradually loaded with the force arm Q until the plate broke. The deflection of the plate was continuously recorded.

Figure 21 – Tested thin plate samples

The result of the experiment is the deflections of the plate under a certain load. The same load and geometry will be applied for the numerical model of „Special Axis and Material Symmetry" and the results will be compared.

8.5.2 Thick plate

From the point of view of mechanics, we distinguish between thin and thick plates. While thin plates can be examined without taking into account the shear stress along the thickness of the plate, in thick plates the shear stress is often the cause of plate failure. Similar to the thin plates, the experiment was approached for the purpose of verifying the numerical model. Since it is generally known and verified by research that the Kirchhoff-Love Plate Theory is not reliable when applied to thick plates and the remaining theories deviate from CPT, several plates manufactured by Stora Enso, Pfeifer and Naturfor were tested for bending to verify the numerical models. The geometry of the tested plates is given in the *Table 2*.

Table 2 – Selected CLT panel geometry

Plate	Number of layers	Layer thicknesses [mm]	Orientation of layers [°]	Material	Plate width [mm]	Plate length [mm]
NaturFor	3	30 - 30 - 30	0- 90 - 0	C24	300	1500
Stora Enso	3	30 - 30 - 30	0- 90 - 0	C24	300	1500
Pfiefer	3	30 - 30 - 30	0- 90 - 0	C24	300	1500

As is displayed in the *Figure 22* each of the plates was placed on supports and progressively loaded with the force Q until the plate broke. The deflection of the plate was continuously recorded. The plates were placed on supports 1200 mm apart and loaded with the load arm of the tearing machine.
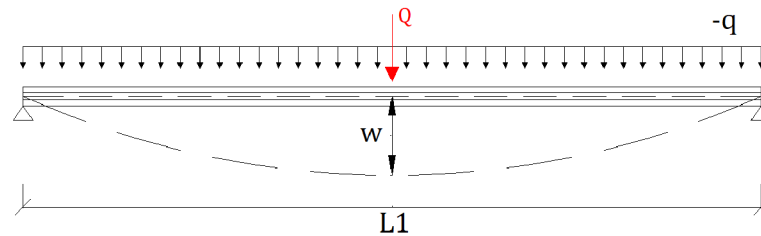
Figure 22 – Loading scheme of the thick plate

8.6 Model Verification

Verification of the numerical models was performed in two ways. The first way of verification is to compare the results of the numerical models. Since the geometry, loading and material characteristics are the same in all models and the fundamentals of the numerical models (displacement field, strains and curvatures, equilibrium equations, stress-strain relationships, governing plate equations) are different, the numerical models should agree in their results when the model is correctly built.

The second way of verification is to compare the results of deflections from numerical models and experimental measurements. Such verification will be performed only for the

full symmetry variant, i.e. the variant in which the thickness of the layers is axially symmetric and the orientation of the layers is 90°-0°-90° or 0°-90°-0°. Since all numerical models are built for generally orthotropic plates, the slightest error can result in different results by orders of magnitude.

8.6.1 Special Axis Symmetry and Material Symmetry

Special axis and material symmetry refers to the geometry and composition of the panel in which the symmetry in the orientation of the layers at angles of 0°-90°-0° and the material of the lamellas is maintained, with the plane of symmetry being the neutral and geometric centre plane of the panel. Since this is a composition that is typical of commercially produced panels, verification was performed in both ways - that is, by comparing the deflections of the thick and thin plate experiments with the numerical models and by comparing the results from the numerical models with each other.
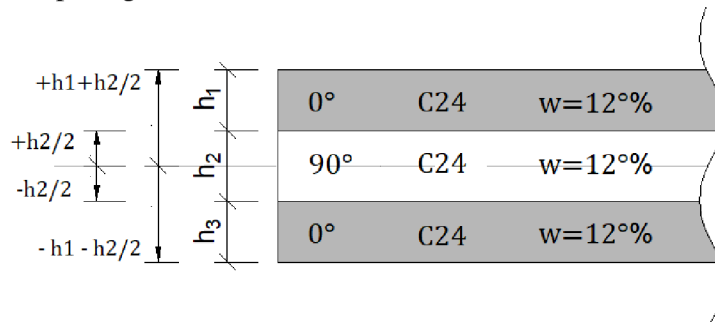
Figure 23 – Geometry of a specially axisymmetric and material-symmetric plate

8.6.2 General Axis Symmetry

Special axial and material symmetry refers to the geometry and composition of the panel in which symmetry in the orientation of the material layers is maintained, with the plane of symmetry being the neutral and geometric centre plane of the panel. The difference from special axial and material symmetry is the orientation of the individual laminae, which do not necessarily have to be oriented at 0°-90°-0°, but for example 20°-70°-20°.
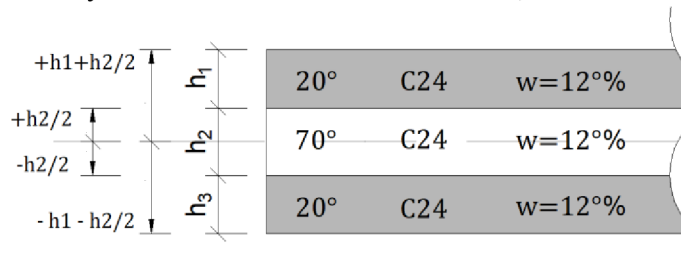
Figure 24 – Geometry of a generally axisymmetric plate

8.6.3 Axial Asymmetry

Axial asymmetry refers to the geometry and composition of the panel in which the symmetry in the orientation of the lamella material layers is not maintained. The

difference from special axial and material symmetry and general axial symmetry is the orientation of the individual lamellae, which is not geometrically symmetrical in the panel width. An example of a panel with axisymmetry can be a panel with a 0°-90°-30° fiber orientation.
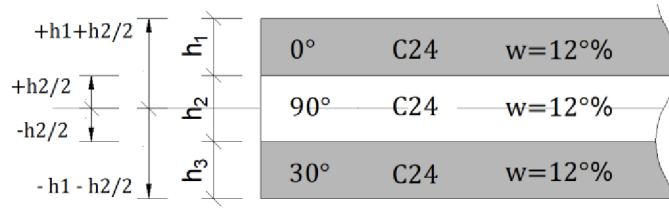
Figure 25 – Geometry of an axially non-symmetrical plate

8.6.4 Material Asymmetry

Material asymmetry refers to the geometry and composition of the panel in which the symmetry in the orientation of the layers of the lamella material is maintained, but the symmetry of the materials of which the material is composed is not maintained. An example would be a panel composed of three laminae, each of which is made of a different wood or wood strength.
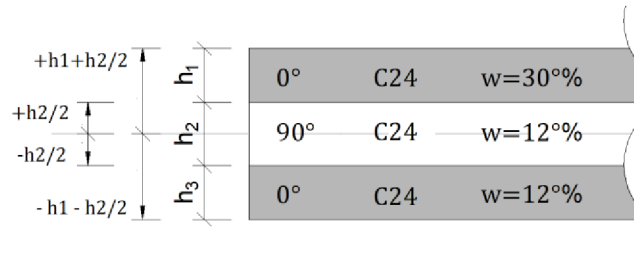
Figure 26 – Example of a materially unsymmetrical plate

9 Results and Discussion

9.1 CLT panel moisture content change

In this chapter, the results of a numerical model that investigated the CLT panel moisture content change rate are described. The solution was a numerical script constructed based on the knowledge of non-stationary diffusion.
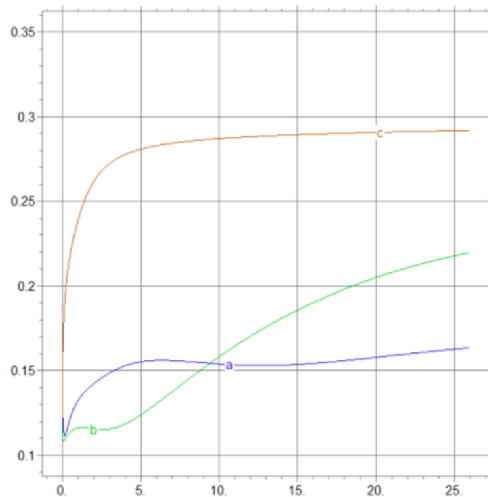
Graph 1 - Non-stationary 3D moisture diffusion over time; y-axis – moisture content (-), x-axis time (t), a – bottom plane of the plate, b – middle plane of the plate, c – top plane of the plate
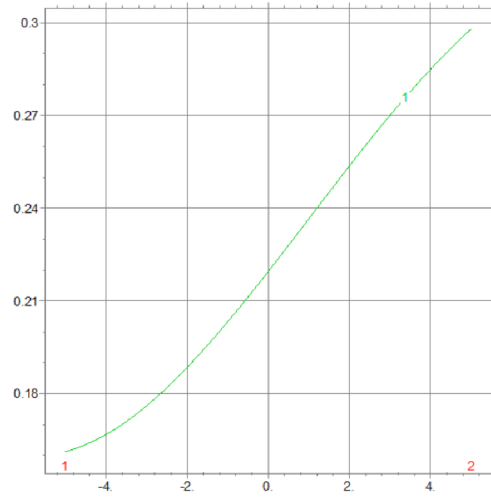
Graph 2 -Non-stacionary 3D moisture diffusion – moisture content in Z-axis (thickness of the plate), y-axis – moisture content, x-axis -thickness of the plate [m]
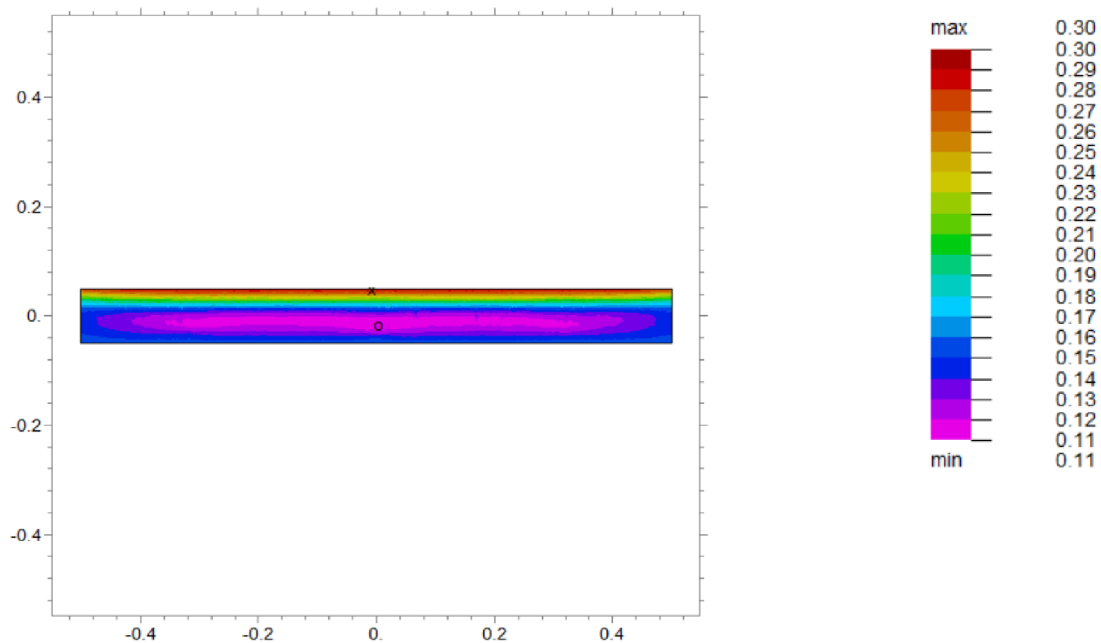
Graph 3 - Non-stacionary 3D moisture diffusion moisture distribution in the XZ plane, t = 5.18e5; x axis – length of the plate, y axis – thickness of the plate

53

Based on the findings from the *Graph 1 and Graph 3*, we can conclude that under the given boundary conditions, the top lamella of the CLT panel under consideration is soaked to the cell wall saturation limit (28% material moisture) in 143.8 hours, respectively 5.7 days. It is important to note that although this is a non-stationary diffusion model, it is only a simplified model that does not consider the presence of adhesive in CLT panels, which has different diffusion properties than wood. It can be expected that the wetting time will be longer if the glued joint is included in the calculation. The moisture gradient along the thickness of the panel would not be linear as in *Graph 2*, but the moisture profile would show large differences in moisture content at the glued joint. An example of such a moisture gradient can be seen in the *Graph 4*, which represents the moisture profile of a three-layer CLT panel with 0.1 mm glued joints. From this graph, presented by Gereke (2009), it is clear that there is a jump in moisture content at the glued joint. The question remains as to what effect the glued joint has on the wetting rate of a unilaterally moisture loaded panel. The answer to this question could be the non-stationary diffusion model involving the glued joint presented in "Combined loading of laminated structural elements" by Valášek (2021).
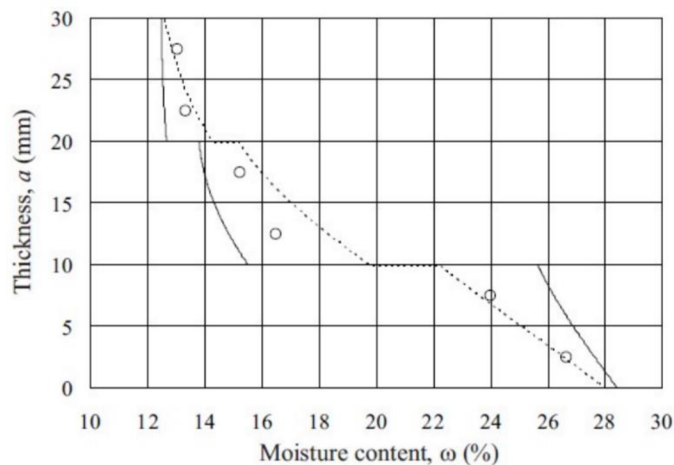
Graph 4 - Moisture profiles along the thickness of a CLT panel involving a glued joint with constant glue diffusion coefficients compared to measurements; 14 days (Gereke, 2009)

The numerical model is not a unified solution, and the result is influenced by a number of factors. These factors include the thickness of the layers of the CLT panel, the thickness of the adhesive, the type of adhesive, the wood species used to produce the CLT panel, the diffusion properties of the adhesive, the method used to calculate the moisture distribution, the effect of stationary or non-stationary conditions, or the chosen neglect of the effect of temperature on the rate of wetting. The calculation itself was undertaken to test the hypothesis that exposure of the ceiling panel to rainwater may lead to significant degradation of the material properties of the CLT panel surface. If the construction of a timber building using CLT ceiling panels is properly designed and constructed, such extreme moisture loading cannot occur during the use of the building. However, what is often not included in the calculations and considerations is the construction phase of the

rough construction, during which entire floors may become covered with rainwater or snow (as can be seen on *Figure 27*).

Figure 27 - CLT panel ceiling exposed to pooled water (Olsson, 2020)

Such moisture loads are examined from the perspective of protection against mold and wood-boring fungi and are not considered from the perspective of reduction or change in mechanical properties (Öberg, 2018). The software (AxisVM, Abaqus, Dlubal, Ansys) used for the design of structures or joints does not allow the inclusion of moisture deformations in the calculation (AxisVM support [online]; Abaqus Analysis [online]; Dlubal manual [online]; Ansys workbench [online]). In the design of timber-based structures, the exposure of timber to moisture is only possible through the k_{def} coefficient defined by the service class, which is determined during design for the service stage of the structure, not for the design stage (Koželouh, 1998; Eurocode 5, 1994).

9.2 Verification 1 – thin plate

9.2.1 Experiment 1

This chapter describes the results of individual measurements and their subsequent comparison with numerical models. Specific values of the deflection of the plates are described. The results are valid for a plate with a temperature of 20°C and a relative humidity of 12%. The results are described and illustrated in graphs and tables.
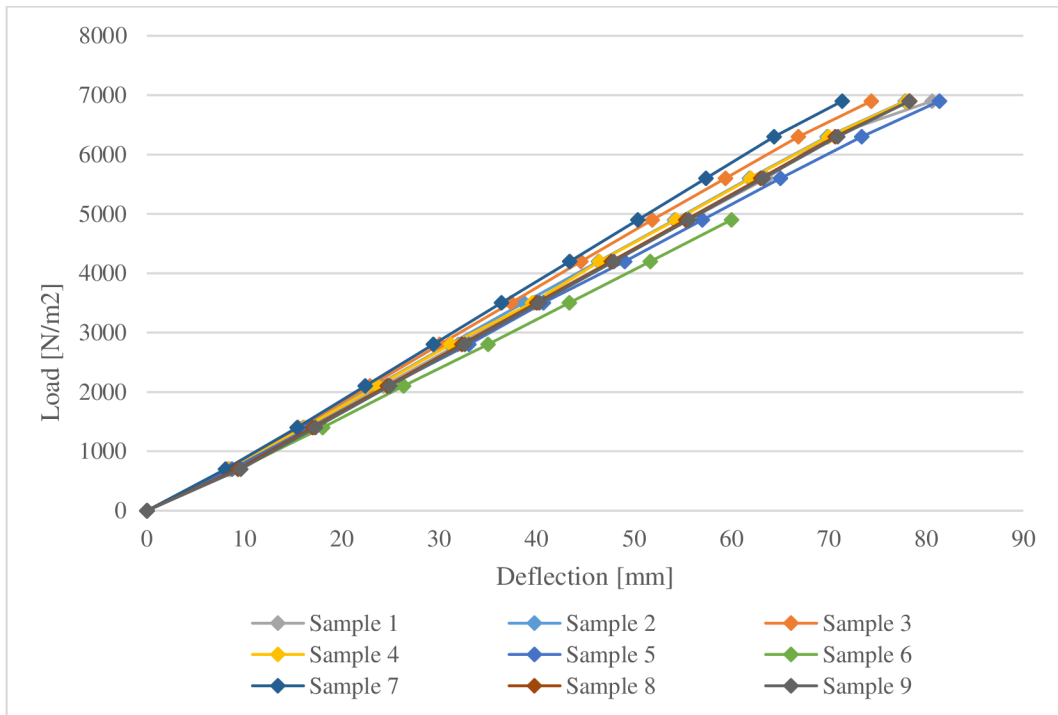
Graph 5 – Results of experimental measurement of deflection of thin plates

In the Graph 5 it can be seen the deflections of individual plate samples depending on the applied surface load [N/m^2]. It can be seen from the graph that at the highest load observed, i.e., at 6900 N/m^2, the deflection ranged from 71.4 to 81.4 mm. The largest deflection at the highest observed load occurred in sample 5. The smallest deflection was observed in sample 7.

Table 3 – Results of experimental measurement of deflection of a thin plate

Load [N/m2]	Deformation [mm]									Arithmetic mean
	Sample 1	Sample 2	Sample 3	Sample 4	Sample 5	Sample 6	Sample 7	Sample 8	Sample 9	
700	8.62	8.37	8.23	8.49	8.73	9.36	8.06	9.34	9.62	8.76
1400	16.46	16.04	15.56	16.18	16.73	18.03	15.4	17.01	17.28	16.52
2100	24.29	23.54	22.9	23.65	24.73	26.36	22.4	24.68	24.95	24.17
2800	31.96	31.04	30.06	31.2	33.06	35.03	29.4	32.34	32.62	31.86
3500	39.79	38.7	37.4	39.6	40.73	43.36	36.4	40.01	40.28	39.59
4200	47.62	46.37	44.56	46.48	49.06	51.7	43.4	47.68	47.95	47.20
4900	55.62	54.2	51.9	54.33	57.06	60.03	50.4	55.34	55.62	54.94
5600	63.62	61.87	59.4	62.02	65.06	-	57.4	63.01	63.28	61.96
6300	69.98	69.87	66.9	69.98	73.4	-	64.4	70.68	70.95	69.52
6900	80.62	77.87	74.4	77.97	81.4	-	71.4	78.34	78.28	77.54

Table 3 shows the results of the experimental measurements together with the arithmetic mean used in the subsequent comparison of the values from the numerical calculations.

9.2.2 Numerical models

This chapter describes the results resulting from the numerical scripts. The boundary conditions and loads that were entered into the scripts were based on the conditions of Experiment 1. The deflection was calculated for loads from 0 to 6900 N/m^2.

Table 4 – Results of deflection of thin plates from numerical models

Load [N/m2]	Deformation [mm]				Standard deviation
	CPT	FOSDT	SOSDT	TOSDT	
700	8.71	8.39	8.42	8.45	0.13
1400	16.91	16.84	16.87	16.9	0.03
2100	24.36	24.07	24.1	24.13	0.11
2800	32.01	31.78	31.81	31.84	0.09
3500	39.84	39.47	39.5	39.53	0.15
4200	47.34	47.13	47.16	47.19	0.08
4900	55.24	54.82	54.85	54.88	0.17
5600	62.36	61.8	61.83	61.86	0.23
6300	69.77	69.4	69.43	69.46	0.15
6900	77.78	77.39	77.42	77.55	0.15

In the Table 4 we can see that the results of the numerical theories are similar. FOST, SODT and TODT differ in their deflection results in hundredths of millimeters, while CPT differs in tenths of millimeters. Due to the low standard deviation, the results can be considered relevant. The smallest deflection at the maximum considered load of 6900 N/m^2 resulted from FODT. The highest deformation at the maximum considered load resulted from CPT.

9.2.3 Comparison of verification results 1

In this chapter, a comparison between experimental measurements and numerical model results is presented.

Table 5 – Comparison of verification results 1

Load [N/m2]	Deformation [mm]					Standard deviation
	Experiment 1 – average value	CPT	FODT	SODT	TODT	
700	8.76	8.71	8.39	8.42	8.45	0.16
1400	16.52	16.91	16.84	16.87	16.9	0.15
2100	24.17	24.36	24.07	24.1	24.13	0.10
2800	31.86	32.01	31.78	31.81	31.84	0.08
3500	39.59	39.84	39.47	39.5	39.53	0.13
4200	47.20	47.34	47.13	47.16	47.19	0.07
4900	54.94	55.24	54.82	54.85	54.88	0.15
5600	61.96	62.36	61.8	61.83	61.86	0.21
6300	69.52	69.77	69.4	69.43	69.46	0.13
6900	77.54	77.78	77.39	77.42	77.55	0.14

The *Table 5* shows the comparison of the results of verification 1, i.e. the comparison of the deflection of the plate loaded experimentally measured and numerically calculated. The differences between the numerical theories and the experimental measurements are in the order of tenths of millimeters to hundredths of millimeters. The standard deviation is in the interval from 0.07 to 0.21. Because the standard deviation is so low, we can consider the results relevant.

Referring to results of experimental measurement 1 (measuring the deflection of the thin plate) from *Graph 5* and *Table 3*, it can be said that the mechanical response of all 9 plates showed the same deflection values. It should be stated that since the numerical models derived were only linear Hooke's law based, only the elastic behavior of the plates was investigated and therefore the failure is not included in the working graphs from the experimental measurements. Based on the results of the numerical models in *Table 4*, it can be concluded that all numerical models agree in the deflection results. Based on the findings from *Table 5*, it can be concluded that the deflection observed in the experimental measurements and the deflection given by the numerical theories are in agreement and it can be concluded that the numerical theories were correctly derived for the bending of the thin plates.

9.3 Verification 2 – thick plate

9.3.1 Experiment 2

This chapter describes the results of individual measurements and their subsequent comparison with numerical models. Specific values of the deflection of the plates are described. The results are valid for a plate with a temperature of 20°C and a relative moisture content of 12%. The results are described and illustrated in graphs and tables.
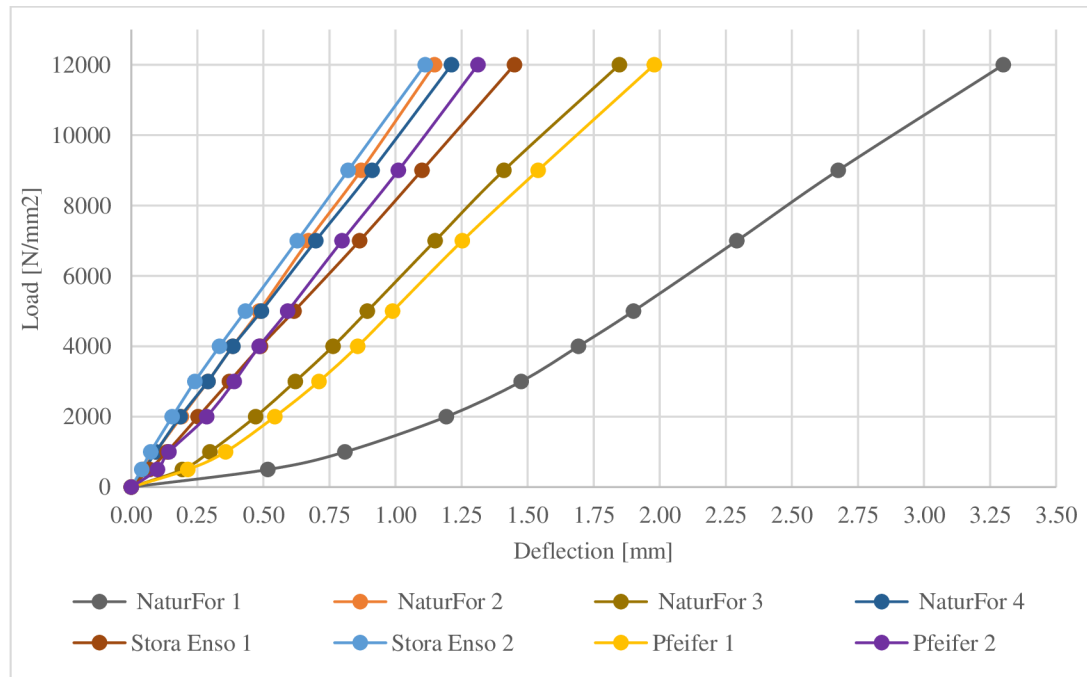
Graph 6 - Results of experimental measurement of deflection of thick plates

In the Graph 6 it can be seen the deflections of the individual plate samples depending on the applied surface load [N/m^2]. The graph shows that at the highest observed load, i.e. 12000 N/m^2, the deflection ranged from 0.039 to 3.3 mm. The largest deflection at the highest observed load was for NaturFor 1 and the smallest for Stora Enso 2.

Table 6 - Results of experimental measurement of deflection of a thick plate

Load [N/m2]	Deformation [mm]								Arithmetic mean	Standard deviation	Selective standard deviation
	NaturFor 1	NaturFor 2	NaturFor 3	NaturFor 4	Stora Enso 1	Stora Enso 2	Pfeifer 1	Pfeifer 2			
500	0.517	0.044	0.194	0.049	0.069	0.039	0.214	0.099	0.153	0.152	0.061
1000	0.809	0.092	0.297	0.093	0.135	0.073	0.357	0.143	0.250	0.232	0.096
2000	1.192	0.190	0.470	0.185	0.253	0.155	0.543	0.285	0.409	0.323	0.130
3000	1.475	0.290	0.620	0.290	0.371	0.240	0.710	0.390	0.548	0.383	0.155
4000	1.692	0.384	0.764	0.384	0.489	0.334	0.856	0.484	0.673	0.423	0.174
5000	1.900	0.484	0.894	0.492	0.616	0.432	0.989	0.592	0.800	0.456	0.185
7000	2.292	0.670	1.150	0.698	0.864	0.628	1.253	0.798	1.044	0.517	0.210
9000	2.675	0.870	1.410	0.911	1.100	0.821	1.539	1.011	1.292	0.576	0.241
12000	3.300	1.147	1.847	1.212	1.450	1.112	1.979	1.312	1.670	0.685	0.295

The Table 6 shows the results of the experimental measurements together with the arithmetic mean, which is used in the subsequent comparison of the values from the numerical calculations. The overall standard deviation takes values up to 1.67. This is mainly due to the NaturFor 1 and NaturFor 4 samples, where partial delamination of the panel layers occurred. This had a significant effect on the final deflection at the observed maximum load. When these specimens are declared unsuitable and excluded from the statistics, the sample standard deviation values are such that the results can be declared relevant. Samples NaturFor 1 and NaturFor 4 are shown on Figure 28.

Sample NaturFor 1	*Sample NaturFor 4*
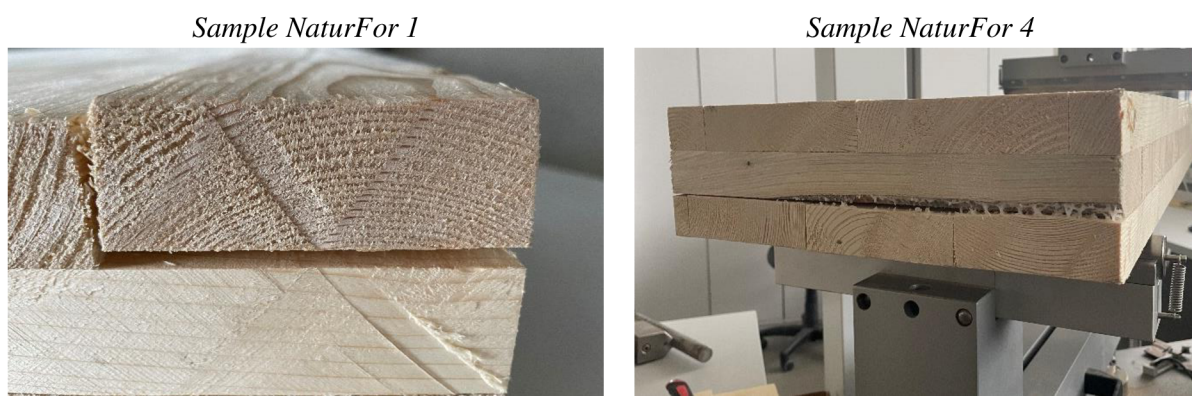
Figure 28 – Samples NaturFor 1 and NaturFor 4 excluded from statistics

9.3.2 Numerical models

This chapter describes the results resulting from the numerical scripts. The boundary conditions and loads that were entered into the scripts were based on the conditions of Experiment 2. Deflection was calculated for loads from 0 to 12000 N/m^2.

Table 7 - Deflection results of thick plates from numerical models

Load [N/m2]	Deformation [mm]				Standard deviation
	CPT	FOSDT	SOSDT	TOSDT	
500	0.0879	0.092	0.092	0.092	0.002
1000	0.138	0.146	0.145	0.146	0.003
2000	0.241	0.253	0.251	0.253	0.005
3000	0.335	0.360	0.337	0.360	0.012
4000	0.444	0.467	0.435	0.467	0.014
5000	0.546	0.574	0.531	0.574	0.019
7000	0.752	0.788	0.743	0.788	0.020
9000	0.96	1.050	0.950	1.050	0.048
12000	1.26	1.320	1.270	1.320	0.028

In the *Table 7* the results of the numerical theories are very similar. The results of FOSDT, SOSDT and TOSDT are almost identical throughout the measurement period. The CPT results start to move away from the other models as the load increases. Due to the low standard deviation, the results can be considered relevant. The smallest deformation at the maximum considered load of 12000 N/m^2 resulted from CPT. The highest deformation at the maximum considered load resulted identically from FOSDT and TOSDT.

9.3.3 Comparison of verification results 2

In this chapter a comparison between experimental measurements, results of selected finite element methods software and results of numerical models is presented.

Table 8 - Comparison of verification results 2

Load [N/m2]	Deformation [mm]							Standard deviation
	Experiment 2 - Average value	CPT	FOSDT	SOSDT	TOSDT	AxisVM	Abaqus	
500	0.086	0.0879	0.092	0.092	0.092	0.059	0.054	0.015
1000	0.149	0.138	0.146	0.145	0.146	0.115	0.107	0.016
2000	0.269	0.241	0.253	0.251	0.253	0.233	0.213	0.016
3000	0.382	0.335	0.360	0.337	0.360	0.351	0.320	0.019
4000	0.488	0.444	0.467	0.435	0.467	0.469	0.426	0.020
5000	0.601	0.546	0.574	0.531	0.574	0.586	0.539	0.024
7000	0.819	0.752	0.788	0.743	0.788	0.824	0.753	0.030
9000	1.042	0.96	1.050	0.950	1.050	1.050	0.959	0.045
12000	1.369	1.26	1.320	1.270	1.320	1.390	1.279	0.046

The Table 8 shows the comparison of the results of verification 2, i.e. the comparison of the deflection of the plate loaded in area, which was experimentally measured, solved in finite element software and numerically calculated by the derived models. The differences between numerical theories, experimental measurements and FEM software are in the

order of tenths of millimeters to hundredths of millimeters. The standard deviation is in the interval from 0.015 to 0.046.

The experimental measurement of the mechanical response of the thick plate in the form of deflection was observed only in the elastic behavior region for the same reason as the experimental measurement of the thin plate. Based on the findings from *Table 6* and *Graph 6*, it can be said that NaturFor 1 and NaturFor 3 a samples achieved significantly higher deflection than other samples at the same stress. This significant difference in deflection was most likely due to the slight delamination of these samples before the experiment was conducted, which was caused by the improper storage of these samples. The delamination of these samples is shown in *Figure 28,* and it can be stated that even a small amount of delamination has a significant effect on the mechanical behavior of the CLT panels. These samples were considered as defective and excluded from the subsequent statistics. Based on Table 7, it can be concluded that the agreement between the results of the numerical theories was significantly higher than that of the thin plate results, as evidenced by the standard deviations, which reach a maximum value of 0.048 for the thick plate. For the thick plate verification case, in addition to the experiment, modelling was proceeded with the FEM software AxisVM and Abaqus while the results from these software served as further comparison of the results of the numerical scripts. Based on the results from *Table 8*, it can be concluded that the numerical theories were derived correctly for the thick plate model case.

9.4   Results of numerical models

Depending on the composition of the laminate, there are several types of symmetry and non-symmetry - material and axial. Material symmetry refers to a laminate that is geometrically symmetrical with respect to the materials used in the individual layers. Axial symmetry refers to laminates that are symmetrical with respect to the orientation of the fibers in the individual plies. A special case may be so-called special orthotropy, by which we mean laminates in which the plies are oriented at 90° and 0° angles. In this chapter, the stress results of the numerical theories are compared with respect to the symmetric or unsymmetric plate under investigation.

The following notations is used in the following chapters:

- CPT – Classical plate theory (Kirchhoff-Love Plate Theory),
- FOSDT – First Order Shear Deformation Theory (Mindlin-Reissner Shear Deformation Theory),
- SOSDT – Second Order Shear Deformation Theory,
- TOSDT – Third Order Shear Deformation Theory.

The notation "*S1 CPT L1/2, L2/2*" in graphs indicates the Classical Plate Theory stress σ_1 observed in a section through half the length and half the width of the plate.

9.4.1 Special Axis Symmetry and Material Symmetry (SASMS)

This chapter describes the results of the numerical models in the form of stress distributions and their comparison between the different numerical theories. The geometry and material properties used in the model are derived from the plate geometry used in Experiment 2.
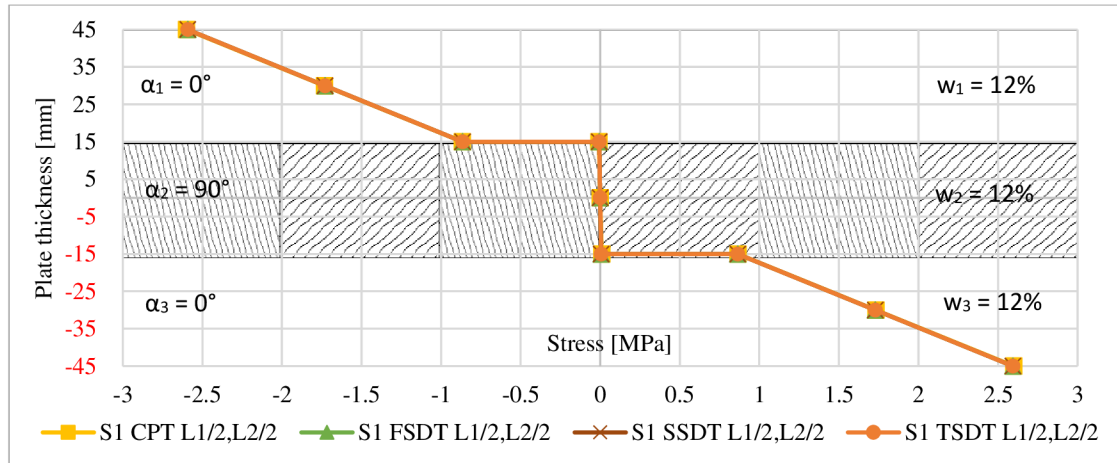
Graph 7 – (SASMS) σ_1 across the thickness of the plate

Table 9 – (SASMS) σ_1 stress comparison

S1 [MPa]	Layer 1			Layer 2			Layer 3		
	TOP	MID	BOT	TOP	MID	BOT	TOP	MID	BOT
CPT	-2,6	-1,734	-0.867	-0.009	0	0.009	0.867	1.734	2.600
FSDT	-2.593	-1.729	-0.864	-0.006	0	0.006	0.864	1.729	2.593
SSDT	-2.593	-1.729	-0.864	-0.006	0	0.006	0.864	1.729	2.593
TSDT	-2.593	-1.729	-0.864	-0.006	0	0.006	0.864	1.729	2.593

Considering the findings from the *Graph 7* and *Table 9*, it can be stated that all four numerical models agree in their results for the specially axially and materially symmetric plates for σ_1 stresses (stresses in the fiber direction). The progression of the σ_1 stress through the thickness of the plate represents a result that corresponds in form to the stress in its shape - that is, the pressure in the upper part of the laminate that is generated by the compression of the fibers, and the stress in the bottom layer of the laminate represents the tension that corresponds to the bending of the fibers. The stresses in the transversely oriented middle layer are minimal or non-existent because there is no stress in the direction of the fibers in this layer. Considering the form of the stress distribution σ_1, it can be concluded that the result corresponds to a specially orthotropic plate.
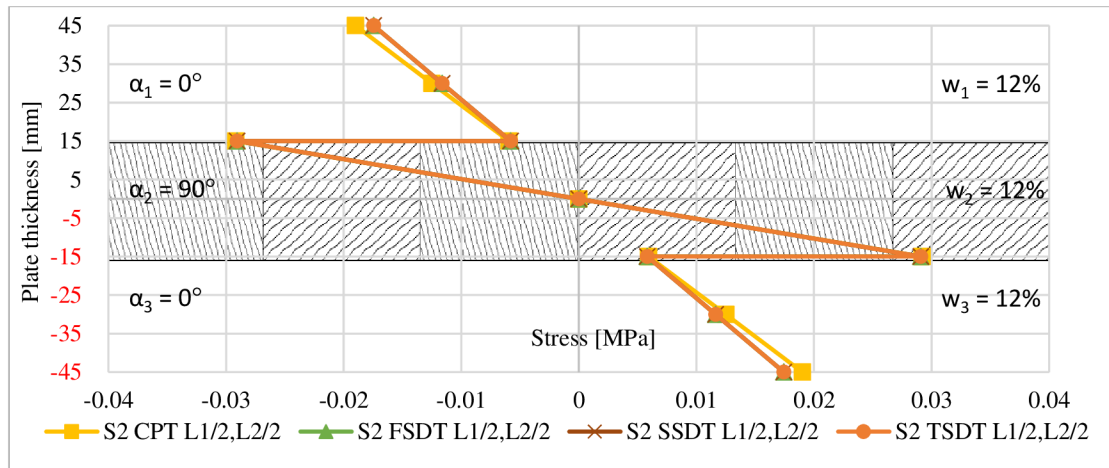
Graph 8 - (SASMS) σ_2 stresses across the fibers across the thickness of the plate

Table 10 - (SASMS) σ_2 stress comparison

S2 [MPa]	Layer 1			Layer 2			Layer 3		
	TOP	MID	BOT	TOP	MID	BOT	TOP	MID	BOT
CPT	-0.019	-0.013	-0.006	-0.029	0	0.029	0.006	0.013	0.019
FSDT	-0.017	-0.012	-0.006	-0.029	0	0.029	0.006	0.012	0.017
SSDT	-0.017	-0.012	-0.006	-0.029	0	0.029	0.006	0.012	0.017
TSDT	-0.017	-0.012	-0.006	-0.029	0	0.029	0.006	0.012	0.017

Considering the results shown in the Graph 8 and *Table 10*, it can be concluded that all four numerical models are consistent with the results for the special axially symmetric and material symmetric plates for σ_2 stresses (stresses across the fibers), only the classical plate theory shows a slight deviation from the other theories. This deviation is probably due to the computational complexity of the numerical model of Kirchhoff's plate theory, which, in its modification for the analysis of generally orthotropic plates, contains fourth-order partial derivatives that must be solved in the software FlexPDE by using a substitution that generates additional variables to allow this substitution. The inaccuracy of the calculation is well observed in the progression of the stresses σ_1 and σ_2 along the length of the plate, which is shown in the *Graph 9* and *Graph 10*. The Kirchhoff-Love plate theory derived only for specially orthotropic plates does not exhibit these deviations (Valášek, 2021), and therefore it can be concluded that Kirchhoff-Love plate theory is not suitable for solving general geometric and boundary conditions, and for each specific problem it is more appropriate to derive this theory or to choose software that provides solutions of partial derivatives of higher than third order. The progression of σ_2 stresses through the thickness of the plate presents a result that is consistent in form with these stresses - i.e., minimal or no stresses are generated in the top layer of the laminate due to the fact that this layer is not subjected to loads applied across the fibers. The increase in stress is observed in the middle layer, which is oriented at 90° to the longitudinal axis of the plate and is therefore subject to stresses across the fibers.
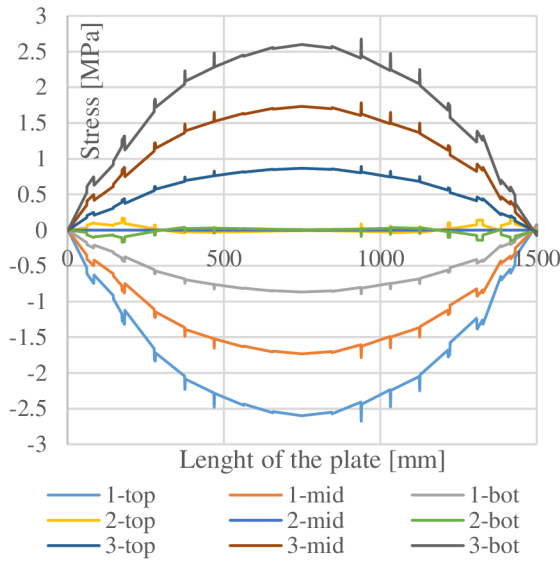
Graph 9 - (SASMS) stress distribution σ_1 along the length of the plate according to CPT
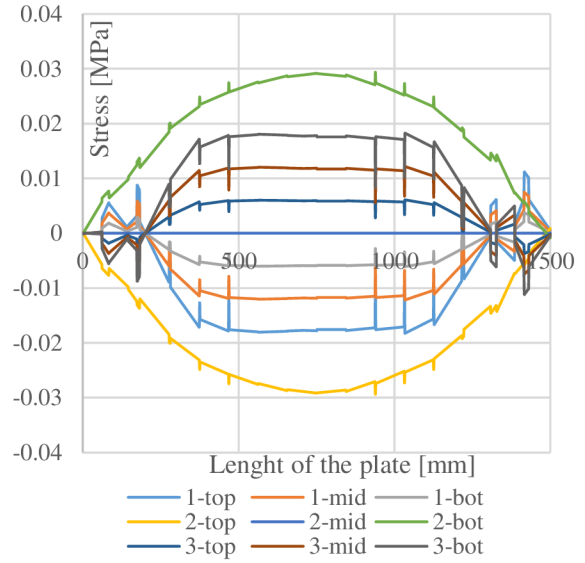
Graph 10 - (SASMS) stress distribution σ_2 along the length of the plate according to CPT
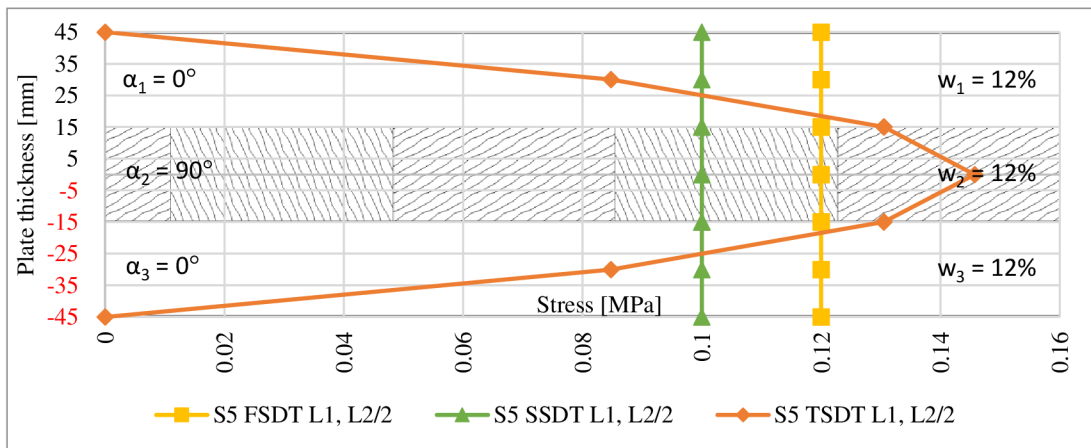
Graph 11 - (SASMS) σ_5 stresses by plate thickness

Table 11 - (SASMS) stress σ_5 comparison

S5	Layer 1			Layer 2			Layer 3		
[MPa]	TOP	MID	BOT	TOP	MID	BOT	TOP	MID	BOT
CPT	-	-	-	-	-	-	-	-	-
FSDT	-0.12	-0.12	-0.12	-0.12	-0.12	-0.12	-0.12	-0.12	-0.12
SSDT	-0.13	-0.13	-0.13	-0.13	-0.13	-0.13	-0.13	-0.13	-0.13
TSDT	0	-0.085	-0.130	-0.130	-0.146	-0.130	-0.130	-0.085	0

Based on the *Graph 11* and the *Table 11*, it can be said that in the case of σ_5 stresses, i.e. shear stress xz, the first difference in the results of the stress progression through the thickness of the plate can be seen, even though these stresses are very small. FSDT and TSDT agree in the maximum of the σ_5 stress. SSDT deviates slightly from the maximum in its value. It can also be seen that the FSDT and SSDT only give maximum stress values. TSDT is a more advanced theory in this aspect and can plot the stress distribution from 0

to maximum. The TSDT stress distribution is an example of a bending shear stress distribution that is zero at the material surface and maximum in the geometric and neutral planes. Kirchhoff's plate theory does not allow the calculation of the shear stress and is therefore not shown in the *Table 11*.

9.4.2   General Axis Symmetry (GAS)

This chapter describes the results of the numerical models in the form of stress distributions and their comparison between the different numerical theories. The geometry and material properties used in the model are described in the methodology.
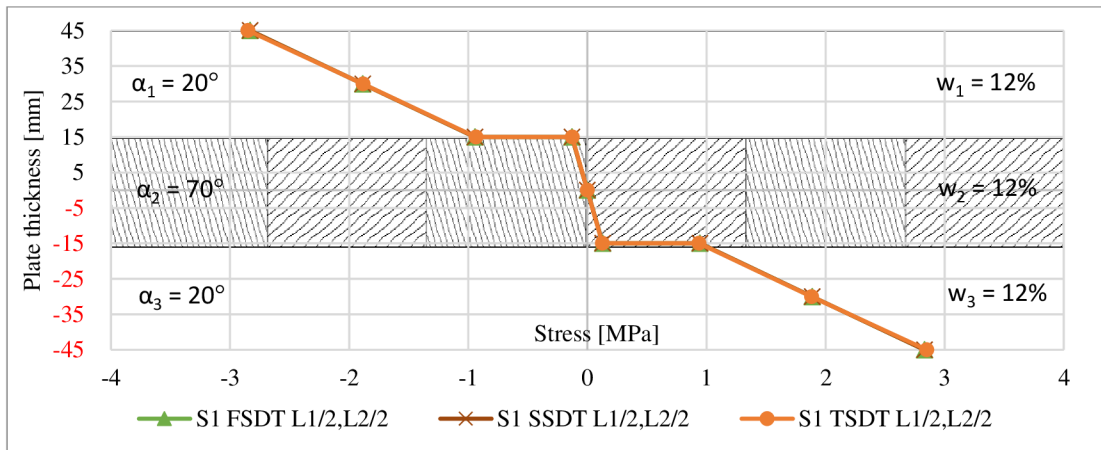
Graph 12 - (GAS) σ_1 across the thickness of the plate

Table 12 - (GAS) stress σ_1 Comparison

S1 [MPa]	Layer 1			Layer 2			Layer 3		
	TOP	MID	BOT	TOP	MID	BOT	TOP	MID	BOT
CPT	-	-	-	-	-	-	-	-	-
FSDT	-2.83	-1.89	-0.94	-0.13	0	0.13	0.94	1.89	2.83
SSDT	-2.83	-1.89	-0.94	-0.13	0	0.13	0.94	1.89	2.83
TSDT	-2.85	-1.88	-0.94	-0.13	0	0.13	0.94	1.88	2.85

Based on the findings from the *Graph 12* and *Table 12* it can be concluded that all four numerical models agree in their results for σ_1 stresses (stresses in the fiber direction). The progression of the σ_1 stress through the thickness of the plate represents the result that corresponds to the stress in its form - that is, the pressure in the top of the laminate resulting from the compression of the fibers. The stress in the bottom layer of the laminate is tension, which corresponds to the fibers being pulled as laminate bend. The difference from the previous case of symmetry can be seen in the stress in the middle layer of the laminate, which higher values by an order of magnitude. This stress is due to the orientation of the layer itself, which is oriented at 70°, not 90°.
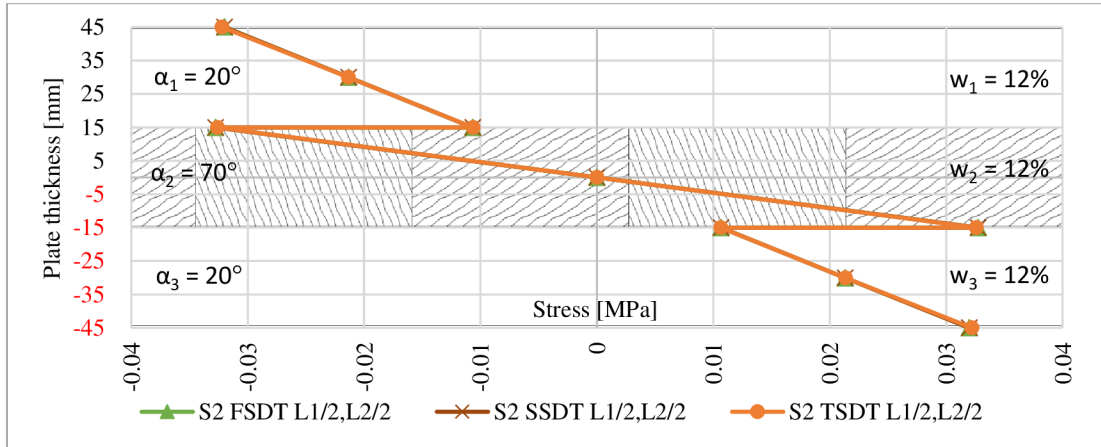
Graph 13 - (GAS) σ_2 Stresses Across Plate Thickness

Table 13 - (GAS) Stress σ_2 comparison

S2	Layer 1			Layer 2			Layer 3		
[MPa]	TOP	MID	BOT	TOP	MID	BOT	TOP	MID	BOT
CPT	-	-	-	-	-	-	-	-	-
FSDT	-0.032	-0.021	-0.011	-0.033	0	0.033	0.011	0.021	0.032
SSDT	-0.032	-0.021	-0.011	-0.033	0	0.033	0.011	0.021	0.032
TSDT	-0.032	-0.021	-0.011	-0.033	0	0.033	0.011	0.021	0.032

Based on the findings from the *Graph 13* and *Table 13* it can be concluded that all four numerical models match the results for σ_2 stresses (stresses across fibers). The stress maximums in all layers reach similar values due to their orientation, which is close to a 45° deviation from the 0°-90°-0° laminate orientation, specifically in this case a 20° deviation of the fibers in each layer. The internal forces are therefore distributed both in the direction of the fibers and across the fibers. The maximum compressive stress is observed at the top surface of layer 1 and the top surface of layer 2. The maximum tensile stress is then observed on the bottom surface of layer 2 and the bottom surface of layer 3.
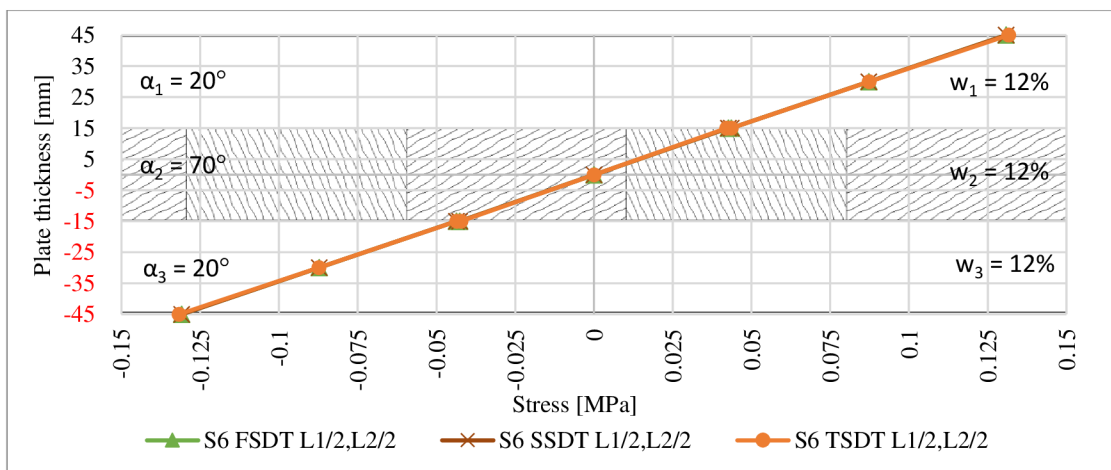
Graph 14 - (GAS) σ_6 stresses by plate thickness

Table 14 - (GAS) Stress σ_6 Comparison

S6	Layer 1			Layer 2			Layer 3		
[MPa]	TOP	MID	BOT	TOP	MID	BOT	TOP	MID	BOT
CPT	-	-	-	-	-	-	-	-	-
FSDT	0.131	0.087	0.044	0.043	0	-0.043	-0.044	-0.087	-0.131
SSDT	0.131	0.087	0.044	0.043	0	-0.043	-0.044	-0.087	-0.131
TSDT	0.132	0.087	0.044	0.042	0	-0.042	-0.044	-0.087	-0.132

Based on the findings from the *Graph 14* and *Table 14* it can be concluded that because the geometry and composition of the laminate is different from the special axis and material symmetry, shear stresses that result from layer orientations other than 0°-90°-0° can be expected. The σ_6 stress, respectively the stress in the XY plane of the plate, is observed to be maximum at the surface of the plate and decreasing linearly towards the neutral plane of the plate to the bottom surface of the plate where it takes a second maximum. The numerical theories agree almost identically in their results, except for the TSDT, which deviates in the thousands of the value of the stress in MPa.
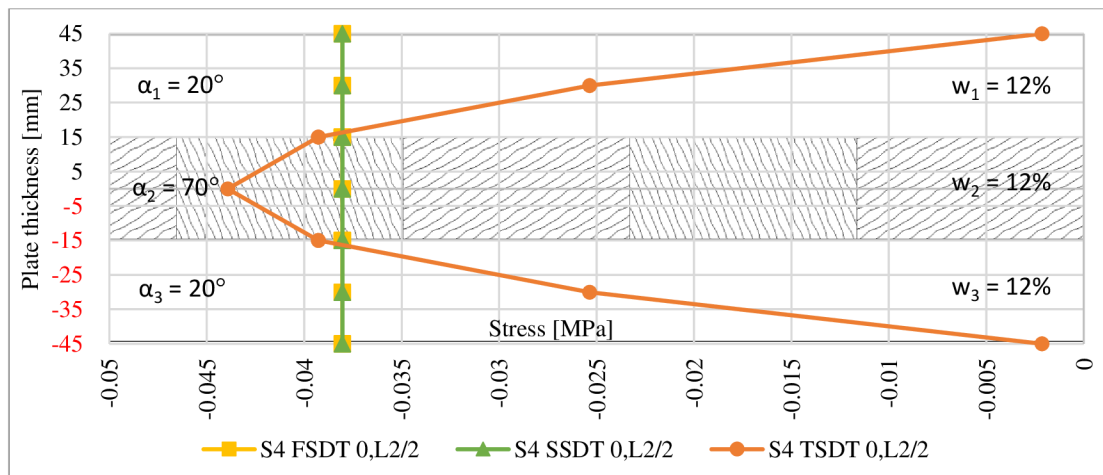
Graph 15 - (GAS) σ_4 stresses by plate thickness

Table 15 - (GAS) Stress σ_4 Comparison

S4	Layer 1			Layer 2			Layer 3		
[MPa]	TOP	MID	BOT	TOP	MID	BOT	TOP	MID	BOT
CPT	-	-	-	-	-	-	-	-	-
FSDT	-0.038	-0.038	-0.038	-0.038	-0.038	-0.038	-0.038	-0.038	-0.038
SSDT	-0.038	-0.038	-0.038	-0.038	-0.038	-0.038	-0.038	-0.038	-0.038
TSDT	-0.002	-0.025	-0.039	-0.039	-0.044	-0.039	-0.039	-0.025	-0.002

Based on the findings from the *Graph 15* and *Table 15* it can be concluded that in contrast to the previous type of symmetry, in this case it is possible to investigate the σ_4 stress, i.e., the YZ shear stress. This stress, like σ_6, is due to the different orientation of the fibers in the individual layers. In this case of general symmetry, FSDT and SSDT correspond and express only the maximum value of the stress. The TSDT is expressed by a parabolic

68

progression of stresses from zero values to the maximum. At the maximum, TSDT differs from the other theories.
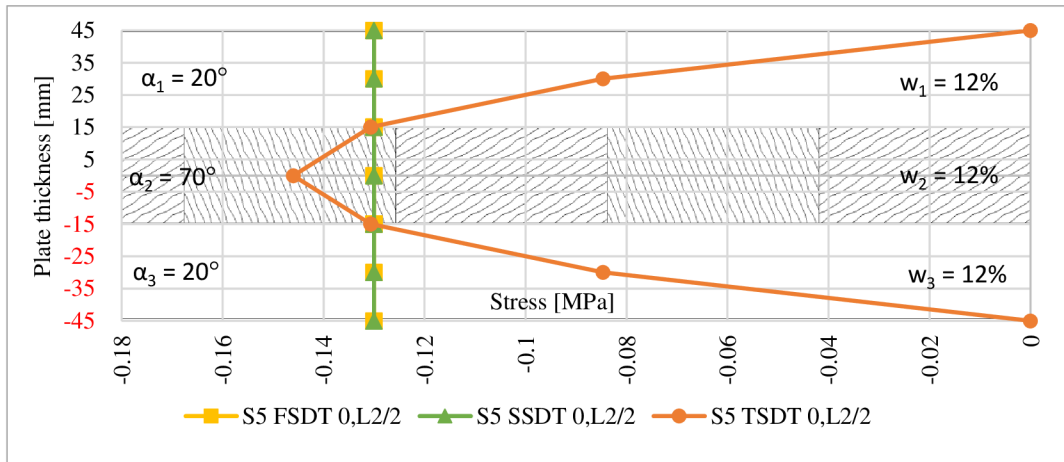
Graph 16 - (GAS) σ_5 stresses by plate thickness

Table 16 – (GAS) Stress σ_5 Comparison

S5	Layer 1			Layer 2			Layer 3		
[MPa]	TOP	MID	BOT	TOP	MID	BOT	TOP	MID	BOT
CPT	-	-	-	-	-	-	-	-	-
FSDT	-0.13	-0.13	-0.13	-0.13	-0.13	-0.13	-0.13	-0.13	-0.13
SSDT	-0.13	-0.13	-0.13	-0.13	-0.13	-0.13	-0.13	-0.13	-0.13
TSDT	0	-0.085	-0.131	-0.131	-0.146	-0.131	-0.131	-0.085	0

Based on the findings from the *Table 16* and *Graph 16* it can be concluded that in the case of the σ_5 stress, i.e. the shear stress xz, the difference in the results of the stress progression through the plate thickness is visible, even though these stresses are small. FSDT and SSDT agree in the maximum of the σ_5 stresses. It can also be seen that FSDT and SSDT only give maximum stress values. TSDT is the more advanced theory in this regard and is able to plot the stress progression from zero to maximum. The TSDT stress progression is an example of a bending shear stress progression which is zero at the surface of the material and maximum in the geometric and neutral planes.

9.4.3 Axis Asymmetry (AA)

This chapter describes the results of the numerical models in the form of stress distributions and their comparison between the different numerical theories. The geometry and material properties used in the model are described in the methodology.
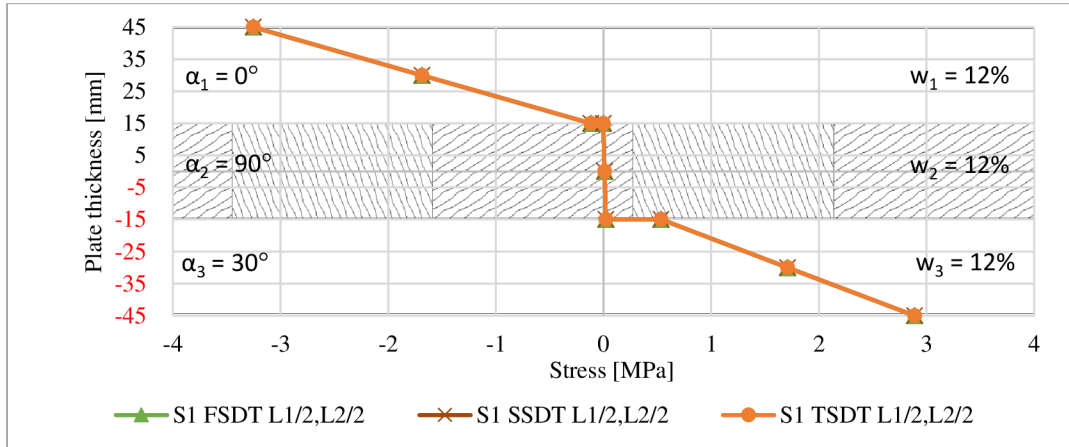
Graph 17 – (AA) σ_1 stresses by plate thickness

Table 17 - (AA) Stress σ_1 Comparison

S1	Layer 1			Layer 2			Layer 3		
[MPa]	TOP	MID	BOT	TOP	MID	BOT	TOP	MID	BOT
CPT	-	-	-	-	-	-	-	-	-
FSDT	-3.25	-1.69	-0.12	0.00	0.01	0.02	0.53	1.71	2.89
SSDT	-3.25	-1.69	-0.12	0.00	0.01	0.02	0.53	1.71	2.89
TSDT	-3.25	-1.69	-0.12	0.00	0.01	0.02	0.53	1.71	2.89

Based on the findings from the *Graph 17* and *Table 17* it can be concluded that the σ_1 stress (stress along the fibers) in the case of axial non-symmetry reaches corresponding values along the thickness of the plate. The highest tensile stress is present at the bottom of layer 3 where the fibers are pulled. The highest compressive stress is present on the upper surface of layer 1 where the fibers are compressed. The individual numerical models agree in their results to within hundredths.
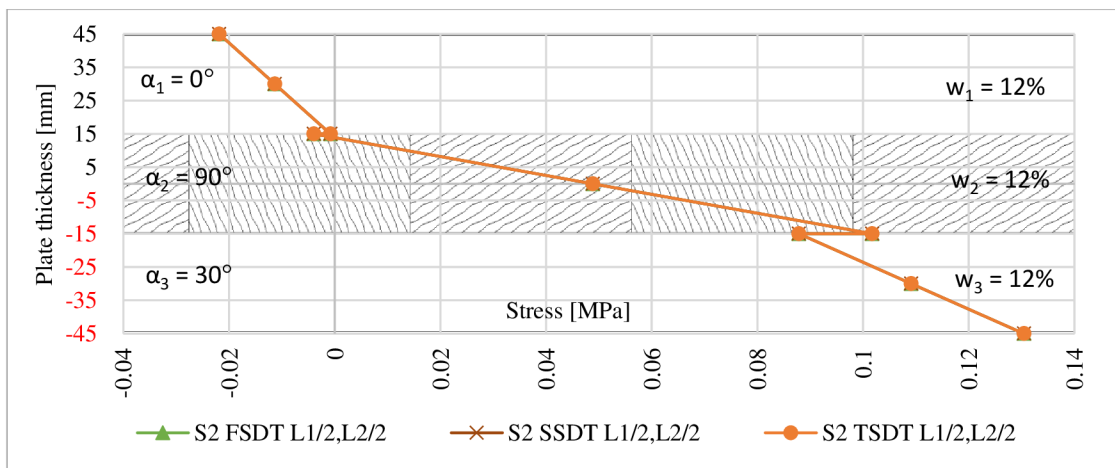
Graph 18 - (AA) σ_2 stresses by plate thickness

Table 18 - (AA) σ₂ Stress Comparison

S2	Layer 1			Layer 2			Layer 3		
[MPa]	TOP	MID	BOT	TOP	MID	BOT	TOP	MID	BOT
CPT	-	-	-	-	-	-	-	-	-
FSDT	-0.022	-0.011	-0.001	-0.004	0.049	0.102	0.088	0.109	0.130
SSDT	-0.022	-0.011	-0.001	-0.004	0.049	0.102	0.088	0.109	0.130
TSDT	-0.022	-0.011	-0.001	-0.004	0.049	0.102	0.088	0.109	0.130

Based on the findings from the *Table 18* and *Graph 18* it can be concluded that for the σ_2 stress progression through the thickness of the plate (stress across the fibers), the highest value of tensile stress can be observed on the bottom surface of layer 3, which is oriented at an angle of 30° from the longitudinal x-axis. The highest compressive stress is observed on the upper surface of layer 1. In this case of symmetry, it can be seen that the compressive and tensile stresses do not reach the same values as in the case of special axis and material symmetry. From the *Table 18* it can be seen that the neutral plane in which the σ_2 stresses should reach zero values no longer matches the geometric plane. The values of all the numerical models compared agree in the result.
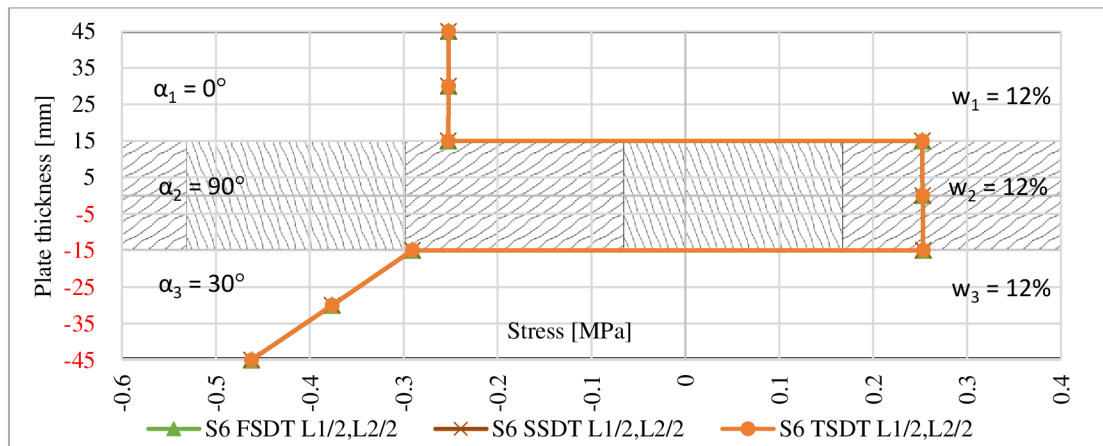
Graph 19- (AA) σ₆ stresses by plate thickness

Table 19 – (AA) σ₆ Stress Comparison

S1	Layer 1			Layer 2			Layer 3		
[MPa]	TOP	MID	BOT	TOP	MID	BOT	TOP	MID	BOT
CPT	-	-	-	-	-	-	-	-	-
FSDT	-0.252	-0.252	-0.253	0.253	0.253	0.253	-0.291	-0.376	-0.462
SSDT	-0.252	-0.252	-0.253	0.253	0.253	0.253	-0.291	-0.376	-0.462
TSDT	-0.252	-0.252	-0.253	0.253	0.253	0.253	-0.291	-0.376	-0.462

Based on the findings from the *Graph 19* and *Table 19* it can be concluded that in the case of the σ_6 stress progression (stress in the plane of the plate), we can observe a large difference between the XY shear stress in the individual layers. In this case of symmetry, the stresses on the upper and lower surfaces of the laminate no longer coincide and the zero-shear stress is no longer left in the geometric centre plane. The top layer of the laminate, which is not rotated from the longitudinal x-axis, achieves a linear stress

progression through the layer thickness. All numerical theories agree in the values of the results.
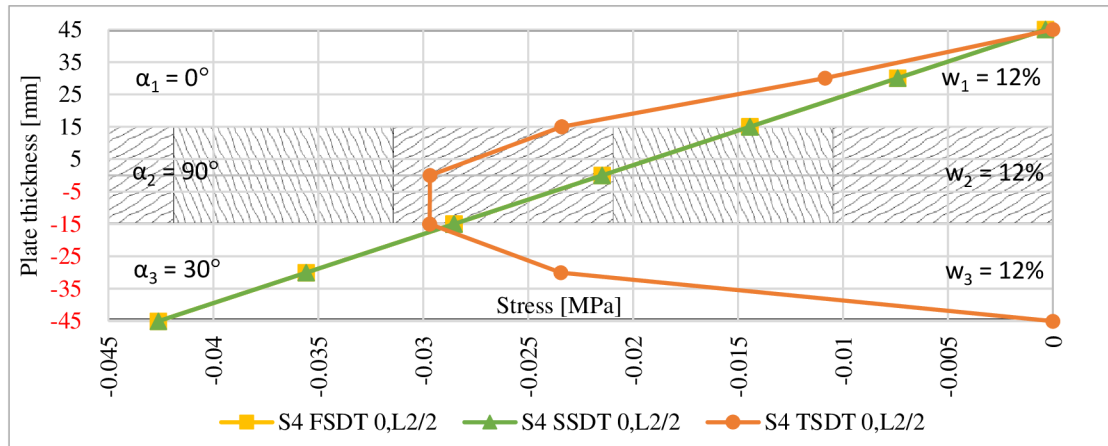
Graph 20 - (AA) σ_4 stresses by plate thickness

Table 20 - (AA) σ_4 Stress Comparison

S4	Layer 1			Layer 2			Layer 3		
[MPa]	TOP	MID	BOT	TOP	MID	BOT	TOP	MID	BOT
CPT	-	-	-	-	-	-	-	-	-
FSDT	0.000	-0.007	-0.014	-0.014	-0.021	-0.029	-0.029	-0.036	-0.043
SSDT	0.000	-0.007	-0.014	-0.014	-0.021	-0.029	-0.029	-0.036	-0.043
TSDT	0.000	-0.011	-0.023	-0.023	-0.030	-0.030	-0.030	-0.023	-0

Based on the findings from the *Table 20* and *Graph 20* it can be concluded that in the case of in the case of σ_4, the stress progression across the thickness of the plate is significantly different from the previous cases. Whereas in the previous cases the shear stress reached a maximum in the middle plane of the plate, in this type of symmetry/unsymmetry the shear stress according to FSDT and SSDT reaches a maximum value on the bottom surface of layer 3 and a zero value on the top surface of layer 1. The shear stress progression was achieved by changing the fiber orientation of the third layer by 30°. Also in this case, the results obtained from the different numerical models agree in values.
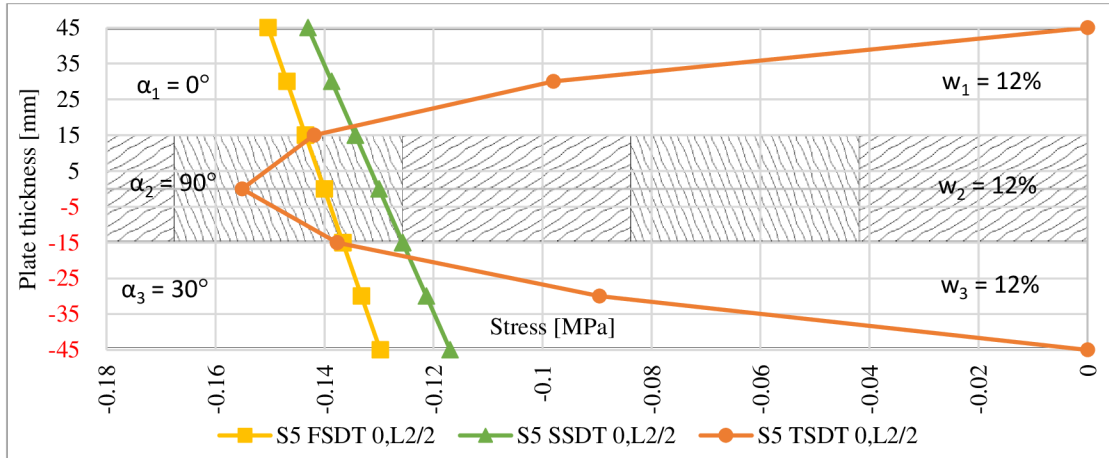
Graph 21 - (AA) σ_5 stresses by plate thickness

Table 21 - (AA) σ_5 Stress Comparison

S5	Layer 1			Layer 2			Layer 3		
[MPa]	TOP	MID	BOT	TOP	MID	BOT	TOP	MID	BOT
CPT	-	-	-	-	-	-	-	-	-
FSDT	-0.150	-0.147	-0.143	-0.143	-0.140	-0.137	-0.137	-0.133	-0.130
SSDT	-0.143	-0.139	-0.134	-0.134	-0.130	-0.126	-0.126	-0.121	-0.117
TSDT	0.000	-0.098	-0.142	-0.142	-0.155	-0.138	-0.138	-0.090	0.000

Based on the findings from the *Graph 21* and *Table 21* it can be concluded that in the case of the σ_5 stress (shear stress in the XZ plane), we can observe the first variations in the stress evolution along the plate thickness according to the individual numerical models. FSDT and SSDT show a linear XZ shear stress waveform, while TSDT shows a quadratic one. According to TSDT, the minimum stress occurs on the top surface of the first layer and on the bottom surface of the third layer. In the shear stress waveform after the thickness of the second layer, all numerical models are in agreement. In the case of the surface layers, the FSDT and SSDT models differ slightly.

9.4.4   Material Asymmetry (MA)

This chapter describes the results of the numerical models in the form of stress distributions and their comparison between the different numerical theories. The geometry and material properties used in the model are described in the methodology.
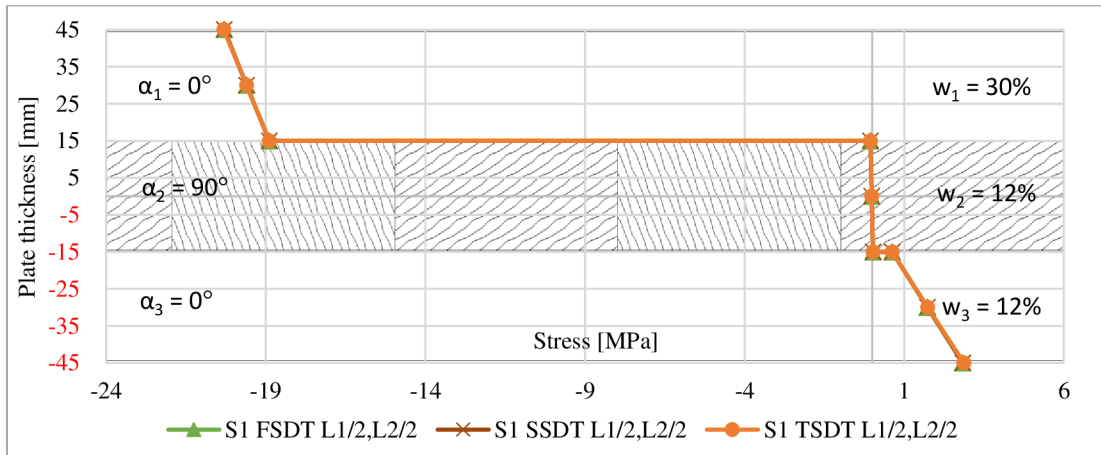
Graph 22 - (MA) Stress σ_1 across the thickness of the plate

Table 22 - (MA) σ_1 Stress Comparison

S1	Layer 1			Layer 2			Layer 3		
[MPa]	TOP	MID	BOT	TOP	MID	BOT	TOP	MID	BOT
CPT	-	-	-	-	-	-	-	-	-
FSDT	-20.30	-19.60	-18.89	-0.05	-0.02	0.02	0.63	1.73	2.83
SSDT	-20.30	-19.60	-18.90	-0.05	-0.02	0.02	0.62	1.73	2.84
TSDT	-20.32	-19.60	-18.89	-0.05	-0.02	0.02	0.63	1.73	2.87

In the case of σ_1 stresses (stresses in the direction of the fibers) in the case of material asymmetry, when the elastic moduli of the first layer are reduced to the equivalent of 30% of the moisture content of the layer, i.e. a moisture content that corresponds approximately to the saturation limit of the fibers, a significant increase in the stresses in the first layer of the laminate can be observed from the *Graph 22*. This increase is due not only to the lower elastic moduli but also to the moisture deformations that occur naturally when the moisture content of the wood increases (swelling/drying). The *Graph 22* shows that while the stress on the bottom surface of the 3rd layer of the laminate is around 2.83 MPa (corresponding to the tensile stress resulting from the bending and stretching of the fibers), the stress on the top surface of the first layer reaches a compression stress of 20.3 MPa. The table shows that the neutral plane has moved further away from the geometric plane of the plate, and according to the stress values from the middle plane of the 2nd layer and the bottom plane of the 2nd layer, the neutral plane of the plate has moved from the geometric middle plane lower in laminate.
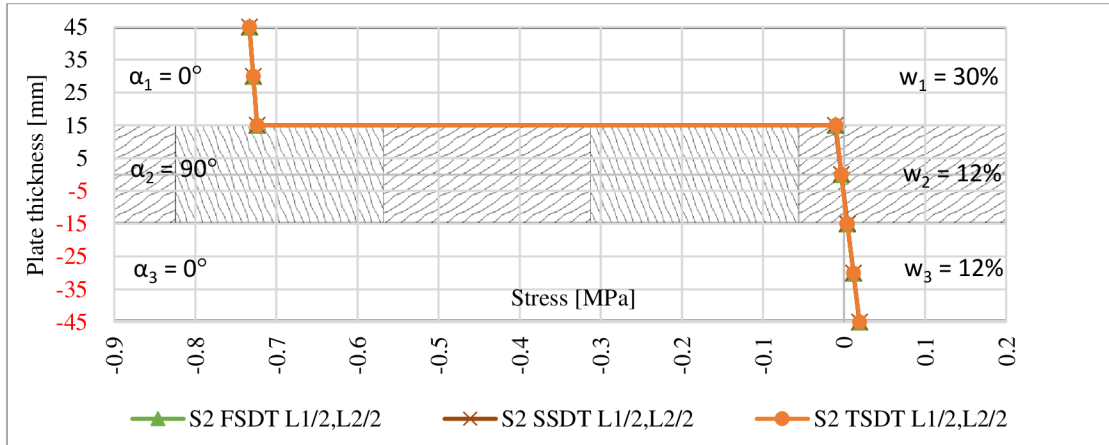
Graph 23 - (MA) σ_2 Stress by Plate Thickness

Table 23 - (MA) σ_2 Stress Comparison

S2	Layer 1			Layer 2			Layer 3		
[MPa]	TOP	MID	BOT	TOP	MID	BOT	TOP	MID	BOT
CPT	-	-	-	-	-	-	-	-	-
FSDT	-0.733	-0.729	-0.724	-0.011	-0.003	0.004	0.004	0.012	0.019
SSDT	-0.733	-0.729	-0.724	-0.011	-0.003	0.004	0.004	0.012	0.019
TSDT	-0.733	-0.729	-0.724	-0.010	-0.003	0.004	0.004	0.012	0.019

Based on the findings from the *Table 23* and *Graph 23* it can be concluded that in the case of in the case of stresses across the fibers (σ_2 stresses), there is a significant increase in stress due to a reduction in the elastic moduli and swelling in the transverse direction of the plate. According to the *Graph 23* and *Table 23*, the difference between the stress on the bottom surface of layer 3 (0.019 MPa) and the top surface of layer 1 (-0.733 MPa) is almost 39 times higher.
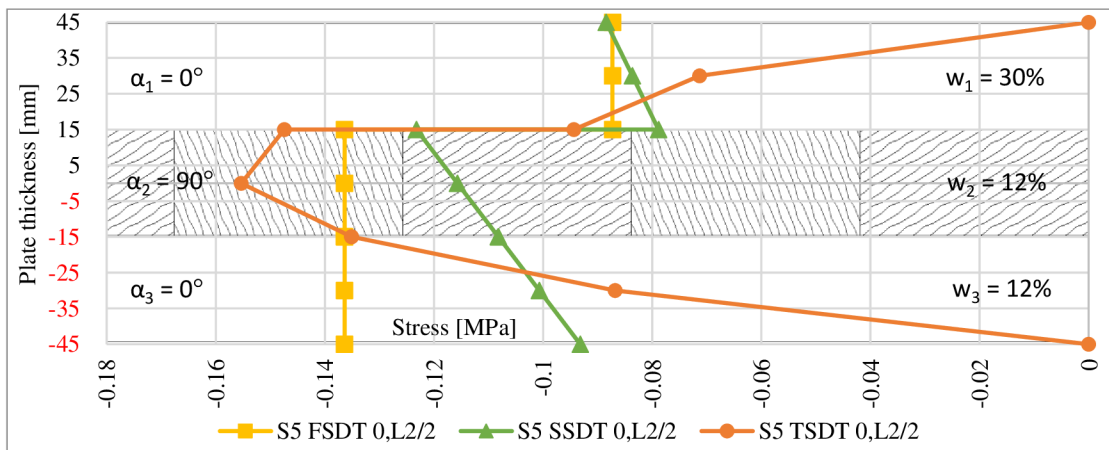
Graph 24 - (MA) σ_5 stress by plate thickness

Table 24 - (MA) σ_5 Stress Comparison

S5 [MPa]	Layer 1			Layer 2			Layer 3		
	TOP	MID	BOT	TOP	MID	BOT	TOP	MID	BOT
CPT	-	-	-	-	-	-	-	-	-
FSDT	-0.087	-0.087	-0.087	-0.136	-0.136	-0.136	-0.136	-0.136	-0.136
SSDT	-0.088	-0.084	-0.079	-0.123	-0.116	-0.108	-0.108	-0.101	-0.093
TSDT	0.000	-0.071	-0.094	-0.147	-0.155	-0.135	-0.135	-0.087	0.000

The difference between the models based on different shear theories can be clearly observed at *Graph 24* (shear stress in the XZ plane). The first (FOSDT) and second (SOSDT) order theories show the shear along the plate thickness in the form of linear maximums. The third-order theory plots the shear stress along the plate thickness parabolically and plots both maxima and minima, maintaining zero stress on the bottom surface of layer 3 and the top surface of layer 1.

Evaluation of numerical model results

By analyzing the stress distribution along the thickness of the plate and based on the results, it can be stated that numerical models for the analysis of generally orthotropic materials in any configuration, taking into account the effect of moisture, have been successfully developed, also in terms of swelling and slumping. However, the numerical models (which are included in the appendix 13.5 – 13.10) do not include the effect of temperature. The influence of temperature has been neglected mainly because the stresses and strains that occur when the temperature of the timber changes are negligible in a stationary calculation. The incorporation of the effect of temperature would make sense if connected to the model of non-uniform distribution of moisture and temperature described by Valášek (2021) in his thesis, which also deals with the principle of mechanosorption. In such a case, the model would be extended by defining temperature changes that would look similar to those of moisture with the difference of different coefficients (temperature expansion coefficients) and the resulting deformations would be added to the superposition with mechanical and moisture deformations.

Another point that can be noticed is that, apart from the special axis and material symmetry, the results do not contain values coming from Kirchhoff's thin plate theory. The reason for this is the computational difficulty that results from the presence of fourth order partial differential equations and their input into the chosen software for solving differential systems, FlexPDE. The software does not allow specifying partial terms in fourth order and the input has to be solved by substitution as given in equation (87), where the left side of the equation represents the mathematical notation and the right side of the equation the syntax of the FlexPDE software.

$$\frac{d^4 w_0}{dx^4} = dxx(wxx) \sim \frac{d^2 w_0}{dx^2} = wxx \qquad (87)$$

By using the substitution term, a new variable wxx is defined in the software for which a boundary condition needs to be defined, which was not successfully done and therefore for the remaining symmetry/unsymmetry cases the CPT evaluation is not present. It is necessary to add that the fourth order partial differential equations occur in the equation in product with coupling matrices B, which take zero values in the case of special axis and material symmetry. For such a symmetry condition, the CPT is a sufficient solution for the analysis of thin plates. From the point of view of the results, the model based on the Third Order Shear Deformation Theory seems to be the most suitable model for the analysis of timber-based laminated plates.

Comparison of SASMS and MA stress distribution

As mentioned in chapter *"9.1 CLT panel moisture content change"* a situation where moisture content of the top lamella of a CLT panel is high is possible and therefore a comparison of the Special Axis and Material Symmetry (SASMS) and Material Asymmetry (MA) cases was performed. For comparison, only the TOSDT results were used.
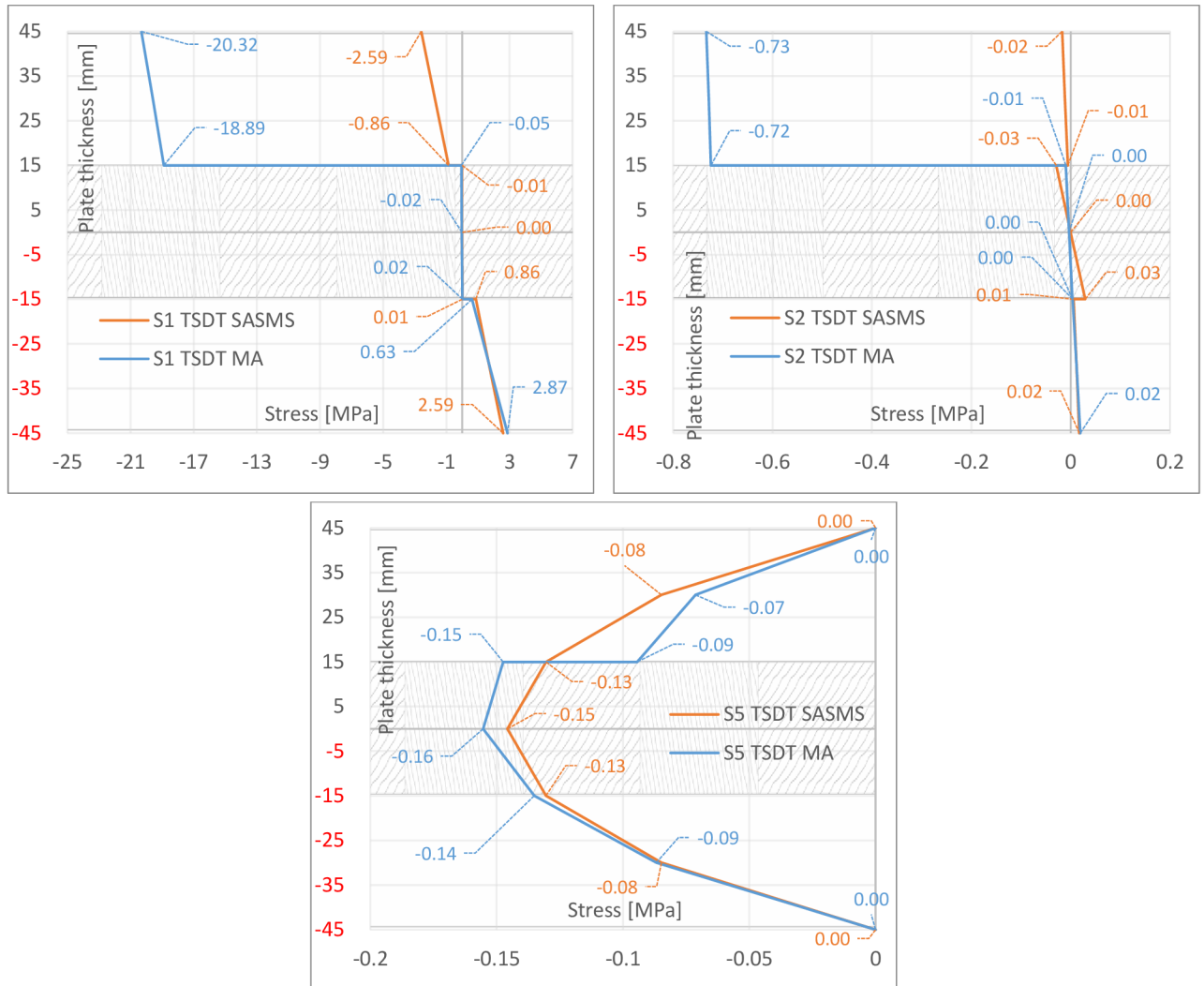
Graph 25 - Comparison of stress distribution along the laminate thickness of special material & axial symmetry (SASMS) and material asymmetry (MA).

The results obtained from the MA are the results for the extreme case, where the cell wall of the first layer of the CLT panel is completely saturated and therefore the largest possible decrease in stiffness and strength of this layer occurs. As can be seen from the *Graph 25*, moisture has a major effect on the stress increase. The combination of the modulus of elasticity, which decreases by approximately 36% at cell wall saturation limit, and the moisture stresses that occur due to the constraints on the movement of the laminae in the width and length direction of the panel, resulted in an increase in compressive stress

in the fiber direction by 784% in the case of σ_1 stress (17.73 MPa in absolute value, to a value of 20.32 MPa), which is almost the characteristic compressive strength in the fiber direction of the C24 material (21 MPa) used for the manufacture of the laminae. In the case of the compressive stress across the σ_2 fibers, the change is from 0.02 MPa to 0.73 MPa. Surprisingly, for the shear stress σ_5, a decrease in stress in the middle and bottom planes of the first lamella and, on the contrary, an increase in stress in the middle lamella is observed.

Field	$f_{m,k}$	γ_m	k_{mod}	$k_{sys,y}$	$f_{m,y,d}$	$M_{y,d}$	$\sigma_{m,y,d}$	Utilization
	[N/mm²]	[-]	[-]	[-]	[N/mm²]	[kNm]	[N/mm²]	
1	24.00	1.25	0.60	1.10	12.67	-0.85	-2.18	17 %

Field	$f_{r,k}$	γ_m	k_{mod}	$f_{r,d}$	V_d	$\tau_{r,d}$	Utilization
	[N/mm²]	[-]	[-]	[N/mm²]	[kN]	[N/mm²]	
1	1.15	1.25	0.60	0.55	-2.84	0.15	26 %

Field	$f_{v,k}$	γ_m	k_{mod}	$f_{v,d}$	V_d	$\tau_{v,d}$	Utilization
	[N/mm²]	[-]	[-]	[N/mm²]	[kN]	[N/mm²]	
1	4.00	1.25	0.60	1.92	-2.84	0.15	8 %

Figure 29 ULS Utilization of analyzed CLT panel (load = 12 000 Pa) according to Calculatis (Stora Enso [online])

The internal stresses from *Graph 25* are the result for an area load of 12 kN/m2, which, according to Calculatis (STORA ENSO [online]), corresponds to 26% of the panel load bearing capacity in ULS perspective (*Figure 29*) after reduction of the elastic moduli by γ_M. At a load close to 100% of the load bearing capacity at the moisture limit of the cell wall saturation limit (28-30%), the stresses in the first lamella would certainly exceed the compressive strength in the grain direction, resulting in the compression thickening of the wood grain and possible lamella failure or permanent reduction of the load bearing capacity of the CLT panel.

9.5   TOSDT Coupling Phenomenon of the ABDEFGH matrix

For the classical ABD matrix used in the numerical script based on the Kirchhoff-Love Plate Theory, it is possible to "predict" the laminate behavior based on the knowledge of the matrices elements of the ply stiffnesses, the elastic moduli, the ply orientation and the Poisson's ratio, without solving higher order partial differential equations. When constructing the script for TOSDT and then evaluating the results for each symmetry/asymmetry condition, a similar phenomenon was observed for the ABDEFGH matrix. This chapter is focused on describing the coupling phenomenon for the matrix used in deriving the relations for TOSDT. Denoting matrices from the stress-strain relation for TOSDT:

The following figure describes the behavior of the laminate when some elements of the matrix are non-zero. The result is a description of the so-called TOSDT coupling phenomenon. TOSDT coupling matrix is denoted on Figure 30.

Figure 30 – Denoting matrices ABDEFGH
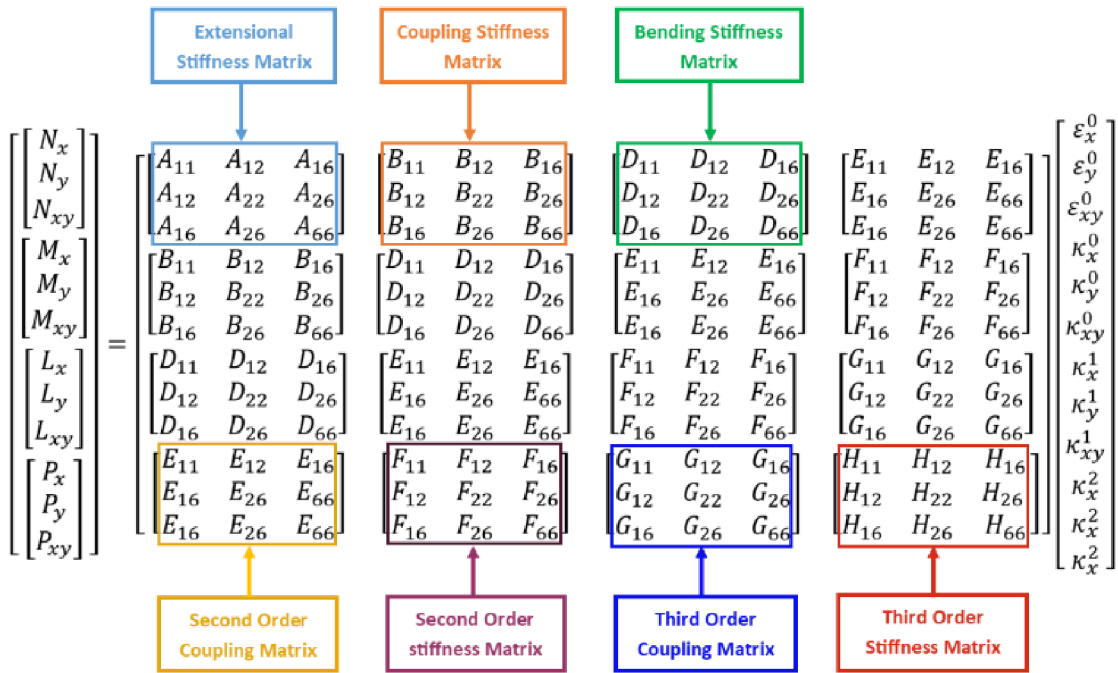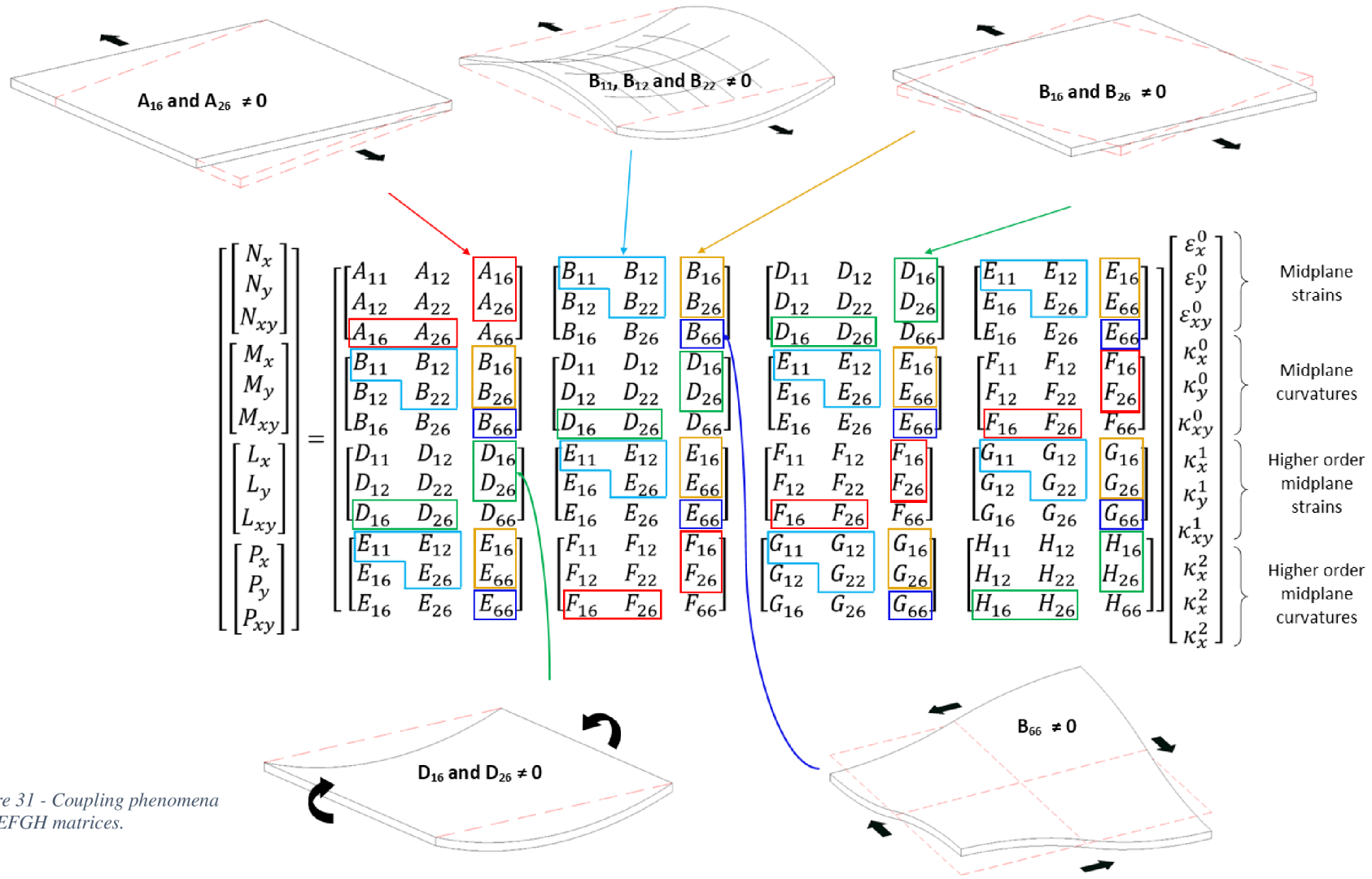
Figure 31 - Coupling phenomena ABDEFGH matrices.

10 The benefits for science and practice

Solid timber structures, especially glued CLT panels, have a great potential to become an ideal construction material for residential and multi-storey buildings. In order for this potential to be fulfilled at least in part, it is first necessary to study the behavior of such material under various conditions in the greatest detail. Since wood is a hygroscopic material, its properties are largely influenced by moisture. It is therefore essential to find out how a given structural element will behave at a given moisture content. In order to do this, it is necessary to determine the effect of moisture, particularly on laminated wood-based materials, as accurately as possible. Current practice uses software that does not go further than the building codes in the case of moisture exposure. In the Czech Republic, to date, we do not have standards describing the design of CLT elements or standards for the construction of timber structures. It is during the construction phase of timber-based buildings that most moisture-related problems arise, both in terms of the risk of mould growth and the reduction of the mechanical properties of the timber. In fact, Sweden places clear requirements in its Building Code to protect construction products and construction materials from moisture during the construction phase. For large constructions, the law requires documented inspections, measurements, and analyses. Material specifications under the legislation require "Wood materials and wood products to be protected from moisture during and after assembly to avoid microbial growth and other problems" (Olsson, 2020). If we are to take timber construction further in the Czech Republic, we need to be inspired by similar requirements and enforce the requirements for the protection of timber buildings during the construction process by legislation and standards. The results of this work provide relevant arguments for stricter protection of building materials during construction and can be the basis for the development of suitable standards for the implementation of timber buildings. Furthermore, the numerical models can be used as a tool to verify the load-bearing capacity of moisture-stressed CLT panels.

From the point of view of further research, the derived numerical models can be used in the design of new laminates made of arbitrary materials (not only wood) and the analysis of their behavior using "TOSDT Coupling Phenomena" according to the chosen composition and the presence of individual components of the ABDEFGH matrix. The model can be modified and freely extended to include other variables such as temperature or to incorporate the effect of mechanosorption. The model can be modified quite easily for dynamic response and vibration analysis. In general, the model offers a solid basis for investigating the behavior of laminates.

11 Conclusions

The thesis deals with the development and validation of computational models for the analysis of bending, deformation, and internal stresses of laminated panels (CLT) with arbitrarily oriented layers and composed of different materials under transverse loading. The numerical models were developed based on four plate theories in a form for the analysis of generally orthotropic panels. It was found that:

- The model based on the Kirchhoff-Love Plate Theory, unlike the other models, does not allow for shear stress analysis along the thickness of the laminate. In addition to this, it is the most computationally demanding in its general form, which places higher requirements on the differential solver used and therefore, from this point of view, it is not suitable for the analysis of wood-based laminates.
- The most difficult model to derive and the most suitable in terms of the provided results is the model based on Third Order Shear Deformation Theory. This model is suitable for the analysis of generally orthotropic laminates.
- The behavior of an arbitrarily composed laminate can be estimated only on the basis of the composition of the laminate matrix (in the case of TOSDT this is the ABDEFGH matrix). Thus, the torsion, bending or shear deformation of the laminate can be predicted without the need to solve a system of higher order partial differential equations.
- Based on the results obtained, it can be argued that a situation where the moisture content of the upper lamellas of the CLT panels at the cell wall saturation limit can occur. At such a change in moisture content, internal stresses approaching the strength of the material can be generated even at relatively low external loads, and even at loads equivalent to 25% of the panel load bearing capacity.

The result of this thesis may help in future efforts to further understand the effect of moisture on CLT panels and the effect on the overall load bearing capacity. However, it should be taken into account that the numerical models are a stationary models and did not take into account the fact that the change and equilibration of moisture will occur not only in one laminate but throughout the thickness of the laminate as described by the nonstationary diffusion principle. The findings suggest that moisture has a significant effect on the load-bearing capacity of the panel and that this type of stress must be taken into account in the future when dimensioning these structural elements or when carrying out construction.

12 References

1. ABBAS, M., ELSHAFEI, M., NEGM, H. (2013). *"Modeling and Analysis of Laminated Composite Plate Using Modified Higher Order Shear Deformation Theory"*, International Conference on Aerospace Sciences and Aviation Technology, 15, pp. 1-25. doi: 10.21608/asat.2013.22182

2. AGARWAL, D. Bhagwan., BROUTMAN, J., CHANDRASHEKHERA, K.. (2015). *"Analysis and Performance of Fiber Composites"*. Third Edition. Wiley India. ISBN: 978-81-265-3636-8

3. ANSYS, Inc. and ANSYS Europe. *"ANSYS Workbench – Product release notes 10.0"*. Canonsburg, PA 15317. [cit. 2023-03-10]. Available from: https://kashanu.ac.ir/Files/Content/ANSYS%20Workbench.pdf

4. BALOGH, Bence (2013). *"Computer program for the calculation of Mindlin Plates "*. Department of Structural Mechanics, BUTE, Budapest. Thesis supervisor: Dr. Imre Bojtár

5. BITTNAR & ŠEJNOHA. (1992). *"Numerické metody mechaniky 1"*. Praha. 1992. ČVUT. ISBN: 80-01-00855-x

6. ČESKÝ STATISTICKÝ ÚŘAD (2018): *"Staví se stále více úsporných domů [online] "*; available from [cit. 10. 03. 2023]: https://www.czso.cz/csu/czso/stavi-se-stale-vice-uspornych-domu

7. DLUBAL SOFTWARE. (2020). *"Rfem 5 – Spacial Models Calculated According to Finite Element Method [online]"*. [cit. 2023-03-10]. Available from: https://www.dlubal.com/-/media/Files/website/documents/manuals/rfem-fea-software/rfem-5/rfem-5-manual-en.pdf?la=en&mlid=1940DA1D4C7242DCB72553023E0C2DAB&hash=4AE0E597004925B09F37ACB257107A8594F43B11

8. DUSHMAN S., LAFFERTY J.M. (1962). *"Scientific Foundations of Vacuum Technique"*. Wiley - New York. ISBN: 978-0471228035

9. EUROPEAN COMMITTEE FOR STANDARDIZATION (1994): „*Eurocode 5: design of timber structure*", Brussels, BSI; ISBN: 9780470675007

10. GEREKE, Thomas Verfasser. (2009): *"Moisture-Induced Stresses in Cross Laminated Wood Panels"*. Moisture-Induced Stresses in Cross-Laminated Wood Panels. Zürich: ETH,

11. GHIAMY, Ali., HOSSEIN, Amoushahi. (2022) *"Thin-Walled Structures: Dynamic stability of different kinds of sandwich plates using third order shear deformation theory "*. Vol 172. Department of Civil Engineering, Faculty of Civil Engineering and Transportation: Department of Civil Engineering, Faculty of Civil Engineering and Transportation. ISSN 0263-8231

12. HORÁČEK, P. (2008). „*Fyzikální a mechanické vlastnosti dřeva I*". Brno: Mendelova zemědělská a lesnická univerzita v Brně. ISBN 978-80-7375-169-2

13. HORÁČEK P. (2010). „*Mechanické vlastnosti dřeva [online]*". *Available* from [cit 10. 03. 2023]:
14. https://is.mendelu.cz/lide/clovek.pl?zalozka=13;id=7038;studium=17869;zp=143 44;download_prace=1;lang=sk
15. INTER-CAD KFT. *"AxisVM – Advanced Step by Step Tutorial [online]"*. 2019 [cit. 2023-03-10]. Available from: https://axisvmsupport.hu/manual/axisvm_advancedstepbystepbook.pdf
16. KHDEIR, A., REDDY, J.N. (1999). *"Free vibrations of laminated composite plates using second-order shear deformation theory "*. Computers & Structures. Vol 71, Issue 6, Pages 617-626. ISSN 0045-7949
17. KOLLMANN, F., CÔTÉ, W.A. (1968). *"Principles of Wood Science and Technology"*, Springer, Berlin, ISBN: 978-3-642-87930-2
18. KOLVIK, Gjermund Mæsel (2012). *"Higher Order Shear Deformation Plate Theory"*. Faculty of Mathematics and Natural Sciences, University of Oslo. Thesis supervisor: Noël Challamel, Jostein Hellesland
19. KOŽELOUH B. (1998). „*Dřevěné Konstrukce podle Eurokódu 5: Step 1 – Navrhování a konstrukční materiály"*. KODR Zlín. ISBN 80-238-2620–4
20. NAMI, Rahim Mohammad., JANGHORBAN, Maziar. DAMADAM, Mohsen. (2015). *"Thermal buckling analysis of functionally graded rectangular nanoplates based on nonlocal third-order shear deformation theory"*. Journal of Aerospace Science and Technology. Vol 41. Pages 7-15. DOI: 10.1016/j.ast.2014.12.001
21. NETTLES A. T. (1994). *"Basic Mechanics of Laminated Composite Plates "*. NASA Alabama. ISBN 1730984487
22. OLSSON, Lars. (2020). *"Moisture safety in CLT construction without weather protection – Case studies, literature review and interviews "*. E3S Web of Conferences 172. RISE Research Institutes of Sweden, Division Build Environment, Building Technology, Sweden.
23. ORMARSSON, S. (1998). *"Numerical analysis of moisture-related distortions in sawn timber"*, PhD thesis, Chalmers University of Technology
24. ÖBERG, Johan. (2018). *"Moisture risks with CLT-panels subjected to outdoor climate during construction -focus on mould and wetting process"*. PolygonAK (Polygon Sverige AB). Graduate thesis supervisor: Erik Wiege
25. PANYATONG, Monchai., CHINNABOON, Boonme., CHUCHEEPSAKUL, Somchai. (2015). *"Nonlocal second-order shear deformation plate theory for free vibration of nanoplates"*. Suranaree Journal of Science and Technology. Vol 22. Available from [cit. 18.03.2023]: https://www.thaiscience.info/journals/Article/SJST/10984529.pdf
26. PAVLAS, Marek. (2006). *"Dřevostavby z vrstvených masivních panelů – technologie CLT"*. Grada Publishing. ISBN 978-80-271-0055-2
27. POŽGAJ A., CHOVANEC D., KURJATKO S., BABIAK M. (1997). *"Štruktúra a vlasnosti dreva"*. Bratislava: Príroda. ISBN 80-07-00960-4
28. SIAU, J.F. (1995). *"Wood: Influence of moisture on physical properties "*. Department of Wood Science and Forest Products, Virginia Polytechnic Institute and State University, Blacksburg, USA, ISBN: 978-0962218101

29. SIMULIA. Abaqus 6.12 Analysis User´s Manual, *"Volume I: Introduction, Spacial Modeling, Execution & Output [online]"*. United States, Fremont, CA. [cit. 2023-03-10]. Available from:
    http://dsk-016-1.fsid.cvut.cz:2080/v6.12/pdf_books/ANALYSIS_1.pdf

30. SHAFEI, Erfan., FAROUGHI, Shirko., REALI, Alessandro. (2020). *"Geometrically nonlinear vibration of anisotropic composite beams using isogeometric third-order shear deformation theory"*. Journal of Composite Structures. Vol 252. DOI: 10.1016/j.compstruct.2020.112627

31. SHAHRJERDI & BAYAT, SAPUAN, S.M., ZAHARI, R. (2010). *"Second-Order Shear Deformation Theory to Analyze Stress Distribution for Solar Functionally Graded Plates "*. Journal of Mechanics Based Design of Structures and Machines. Vol 38. Issue 3. Pages 348-361. DOI: 10.1080/15397731003744603

32. SHAHRJERDI A., MUSTAPHA F. (2011). *"Second Order Shear Deformation Theory (SSDT) for Free Vibration Analysis on a Functionally Graded Quadrangle Plate"*. Journal of Recent Advances in Vibration Analysis. InTech. DOI: 10.5772/22245.

33. SHAOBO L., GU H., BERGMAN R., KELLEY S. (2020): *"Comparative life-cycle assessment of a mass timber building and concrete alternative "*. Wood and Fiber Science [online]; Society of Wood and Technology; [cit. 10. 03. 2023] available from:
    https://www.researchgate.net/publication/340960305_Comparative_lifecycle_assessment_of_a_mass_timber_building_and_concrete_alternative

34. SHOKRIEH, M.M., PARKESTANI, A. Nouri. (2017). *"Post buckling analysis of shallow composite shells based on the third order shear deformation theory"*. Aerospace Science and Technology. Vol 66. Pages 332-341. DOI: 10.1016/j.ast.2017.01.011

35. STORA ENSO. *„Calculatis [Online] „*. Available from [cit. 10.30.2023]:
    https://calculatis.storaenso.com/

36. SULZBERGER, P. H. (1953). *"The Effect of Temperature on the Strength of Wood, Plywood and Glued Joints"*. Rept. ACA-46, Dept. Supply, Aeronait. Res. Consult. Com., Commonwealth of Australia,

37. SZEKRÉNYES, András. (2014). *"Stress and fracture analysis in delaminated orthotropic composite plates using third-order shear deformation theory "*. Applied Mathematical Modelling. Vol 38, Issues 15–16. Pages 3897-3916. DOI: 10.1016/j.apm.2013.11.064.

38. SZILARD, Rudolph. (2004). *"Theory and Application of Plate Analysis: Classical numerical and engineering methods"*. John Wiley & Sons, Inc., Hoboken, New Jersey. ISBN 0-471-42989-9

39. THAI, Huu-Tai., CHOI, Dong-ho (2013). *"A simple first-order shear deformation theory for laminated composite plates"*. Composite Structures. Vol 106. Pages 754-763. ISSN 0263-8223

40. TIAN, Yuhang., LI, Qingya., WU, Di., CHEN, Xiaojun., GAO, Wei. (2022). *"Nonlinear dynamic stability analysis of clamped and simply*

supported organic solar cells via the third-order shear deformation plate theory". Engineering Structures. Vol 252. ISSN 0141-0296

41. VALÁŠEK, Václav. *„Kombinované zatížení vrstvených konstrukčních prvků"*. 2021. Theses. Supervisor: prof. Dr. Ing. Petr Horáček

42. VENTSEL, Eduard. (2001). *"Theory, Analysis and Applications - Thin Plates and Shells"*. The Pennsylvania State University, Pennsylvania. Marcel Dekker Inc. New York. ISBN: 0-8247-0575-0

43. VRBKA, Jan. (2008). *"Mechanika kompozitů [online]"*. Brno: Ústav mechaniky těles, mechatroniky a biomechaniky. Fakulta strojního inženýrství VUT v Brně. Available from [cit. 2023-03-10]:
https://www.vutbr.cz/www_base/priloha.php?dpid=83340

44. ZHANG, Shunqi. (2014). *"Nonlinear FE Simulation and Active Vibration Control of Piezoelectric Laminated Thin-Walled Smart Structures"*. Institute of General Mechanics RWTH Aachen University. Ph.D. dissertation Supervisor: apl. Prof. Dr.-Ing. Rüdiger Schmidt

13 Appendix

13.1 Derivation of relations according to Kirchhoff-Love Plate Theory

13.1.1 Strains and curvatures

From equations defining displacement field the strains and curvatures are defined according to Nettles (1994) as:

$$\varepsilon_x = \frac{du}{dx} = \frac{du_0}{dx} - z\frac{d^2w}{dx^2} \tag{88}$$

$$\varepsilon_y = \frac{dv}{dy} = \frac{dv_0}{dy} - z\frac{d^2w}{dy^2} \tag{89}$$

$$\gamma_{xy} = \frac{du}{dy} + \frac{dv}{dx} = \frac{du_0}{dy} + \frac{dv_0}{dx} - 2z\frac{d^2w}{dxdy} \tag{90}$$

Defining:

$$\frac{du_0}{dx_0} \text{ as } \varepsilon_x^0 \;\; ; \;\; \frac{dv_0}{dy_0} \text{ as } \varepsilon_y^0 \;\; ; \;\; \frac{du_0}{dy_0} + \frac{dv_0}{dx_0} \text{ as } \gamma_{xy}^0 \tag{91}$$

To be the midplane strains and defining:

$$-\frac{d^2w}{dx^2} \text{ as } \kappa_x \;\; ; \;\; -\frac{d^2w}{dy^2} \text{ as } \kappa_y \;\; ; \;\; -2\frac{d^2w}{dxy} \text{ as } \kappa_{xy} \tag{92}$$

to be the plate curvatures will make notation easier. The above equations can be expressed in matrix notation as follows:

$$\begin{bmatrix} \varepsilon_x \\ \varepsilon_y \\ \gamma_{xy} \end{bmatrix} = \begin{bmatrix} \varepsilon_x^0 \\ \varepsilon_y^0 \\ \gamma_{xy}^0 \end{bmatrix} + z \begin{bmatrix} \kappa_x \\ \kappa_y \\ \kappa_{xy} \end{bmatrix} \tag{93}$$

As illustrated in the Figure 32, the plate's curvature Kx or Ky represents the change in slope of the bending plate along the x- or y-axis, respectively. The term K_{xy} refers to the amount of bending in the x-direction along the y-axis, also known as twisting.
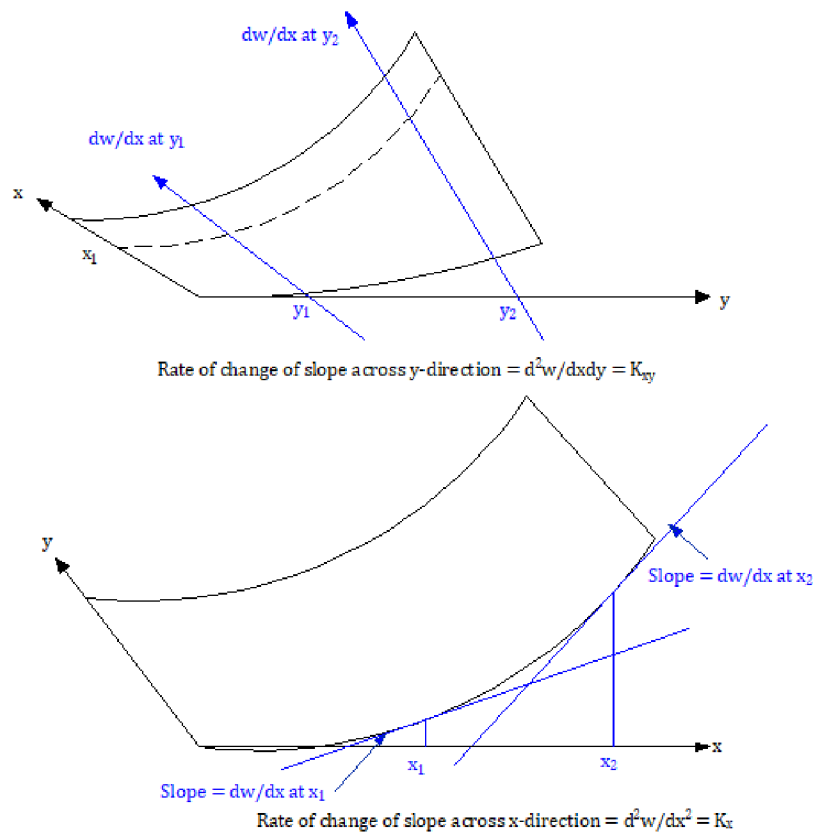
Figure 32 – Definitions of plate curvatures (Nettles, 1994)

13.1.2 Equilibrium equations

The *Figure 33* illustrates the directions for all stress and moment resultants. The double-headed arrow indicates torque in the direction determined by the right-hand rule (i.e., point your right-hand thumb in the direction of the double-headed arrows, and the direction of the torque's rotation is in the direction your fingers are pointing). The M_x and M_y components will result in the board bending, while the M_{xy} component will cause twisting of the board (Nettles, 1994).

89
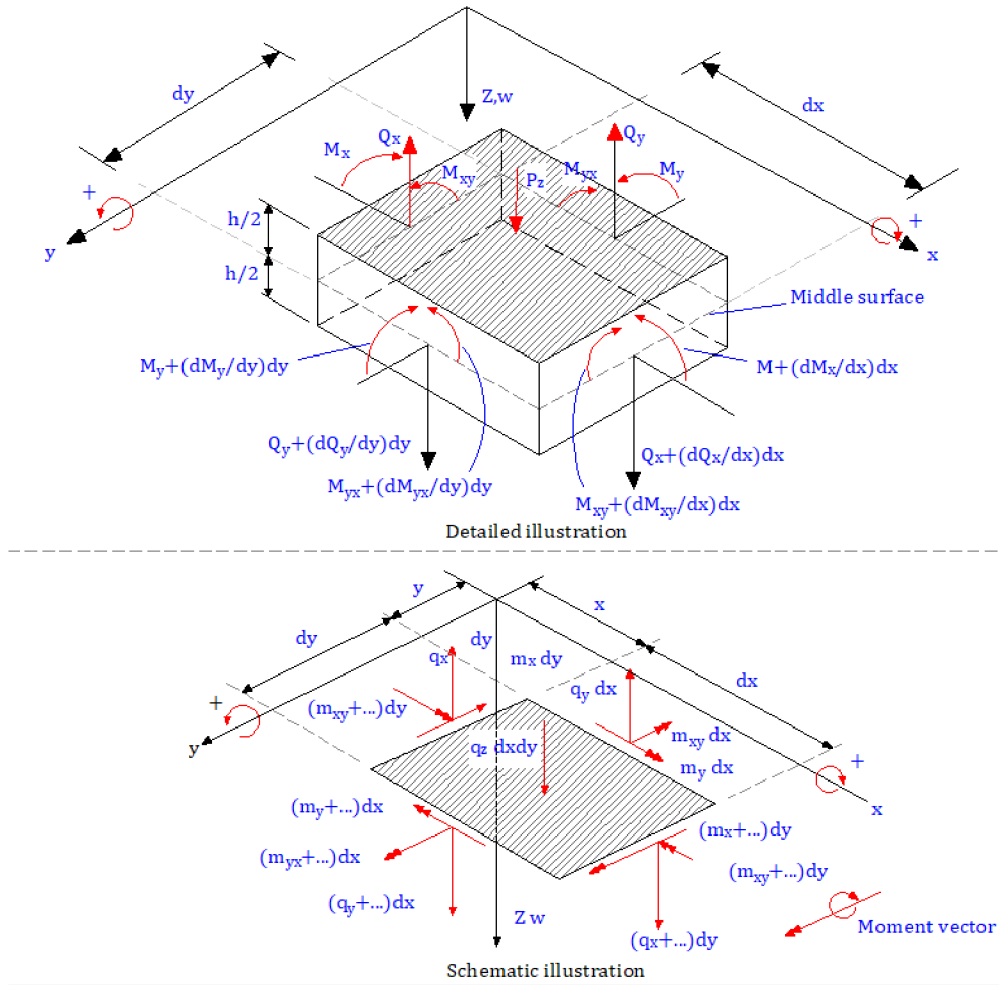
Figure 33 – External and internal forces on the element of the middle surface (Szilard, 2004)

Based on the *Figure 33* and the strain and curvature relations (as discussed in the previous chapter), we can derive the equilibrium equations for shell plates, which can be expressed in the following form:

- Equilibrium equation for forces in the x-direction:

$$-N_x dy + \left(N_x + \frac{dN_x}{d_x} dx\right) dy - N_{xy} dx + \left(N_{xy} + \frac{dN_{xy}}{dy} dy\right) dx = 0 \quad (94)$$

in reduced form for forces in x, y-direction:

$$\frac{dN_x}{dx} + \frac{dN_{xy}}{dy} = 0 \quad ; \quad \frac{dN_{xy}}{dx} + \frac{dN_y}{dy} = 0 \tag{95}$$

- Equilibrium equation for forces in the z-direction:

$$-R_{xz} dy + \left(R_{xz} + \frac{dR_{xz}}{dx} dx\right) dy - R_{yz} dx + \left(R_{yz} + \frac{dR_{yz}}{dy}\right) dx$$
$$+ p\, dx dy = 0 \tag{96}$$

90

in reduced form:

$$\frac{dR_{xz}}{dx} = \frac{dR_{yz}}{dy} + p = 0 \tag{97}$$

- Moment equations of equilibrium around the x-axis:

$$M_y dx - \left(M_y + \frac{dM_y}{dy} dy \right) dx + M_{xy} dy - \left(M_{xy} + \frac{dM_{xy}}{dx} dx \right) dy$$

$$+ \left(R_{yz} + \frac{R_{yz}}{dy} dy \right) dxdy + \frac{dy}{2} \left(R_{xz} + \frac{dR_{xz}}{dx} dx \right) dy \tag{98}$$

$$- \frac{dy}{2} R_{xz} dy + \frac{dy}{2} p \, dxdy = 0$$

In reduced form:

$$\frac{dM_x}{dx} = \frac{dM_{xy}}{dy} - R_{xz} = 0 \tag{99}$$

Similarly, the moment equations of equilibrium about the y-axis:

$$\frac{dM_{xy}}{dx} + \frac{dM_y}{dy} - R_{yz} = 0 \tag{100}$$

Substituting the (moment) equation into the equilibrium equations in the z-direction, we can derive the equilibrium equation for the plate:

$$\frac{d^2 M_x}{dx^2} + 2\frac{d^2 M_{xy}}{dxdy} + \frac{d^2 M_y}{dy^2} + p = 0 \tag{101}$$

These three equilibrium equations serve as the basis for establishing the governing plate equations in terms of displacement for the Kirchhoff-Love Plate Theory, which will be discussed in the following chapters.

13.1.3 Orthotropic plate stress-strain relationship

As previously mentioned (in the Hook's Law chapter), the stress in each lamination can be expressed in terms of strain and curvature as follows:

$$\begin{bmatrix} \sigma_x \\ \sigma_y \\ \tau_{xy} \end{bmatrix} = \begin{bmatrix} \bar{Q}_{11} & \bar{Q}_{12} & \bar{Q}_{16} \\ \bar{Q}_{12} & \bar{Q}_{22} & \bar{Q}_{26} \\ \bar{Q}_{16} & \bar{Q}_{26} & \bar{Q}_{66} \end{bmatrix} \begin{bmatrix} \varepsilon_x^0 \\ \varepsilon_y^0 \\ \gamma_{xy}^0 \end{bmatrix} + z \begin{bmatrix} \bar{Q}_{11} & \bar{Q}_{12} & \bar{Q}_{16} \\ \bar{Q}_{12} & \bar{Q}_{22} & \bar{Q}_{26} \\ \bar{Q}_{16} & \bar{Q}_{26} & \bar{Q}_{66} \end{bmatrix} \begin{bmatrix} \kappa_x \\ \kappa_y \\ \kappa_{xy} \end{bmatrix} \tag{102}$$

The stresses in each layer may vary due to the thickness of the layer, thus it is necessary to define the stresses in terms of equivalent forces acting on the midplane of the plate. Referring to the Figure 34, we can observe that the stresses acting on the plate can be divided into increments and then summed. The resulting relationship in integral form is defined as the stress resultant and is denoted by N_i. This stress resultant has a unit force per length and acts in the same direction as the applied stress.
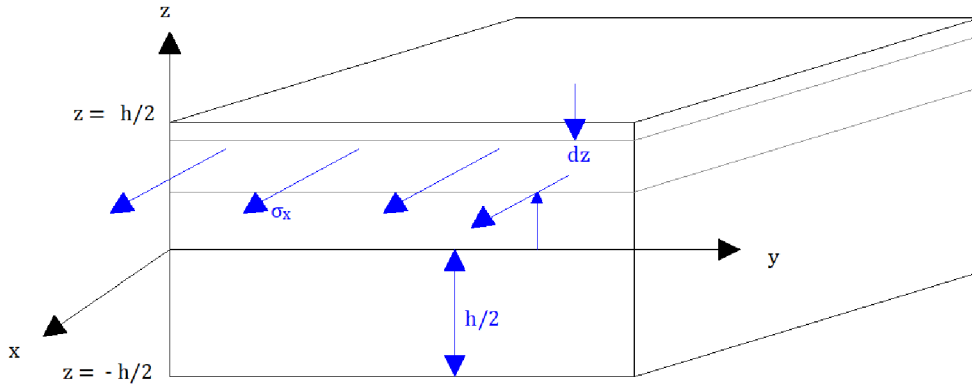
Figure 34 – Scheme of midplane notation

The figure can be rearranged to represent the components in the y-axis direction and the in-plane shear stress as follows:

$$N_x = \int_{-h/2}^{h/2} \sigma_x dz \tag{103}$$

$$N_y = \int_{-h/2}^{h/2} \sigma_y dz \tag{104}$$

$$N_{xy} = \int_{-h/2}^{h/2} \tau_{xy} dz \tag{105}$$

From the figure presented earlier, it is evident that the applied stress on the plate generates a moment in the midline plane of the plate. The magnitude of this moment is dependent on the distance z from the midplane. These moments can be defined around all axes based on this principle.

$$M_x = \int_{-h/2}^{h/2} \sigma_x z dz \tag{106}$$

$$M_y = \int_{-h/2}^{h/2} \sigma_y z dz \tag{107}$$

$$M_{xy} = \int_{-h/2}^{h/2} \tau_{xy} z dz \tag{108}$$

These moment resultants have units of torque per unit length. The Figure 35 illustrates the directions of all stress and moment resultants (Nettles, 1994):
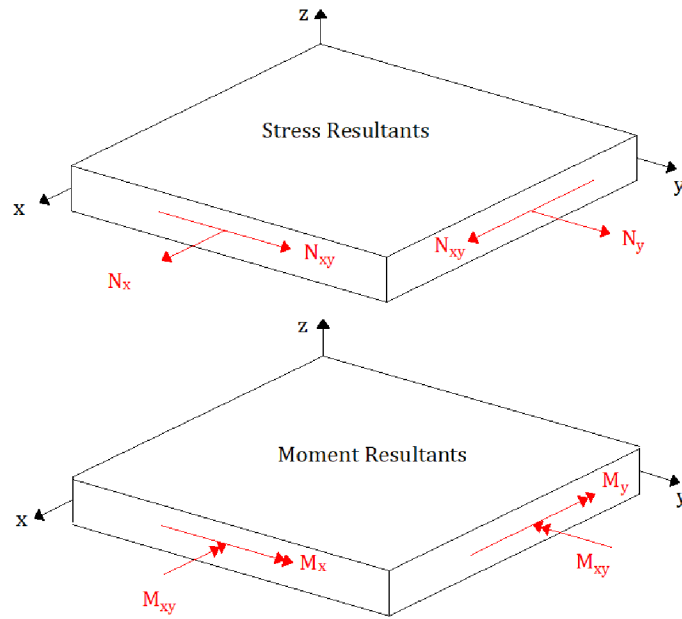
Figure 35 – Stress and moment resultants (Nettles, 1994)

Equations (for N_x, N_y, N_{xy}) written in matrix form:

$$\begin{bmatrix} N_x \\ N_y \\ N_{xy} \end{bmatrix} = \int_{-h/2}^{h/2} \begin{bmatrix} \sigma_x \\ \sigma_y \\ \tau_{xy} \end{bmatrix} \tag{109}$$

Equations (for M_x, M_y, M_{xy}) written in matrix form:

$$\begin{bmatrix} M_x \\ M_y \\ M_{xy} \end{bmatrix} = \int_{-h/2}^{h/2} \begin{bmatrix} \sigma_x \\ \sigma_y \\ \tau_{xy} \end{bmatrix} z dz \tag{110}$$

These integral notations must be applied for each individual lamination and added together if there is a discontinuity in the stresses between the layers.
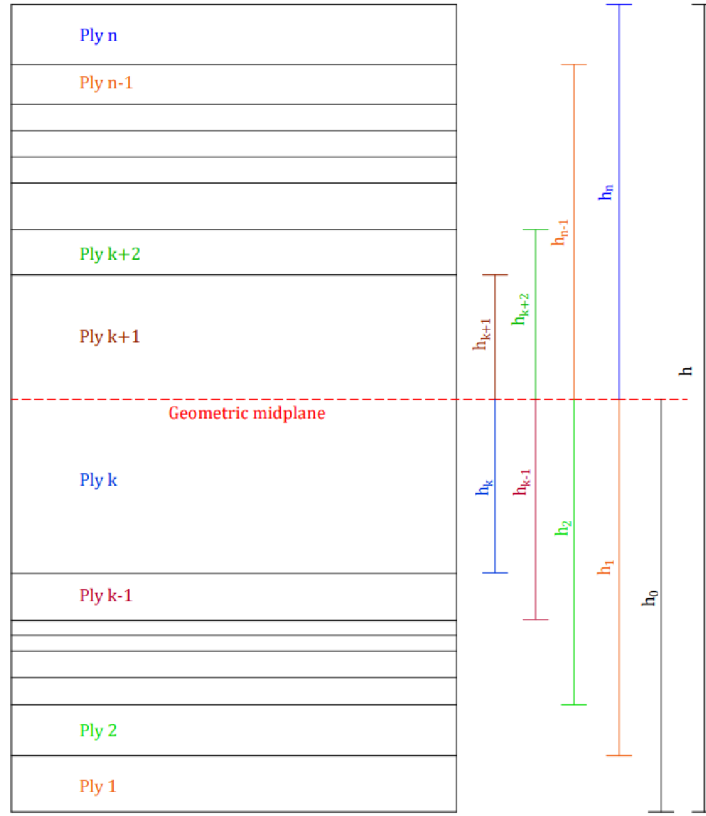
Figure 36 – Cross section of a laminate

The equations (N_x, N_y, N_{xy}, M_y, ...) must be expressed in the form using the figure provided above:

$$\begin{bmatrix} N_x \\ N_y \\ N_{xy} \end{bmatrix} = \sum_{k=1}^{n} \int_{h_{k-1}}^{h_k} \begin{bmatrix} \sigma_x \\ \sigma_y \\ \tau_{xy} \end{bmatrix}_k dz \tag{111}$$

$$\begin{bmatrix} M_x \\ M_y \\ M_{xy} \end{bmatrix} = \sum_{k=1}^{n} \int_{h_{k-1}}^{h_k} \begin{bmatrix} \sigma_x \\ \sigma_y \\ \tau_{xy} \end{bmatrix}_k zdz \tag{112}$$

By substituting the aforementioned equations into the equation for stress, we obtain:

$$\begin{bmatrix} N_x \\ N_y \\ N_{xy} \end{bmatrix} = \sum_{k=1}^{n} \left\{ \int_{h_{k-1}}^{k_k} \begin{bmatrix} \bar{Q}_{11} & \bar{Q}_{12} & \bar{Q}_{16} \\ \bar{Q}_{12} & \bar{Q}_{22} & \bar{Q}_{26} \\ \bar{Q}_{16} & \bar{Q}_{26} & \bar{Q}_{66} \end{bmatrix} \begin{bmatrix} \varepsilon_x^0 \\ \varepsilon_y^0 \\ \gamma_{xy}^0 \end{bmatrix} dz \right.$$
$$\left. + \int_{h_{k-1}}^{k_k} \begin{bmatrix} \bar{Q}_{11} & \bar{Q}_{12} & \bar{Q}_{16} \\ \bar{Q}_{12} & \bar{Q}_{22} & \bar{Q}_{26} \\ \bar{Q}_{16} & \bar{Q}_{26} & \bar{Q}_{66} \end{bmatrix} \begin{bmatrix} \kappa_x \\ \kappa_y \\ \kappa_{xy} \end{bmatrix} zdz \right\} \tag{113}$$

Since strains and curvatures ($\varepsilon_0.\kappa_0$) do not vary with z (their values are always 0 in the median plane), they do not need to be included in the integration. Additionally,

94

the stiffness matrix of the laminate is constant for each layer and thus will remain constant during the integration over the thickness of the laminate. Therefore, subtracting these constants before integrating over the thickness yields:

$$
\begin{bmatrix} N_x \\ N_y \\ N_{xy} \end{bmatrix} = \sum_{k=1}^{n} \left\{ \begin{bmatrix} \bar{Q}_{11} & \bar{Q}_{12} & \bar{Q}_{16} \\ \bar{Q}_{12} & \bar{Q}_{22} & \bar{Q}_{26} \\ \bar{Q}_{16} & \bar{Q}_{26} & \bar{Q}_{66} \end{bmatrix} \begin{bmatrix} \varepsilon_x^0 \\ \varepsilon_y^0 \\ \gamma_{xy}^0 \end{bmatrix} \int_{h_{k-1}}^{h_k} dz \right.
$$
$$
\left. + \begin{bmatrix} \bar{Q}_{11} & \bar{Q}_{12} & \bar{Q}_{16} \\ \bar{Q}_{12} & \bar{Q}_{22} & \bar{Q}_{26} \\ \bar{Q}_{16} & \bar{Q}_{26} & \bar{Q}_{66} \end{bmatrix} \begin{bmatrix} \kappa_x \\ \kappa_y \\ \kappa_{xy} \end{bmatrix} \int_{h_{k-1}}^{h_k} z\,dz \right\} \tag{114}
$$

$$
\begin{bmatrix} M_x \\ M_y \\ M_{xy} \end{bmatrix} = \sum_{k=1}^{n} \left\{ \begin{bmatrix} \bar{Q}_{11} & \bar{Q}_{12} & \bar{Q}_{16} \\ \bar{Q}_{12} & \bar{Q}_{22} & \bar{Q}_{26} \\ \bar{Q}_{16} & \bar{Q}_{26} & \bar{Q}_{66} \end{bmatrix} \begin{bmatrix} \varepsilon_x^0 \\ \varepsilon_y^0 \\ \gamma_{xy}^0 \end{bmatrix} \int_{h_{k-1}}^{h_k} z\,dz \right.
$$
$$
\left. + \begin{bmatrix} \bar{Q}_{11} & \bar{Q}_{12} & \bar{Q}_{16} \\ \bar{Q}_{12} & \bar{Q}_{22} & \bar{Q}_{26} \\ \bar{Q}_{16} & \bar{Q}_{26} & \bar{Q}_{66} \end{bmatrix} \begin{bmatrix} \kappa_x \\ \kappa_y \\ \kappa_{xy} \end{bmatrix} \int_{h_{k-1}}^{h_k} z^2\,dz \right\} \tag{115}
$$

By performing a simple integration, we get:

$$
\begin{bmatrix} N_x \\ N_y \\ N_{xy} \end{bmatrix} = \sum_{k=1}^{n} \left\{ \begin{bmatrix} \bar{Q}_{11} & \bar{Q}_{12} & \bar{Q}_{16} \\ \bar{Q}_{12} & \bar{Q}_{22} & \bar{Q}_{26} \\ \bar{Q}_{16} & \bar{Q}_{26} & \bar{Q}_{66} \end{bmatrix}_k \begin{bmatrix} \varepsilon_x^0 \\ \varepsilon_y^0 \\ \gamma_{xy}^0 \end{bmatrix} (h_k - h_{h-1}) \right.
$$
$$
\left. + \begin{bmatrix} \bar{Q}_{11} & \bar{Q}_{12} & \bar{Q}_{16} \\ \bar{Q}_{12} & \bar{Q}_{22} & \bar{Q}_{26} \\ \bar{Q}_{16} & \bar{Q}_{26} & \bar{Q}_{66} \end{bmatrix}_k \begin{bmatrix} \kappa_x \\ \kappa_y \\ \kappa_{xy} \end{bmatrix} \frac{1}{2}(h_k^2 - h_{k-1}^2) \right\} \tag{116}
$$

$$
\begin{bmatrix} M_x \\ M_y \\ M_{xy} \end{bmatrix} = \sum_{k=1}^{n} \left\{ \begin{bmatrix} \bar{Q}_{11} & \bar{Q}_{12} & \bar{Q}_{16} \\ \bar{Q}_{12} & \bar{Q}_{22} & \bar{Q}_{26} \\ \bar{Q}_{16} & \bar{Q}_{26} & \bar{Q}_{66} \end{bmatrix}_k \begin{bmatrix} \varepsilon_x^0 \\ \varepsilon_y^0 \\ \gamma_{xy}^0 \end{bmatrix} \frac{1}{2}(h_k^2 - h_{h-1}^2) \right.
$$
$$
\left. + \begin{bmatrix} \bar{Q}_{11} & \bar{Q}_{12} & \bar{Q}_{16} \\ \bar{Q}_{12} & \bar{Q}_{22} & \bar{Q}_{26} \\ \bar{Q}_{16} & \bar{Q}_{26} & \bar{Q}_{66} \end{bmatrix}_k \begin{bmatrix} \kappa_x \\ \kappa_y \\ \kappa_{xy} \end{bmatrix} \frac{1}{3}(h_k^3 - h_{k-1}^3) \right\} \tag{117}
$$

Since the deformation and curvature of the shear plane are not part of the sums, the laminate stiffness matrix and h_k terms that can be seen in Figure 36 can be combined to create new matrices.

$$
A_{ij} = \sum_{k=1}^{n} [\bar{Q}_{ij}]_k (h_k - h_{k-1}) \tag{118}
$$

$$B_{ij} = \frac{1}{2} \sum_{k=1}^{n} \left[\bar{Q}_{ij} \right]_k (h_k^2 - h_{k-1}^2) \qquad (119)$$

$$D_{ij} = \frac{1}{3} \sum_{k=1}^{n} \left[\bar{Q}_{ij} \right]_k (h_k^3 - h_{k-1}^3) \qquad (120)$$

The extensional stiffness matrix is denoted as matrix A, the coupling stiffness matrix as matrix B, and the bending stiffness matrix as matrix D_{ij}. The bending stiffness matrix relates the amount of plate curvatures with the bending moments. In matrix notation, stress-strain relationship can be written as:

$$
\begin{bmatrix}
N_x \\
N_y \\
N_{xy} \\
- \\
M_x \\
M_y \\
M_{xy}
\end{bmatrix}
=
\begin{bmatrix}
A_{11} & A_{12} & A_{16} & | & B_{11} & B_{12} & B_{16} \\
A_{12} & A_{22} & A_{26} & | & B_{12} & B_{22} & B_{26} \\
A_{16} & A_{26} & A_{66} & | & B_{16} & B_{26} & B_{66} \\
- & - & - & | & - & - & - \\
B_{11} & B_{12} & B_{16} & | & D_{11} & D_{12} & D_{16} \\
B_{12} & B_{22} & B_{26} & | & D_{12} & D_{22} & D_{26} \\
B_{16} & B_{26} & B_{66} & | & D_{16} & D_{26} & D_{66}
\end{bmatrix}
\begin{bmatrix}
\varepsilon_x^0 \\
\varepsilon_y^0 \\
\gamma_{xy}^0 \\
- \\
\kappa_x \\
\kappa_y \\
\kappa_{xy}
\end{bmatrix}
\qquad (121)
$$

13.1.4 Governing plate equations in terms of displacement

By substituting the plate equilibrium equations into the stress-strain relations and then substituting the equations for strain and curvatures, we can derive the governing plate equations in terms of displacement u_0, v_0, and w_0. Further mathematical manipulations lead to:

1) Displacement u_0 (in the x-axis direction):

$$
A_{11} \frac{d^2 u_0}{dx^2} + 2A_{16} \frac{d^2 u_0}{dxdy} + A_{66} \frac{d^2 u_0}{dy^2} + A_{16} \frac{d^2 v_0}{dx^2} + (A_{12} + A_{66}) \frac{d^2 v_0}{dxdy}
$$
$$
+ A_{26} \frac{d^2 v_0}{dy^2} - B_{11} \frac{d^3 w_0}{dx^3} - 3B_{16} \frac{d^3 w_0}{dx^2 dy} \qquad (122)
$$
$$
- (B_{12} + 2B_{66}) \frac{d^3 w_0}{dxdy^2} - B_{26} \frac{d^3 w_0}{dy^3} = 0
$$

2) Displacement v_0 (in the y-axis direction)

$$
A_{16} \frac{d^2 u_0}{dx^2} + (A_{12} + A_{66}) \frac{d^2 u_0}{dxdy} + A_{26} \frac{d^2 u_0}{dy^2} + A_{66} \frac{d^2 v_0}{dx^2} + 2A_{26} \frac{d^2 v_0}{dxdy}
$$
$$
+ A_{22} \frac{d^2 v_0}{dy^2} - B_{16} \frac{d^3 w_0}{dx^3} - (B_{12} + 2B_{66}) \frac{d^3 w_0}{dx^2 dy} \qquad (123)
$$
$$
- 3B_{26} \frac{d^3 w_0}{dxdy^2} - B_{22} \frac{d^3 w_0}{dy^3} = 0
$$

3) Displacement w_0 (in the z-axis direction)

$$D_{11} \frac{d^4 w_0}{dx^4} + 4D_{16} \frac{d^4 w_0}{dx^3 dy} + 2(D_{12} + 2D_{66}) \frac{d^4 w_0}{dx^2 dy^2} + 4D_{26} \frac{d^4 w_0}{dxdy^3}$$

$$+ D_{22} \frac{d^4 w_0}{dy^4} - B_{11} \frac{d^3 u_0}{dx^3} - 3B_{16} \frac{d^3 u_0}{dx^2 dy}$$

$$- (B_{12} + 2B_{66}) \frac{d^3 u_0}{dxdy^2} - B_{26} \frac{d^3 u_0}{dy^3} - B_{16} \frac{d^3 v_0}{dx^3}$$

$$- (B_{12} + 2B_{66}) \frac{d^3 v_0}{dx^2 dy} - 3B_{26} \frac{d^3 v_0}{dxdy^2} - B_{22} \frac{d^3 v_0}{dy^3} = q$$

(124)

13.2 Derivation of relations according to Mindlin-Reissner Plate Theory

13.2.1 Strains and curvatures

The linear strains associated with the displacement field in Eq. (65), (66) and (67) are:

$$\varepsilon_x = \varepsilon_x^0 + z\kappa_x^0 \quad ; \quad \varepsilon_y = \varepsilon_y^0 + z\kappa_y^0 \quad ; \quad \varepsilon_{xy} = \varepsilon_{xy}^0 + z\kappa_{xy}^0 \tag{125}$$

$$\varepsilon_{yz} = \gamma_{yz}^0 \quad ; \quad \varepsilon_{xz} = \gamma_{xz}^0 \tag{126}$$

The strain and curvature displacement equations of linear strain are given by:

$$\kappa_x^0 = \frac{d\phi_x}{dx} \quad ; \quad \kappa_y^0 = \frac{d\phi_y}{dy} \quad ; \quad \kappa_{xy}^0 = \left(\frac{d\phi_x}{dy} + \frac{d\phi_y}{dx} \right) \tag{127}$$

$$\varepsilon_x^0 = \frac{du_0}{dx} \quad ; \quad \varepsilon_y^0 = \frac{dv_0}{dy} \quad ; \quad \varepsilon_{xy}^0 = \left(\frac{du_0}{dy} + \frac{dv_0}{dx} \right) \tag{128}$$

$$\gamma_{yz}^0 = \phi_y + \frac{dw}{dy} \quad ; \quad \gamma_{xz}^0 = \phi_x + \frac{dw}{dx} \tag{129}$$

In matrix form:

$$[\kappa] = \begin{bmatrix} \kappa_x \\ \kappa_y \\ \kappa_{xy} \end{bmatrix} = \begin{bmatrix} \dfrac{d\phi_x}{dx} \\ \dfrac{d\phi_y}{dy} \\ \left(\dfrac{d\phi_x}{dy} + \dfrac{d\phi_y}{dx} \right) \end{bmatrix} \quad ; \quad [\varepsilon] = \begin{bmatrix} \varepsilon_x \\ \varepsilon_y \\ \varepsilon_{xy} \end{bmatrix} = \begin{bmatrix} \dfrac{du_0}{dx} \\ \dfrac{dv_0}{dy} \\ \left(\dfrac{du_0}{dy} + \dfrac{dv_0}{dx} \right) \end{bmatrix} \tag{130}$$

$$[\gamma] = \begin{bmatrix} \gamma_{yz} \\ \gamma_{xz} \end{bmatrix} = \begin{bmatrix} \phi_y + \dfrac{dw}{dy} \\ \phi_x + \dfrac{dw}{dx} \end{bmatrix} \tag{131}$$

13.2.2 Equilibrium equations

If we do not proceed from the assumptions of Kirchhoff-Love's thin plate theory that the shear stresses R_{xz} and R_{yz} are zero over the thickness of the plate, then the equations of equilibrium can be rewritten in the following form:

- Equilibrium equation o of forces in the x-axis direction:

$$-N_x\,dy + \left(N_x + \frac{dN_x}{dx}dx\right)dy - N_{xy}dx + \left(N_{xy} + \frac{dN_{xy}}{dy}dy\right)dx = 0 \quad (132)$$

in reduced form in x and y-direction:

$$\frac{dN_x}{dx} + \frac{dN_{xy}}{dy} = 0 \;\; ; \;\; \frac{dN_{xy}}{dx} + \frac{dN_y}{dy} = 0 \quad\quad (133)$$

- Equation of balance of forces in the z-axis direction:

$$-R_{xz}dy + \left(R_{xz} + \frac{dR_{xz}}{dx}dx\right)dy - R_{yz}dx + \left(R_{yz} + \frac{dR_{yz}}{dy}dy\right)dx$$
$$+ p\,dxdy = 0 \quad\quad (134)$$

in reduced form:

$$\frac{dR_{xz}}{dx} + \frac{dR_{yz}}{dy} + p = 0 \quad\quad (135)$$

- Moment equations of equilibrium around the x-axis:

$$M_y dx - \left(M_y + \frac{dM_y}{dy}dy\right)dx + M_{xy}dy - \left(M_{xy} + \frac{dM_{xy}}{dx}dx\right)dy$$
$$+ \left(R_{yz} + \frac{dR_{yz}}{dy}dy\right)dxdy + \frac{dy}{2}\left(R_{xz} + \frac{dR_{xz}}{dx}dx\right)dy \quad\quad (136)$$
$$- \frac{dy}{2}R_{xz}dy + p\,dxdy = 0$$

in reduced form:

$$\frac{dM_x}{dx} + \frac{dM_{xy}}{dy} - R_{xz} = 0 \quad\quad (137)$$

- Similarly, the moment equations of equilibrium about the y-axis:

$$\frac{dM_{xy}}{dx} + \frac{dM_y}{dy} - R_{yz} = 0 \quad\quad (138)$$

These four resulting equilibrium equations are the foundation for the establishment of governing plate equations in terms of displacement for Mindlin-Reissner plate theory in the following chapters.

13.2.3 Orthotropic plate stress-strain relationship

Similar to Kirchhoff-Love plate theory, the stress-strain relationship for an orthotropic laminate with layers of different orientations can be written as:

$$\begin{bmatrix} \sigma_x \\ \sigma_y \\ \sigma_{xy} \\ \sigma_{yz} \\ \sigma_{xz} \end{bmatrix} = \begin{bmatrix} \bar{Q}_{11} & \bar{Q}_{12} & \bar{Q}_{16} & 0 & 0 \\ \bar{Q}_{12} & \bar{Q}_{22} & \bar{Q}_{26} & 0 & 0 \\ \bar{Q}_{16} & \bar{Q}_{26} & \bar{Q}_{66} & 0 & 0 \\ 0 & 0 & 0 & \bar{Q}_{44} & \bar{Q}_{45} \\ 0 & 0 & 0 & \bar{Q}_{45} & \bar{Q}_{55} \end{bmatrix}_k \begin{bmatrix} \varepsilon_x \\ \varepsilon_y \\ \gamma_{xy} \\ \gamma_{yz} \\ \gamma_{xz} \end{bmatrix} \qquad (139)$$

Where $\bar{Q}_{ij}$ is the transformed stiffness matrix. Stress-resultants for Mindlin-Reissner can be derived, as in Kirchhoff-Love plate theory, from the relations:

$$(N_x, N_y, N_{xy}) = \int_{-h/2}^{h/2} (\sigma_x, \sigma_y \sigma_{xy}) dz \qquad (140)$$

$$(M_x, M_y, M_{xy}) = \int_{-h/2}^{h/2} (\sigma_x, \sigma_y \sigma_{xy}) z dz \qquad (141)$$

$$(Q_x, Q_y) = \int_{-h/2}^{h/2} (\sigma_{xz}, \sigma_{yz}) dz \qquad (142)$$

Similar to Kirchhoff-Love plate theory, the stress-strain relationship for an orthotropic laminate with layers of different orientations written according to Thai (2013) as:

$$\begin{bmatrix} N_x \\ N_y \\ N_{xy} \\ M_x \\ M_y \\ M_{xy} \end{bmatrix} = \begin{bmatrix} A_{11} & A_{12} & A_{16} & B_{11} & B_{12} & B_{16} \\ A_{12} & A_{22} & A_{26} & B_{12} & B_{22} & B_{26} \\ A_{16} & A_{26} & A_{66} & B_{16} & B_{26} & B_{66} \\ B_{11} & B_{12} & B_{16} & D_{11} & D_{12} & D_{16} \\ B_{12} & B_{22} & B_{26} & D_{12} & D_{22} & D_{26} \\ B_{16} & B_{26} & B_{66} & D_{16} & D_{26} & D_{66} \end{bmatrix} \begin{bmatrix} \varepsilon_x \\ \varepsilon_y \\ \varepsilon_{xy} \\ \kappa_x \\ \kappa_y \\ \kappa_{xy} \end{bmatrix} \qquad (143)$$

Where

$$A_{ij} = \sum_{k=1}^{N} (\bar{Q}_{ij})_{(k)} (z_{k+1} - z_k) \qquad (144)$$

$$B_{ij} = \frac{1}{2} \sum_{k=1}^{N} (\bar{Q}_{ij})_{(k)} (z_{k+1}^2 - z_k^2) \qquad (145)$$

$$D_{ij} = \frac{1}{3} \sum_{k=1}^{N} (\bar{Q}_{ij})_{(k)} (z_{k+1}^3 - z_k^3) \qquad (146)$$

In addition, according to Balogh (2013) following laminate constitutive equations:

$$\begin{bmatrix} Q_y \\ Q_x \end{bmatrix} = \begin{bmatrix} A_{44} & A_{45} \\ A_{45} & A_{55} \end{bmatrix} \begin{bmatrix} \phi_y + \dfrac{dw}{dy} \\ \phi_y + \dfrac{dw}{dx} \end{bmatrix} \tag{147}$$

where

$$A_{ij} = \sum_{k=1}^{N} \left(\bar{Q}_{ij} \right)_{(k)} (z_{k+1} - z_k) \tag{148}$$

13.2.4 Governing plate equations in terms of displacement

After substituting the plate equilibrium equations into the stress-strain relations and then replacing the strain curvatures equations, we obtain the governing plate equations in terms of displacement u_0, v_0, w_0, ϕ_x, and ϕ_y. Further mathematical modifications result in:

1) Equation for displacement u_0 (in the x-axis direction):

$$\begin{aligned}
A_{11} \frac{\partial^2 u_0}{\partial x^2} &+ A_{12} \frac{\partial^2 v_0}{\partial x \partial y} + A_{16} \left(\frac{\partial^2 u_0}{\partial x \partial y} + \frac{\partial^2 v_0}{\partial x^2} \right) + B_{11} \frac{\partial^2 \phi_x}{\partial x^2} + B_{12} \frac{\partial^2 \phi_y}{\partial x \partial y} \\
&+ B_{16} \left(\frac{\partial^2 \phi_x}{\partial x \partial y} + \frac{\partial^2 \phi_y}{\partial x^2} \right) + A_{16} \frac{\partial^2 u_0}{\partial x \partial y} + A_{26} \frac{\partial^2 v_0}{\partial y^2} \\
&+ A_{66} \left(\frac{\partial^2 u_0}{\partial y^2} + \frac{\partial^2 v_0}{\partial x \partial y} \right) + B_{16} \frac{\partial^2 \phi_x}{\partial x \partial y} + B_{26} \frac{\partial^2 \phi_y}{\partial y^2} \\
&+ B_{66} \left(\frac{\partial^2 \phi_x}{\partial y^2} + \frac{\partial^2 \phi_y}{\partial x \partial y} \right) = 0
\end{aligned} \tag{149}$$

1) Equation for displacement v_0 (in the y-axis direction):

$$\begin{aligned}
A_{16} \frac{\partial^2 u_0}{\partial x^2} &+ A_{26} \frac{\partial^2 v_0}{\partial x \partial y} + A_{66} \left(\frac{\partial^2 u_0}{\partial y \partial x} + \frac{\partial^2 v_0}{\partial x^2} \right) + B_{16} \frac{\partial^2 \phi_x}{\partial x^2} + B_{26} \frac{\partial^2 \phi_y}{\partial x \partial y} \\
&+ B_{66} \left(\frac{\partial^2 \phi_x}{\partial x \partial y} + \frac{\partial^2 \phi_y}{\partial x^2} \right) + A_{12} \frac{\partial^2 u_0}{\partial x \partial y} + A_{22} \frac{\partial^2 v_0}{\partial y^2} \\
&+ A_{26} \left(\frac{\partial^2 u_0}{\partial y^2} + \frac{\partial^2 v_0}{\partial x \partial y} \right) + B_{12} \frac{\partial^2 \phi_x}{\partial x \partial y} + B_{22} \frac{\partial^2 \phi_y}{\partial y^2} \\
&+ B_{26} \left(\frac{\partial^2 \phi_x}{\partial y^2} + \frac{\partial^2 \phi_y}{\partial x \partial y} \right) = 0
\end{aligned} \tag{150}$$

2) Equation for displacement w_0 (in the z-axis direction):

$$\begin{aligned}
A_{45} \left(\frac{\partial \phi_y}{\partial x} + \frac{\partial^2 w}{\partial x \partial y} \right) &+ A_{55} \left(\frac{\partial \phi_x}{\partial x} + \frac{\partial^2 w}{\partial x^2} \right) + A_{44} \left(\frac{\partial \phi_y}{\partial y} + \frac{\partial^2 w}{\partial y^2} \right) \\
&+ A_{45} \left(\frac{\partial \phi_x}{\partial y} + \frac{\partial^2 w}{\partial x \partial y} \right) + p = 0
\end{aligned} \tag{151}$$

3) Equation for displacement ϕ_x (rotation of the perpendicular to the midplane in the zx-plane)

$$B_{11}\frac{\partial^2 u_0}{\partial x^2} + B_{12}\frac{\partial^2 v_0}{\partial x\partial y} + B_{16}\left(\frac{\partial^2 u_0}{\partial x\partial y} + \frac{\partial^2 v_0}{\partial x^2}\right) + D_{11}\frac{\partial^2 \phi_x}{\partial x^2} + D_{12}\frac{\partial^2 \phi_y}{\partial x\partial y}$$
$$+ D_{16}\left(\frac{\partial^2 \phi_x}{\partial x\partial y} + \frac{\partial^2 \phi_y}{\partial x^2}\right) + B_{16}\frac{\partial^2 u_0}{\partial x\partial y} + B_{26}\frac{\partial^2 v_0}{\partial y^2}$$
$$+ B_{66}\left(\frac{\partial^2 u_0}{\partial y^2} + \frac{\partial^2 v_0}{\partial x\partial y}\right) + D_{16}\frac{\partial^2 \phi_x}{\partial x\partial y} + D_{26}\frac{\partial^2 \phi_y}{\partial y^2}$$
$$+ D_{66}\left(\frac{\partial^2 \phi_x}{\partial y^2} + \frac{\partial^2 \phi_y}{\partial x\partial y}\right) = A_{45}\left(\phi_y + \frac{\partial w}{\partial y}\right) + A_{55}\left(\phi_x + \frac{\partial w}{\partial x}\right) \tag{152}$$

4) Equation for displacement ϕ_y (rotation of the perpendicular to the midplane in the zy-plane)

$$B_{16}\frac{\partial^2 u_0}{\partial x^2} + B_{26}\frac{\partial^2 v_0}{\partial x\partial y} + B_{66}\left(\frac{\partial^2 u_0}{\partial x\partial y} + \frac{\partial^2 v_0}{\partial x^2}\right) + D_{16}\frac{\partial^2 \phi_x}{\partial x^2} + D_{26}\frac{\partial^2 \phi_y}{\partial x\partial y}$$
$$+ D_{66}\left(\frac{\partial^2 \phi_x}{\partial x\partial y} + \frac{\partial^2 \phi_y}{\partial x^2}\right) + B_{12}\frac{\partial^2 u_0}{\partial x\partial y} + B_{22}\frac{\partial^2 v_0}{\partial y^2}$$
$$+ B_{26}\left(\frac{\partial^2 u_0}{\partial y^2} + \frac{\partial^2 v_0}{\partial x\partial y}\right) + D_{12}\frac{\partial^2 \phi_x}{\partial x\partial y} + D_{22}\frac{\partial^2 \phi_y}{\partial y^2}$$
$$+ D_{26}\left(\frac{\partial^2 \phi_x}{\partial y^2} + \frac{\partial^2 \phi_y}{\partial x\partial y}\right)$$
$$= A_{44}\left(\phi_y + \frac{\partial w}{\partial y}\right) + A_{45}\left(\phi_x + \frac{\partial w}{\partial x}\right) \tag{153}$$

13.3 Derivation of relations according to Second Order Shear Deformation Theory

13.3.1 Strains and curvatures

The linear strains associated with the displacement field in Eq. (68), (69) and (70) are according to Khdeir (1999):

$$\varepsilon_x = \varepsilon_x^0 + z\kappa_x^0 + z^2\kappa_x^1 \quad ; \quad \varepsilon_y = \varepsilon_y^0 + z\kappa_y^0 + z^2\kappa_y^1 \tag{154}$$

$$\gamma_{yz} = \gamma_{yz}^0 + \gamma_{yz}^1 \quad ; \quad \gamma_{xz} = \gamma_{xz}^0 + \gamma_{xz}^1 \tag{155}$$

$$\varepsilon_{xy} = \varepsilon_{xy}^0 + \kappa_{xy}^0 + \kappa_{xy}^1 \tag{156}$$

where

$$\varepsilon_x^0 = \frac{du_0}{dx} \quad ; \quad \varepsilon_y^0 = \frac{dv_0}{dy} \quad ; \quad \varepsilon_{xy}^0 = \gamma_{xy}^0 = \left(\frac{du_0}{dy} + \frac{dv_0}{dx}\right) \tag{157}$$

$$\kappa_x^0 = \frac{d\phi_1}{dx} \quad ; \quad \kappa_y^0 = \frac{d\psi_1}{dy} \quad ; \quad \kappa_{xy}^0 = \left(\frac{d\phi_1}{dy} + \frac{d\psi_1}{dx}\right) \tag{158}$$

$$\kappa_x^1 = \frac{d\phi_2}{dx} \quad ; \quad \kappa_y^1 = \frac{d\psi_2}{dy} \quad ; \quad \kappa_{xy}^1 = \left(\frac{d\phi_2}{dy} + \frac{d\psi_2}{dx}\right) \tag{159}$$

$$\gamma_{yz}^0 = \left(\psi_1 + \frac{dw_0}{dy}\right) \quad ; \quad \gamma_{xz}^0 = \left(\phi_1 + \frac{dw_0}{dx}\right) \tag{160}$$

$$\gamma_{yz}^1 = 2\psi_2 \quad ; \quad \gamma_{xz}^1 = 2\phi_2 \tag{161}$$

In matrix form:

$$[\varepsilon^0] = \begin{bmatrix} \varepsilon_x^0 \\ \varepsilon_y^0 \\ \varepsilon_{xy}^0 \end{bmatrix} = \begin{bmatrix} \dfrac{du_0}{dx} \\ \dfrac{dv_0}{dy} \\ \left(\dfrac{du_0}{dy} + \dfrac{dv_0}{dx}\right) \end{bmatrix} \quad ; \quad [\kappa^0] = \begin{bmatrix} \kappa_x^0 \\ \kappa_y^0 \\ \kappa_{xy}^0 \end{bmatrix} = \begin{bmatrix} \dfrac{d\phi_1}{dx} \\ \dfrac{d\psi_1}{dy} \\ \left(\dfrac{d\phi_1}{dy} + \dfrac{d\psi_1}{dx}\right) \end{bmatrix} \tag{162}$$

$$[\kappa^1] = \begin{bmatrix} \kappa_x^1 \\ \kappa_y^1 \\ \kappa_{xy}^1 \end{bmatrix} = \begin{bmatrix} \dfrac{d\phi_2}{dx} \\ \dfrac{d\psi_2}{dy} \\ \left(\dfrac{d\phi_2}{dy} + \dfrac{d\psi_2}{dx}\right) \end{bmatrix} \tag{163}$$

$$[\gamma^0] = \begin{bmatrix} \gamma_{yz}^0 \\ \gamma_{xz}^0 \end{bmatrix} = \begin{bmatrix} \left(\psi_1 + \dfrac{dw_0}{dy}\right) \\ \left(\phi_1 + \dfrac{dw_0}{dx}\right) \end{bmatrix} \quad [\gamma^1] = \begin{bmatrix} \gamma_{yz}^1 \\ \gamma_{xz}^1 \end{bmatrix} = \begin{bmatrix} 2\psi_2 \\ 2\phi_2 \end{bmatrix} \tag{164}$$

13.3.2 Equilibrium equations

Similar to CPT and FSDT, the equation of equilibrium is determined from the forces and moments acting in the plane of the plate.

Stress resultant in x and y-direction:

$$\frac{dN_x}{dx} + \frac{dN_{xy}}{dy} = 0 \quad ; \quad \frac{dN_{xy}}{dx} + \frac{dN_y}{dy} = 0 \tag{165}$$

Stress resultant in z-direction:

$$\frac{dQ_x}{dx} + \frac{dQ_y}{dy} + p(x,y) = 0 \tag{166}$$

Moment resultant about x and y-axis:

$$\frac{dM_x}{dx} + \frac{dM_{xy}}{dy} - Q_x = 0 \quad ; \quad \frac{dM_{xy}}{dx} + \frac{dM_y}{dy} - Q_y = 0 \qquad (167)$$

The components representing second order stress resultants in x and y-direction are then written as:

$$\frac{dL_x}{dx} + \frac{dL_{xy}}{dy} - 2R_x = 0 \quad ; \quad \frac{dL_{xy}}{dx} + \frac{dL_y}{dy} - 2R_y = 0 \qquad (168)$$

13.3.3 Orthotropic plate stress-strain relationship

The stress-strain relations for the kth lamina in the laminate coordinates are given by:

$$
\begin{bmatrix} \sigma_x \\ \sigma_y \\ \sigma_{xy} \\ \sigma_{yz} \\ \sigma_{xz} \end{bmatrix}_{(k)}
=
\begin{bmatrix}
\bar{Q}_{11} & \bar{Q}_{12} & \bar{Q}_{16} & 0 & 0 \\
\bar{Q}_{12} & \bar{Q}_{22} & \bar{Q}_{26} & 0 & 0 \\
\bar{Q}_{16} & \bar{Q}_{26} & \bar{Q}_{66} & 0 & 0 \\
0 & 0 & 0 & \bar{Q}_{44} & \bar{Q}_{45} \\
0 & 0 & 0 & \bar{Q}_{45} & \bar{Q}_{55}
\end{bmatrix}_{(k)}
\begin{bmatrix} \varepsilon_x \\ \varepsilon_y \\ \varepsilon_{xy} \\ \varepsilon_{yz} \\ \varepsilon_{xz} \end{bmatrix}
\qquad (169)
$$

Where $\bar{Q}_{ij}$ is the transformed stiffness matrix.

Stress-resultants for SSDT are according to Khdeir (1999) defined as:

$$(N_x, N_y, N_{xy}) = \sum_{k=1}^{N} \int_{-h/2}^{h/2} (\sigma_x, \sigma_y, \sigma_{xy}) dz \qquad (170)$$

$$(M_x, M_y, M_{xy}) = \sum_{k=1}^{N} \int_{-h/2}^{h/2} (\sigma_x, \sigma_y, \sigma_{xy}) z\, dz \qquad (171)$$

$$(L_x, L_y, L_{xy}) = \sum_{k=1}^{N} \int_{-h/2}^{h/2} (\sigma_x, \sigma_y \sigma_{xy}) z^2\, dz \qquad (172)$$

$$(Q_y, Q_x) = \sum_{k=1}^{N} \int_{-h/2}^{h/2} (\sigma_{yz}, \sigma_{xz}) dz \qquad (173)$$

$$(R_y, R_x) = \sum_{k=1}^{N} \int_{-h/2}^{h/2} (\sigma_{yz}, \sigma_{xz}) z\, dz \qquad (174)$$

Substituting equations (170) - (174) into equation (169) we obtain the following relations:

$$\begin{bmatrix} N_x \\ N_y \\ N_{xy} \end{bmatrix} = \sum_{k=1}^{n} \left\{ \int_{h_{k-1}}^{h_k} \begin{bmatrix} \bar{Q}_{11} & \bar{Q}_{12} & \bar{Q}_{16} \\ \bar{Q}_{12} & \bar{Q}_{22} & \bar{Q}_{26} \\ \bar{Q}_{16} & \bar{Q}_{26} & \bar{Q}_{66} \end{bmatrix} \begin{bmatrix} \varepsilon_x^0 \\ \varepsilon_y^0 \\ \varepsilon_{xy}^0 \end{bmatrix} dz \right.$$
$$+ \int_{h_{k-1}}^{h_k} \begin{bmatrix} \bar{Q}_{11} & \bar{Q}_{12} & \bar{Q}_{16} \\ \bar{Q}_{12} & \bar{Q}_{22} & \bar{Q}_{26} \\ \bar{Q}_{16} & \bar{Q}_{26} & \bar{Q}_{66} \end{bmatrix} \begin{bmatrix} \kappa_x^0 \\ \kappa_y^0 \\ \kappa_{xy}^0 \end{bmatrix} z\,dz \tag{175}$$
$$\left. + \int_{h_{k-1}}^{h_k} \begin{bmatrix} \bar{Q}_{11} & \bar{Q}_{12} & \bar{Q}_{16} \\ \bar{Q}_{12} & \bar{Q}_{22} & \bar{Q}_{26} \\ \bar{Q}_{16} & \bar{Q}_{26} & \bar{Q}_{66} \end{bmatrix} \begin{bmatrix} \kappa_x^1 \\ \kappa_y^1 \\ \kappa_{xy}^1 \end{bmatrix} z^2\,dz \right\}$$

$$\begin{bmatrix} M_x \\ M_y \\ M_{xy} \end{bmatrix} = \sum_{k=1}^{n} \left\{ \int_{h_{k-1}}^{h_k} \begin{bmatrix} \bar{Q}_{11} & \bar{Q}_{12} & \bar{Q}_{16} \\ \bar{Q}_{12} & \bar{Q}_{22} & \bar{Q}_{26} \\ \bar{Q}_{16} & \bar{Q}_{26} & \bar{Q}_{66} \end{bmatrix} \begin{bmatrix} \varepsilon_x^0 \\ \varepsilon_y^0 \\ \varepsilon_{xy}^0 \end{bmatrix} z\,dz \right.$$
$$+ \int_{h_{k-1}}^{h_k} \begin{bmatrix} \bar{Q}_{11} & \bar{Q}_{12} & \bar{Q}_{16} \\ \bar{Q}_{12} & \bar{Q}_{22} & \bar{Q}_{26} \\ \bar{Q}_{16} & \bar{Q}_{26} & \bar{Q}_{66} \end{bmatrix} \begin{bmatrix} \kappa_x^0 \\ \kappa_y^0 \\ \kappa_{xy}^0 \end{bmatrix} z^2\,dz \tag{176}$$
$$\left. + \int_{h_{k-1}}^{h_k} \begin{bmatrix} \bar{Q}_{11} & \bar{Q}_{12} & \bar{Q}_{16} \\ \bar{Q}_{12} & \bar{Q}_{22} & \bar{Q}_{26} \\ \bar{Q}_{16} & \bar{Q}_{26} & \bar{Q}_{66} \end{bmatrix} \begin{bmatrix} \kappa_x^1 \\ \kappa_y^1 \\ \kappa_{xy}^1 \end{bmatrix} z^3\,dz \right\}$$

$$\begin{bmatrix} L_x \\ L_y \\ L_{xy} \end{bmatrix} = \sum_{k=1}^{n} \left\{ \int_{h_{k-1}}^{h_k} \begin{bmatrix} \bar{Q}_{11} & \bar{Q}_{12} & \bar{Q}_{16} \\ \bar{Q}_{12} & \bar{Q}_{22} & \bar{Q}_{26} \\ \bar{Q}_{16} & \bar{Q}_{26} & \bar{Q}_{66} \end{bmatrix} \begin{bmatrix} \varepsilon_x^0 \\ \varepsilon_y^0 \\ \varepsilon_{xy}^0 \end{bmatrix} z^2\,dz \right.$$
$$+ \int_{h_{k-1}}^{h_k} \begin{bmatrix} \bar{Q}_{11} & \bar{Q}_{12} & \bar{Q}_{16} \\ \bar{Q}_{12} & \bar{Q}_{22} & \bar{Q}_{26} \\ \bar{Q}_{16} & \bar{Q}_{26} & \bar{Q}_{66} \end{bmatrix} \begin{bmatrix} \kappa_x^0 \\ \kappa_y^0 \\ \kappa_{xy}^0 \end{bmatrix} z^3\,dz \tag{177}$$
$$\left. + \int_{h_{k-1}}^{h_k} \begin{bmatrix} \bar{Q}_{11} & \bar{Q}_{12} & \bar{Q}_{16} \\ \bar{Q}_{12} & \bar{Q}_{22} & \bar{Q}_{26} \\ \bar{Q}_{16} & \bar{Q}_{26} & \bar{Q}_{66} \end{bmatrix} \begin{bmatrix} \kappa_x^1 \\ \kappa_y^1 \\ \kappa_{xy}^1 \end{bmatrix} z^4\,dz \right\}$$

$$\begin{bmatrix} Q_y \\ Q_x \end{bmatrix} = \sum_{h_{k-1}}^{n} \left\{ \int_{h_{k-1}}^{h_k} \begin{bmatrix} \bar{Q}_{44} & \bar{Q}_{45} \\ \bar{Q}_{45} & \bar{Q}_{55} \end{bmatrix} \begin{bmatrix} \gamma_{yz}^0 \\ \gamma_{xz}^0 \end{bmatrix} dz \right.$$
$$\left. + \int_{h_{k-1}}^{h_k} \begin{bmatrix} \bar{Q}_{44} & \bar{Q}_{45} \\ \bar{Q}_{45} & \bar{Q}_{55} \end{bmatrix} \begin{bmatrix} \gamma_{yz}^1 \\ \gamma_{xz}^1 \end{bmatrix} z\,dz \right\} \tag{178}$$

$$\begin{bmatrix} R_y \\ R_x \end{bmatrix} = \sum_{h_{k-1}}^{n} \left\{ \int_{h_{k-1}}^{h_k} \begin{bmatrix} \bar{Q}_{44} & \bar{Q}_{45} \\ \bar{Q}_{45} & \bar{Q}_{55} \end{bmatrix} \begin{bmatrix} \gamma_{yz}^0 \\ \gamma_{xz}^0 \end{bmatrix} z\,dz \right.$$
$$\left. + \int_{h_{k-1}}^{h_k} \begin{bmatrix} \bar{Q}_{44} & \bar{Q}_{45} \\ \bar{Q}_{45} & \bar{Q}_{55} \end{bmatrix} \begin{bmatrix} \gamma_{yz}^1 \\ \gamma_{xz}^1 \end{bmatrix} z^2\,dz \right\} \tag{179}$$

Strains and curvatures (ε_0, κ_0) are not a function of z (these values are always 0 in the midplane), they need not be part of the integration. At the same time, the

laminate stiffness matrix is constant for a given layer and thus will be constant in the laminate thickness integration. By expelling these constants before the integral and then integrating, we obtain:

$$
\begin{bmatrix} N_x \\ N_y \\ N_{xy} \end{bmatrix} = \sum_{k=1}^{n} \left\{ \begin{bmatrix} \bar{Q}_{11} & \bar{Q}_{12} & \bar{Q}_{16} \\ \bar{Q}_{12} & \bar{Q}_{22} & \bar{Q}_{26} \\ \bar{Q}_{16} & \bar{Q}_{26} & \bar{Q}_{66} \end{bmatrix}_k \begin{bmatrix} \varepsilon_x^0 \\ \varepsilon_y^0 \\ \varepsilon_{xy}^0 \end{bmatrix} (h_k - h_{k-1}) \right.
$$
$$
+ \begin{bmatrix} \bar{Q}_{11} & \bar{Q}_{12} & \bar{Q}_{16} \\ \bar{Q}_{12} & \bar{Q}_{22} & \bar{Q}_{26} \\ \bar{Q}_{16} & \bar{Q}_{26} & \bar{Q}_{66} \end{bmatrix}_k \begin{bmatrix} \kappa_x^0 \\ \kappa_y^0 \\ \kappa_{xy}^0 \end{bmatrix} \frac{1}{2} (h_k^2 - h_{k-1}^2)
$$
$$
\left. + \begin{bmatrix} \bar{Q}_{11} & \bar{Q}_{12} & \bar{Q}_{16} \\ \bar{Q}_{12} & \bar{Q}_{22} & \bar{Q}_{26} \\ \bar{Q}_{16} & \bar{Q}_{26} & \bar{Q}_{66} \end{bmatrix}_k \begin{bmatrix} \kappa_x^1 \\ \kappa_y^1 \\ \kappa_{xy}^1 \end{bmatrix} \frac{1}{3} (h_k^3 - h_{k-1}^3) \right\} \tag{180}
$$

$$
\begin{bmatrix} M_x \\ M_y \\ M_{xy} \end{bmatrix} = \sum_{k=1}^{n} \left\{ \begin{bmatrix} \bar{Q}_{11} & \bar{Q}_{12} & \bar{Q}_{16} \\ \bar{Q}_{12} & \bar{Q}_{22} & \bar{Q}_{26} \\ \bar{Q}_{16} & \bar{Q}_{26} & \bar{Q}_{66} \end{bmatrix}_k \begin{bmatrix} \varepsilon_x^0 \\ \varepsilon_y^0 \\ \varepsilon_{xy}^0 \end{bmatrix} \frac{1}{2} (h_k^2 - h_{k-1}^2) \right.
$$
$$
+ \begin{bmatrix} \bar{Q}_{11} & \bar{Q}_{12} & \bar{Q}_{16} \\ \bar{Q}_{12} & \bar{Q}_{22} & \bar{Q}_{26} \\ \bar{Q}_{16} & \bar{Q}_{26} & \bar{Q}_{66} \end{bmatrix}_k \begin{bmatrix} \kappa_x^0 \\ \kappa_y^0 \\ \kappa_{xy}^0 \end{bmatrix} \frac{1}{3} (h_k^3 - h_{k-1}^3)
$$
$$
\left. + \begin{bmatrix} \bar{Q}_{11} & \bar{Q}_{12} & \bar{Q}_{16} \\ \bar{Q}_{12} & \bar{Q}_{22} & \bar{Q}_{26} \\ \bar{Q}_{16} & \bar{Q}_{26} & \bar{Q}_{66} \end{bmatrix}_k \begin{bmatrix} \kappa_x^1 \\ \kappa_y^1 \\ \kappa_{xy}^1 \end{bmatrix} \frac{1}{4} (h_k^4 - h_{k-1}^4) \right\} \tag{181}
$$

$$
\begin{bmatrix} L_x \\ L_y \\ L_{xy} \end{bmatrix} = \sum_{k=1}^{n} \left\{ \begin{bmatrix} \bar{Q}_{11} & \bar{Q}_{12} & \bar{Q}_{16} \\ \bar{Q}_{12} & \bar{Q}_{22} & \bar{Q}_{26} \\ \bar{Q}_{16} & \bar{Q}_{26} & \bar{Q}_{66} \end{bmatrix}_k \begin{bmatrix} \varepsilon_x^0 \\ \varepsilon_y^0 \\ \varepsilon_{xy}^0 \end{bmatrix} \frac{1}{3} (h_k^3 - h_{k-1}^3) \right.
$$
$$
+ \begin{bmatrix} \bar{Q}_{11} & \bar{Q}_{12} & \bar{Q}_{16} \\ \bar{Q}_{12} & \bar{Q}_{22} & \bar{Q}_{26} \\ \bar{Q}_{16} & \bar{Q}_{26} & \bar{Q}_{66} \end{bmatrix}_k \begin{bmatrix} \kappa_x^0 \\ \kappa_y^0 \\ \kappa_{xy}^0 \end{bmatrix} \frac{1}{4} (h_k^4 - h_{k-1}^4)
$$
$$
\left. + \begin{bmatrix} \bar{Q}_{11} & \bar{Q}_{12} & \bar{Q}_{16} \\ \bar{Q}_{12} & \bar{Q}_{22} & \bar{Q}_{26} \\ \bar{Q}_{16} & \bar{Q}_{26} & \bar{Q}_{66} \end{bmatrix}_k \begin{bmatrix} \kappa_x^1 \\ \kappa_y^1 \\ \kappa_{xy}^1 \end{bmatrix} \frac{1}{5} (h_k^5 - h_{k-1}^5) \right\} \tag{182}
$$

$$
\begin{bmatrix} Q_y \\ Q_x \end{bmatrix} = \sum_{h_{k-1}}^{n} \left\{ \begin{bmatrix} \bar{Q}_{44} & \bar{Q}_{45} \\ \bar{Q}_{45} & \bar{Q}_{55} \end{bmatrix}_k \begin{bmatrix} \gamma_{yz}^0 \\ \gamma_{xz}^0 \end{bmatrix} (h_k - h_{k-1}) \right.
$$
$$
\left. + \begin{bmatrix} \bar{Q}_{44} & \bar{Q}_{45} \\ \bar{Q}_{45} & \bar{Q}_{55} \end{bmatrix} \begin{bmatrix} \gamma_{yz}^1 \\ \gamma_{xz}^1 \end{bmatrix} \frac{1}{2} (h_k^2 - h_{k-1}^2) \right\} \tag{183}
$$

$$
\begin{bmatrix} R_y \\ R_x \end{bmatrix} = \sum_{h_{k-1}}^{n} \left\{ \begin{bmatrix} \bar{Q}_{44} & \bar{Q}_{45} \\ \bar{Q}_{45} & \bar{Q}_{55} \end{bmatrix}_k \begin{bmatrix} \gamma_{yz}^0 \\ \gamma_{xz}^0 \end{bmatrix} \frac{1}{2} (h_k^2 - h_{k-1}^2) \right.
$$
$$
\left. + \begin{bmatrix} \bar{Q}_{44} & \bar{Q}_{45} \\ \bar{Q}_{45} & \bar{Q}_{55} \end{bmatrix} \begin{bmatrix} \gamma_{yz}^1 \\ \gamma_{xz}^1 \end{bmatrix} \frac{1}{3} (h_k^3 - h_{k-1}^3) \right\} \tag{184}
$$

Since the deformation and curvature of the shear plane are not part of the sums, the laminate stiffness matrix and h_k terms can be combined to create new matrices.

$$A_{ij} = \sum_{k=1}^{n} [\bar{Q}_{ij}]_k (h_k - h_{k-1}) \tag{185}$$

$$B_{ij} = \frac{1}{2} \sum_{k=1}^{n} [\bar{Q}_{ij}]_k (h_k^2 - h_{k-1}^2) \tag{186}$$

$$D_{ij} = \frac{1}{3} \sum_{k=1}^{n} [\bar{Q}_{ij}]_k (h_k^3 - h_{k-1}^3) \tag{187}$$

$$E_{ij} = \frac{1}{4} \sum_{k=1}^{n} [\bar{Q}_{ij}]_k (h_k^4 - h_{k-1}^4) \tag{188}$$

$$F_{ij} = \frac{1}{5} \sum_{k=1}^{n} [\bar{Q}_{ij}]_k (h_k^5 - h_{k-1}^5) \tag{189}$$

Where A_{ij} is extensional stiffness matrix, B_{ij} is extension-bending coupling matrix, D_{ij} is bending stiffness matrix, E_{ij} is second order coupling matrix, F_{ij} is second order stiffness matrix.

$$A_{ij}, B_{ij}, D_{ij}, E_{ij}, F_{ij} = \int_{-\frac{h}{2}}^{\frac{h}{2}} [\bar{Q}_{ij}] (1, z, z^2, z^3, z^4) dz$$
$$\times \begin{cases} A_{ij}, D_{ij}, F_{ij} & (j, i = 1,2,4,5,6) \\ E_{ij}, B_{ij} & (j, i = 1,2,6) \end{cases} \tag{190}$$

Stress-strain relationship in terms of stress resultants in full matrix form according to Shahrjerdi & Bayat (2010):

$$\begin{bmatrix} \begin{bmatrix} N_x \\ N_y \\ N_{xy} \end{bmatrix} \\ \begin{bmatrix} M_x \\ M_y \\ M_{xy} \end{bmatrix} \\ \begin{bmatrix} L_x \\ L_y \\ L_{xy} \end{bmatrix} \end{bmatrix} = \begin{bmatrix} \begin{bmatrix} A_{11} & A_{12} & A_{16} \\ A_{12} & A_{22} & A_{26} \\ A_{16} & A_{26} & A_{66} \end{bmatrix} & \begin{bmatrix} B_{11} & B_{12} & B_{16} \\ B_{12} & B_{22} & B_{16} \\ B_{16} & B_{26} & B_{66} \end{bmatrix} & \begin{bmatrix} D_{11} & D_{12} & D_{16} \\ D_{12} & D_{22} & D_{26} \\ D_{16} & D_{26} & D_{66} \end{bmatrix} \\ \begin{bmatrix} B_{11} & B_{12} & B_{16} \\ B_{12} & B_{22} & B_{16} \\ B_{16} & B_{26} & B_{66} \end{bmatrix} & \begin{bmatrix} D_{11} & D_{12} & D_{16} \\ D_{12} & D_{22} & D_{26} \\ D_{16} & D_{26} & D_{66} \end{bmatrix} & \begin{bmatrix} E_{11} & E_{12} & E_{16} \\ E_{12} & E_{22} & E_{26} \\ E_{16} & E_{26} & E_{66} \end{bmatrix} \\ \begin{bmatrix} D_{11} & D_{12} & D_{16} \\ D_{12} & D_{22} & D_{26} \\ D_{16} & D_{26} & D_{66} \end{bmatrix} & \begin{bmatrix} E_{11} & E_{12} & E_{16} \\ E_{12} & E_{22} & E_{26} \\ E_{16} & E_{26} & E_{66} \end{bmatrix} & \begin{bmatrix} F_{11} & F_{12} & F_{16} \\ F_{12} & F_{22} & F_{26} \\ F_{16} & F_{26} & F_{66} \end{bmatrix} \end{bmatrix} \begin{bmatrix} \begin{bmatrix} \varepsilon_x^0 \\ \varepsilon_y^0 \\ \varepsilon_{xy}^0 \end{bmatrix} \\ \begin{bmatrix} \kappa_x^0 \\ \kappa_y^0 \\ \kappa_{xy}^0 \end{bmatrix} \\ \begin{bmatrix} \kappa_x^1 \\ \kappa_y^1 \\ \kappa_{xy}^1 \end{bmatrix} \end{bmatrix} \tag{191}$$

$$\begin{bmatrix} \begin{bmatrix} Q_y \\ Q_x \end{bmatrix} \\ \begin{bmatrix} R_y \\ R_x \end{bmatrix} \end{bmatrix} = \begin{bmatrix} \begin{bmatrix} A_{44} & A_{45} \\ A_{45} & A_{55} \end{bmatrix} & \begin{bmatrix} B_{44} & B_{45} \\ B_{45} & B_{55} \end{bmatrix} \\ \begin{bmatrix} B_{44} & B_{45} \\ B_{45} & B_{55} \end{bmatrix} & \begin{bmatrix} D_{44} & D_{45} \\ D_{45} & D_{55} \end{bmatrix} \end{bmatrix} \begin{bmatrix} \begin{bmatrix} \gamma_{yz}^0 \\ \gamma_{xz}^0 \end{bmatrix} \\ \begin{bmatrix} \gamma_{yz}^1 \\ \gamma_{xz}^1 \end{bmatrix} \end{bmatrix} \tag{192}$$

Stress-strain relationship in terms of stress resultants in contracted matrix form:

$$\begin{bmatrix} [N] \\ [M] \\ [L] \end{bmatrix} = \begin{bmatrix} [A] & [B] & [D] \\ [B] & [D] & [E] \\ [D] & [E] & [F] \end{bmatrix} \begin{bmatrix} [\varepsilon^0] \\ [\kappa^0] \\ [\kappa^1] \end{bmatrix} \tag{193}$$

$$\begin{bmatrix} [Q] \\ [R] \end{bmatrix} = \begin{bmatrix} [A] & [B] \\ [B] & [D] \end{bmatrix} \begin{bmatrix} [\gamma^0] \\ [\gamma^1] \end{bmatrix} \tag{194}$$

13.3.4 Governing plate equations in terms of displacement

Substitution of the plate equilibrium equations into the previous stress-strain relations and subsequent equation substitution (strain curvatures) yields governing plate equations in terms of displacement u_0, v_0, w_0, ϕ_1, ϕ_2, ψ_1 and ψ_2. By further mathematical adjustments we obtain:

1) Equation for displacement u_0 (in the x-axis direction):

$$A_{11}\frac{\partial^2 u_0}{\partial x^2} + A_{12}\frac{\partial^2 v_0}{\partial x\,\partial y} + A_{16}\left(\frac{\partial^2 u_0}{\partial x\,\partial y} + \frac{\partial^2 v_0}{\partial x^2}\right) + B_{11}\frac{\partial^2 \phi_1}{\partial x^2} + B_{12}\frac{\partial^2 \psi_1}{\partial x\,\partial y}$$

$$+ B_{16}\left(\frac{\partial^2 \phi_1}{\partial x\,\partial y} + \frac{\partial^2 \psi_1}{\partial x^2}\right) + D_{11}\frac{\partial^2 \phi_2}{\partial x^2} + D_{12}\frac{\partial^2 \psi_2}{\partial x\,\partial y} + D_{16}\left(\frac{\partial^2 \phi_2}{\partial x\,\partial y} + \frac{\partial^2 \psi_2}{\partial x^2}\right)$$

$$+ A_{16}\frac{\partial^2 u_0}{\partial x\,\partial y} + A_{26}\frac{\partial^2 v_0}{\partial y^2} + A_{66}\left(\frac{\partial^2 u_0}{\partial y^2} + \frac{\partial^2 v_0}{\partial y\,\partial x}\right) + B_{16}\frac{\partial^2 \phi_1}{\partial x\,\partial y}$$

$$+ B_{26}\frac{\partial^2 \psi_1}{\partial y^2} + B_{66}\left(\frac{\partial^2 \phi_1}{\partial y^2} + \frac{\partial^2 \psi_1}{\partial x\,\partial y}\right) + D_{16}\frac{\partial^2 \phi_2}{\partial x\,\partial y} + D_{26}\frac{\partial^2 \psi_2}{\partial y^2}$$

$$+ D_{66}\left(\frac{\partial^2 \phi_2}{\partial y^2} + \frac{\partial^2 \psi_2}{\partial x\,\partial y}\right) = 0$$

$$\tag{195}$$

2) Equation for displacement v_0 (in the y-axis direction):

$$A_{16}\frac{\partial^2 u_0}{\partial x^2} + A_{26}\frac{\partial^2 v_0}{\partial x \partial y} + A_{66}\left(\frac{\partial^2 u_0}{\partial x \partial y} + \frac{\partial^2 v_0}{\partial x^2}\right) + B_{16}\frac{\partial^2 \phi_1}{\partial x^2} + B_{26}\frac{\partial^2 \psi_1}{\partial x \partial y}$$

$$+ B_{66}\left(\frac{\partial^2 \phi_1}{\partial x \partial y} + \frac{\partial^2 \psi_1}{\partial x^2}\right) + D_{16}\frac{\partial^2 \phi_2}{\partial x^2} + D_{26}\frac{\partial^2 \psi_2}{\partial x \partial y}$$

$$+ D_{66}\left(\frac{\partial^2 \phi_2}{\partial x \partial y} + \frac{\partial^2 \psi_2}{\partial x^2}\right) + A_{12}\frac{\partial^2 u_0}{\partial x \partial y} + A_{22}\frac{\partial^2 v_0}{\partial y^2} + A_{26}\left(\frac{\partial^2 u_0}{\partial y^2} + \frac{\partial^2 v_0}{\partial x \partial y}\right)$$

$$+ B_{12}\frac{\partial^2 \phi_1}{\partial x \partial y} + B_{22}\frac{\partial^2 \psi_1}{\partial y^2} + B_{26}\left(\frac{\partial^2 \phi_1}{\partial y^2} + \frac{\partial^2 \psi_1}{\partial x \partial y}\right) + D_{12}\frac{\partial^2 \phi_2}{\partial x \partial y}$$

$$+ D_{22}\frac{\partial^2 \psi_2}{\partial y^2} + D_{26}\left(\frac{\partial^2 \phi_2}{\partial y^2} + \frac{\partial^2 \psi_2}{\partial x \partial y}\right) = 0$$

$$\tag{196}$$

3) Equation for displacement w_0 (in the z-axis direction)

$$A_{45} \left(\frac{\partial \psi_1}{\partial x} + \frac{\partial^2 w_0}{\partial x \partial y} \right) + A_{55} \left(\frac{\partial \phi_1}{\partial x} + \frac{\partial^2 w_0}{\partial x^2} \right) + B_{45} \frac{\partial (2\psi_2)}{\partial x} + B_{55} \frac{\partial (2\phi_2)}{\partial x}$$

$$+ A_{44} \left(\frac{\partial \psi_1}{\partial y} + \frac{\partial^2 w_0}{\partial y^2} \right) + A_{45} \left(\frac{\partial \phi_1}{\partial y} + \frac{\partial^2 w_0}{\partial x \partial y} \right) + B_{44} \frac{\partial (2\psi_2)}{\partial y}$$

$$+ B_{45} \frac{\partial (2\phi_2)}{\partial y} = -p(x, y)$$

$$(197)$$

4) Equation for displacement ϕ_1 (rotation of the perpendicular to the midplane in the zx plane)

$$B_{11} \frac{\partial^2 u_0}{\partial x^2} + B_{12} \frac{\partial^2 v_0}{\partial x \partial y} + B_{16} \left(\frac{\partial^2 u_0}{\partial x \partial y} + \frac{\partial^2 v_0}{\partial x^2} \right) + D_{11} \frac{\partial^2 \phi_1}{\partial x^2} + D_{12} \frac{\partial^2 \psi_1}{\partial x \partial y}$$

$$+ D_{16} \left(\frac{\partial^2 \phi_1}{\partial x \partial y} + \frac{\partial^2 \psi_1}{\partial x^2} \right) + E_{11} \frac{\partial^2 \phi_2}{\partial x^2} + E_{12} \frac{\partial^2 \psi_2}{\partial x \partial y} + E_{16} \left(\frac{\partial^2 \phi_2}{\partial x \partial y} + \frac{\partial^2 \psi_2}{\partial x^2} \right)$$

$$+ B_{16} \frac{\partial^2 u_0}{\partial x \partial y} + B_{26} \frac{\partial^2 v_0}{\partial y^2} + B_{66} \left(\frac{\partial^2 u_0}{\partial y^2} + \frac{\partial^2 v_0}{\partial x \partial y} \right) + D_{16} \frac{\partial^2 \phi_1}{\partial x \partial y}$$

$$+ D_{26} \frac{\partial^2 \psi_1}{\partial y^2} + D_{66} \left(\frac{\partial^2 \phi_1}{\partial y^2} + \frac{\partial^2 \psi_1}{\partial x \partial y} \right) + E_{16} \frac{\partial^2 \phi_2}{\partial x \partial y} + E_{26} \frac{\partial^2 \psi_2}{\partial y^2}$$

$$+ E_{66} \left(\frac{\partial^2 \phi_2}{\partial y^2} + \frac{\partial^2 \psi_2}{\partial x \partial y} \right)$$

$$- \left[A_{45} \left(\psi_1 + \frac{\partial w_0}{\partial y} \right) + A_{55} \left(\phi_1 + \frac{\partial w_0}{\partial x} \right) + B_{45} 2\psi_2 + B_{55} 2\phi_2 \right] = 0$$

$$(198)$$

5) Equation for displacement ϕ_2 (rotation of the perpendicular to the midplane in the yx plane)

$$B_{16} \frac{\partial^2 u_0}{\partial x^2} + B_{26} \frac{\partial^2 v_0}{\partial x \partial y} + B_{66} \left(\frac{\partial^2 u_0}{\partial x \partial y} + \frac{\partial^2 v_0}{\partial x^2} \right) + D_{16} \frac{\partial^2 \phi_1}{\partial x^2} + D_{26} \frac{\partial^2 \psi_1}{\partial x \partial y}$$

$$+ D_{66} \left(\frac{\partial^2 \phi_1}{\partial x \partial y} + \frac{\partial^2 \psi_1}{\partial x^2} \right) + E_{16} \frac{\partial^2 \phi_2}{\partial x^2} + E_{26} \frac{\partial^2 \psi_2}{\partial x \partial y}$$

$$+ E_{66} \left(\frac{\partial^2 \phi_2}{\partial x \partial y} + \frac{\partial^2 \psi_2}{\partial x^2} \right) + B_{12} \frac{\partial^2 u_0}{\partial x \partial y} + B_{22} \frac{\partial^2 v_0}{\partial y^2} + B_{26} \left(\frac{\partial^2 u_0}{\partial y^2} + \frac{\partial^2 v_0}{\partial x \partial y} \right)$$

$$+ D_{12} \frac{\partial^2 \phi_1}{\partial x \partial y} + D_{22} \frac{\partial^2 \psi_1}{\partial y^2} + D_{26} \left(\frac{\partial^2 \phi_1}{\partial y^2} + \frac{\partial^2 \psi_1}{\partial x \partial y} \right) + E_{12} \frac{\partial^2 \phi_2}{\partial x \partial y}$$

$$+ E_{22} \frac{\partial^2 \psi_2}{\partial y^2} + E_{26} \left(\frac{\partial^2 \phi_2}{\partial y^2} + \frac{\partial^2 \psi_2}{\partial x \partial y} \right)$$

$$- \left[A_{44} \left(\psi_1 + \frac{\partial w_0}{\partial y} \right) + A_{45} \left(\phi_1 + \frac{\partial w_0}{\partial x} \right) + B_{44} 2\psi_2 + B_{45} 2\phi_2 \right] = 0$$

$$(199)$$

6) Second order displacement equation ψ_1 (rotation of the perpendicular to the midplane in the zx plane)

$$D_{11}\frac{\partial^2 u_0}{\partial x^2} + D_{12}\frac{\partial^2 v_0}{\partial x \partial y} + D_{16}\left(\frac{\partial^2 u_0}{\partial x \partial y} + \frac{\partial v_0}{\partial x^2}\right) + E_{11}\frac{\partial^2 \phi_1}{\partial x^2} + E_{12}\frac{\partial^2 \psi_1}{\partial x \partial y}$$

$$+ E_{16}\left(\frac{\partial^2 \phi_1}{\partial x \partial y} + \frac{\partial^2 \psi_1}{\partial x^2}\right) + F_{11}\frac{\partial^2 \phi_2}{\partial x^2} + F_{12}\frac{\partial^2 \psi_2}{\partial x \partial y} + F_{16}\left(\frac{\partial^2 \phi_2}{\partial x \partial y} + \frac{\partial^2 \psi_2}{\partial x^2}\right)$$

$$+ D_{16}\frac{\partial^2 u_0}{\partial x \partial y} + D_{26}\frac{\partial^2 v_0}{\partial y^2} + D_{66}\left(\frac{\partial^2 u_0}{\partial y^2} + \frac{\partial^2 v_0}{\partial x \partial y}\right) + E_{16}\frac{\partial^2 \phi_1}{\partial x \partial y}$$

$$+ E_{26}\frac{\partial^2 \psi_1}{\partial y^2} + E_{66}\left(\frac{\partial^2 \phi_1}{\partial y^2} + \frac{\partial^2 \psi_1}{\partial x \partial y}\right) + F_{16}\frac{\partial^2 \phi_2}{\partial x \partial y} + F_{26}\frac{\partial^2 \psi_2}{\partial y^2}$$

$$+ F_{66}\left(\frac{\partial^2 \phi_2}{\partial y^2} + \frac{\partial^2 \psi_2}{\partial x \partial y}\right)$$

$$- 2\left[B_{45}\left(\psi_1 + \frac{\partial w_0}{\partial y}\right) + B_{55}\left(\phi_1 + \frac{\partial w_0}{\partial x}\right) + D_{45}2\psi_2 + D_{55}2\phi_1\right] = 0$$

$$(200)$$

7) Second order displacement equation ψ_2 (rotation of the perpendicular to the midplane in the zy plane)

$$\left[D_{16}\frac{\partial^2 u_0}{\partial x^2} + D_{26}\frac{\partial^2 v_0}{\partial x \partial y} + D_{66}\left(\frac{\partial^2 u_0}{\partial x \partial y} + \frac{\partial^2 v_0}{\partial x^2}\right) + E_{16}\frac{\partial^2 \phi_1}{\partial x^2} + E_{26}\frac{\partial^2 \psi_1}{\partial x \partial y}\right.$$

$$+ E_{66}\left(\frac{\partial^2 \phi_1}{\partial x \partial y} + \frac{\partial^2 \psi_1}{\partial x^2}\right) + F_{16}\frac{\partial^2 \phi_2}{\partial x^2} + F_{26}\frac{\partial^2 \psi_2}{\partial x \partial y}$$

$$\left.+ F_{66}\left(\frac{\partial^2 \phi_2}{\partial x \partial y} + \frac{\partial^2 \psi_2}{\partial x^2}\right)\right]$$

$$+ \left[D_{12}\frac{\partial^2 u_0}{\partial x \partial y} + D_{22}\frac{\partial^2 v_0}{\partial y^2} + D_{26}\left(\frac{\partial^2 u_0}{\partial y^2} + \frac{\partial^2 v_0}{\partial x \partial y}\right) + E_{12}\frac{\partial^2 \phi_1}{\partial x \partial y}\right.$$

$$+ E_{22}\frac{\partial^2 \psi_1}{\partial y^2} + E_{26}\left(\frac{\partial^2 \phi_1}{\partial y^2} + \frac{\partial^2 \psi_1}{\partial x \partial y}\right) + F_{12}\frac{\partial^2 \phi_2}{\partial x \partial y} + F_{22}\frac{\partial^2 \psi_2}{\partial y^2}$$

$$\left.+ F_{26}\left(\frac{\partial^2 \phi_2}{\partial y^2} + \frac{\partial^2 \psi_2}{\partial x \partial y}\right)\right]$$

$$- 2\left[B_{44}\left(\psi_1 + \frac{\partial w_0}{\partial y}\right) + B_{45}\left(\phi_1 + \frac{\partial w_0}{\partial x}\right) + D_{44}2\psi_2 + D_{45}2\phi_1\right] = 0$$

$$(201)$$

13.4 Derivation of relations according to Third-Order Shear Deformation Theory

13.4.1 Strains and curvatures

The linear strains associated with the displacement field according to Nami (2015):

$$\varepsilon_x = \varepsilon_x^0 + z\kappa_x^0 + z^2\kappa_x^1 + z^3\kappa_x^2 \tag{202}$$

$$\varepsilon_y = \varepsilon_y^0 + z\kappa_y^0 + z^2\kappa_y^1 + z^3\kappa_y^2 \tag{203}$$

$$\gamma_{yz} = \gamma_{yz}^0 + z\gamma_{yz}^1 + z^2\gamma_{yz}^2 \tag{204}$$

$$\gamma_{xz} = \gamma_{xz}^0 + z\gamma_{xz}^1 + z^2\gamma_{xz}^2 \tag{205}$$

$$\varepsilon_{xy} = \varepsilon_{xy}^0 + z\kappa_{xy}^0 + z^2\kappa_{xy}^1 + z^3\kappa_{xy}^2 \tag{206}$$

Where

$$\varepsilon_x^0 = \frac{du_0}{dx} \quad ; \quad \varepsilon_y^0 = \frac{dv_0}{dy} \quad ; \quad \varepsilon_{xy}^0 = \gamma_{xy} = \left(\frac{du_0}{dy} + \frac{dv_0}{dx}\right) \tag{207}$$

$$\kappa_x^0 = \frac{d\psi_x}{dx} \quad ; \quad \kappa_y^0 = \frac{d\psi_y}{dx} \quad ; \quad \kappa_{xy}^0 = \left(\frac{d\psi_x}{dy} + \frac{d\psi_y}{dx}\right) \tag{208}$$

$$\kappa_x^1 = \frac{d\phi_x}{dx} \quad ; \quad \kappa_y^1 = \frac{d\phi_y}{dy} \quad ; \quad \kappa_{xy}^1 = \left(\frac{d\phi_x}{dy} + \frac{d\phi_y}{dx}\right) \tag{209}$$

$$\kappa_x^2 = \frac{d\lambda_x}{dx} \quad ; \quad \kappa_y^2 = \frac{d\lambda_y}{dy} \quad ; \quad \kappa_{xy}^2 = \left(\frac{d\lambda_x}{dy} + \frac{d\lambda_y}{dx}\right) \tag{210}$$

$$\gamma_{yz}^0 = \left(\psi_y + \frac{dw_0}{dy}\right) \quad ; \quad \gamma_{xz}^0 = \left(\psi_x + \frac{dw_0}{dx}\right) \tag{211}$$

$$\gamma_{yz}^1 = 2\phi_y \quad ; \quad \gamma_{xz}^1 = 2\phi_x \tag{212}$$

$$\gamma_{yz}^2 = 3\lambda_y \quad ; \quad \gamma_{xz}^2 = 3\lambda_x \tag{213}$$

In matrix form:

$$\varepsilon^0 = \begin{bmatrix} \varepsilon_x^0 \\ \varepsilon_y^0 \\ \varepsilon_{xy}^0 \end{bmatrix} = \begin{bmatrix} \dfrac{du_0}{dx} \\ \dfrac{dv_0}{dy} \\ \left(\dfrac{du_0}{dy} + \dfrac{dv_0}{dx}\right) \end{bmatrix} \quad ; \quad \kappa^0 = \begin{bmatrix} \kappa_x^0 \\ \kappa_y^0 \\ \kappa_{xy}^0 \end{bmatrix} = \begin{bmatrix} \dfrac{d\psi_x}{dx} \\ \dfrac{d\psi_y}{dx} \\ \left(\dfrac{d\psi_x}{dy} + \dfrac{d\psi_y}{dx}\right) \end{bmatrix} \tag{214}$$

$$\kappa^1 = \begin{bmatrix} \kappa_x^1 \\ \kappa_y^1 \\ \kappa_{xy}^1 \end{bmatrix} = \begin{bmatrix} \dfrac{d\phi_x}{dx} \\ \dfrac{d\phi_y}{dy} \\ \left(\dfrac{d\phi_x}{dy} + \dfrac{d\phi_y}{dx}\right) \end{bmatrix} \quad ; \quad \kappa^2 = \begin{bmatrix} \kappa_x^2 \\ \kappa_y^2 \\ \kappa_{xy}^2 \end{bmatrix} = \begin{bmatrix} \dfrac{d\lambda_x}{dx} \\ \dfrac{d\lambda_y}{dy} \\ \left(\dfrac{d\lambda_x}{dy} + \dfrac{d\lambda_y}{dx}\right) \end{bmatrix} \tag{215}$$

$$\gamma^0 = \begin{bmatrix} \gamma_{xz}^0 \\ \gamma_{yz}^0 \end{bmatrix} = \begin{bmatrix} \left(\psi_x + \dfrac{dw_0}{dx}\right) \\ \left(\psi_y + \dfrac{dw_0}{dy}\right) \end{bmatrix} \tag{216}$$

$$\gamma^2 = \begin{bmatrix} \gamma_{xz}^2 \\ \gamma_{yz}^2 \end{bmatrix} = \begin{bmatrix} 3\lambda_x \\ 3\lambda_y \end{bmatrix} \quad ; \quad \gamma^1 = \begin{bmatrix} \gamma_{xz}^1 \\ \gamma_{yz}^1 \end{bmatrix} = \begin{bmatrix} 2\phi_x \\ 2\phi_y \end{bmatrix} \tag{217}$$

(a) Initial   (b) Deformed
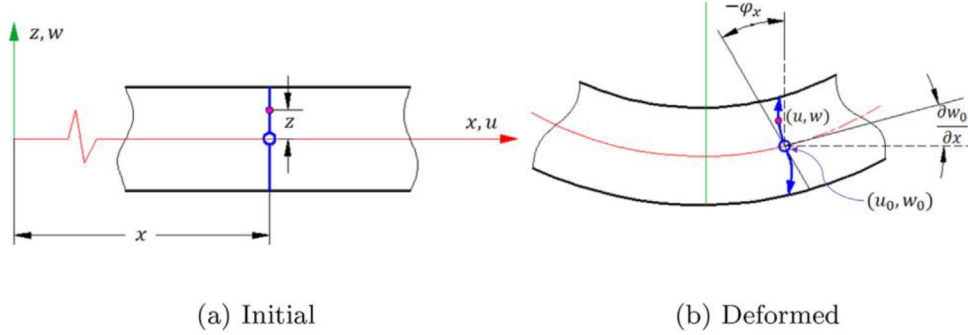
Figure 37 - Initial and deformed geometries of a laminated composite beam under TSDT assumptions (Shafei, 2020)

13.4.2 Equilibrium equations

Similar to CPT, FSDT and SSDT, the equation of equilibrium is determined from the forces and moments acting in the plane of the plate.

Stress resultant in x and y-direction:

$$\frac{dN_x}{dx} + \frac{dN_{xy}}{dy} = 0 \quad ; \quad \frac{dN_{xy}}{dx} + \frac{dN_y}{dy} = 0 \tag{218}$$

Stress resultant in z-direction:

$$\frac{dQ_x}{dx} + \frac{dQ_y}{dy} + p(x,y) = 0 \tag{219}$$

Moment resultant about x and y-axis:

$$\frac{dM_x}{dx} + \frac{dM_{xy}}{dy} - Q_x - S_x = 0 \quad ; \quad \frac{dM_{xy}}{dx} + \frac{dM_y}{dy} - Q_y - S_y = 0 \tag{220}$$

Second order stress resultant in x and y-direction:

$$\frac{dL_x}{dx} + \frac{dL_{xy}}{dy} - 2R_x = 0 \quad ; \quad \frac{dL_{xy}}{dx} + \frac{dL_y}{dy} - 2R_y = 0 \tag{221}$$

The components representing third order stress resultants in x and y-direction are then written as:

$$\frac{dP_x}{dx} + \frac{dP_{xy}}{dy} - 3S_x = 0 \quad ; \quad \frac{dP_{xy}}{dx} + \frac{dP_y}{dy} - 3S_y = 0 \tag{222}$$

13.4.3 Orthotropic plate stress-strain relationship

The stress-strain relations for the kth lamina in the laminate coordinates are given by:

$$\begin{bmatrix} \sigma_x \\ \sigma_y \\ \sigma_{xy} \\ \sigma_{yz} \\ \sigma_{xz} \end{bmatrix} = \begin{bmatrix} \bar{Q}_{11} & \bar{Q}_{12} & \bar{Q}_{16} & 0 & 0 \\ \bar{Q}_{12} & \bar{Q}_{22} & \bar{Q}_{26} & 0 & 0 \\ \bar{Q}_{16} & \bar{Q}_{26} & \bar{Q}_{66} & 0 & 0 \\ 0 & 0 & 0 & \bar{Q}_{44} & \bar{Q}_{45} \\ 0 & 0 & 0 & \bar{Q}_{45} & \bar{Q}_{55} \end{bmatrix} \begin{bmatrix} \varepsilon_x \\ \varepsilon_y \\ \gamma_{xy} \\ \gamma_{yz} \\ \gamma_{xz} \end{bmatrix} \tag{223}$$

Where $\bar{Q}_{ij}$ is the transformed stiffness matrix. Stress-resultants for TSDT are defined according to Szekrényes (2014) as:

$$\left(N_x, N_y, N_{xy}\right) = \sum_{k=1}^{N} \int_{-h/2}^{h/2} \left(\sigma_x, \sigma_y, \sigma_{xy}\right) dz \tag{224}$$

$$\left(M_x, M_y, M_{xy}\right) = \sum_{k=1}^{N} \int_{-h/2}^{h/2} \left(\sigma_x, \sigma_y, \sigma_{xy}\right) z\, dz \tag{225}$$

$$\left(L_x, L_y, L_{xy}\right) = \sum_{k=1}^{N} \int_{-h/2}^{h/2} \left(\sigma_x, \sigma_y, \sigma_{xy}\right) z^2\, dz \tag{226}$$

$$\left(P_x, P_y, P_{xy}\right) = \sum_{k=1}^{N} \int_{-h/2}^{h/2} \left(\sigma_x, \sigma_y, \sigma_{xy}\right) z^2\, dz \tag{227}$$

$$\left(Q_y, Q_x\right) = \sum_{k=1}^{N} \int_{-h/2}^{h/2} \left(\sigma_{yz}, \sigma_{xz}\right) dz \tag{228}$$

$$\left(R_y, R_x\right) = \sum_{k=1}^{N} \int_{-h/2}^{h/2} \left(\sigma_{yz}, \sigma_{xz}\right) z\, dz \tag{229}$$

$$\left(S_y, S_x\right) = \sum_{k=1}^{N} \int_{-h/2}^{h/2} \left(\sigma_{yz}, \sigma_{xz}\right) z^2\, dz \tag{230}$$

Stress-strain relationship according to Tian (2022) in terms of stress resultants in contracted form:

$$\begin{bmatrix} [N] \\ [M] \\ [L] \\ [P] \end{bmatrix} = \begin{bmatrix} [A] & [B] & [D] & [E] \\ [B] & [D] & [E] & [F] \\ [D] & [E] & [F] & [G] \\ [E] & [F] & [G] & [H] \end{bmatrix} \begin{bmatrix} \varepsilon^0 \\ \kappa^0 \\ \kappa^1 \\ \kappa^2 \end{bmatrix} \tag{231}$$

$$\begin{bmatrix} [Q] \\ [R] \\ [S] \end{bmatrix} = \begin{bmatrix} [A] & [B] & [D] \\ [B] & [D] & [E] \\ [D] & [E] & [F] \end{bmatrix} \begin{bmatrix} \gamma^0 \\ \gamma^1 \\ \gamma^2 \end{bmatrix} \tag{232}$$

in full form:

$$
\begin{bmatrix}
\begin{bmatrix} N_x \\ N_y \\ N_{xy} \end{bmatrix} \\[4pt]
\begin{bmatrix} M_x \\ M_y \\ M_{xy} \end{bmatrix} \\[4pt]
\begin{bmatrix} L_x \\ L_y \\ L_{xy} \end{bmatrix} \\[4pt]
\begin{bmatrix} P_x \\ P_y \\ P_{xy} \end{bmatrix}
\end{bmatrix}
=
\begin{bmatrix}
\begin{bmatrix} A_{11} & A_{12} & A_{16} \\ A_{12} & A_{22} & A_{26} \\ A_{16} & A_{26} & A_{66} \end{bmatrix} &
\begin{bmatrix} B_{11} & B_{12} & B_{16} \\ B_{12} & B_{22} & B_{26} \\ B_{16} & B_{26} & B_{66} \end{bmatrix} &
\begin{bmatrix} D_{11} & D_{12} & D_{16} \\ D_{12} & D_{22} & D_{26} \\ D_{16} & D_{26} & D_{66} \end{bmatrix} &
\begin{bmatrix} E_{11} & E_{12} & E_{16} \\ E_{16} & E_{26} & E_{66} \\ E_{16} & E_{26} & E_{66} \end{bmatrix} \\[10pt]
\begin{bmatrix} B_{11} & B_{12} & B_{16} \\ B_{12} & B_{22} & B_{26} \\ B_{16} & B_{26} & B_{66} \end{bmatrix} &
\begin{bmatrix} D_{11} & D_{12} & D_{16} \\ D_{12} & D_{22} & D_{26} \\ D_{16} & D_{26} & D_{66} \end{bmatrix} &
\begin{bmatrix} E_{11} & E_{12} & E_{16} \\ E_{16} & E_{26} & E_{66} \\ E_{16} & E_{26} & E_{66} \end{bmatrix} &
\begin{bmatrix} F_{11} & F_{12} & F_{16} \\ F_{12} & F_{22} & F_{26} \\ F_{16} & F_{26} & F_{66} \end{bmatrix} \\[10pt]
\begin{bmatrix} D_{11} & D_{12} & D_{16} \\ D_{12} & D_{22} & D_{26} \\ D_{16} & D_{26} & D_{66} \end{bmatrix} &
\begin{bmatrix} E_{11} & E_{12} & E_{16} \\ E_{16} & E_{26} & E_{66} \\ E_{16} & E_{26} & E_{66} \end{bmatrix} &
\begin{bmatrix} F_{11} & F_{12} & F_{16} \\ F_{12} & F_{22} & F_{26} \\ F_{16} & F_{26} & F_{66} \end{bmatrix} &
\begin{bmatrix} G_{11} & G_{12} & G_{16} \\ G_{12} & G_{22} & G_{26} \\ G_{16} & G_{26} & G_{66} \end{bmatrix} \\[10pt]
\begin{bmatrix} E_{11} & E_{12} & E_{16} \\ E_{16} & E_{26} & E_{66} \\ E_{16} & E_{26} & E_{66} \end{bmatrix} &
\begin{bmatrix} F_{11} & F_{12} & F_{16} \\ F_{12} & F_{22} & F_{26} \\ F_{16} & F_{26} & F_{66} \end{bmatrix} &
\begin{bmatrix} G_{11} & G_{12} & G_{16} \\ G_{12} & G_{22} & G_{26} \\ G_{16} & G_{26} & G_{66} \end{bmatrix} &
\begin{bmatrix} H_{11} & H_{12} & H_{16} \\ H_{12} & H_{22} & H_{26} \\ H_{16} & H_{26} & H_{66} \end{bmatrix}
\end{bmatrix}
\begin{bmatrix}
\varepsilon_x^0 \\ \varepsilon_y^0 \\ \varepsilon_{xy}^0 \\
\kappa_x^0 \\ \kappa_y^0 \\ \kappa_{xy}^0 \\
\kappa_x^1 \\ \kappa_y^1 \\ \kappa_{xy}^1 \\
\kappa_x^2 \\ \kappa_x^2 \\ \kappa_x^2
\end{bmatrix}
$$

$$\text{(233)}$$

$$
\begin{bmatrix}
\begin{bmatrix} Q_y \\ Q_x \end{bmatrix} \\[4pt]
\begin{bmatrix} R_y \\ R_x \end{bmatrix} \\[4pt]
\begin{bmatrix} S_y \\ S_x \end{bmatrix}
\end{bmatrix}
=
\begin{bmatrix}
\begin{bmatrix} A_{44} & A_{45} \\ A_{45} & A_{55} \end{bmatrix} &
\begin{bmatrix} B_{44} & B_{45} \\ B_{45} & B_{55} \end{bmatrix} &
\begin{bmatrix} D_{44} & D_{45} \\ D_{45} & D_{55} \end{bmatrix} \\[8pt]
\begin{bmatrix} B_{44} & B_{45} \\ B_{45} & B_{55} \end{bmatrix} &
\begin{bmatrix} D_{44} & D_{45} \\ D_{45} & D_{55} \end{bmatrix} &
\begin{bmatrix} E_{44} & E_{45} \\ E_{45} & E_{55} \end{bmatrix} \\[8pt]
\begin{bmatrix} D_{44} & D_{45} \\ D_{45} & D_{55} \end{bmatrix} &
\begin{bmatrix} E_{44} & E_{45} \\ E_{45} & E_{55} \end{bmatrix} &
\begin{bmatrix} F_{44} & F_{45} \\ F_{45} & F_{55} \end{bmatrix}
\end{bmatrix}
\begin{bmatrix}
\gamma_{yz}^0 \\ \gamma_{xz}^0 \\
\gamma_{yz}^1 \\ \gamma_{xz}^1 \\
\gamma_{yz}^2 \\ \gamma_{xz}^2
\end{bmatrix}
\qquad \text{(234)}
$$

Where:

$$
A_{ij}, B_{ij}, D_{ij}, E_{ij}, F_{ij}, G_{ij}, H_{ij} = \int_{-\frac{h}{2}}^{\frac{h}{2}} [C_{ij}] \, (1, z, z^2, z^3, z^4, z^5, z^6) \, dz
$$

$$
\times \begin{cases} A_{ij}, B_{ij}, D_{ij}, E_{ij}, F_{ij} & (j, i = 1,2,4,5,6) \\ H_{ij}, G_{ij} & (j, i = 1,2,6) \end{cases}
\qquad \text{(235)}
$$

For kth layer of the laminate:

$$
A_{ij} = \sum_{k=1}^{n} [\bar{Q}_{ij}]_k (h_k - h_{k-1}) \tag{236}
$$

$$
B_{ij} = \frac{1}{2} \sum_{k=1}^{n} [\bar{Q}_{ij}]_k (h_k^2 - h_{k-1}^2) \tag{237}
$$

$$
D_{ij} = \frac{1}{3} \sum_{k=1}^{n} [\bar{Q}_{ij}]_k (h_k^3 - h_{k-1}^3) \tag{238}
$$

$$
E_{ij} = \frac{1}{4} \sum_{k=1}^{n} [\bar{Q}_{ij}]_k (h_k^4 - h_{k-1}^4) \tag{239}
$$

$$
F_{ij} = \frac{1}{5} \sum_{k=1}^{n} [\bar{Q}_{ij}]_k (h_k^5 - h_{k-1}^5) \tag{240}
$$

$$
G_{ij} = \frac{1}{6} \sum_{k=1}^{n} [\bar{Q}_{ij}]_k (h_k^6 - h_{k-1}^6) \tag{241}
$$

$$
H_{ij} = \frac{1}{7} \sum_{k=1}^{n} [\bar{Q}_{ij}]_k (h_k^7 - h_{k-1}^7) \tag{242}
$$

Where A_{ij} is extensional stiffness matrix, B_{ij} is extension-bending coupling matrix, D_{ij} is bending stiffness matrix, E_{ij} is second order coupling matrix, F_{ij} is second order stiffness matrix, G_{ij} is third order second order stiffness matrix, H_{ij} is third order coupling matrix (Szekrényes, 2014).

13.4.4 Governing plate equations in terms of displacement

Substitution of the plate equilibrium equations into the stress-strain relations above and subsequent equation substitution (strain curvatures) yields governing plate equations in terms of displacement u_0, v_0, w_0, ϕ_x, ϕ_y, ψ_x, ψ_y, λ_x and λ_y. By further mathematical adjustments we obtain:

1) Equation for displacement u_0 (in the x-axis direction):

$$A_{11}\frac{\partial^2 u_0}{\partial x^2} + A_{12}\frac{\partial^2 v_0}{\partial x \partial y} + A_{16}\left(\frac{\partial^2 u_0}{\partial x \partial y} + \frac{\partial^2 v_0}{\partial x^2}\right) + B_{11}\frac{\partial^2 \psi_x}{\partial x^2} + B_{12}\frac{\partial^2 \psi_y}{\partial x \partial y} + B_{16}\left(\frac{\partial^2 \psi_x}{\partial x \partial y} + \frac{\partial^2 \psi_y}{\partial x^2}\right)$$
$$+ D_{11}\frac{\partial^2 \phi_x}{\partial x^2} + D_{12}\frac{\partial^2 \phi_y}{\partial x \partial y} + D_{16}\left(\frac{\partial^2 \phi_x}{\partial x \partial y} + \frac{\partial^2 \phi_y}{\partial x^2}\right) + E_{11}\frac{\partial^2 \lambda_x}{\partial x^2} + E_{12}\frac{\partial^2 \lambda_y}{\partial x \partial y}$$
$$+ E_{16}\left(\frac{\partial^2 \lambda_x}{\partial x \partial y} + \frac{\partial^2 \lambda_y}{\partial x^2}\right) + A_{16}\frac{\partial^2 u_0}{\partial x \partial y} + A_{26}\frac{\partial^2 v_0}{\partial y^2} + A_{66}\left(\frac{\partial^2 u_0}{\partial y^2} + \frac{\partial^2 v_0}{\partial x \partial y}\right)$$
$$+ B_{16}\frac{\partial^2 \psi_x}{\partial x \partial y} + B_{26}\frac{\partial^2 \psi_y}{\partial y^2} + B_{66}\left(\frac{\partial^2 \psi_x}{\partial y^2} + \frac{\partial^2 \psi_y}{\partial x \partial y}\right) + D_{16}\frac{\partial^2 \phi_x}{\partial x \partial y} + D_{26}\frac{\partial^2 \phi_y}{\partial y^2}$$
$$+ D_{66}\left(\frac{\partial^2 \phi_x}{\partial y^2} + \frac{\partial^2 \phi_y}{\partial x \partial y}\right) + E_{16}\frac{\partial^2 \lambda_x}{\partial x \partial y} + E_{26}\frac{\partial^2 \lambda_y}{\partial y^2} + E_{66}\left(\frac{\partial^2 \lambda_x}{\partial y^2} + \frac{\partial^2 \lambda_y}{\partial x \partial y}\right) = 0$$

(243)

2) Equation for displacement v_0 (in the y-axis direction):

$$A_{16}\frac{\partial^2 u_0}{\partial x^2} + A_{26}\frac{\partial^2 v_0}{\partial x \partial y} + A_{66}\left(\frac{\partial^2 u_0}{\partial x \partial y} + \frac{\partial^2 v_0}{\partial x^2}\right) + B_{16}\frac{\partial^2 \psi_x}{\partial x^2} + B_{26}\frac{\partial^2 \psi_y}{\partial x \partial y} + B_{66}\left(\frac{\partial^2 \psi_x}{\partial x \partial y} + \frac{\partial^2 \psi_y}{\partial x^2}\right)$$
$$+ D_{16}\frac{\partial^2 \phi_x}{\partial x^2} + D_{26}\frac{\partial^2 \phi_y}{\partial x \partial y} + D_{66}\left(\frac{\partial^2 \phi_x}{\partial x \partial y} + \frac{\partial^2 \phi_y}{\partial x^2}\right) + E_{16}\frac{\partial^2 \lambda_x}{\partial x^2} + E_{26}\frac{\partial^2 \lambda_y}{\partial x \partial y}$$
$$+ E_{66}\left(\frac{\partial^2 \lambda_x}{\partial x \partial y} + \frac{\partial^2 \lambda_y}{\partial x^2}\right) + A_{12}\frac{\partial^2 u_0}{\partial x \partial y} + A_{22}\frac{\partial^2 v_0}{\partial y^2} + A_{26}\left(\frac{\partial^2 u_0}{\partial y^2} + \frac{\partial^2 v_0}{\partial x \partial y}\right)$$
$$+ B_{12}\frac{\partial^2 \psi_x}{\partial x \partial y} + B_{22}\frac{\partial^2 \psi_y}{\partial y^2} + B_{26}\left(\frac{\partial^2 \psi_x}{\partial y^2} + \frac{\partial^2 \psi_y}{\partial x \partial y}\right) + D_{12}\frac{\partial^2 \phi_x}{\partial x \partial y} + D_{22}\frac{\partial^2 \phi_y}{\partial y^2}$$
$$+ D_{26}\left(\frac{\partial^2 \phi_x}{\partial y^2} + \frac{\partial^2 \phi_y}{\partial x \partial y}\right) + E_{12}\frac{\partial^2 \lambda_x}{\partial x \partial y} + E_{22}\frac{\partial^2 \lambda_y}{\partial y^2} + E_{26}\left(\frac{\partial^2 \lambda_x}{\partial y^2} + \frac{\partial^2 \lambda_y}{\partial x \partial y}\right) = 0$$

(244)

3) Equation for displacement w_0 (in the z-axis direction):

114

$$\left[A_{45} \left(\frac{\partial}{\partial x} \psi_y + \frac{\partial^2 w_0}{\partial x \partial y} \right) + A_{55} \left(\frac{\partial}{\partial x} \psi_x + \frac{\partial^2 w_0}{\partial x^2} \right) + 2B_{45} \frac{\partial}{\partial x} \phi_y + 2B_{55} \frac{\partial}{\partial x} \phi_x + 3D_{45} \frac{\partial}{\partial x} \lambda_y \right.$$

$$\left. + 3D_{55} \frac{\partial}{\partial x} \lambda_x \right]$$

$$+ \left[A_{44} \left(\frac{\partial}{\partial y} \psi_y + \frac{\partial^2 w_0}{\partial y^2} \right) + A_{45} \left(\frac{\partial}{\partial y} \psi_x + \frac{\partial^2 w_0}{\partial x \partial y} \right) + 2B_{44} \frac{\partial}{\partial y} \phi_y + 2B_{45} \frac{\partial}{\partial y} \phi_x \right.$$

$$\left. + 3D_{44} \frac{\partial}{\partial y} \lambda_y + 3D_{45} \frac{\partial}{\partial y} \lambda_x \right] = -p(x,y)$$

<div align="right">(245)</div>

4) Equation for the displacement ψ_x (rotation of the perpendicular to the midplane in the zx plane)

$$B_{11} \frac{\partial^2 u_0}{\partial x^2} + B_{12} \frac{\partial^2 v_0}{\partial x \partial y} + B_{16} \left(\frac{\partial^2 u_0}{\partial x \partial y} + \frac{\partial^2 v_0}{\partial x^2} \right) + D_{11} \frac{\partial^2 \psi_x}{\partial x^2} + D_{12} \frac{\partial^2 \psi_y}{\partial x \partial y} + D_{16} \left(\frac{\partial^2 \psi_x}{\partial x \partial y} + \frac{\partial^2 \psi_y}{\partial x^2} \right)$$

$$+ E_{11} \frac{\partial^2 \phi_x}{\partial x^2} + E_{12} \frac{\partial^2 \phi_y}{\partial x \partial y} + E_{16} \left(\frac{\partial^2 \phi_x}{\partial x \partial y} + \frac{\partial^2 \phi_y}{\partial x^2} \right) + F_{11} \frac{\partial^2 \lambda_x}{\partial x^2} + F_{12} \frac{\partial^2 \lambda_y}{\partial x \partial y}$$

$$+ F_{16} \left(\frac{\partial^2 \lambda_x}{\partial x \partial y} + \frac{\partial^2 \lambda_y}{\partial x^2} \right) + B_{16} \frac{\partial^2 u_0}{\partial x \partial y} + B_{26} \frac{\partial^2 v_0}{\partial y^2} + B_{66} \left(\frac{\partial^2 u_0}{\partial y^2} + \frac{\partial^2 v_0}{\partial x \partial y} \right)$$

$$+ D_{16} \frac{\partial^2 \psi_x}{\partial x \partial y} + D_{26} \frac{\partial^2 \psi_y}{\partial y^2} + D_{66} \left(\frac{\partial^2 \psi_x}{\partial y^2} + \frac{\partial^2 \psi_y}{\partial x \partial y} \right) + E_{16} \frac{\partial^2 \phi_x}{\partial x \partial y} + E_{26} \frac{\partial^2 \phi_y}{\partial y^2}$$

$$+ E_{66} \left(\frac{\partial^2 \phi_x}{\partial y^2} + \frac{\partial^2 \phi_y}{\partial x \partial y} \right) + F_{16} \frac{\partial^2 \lambda_x}{\partial x \partial y} + F_{26} \frac{\partial^2 \lambda_y}{\partial y^2} + F_{66} \left(\frac{\partial^2 \lambda_x}{\partial y^2} + \frac{\partial^2 \lambda_y}{\partial x \partial y} \right)$$

$$- \left[A_{45} \left(\psi_y + \frac{\partial w_0}{\partial y} \right) + A_{55} \left(\psi_x + \frac{\partial w_0}{\partial x} \right) + 2B_{45} \phi_y + 2B_{55} \phi_x + 3D_{45} \lambda_y \right.$$

$$\left. + 3D_{55} \lambda_x \right]$$

$$- \left[D_{45} \left(\psi_y + \frac{\partial w_0}{\partial y} \right) + D_{55} \left(\psi_x + \frac{\partial w_0}{\partial x} \right) + 2E_{45} \phi_y + 2E_{55} \phi_x + 3F_{45} \lambda_y \right.$$

$$\left. + 3F_{55} \lambda_x \right] = 0$$

<div align="right">(246)</div>

5) Equation for the displacement ψ_y (rotation of the perpendicular to the midplane in the zy plane)

$$B_{16}\frac{\partial^2 u_0}{\partial x^2} + B_{26}\frac{\partial^2 v_0}{\partial x\partial y} + B_{66}\left(\frac{\partial^2 u_0}{\partial x\partial y} + \frac{\partial^2 v_0}{\partial x^2}\right) + D_{16}\frac{\partial^2 \psi_x}{\partial x^2} + D_{26}\frac{\partial^2 \psi_y}{\partial x\partial y} + D_{66}\left(\frac{\partial^2 \psi_x}{\partial x\partial y} + \frac{\partial^2 \psi_y}{\partial x^2}\right)$$

$$+ E_{16}\frac{\partial^2 \phi_x}{\partial x^2} + E_{26}\frac{\partial^2 \phi_y}{\partial x\partial y} + E_{66}\left(\frac{\partial^2 \phi_x}{\partial x\partial y} + \frac{\partial^2 \phi_y}{\partial x^2}\right) + F_{16}\frac{\partial^2 \lambda_x}{\partial x^2} + F_{26}\frac{\partial^2 \lambda_y}{\partial x\partial y}$$

$$+ F_{66}\left(\frac{\partial^2 \lambda_x}{\partial x\partial y} + \frac{\partial^2 \lambda_y}{\partial x^2}\right) + B_{12}\frac{\partial^2 u_0}{\partial x\partial y} + B_{22}\frac{\partial^2 v_0}{\partial y^2} + B_{26}\left(\frac{\partial^2 u_0}{\partial y^2} + \frac{\partial^2 v_0}{\partial x\partial y}\right)$$

$$+ D_{12}\frac{\partial^2 \psi_x}{\partial x\partial y} + D_{22}\frac{\partial^2 \psi_y}{\partial y^2} + D_{26}\left(\frac{\partial^2 \psi_x}{\partial y^2} + \frac{\partial^2 \psi_y}{\partial x\partial y}\right) + E_{12}\frac{\partial^2 \phi_x}{\partial x\partial y} + E_{22}\frac{\partial^2 \phi_y}{\partial y^2}$$

$$+ E_{26}\left(\frac{\partial^2 \phi_x}{\partial y^2} + \frac{\partial^2 \phi_y}{\partial x\partial y}\right) + F_{12}\frac{\partial^2 \lambda_x}{\partial x\partial y} + F_{22}\frac{\partial^2 \lambda_y}{\partial y^2} + F_{26}\left(\frac{\partial^2 \lambda_x}{\partial y^2} + \frac{\partial^2 \lambda_y}{\partial x\partial y}\right)$$

$$- \left[A_{44}\left(\psi_y + \frac{\partial w_0}{\partial y}\right) + A_{45}\left(\psi_x + \frac{\partial w_0}{\partial x}\right) + 2B_{44}\phi_y + 2B_{45}\phi_x + 3D_{44}\lambda_y\right.$$

$$\left. + 3D_{45}\lambda_x\right]$$

$$- \left[D_{44}\left(\psi_y + \frac{\partial w_0}{\partial y}\right) + D_{45}\left(\psi_x + \frac{\partial w_0}{\partial x}\right) + 2E_{44}\phi_y + 2E_{45}\phi_x + 3F_{44}\lambda_y\right.$$

$$\left. + 3F_{45}\lambda_x\right] = 0$$

(247)

6) Equation for second order displacement ϕ_x (rotation of the perpendicular to the midplane in the zx plane)

$$D_{11}\frac{\partial^2 u_0}{\partial x^2} + D_{12}\frac{\partial^2 v_0}{\partial x\partial y} + D_{16}\left(\frac{\partial^2 u_0}{\partial x\partial y} + \frac{\partial^2 v_0}{\partial x^2}\right) + E_{11}\frac{\partial^2 \psi_x}{\partial x^2} + E_{12}\frac{\partial^2 \psi_y}{\partial x\partial y} + E_{16}\left(\frac{\partial^2 \psi_x}{\partial x\partial y} + \frac{\partial^2 \psi_y}{\partial x^2}\right)$$

$$+ F_{11}\frac{\partial^2 \phi_x}{\partial x^2} + F_{12}\frac{\partial^2 \phi_y}{\partial x\partial y} + F_{16}\left(\frac{\partial^2 \phi_x}{\partial x\partial y} + \frac{\partial^2 \phi_y}{\partial x^2}\right) + G_{11}\frac{\partial^2 \lambda_x}{\partial x^2} + G_{12}\frac{\partial^2 \lambda_y}{\partial x\partial y}$$

$$+ G_{16}\left(\frac{\partial^2 \lambda_x}{\partial x\partial y} + \frac{\partial^2 \lambda_y}{\partial x^2}\right) + D_{16}\frac{\partial^2 u_0}{\partial x\partial y} + D_{26}\frac{\partial^2 v_0}{\partial y^2} + D_{66}\left(\frac{\partial^2 u_0}{\partial y^2} + \frac{\partial^2 v_0}{\partial x\partial y}\right)$$

$$+ E_{16}\frac{\partial^2 \psi_x}{\partial x\partial y} + E_{26}\frac{\partial^2 \psi_y}{\partial y^2} + E_{66}\left(\frac{\partial^2 \psi_x}{\partial y^2} + \frac{\partial^2 \psi_y}{\partial x\partial y}\right) + F_{16}\frac{\partial^2 \phi_x}{\partial x\partial y} + F_{26}\frac{\partial^2 \phi_y}{\partial y^2}$$

$$+ F_{66}\left(\frac{\partial^2 \phi_x}{\partial y^2} + \frac{\partial^2 \phi_y}{\partial x\partial y}\right) + G_{16}\frac{\partial^2 \lambda_x}{\partial x\partial y} + G_{26}\frac{\partial^2 \lambda_y}{\partial y^2} + G_{66}\left(\frac{\partial^2 \lambda_x}{\partial y^2} + \frac{\partial^2 \lambda_y}{\partial x\partial y}\right)$$

$$- 2\left[B_{45}\left(\psi_y + \frac{\partial w_0}{\partial y}\right) + B_{55}\left(\psi_x + \frac{\partial w_0}{\partial x}\right) + D_{45}2\phi_y + D_{55}2\phi_x + E_{45}3\lambda_y\right.$$

$$\left. + E_{55}3\lambda_x\right] = 0$$

(248)

7) Equation for second order displacement ϕ_y (rotation of the perpendicular to the midplane in the zy plane)

116

$$E_{11}\frac{\partial^2 u_0}{\partial x^2} + E_{12}\frac{\partial^2 v_0}{\partial x \partial y} + E_{16}\left(\frac{\partial^2 u_0}{\partial x \partial y} + \frac{\partial^2 v_0}{\partial x^2}\right) + F_{11}\frac{\partial^2 \psi_x}{\partial x^2} + F_{12}\frac{\partial^2 \psi_y}{\partial x \partial y} + F_{16}\left(\frac{\partial^2 \psi_x}{\partial x \partial y} + \frac{\partial^2 \psi_y}{\partial x^2}\right)$$

$$+ G_{11}\frac{\partial^2 \phi_x}{\partial x^2} + G_{12}\frac{\partial^2 \phi_y}{\partial x \partial y} + G_{16}\left(\frac{\partial^2 \phi_x}{\partial x \partial y} + \frac{\partial^2 \phi_y}{\partial x^2}\right) + H_{11}\frac{\partial^2 \lambda_x}{\partial x^2} + H_{12}\frac{\partial^2 \lambda_y}{\partial x \partial y}$$

$$+ H_{16}\left(\frac{\partial^2 \lambda_x}{\partial x \partial y} + \frac{\partial^2 \lambda_y}{\partial x^2}\right) + E_{16}\frac{\partial^2 u_0}{\partial x \partial y} + E_{26}\frac{\partial^2 v_0}{\partial y^2} + E_{66}\left(\frac{\partial^2 u_0}{\partial y^2} + \frac{\partial^2 v_0}{\partial x \partial y}\right)$$

$$+ F_{16}\frac{\partial^2 \psi_x}{\partial x \partial y} + F_{26}\frac{\partial^2 \psi_y}{\partial y^2} + F_{66}\left(\frac{\partial^2 \psi_x}{\partial y^2} + \frac{\partial^2 \psi_y}{\partial x \partial y}\right) + G_{16}\frac{\partial^2 \phi_x}{\partial x \partial y} + G_{26}\frac{\partial^2 \phi_y}{\partial y^2}$$

$$+ G_{66}\left(\frac{\partial^2 \phi_x}{\partial y^2} + \frac{\partial^2 \phi_y}{\partial x \partial y}\right) + H_{16}\frac{\partial^2 \lambda_x}{\partial x \partial y} + H_{26}\frac{\partial^2 \lambda_y}{\partial y^2} + H_{66}\left(\frac{\partial^2 \lambda_x}{\partial y^2} + \frac{\partial^2 \lambda_y}{\partial x \partial y}\right)$$

$$- 3\left[D_{45}\left(\psi_y + \frac{\partial w_0}{\partial y}\right) + D_{55}\left(\psi_x + \frac{\partial w_0}{\partial x}\right) + 2E_{45}\phi_y + 2E_{55}\phi_x + 3F_{45}\lambda_y\right.$$

$$\left. + 3F_{55}\lambda_x\right] = 0$$

$$(249)$$

8) Equation for the third order displacement λ_y (rotation of the perpendicular to the midplane in the zy plane)

$$E_{16}\frac{\partial^2 u_0}{\partial x^2} + E_{26}\frac{\partial^2 v_0}{\partial x \partial y} + E_{66}\left(\frac{\partial^2 u_0}{\partial x \partial y} + \frac{\partial^2 v_0}{\partial x^2}\right) + F_{16}\frac{\partial^2 \psi_x}{\partial x^2} + F_{26}\frac{\partial^2 \psi_y}{\partial x \partial y} + F_{66}\left(\frac{\partial^2 \psi_x}{\partial x \partial y} + \frac{\partial^2 \psi_y}{\partial x^2}\right)$$

$$+ G_{16}\frac{\partial^2 \phi_x}{\partial x^2} + G_{26}\frac{\partial^2 \phi_y}{\partial x \partial y} + G_{66}\left(\frac{\partial^2 \phi_x}{\partial x \partial y} + \frac{\partial^2 \phi_y}{\partial x^2}\right) + H_{16}\frac{\partial^2 \lambda_x}{\partial x^2} + H_{26}\frac{\partial^2 \lambda_y}{\partial x \partial y}$$

$$+ H_{66}\left(\frac{\partial^2 \lambda_x}{\partial x \partial y} + \frac{\partial^2 \lambda_y}{\partial x^2}\right) + E_{12}\frac{\partial^2 u_0}{\partial x \partial y} + E_{22}\frac{\partial^2 v_0}{\partial y^2} + E_{26}\left(\frac{\partial^2 u_0}{\partial y^2} + \frac{\partial^2 v_0}{\partial x \partial y}\right)$$

$$+ F_{12}\frac{\partial^2 \psi_x}{\partial x \partial y} + F_{22}\frac{\partial^2 \psi_y}{\partial y^2} + F_{26}\left(\frac{\partial^2 \psi_x}{\partial y^2} + \frac{\partial^2 \psi_y}{\partial x \partial y}\right) + G_{12}\frac{\partial^2 \phi_x}{\partial x \partial y} + G_{22}\frac{\partial^2 \phi_y}{\partial y^2}$$

$$+ G_{26}\left(\frac{\partial^2 \phi_x}{\partial y^2} + \frac{\partial^2 \phi_y}{\partial x \partial y}\right) + H_{12}\frac{\partial^2 \lambda_x}{\partial x \partial y} + H_{22}\frac{\partial^2 \lambda_y}{\partial y^2} + H_{26}\left(\frac{\partial^2 \lambda_x}{\partial y^2} + \frac{\partial^2 \lambda_y}{\partial x \partial y}\right)$$

$$- 3\left[D_{44}\varepsilon_{yz}^0 + D_{45}\varepsilon_{xz}^0 + E_{44}\varepsilon_{yz}^1 + E_{45}\varepsilon_{xz}^1 + F_{44}\varepsilon_{yz}^2 + F_{45}\varepsilon_{xz}^2\right] = 0$$

$$(250)$$

9) Equation for the third order displacement λ_x (rotation of the perpendicular to the midplane in the zx plane)

$$D_{16}\frac{\partial^2 u_0}{\partial x^2} + D_{26}\frac{\partial^2 v_0}{\partial x \partial y} + D_{66}\left(\frac{\partial^2 u_0}{\partial x \partial y} + \frac{\partial^2 v_0}{\partial x^2}\right) + E_{16}\frac{\partial^2 \psi_x}{\partial x^2} + E_{26}\frac{\partial^2 \psi_y}{\partial x \partial y} + E_{66}\left(\frac{\partial^2 \psi_x}{\partial x \partial y} + \frac{\partial^2 \psi_y}{\partial x^2}\right)$$

$$+ F_{16}\frac{\partial^2 \phi_x}{\partial x^2} + F_{26}\frac{\partial^2 \phi_y}{\partial x \partial y} + F_{66}\left(\frac{\partial^2 \phi_x}{\partial x \partial y} + \frac{\partial^2 \phi_y}{\partial x^2}\right) + G_{16}\frac{\partial^2 \lambda_x}{\partial x^2} + G_{26}\frac{\partial^2 \lambda_y}{\partial x \partial y}$$

$$+ G_{66}\left(\frac{\partial^2 \lambda_x}{\partial x \partial y} + \frac{\partial^2 \lambda_y}{\partial x^2}\right) + D_{12}\frac{\partial^2 u_0}{\partial x \partial y} + D_{22}\frac{\partial^2 v_0}{\partial y^2} + D_{26}\left(\frac{\partial^2 u_0}{\partial y^2} + \frac{\partial^2 v_0}{\partial x \partial y}\right)$$

$$+ E_{12}\frac{\partial^2 \psi_x}{\partial x \partial y} + E_{22}\frac{\partial^2 \psi_y}{\partial y^2} + E_{26}\left(\frac{\partial^2 \psi_x}{\partial y^2} + \frac{\partial^2 \psi_y}{\partial x \partial y}\right) + F_{12}\frac{\partial^2 \phi_x}{\partial x \partial y} + F_{22}\frac{\partial^2 \phi_y}{\partial y^2}$$

$$+ F_{26}\left(\frac{\partial^2 \phi_x}{\partial y^2} + \frac{\partial^2 \phi_y}{\partial x \partial y}\right) + G_{12}\frac{\partial^2 \lambda_x}{\partial x \partial y} + G_{22}\frac{\partial^2 \lambda_y}{\partial y^2} + G_{26}\left(\frac{\partial^2 \lambda_x}{\partial y^2} + \frac{\partial^2 \lambda_y}{\partial x \partial y}\right)$$

$$- 2\left[B_{44}\left(\psi_y + \frac{\partial w_0}{\partial y}\right) + B_{45}\left(\psi_x + \frac{\partial w_0}{\partial x}\right) + 2D_{44}\phi_y + 2D_{45}\phi_x + 3E_{44}\lambda_y\right.$$

$$\left. + 3E_{45}\lambda_x\right] = 0$$

<div align="right">(251)</div>

13.5 Effects of moisture and fiber orientation on material parameters of wood

As can be seen from the Graph 26-Graph 36, the material constants depend on both moisture content and fiber orientation. In the case of the stiffness matrix C11, the greater the fiber deflection and the greater the moisture content, the more the modulus of elasticity decreases. In the case of stiffness matrix $C_{11}=10000$ MPa, which we transform to an angle of 90° and convert to a material moisture content of 30%, then C_{11} is around 212 MPa. The stiffness matrix is therefore reduced by 98% of its original value. When only the moisture content is changed, the stiffness matrix is reduced by 36%.

The following graphs are expressions of the dependence of the material constants on moisture content and fiber deflection separately and the dependence on moisture content and fiber deflection simultaneously.
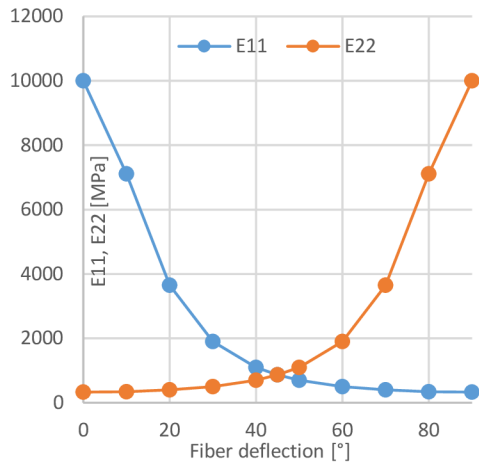
Graph 26 - the dependence of the elastic moduli E11 and E22 on the fibre deflection
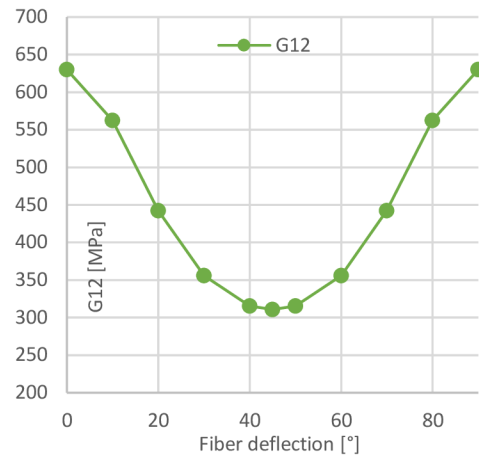
Graph 27 - the dependence of the elastic moduli G12 on the fibre deflection
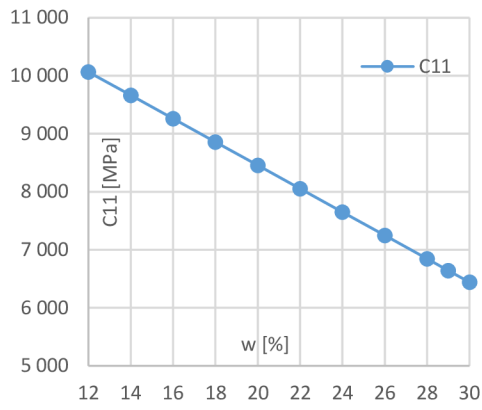
Graph 28 the dependence of the stiffness parameter C11 on the moisture content
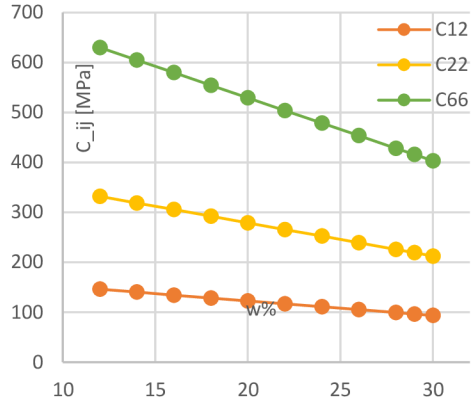
Graph 29 - the dependence of the stiffness parameter C12, C22, C66 on the moisture content

119
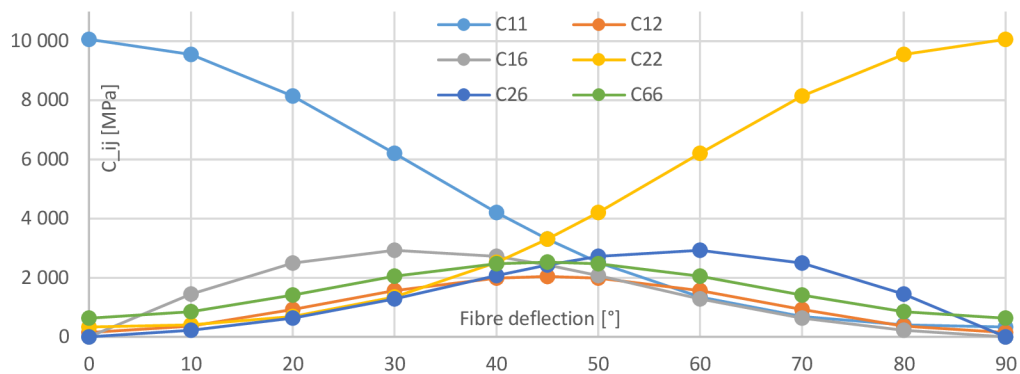
Graph 30 - the dependence of the stiffness parameter C_ij on the fiber deflection
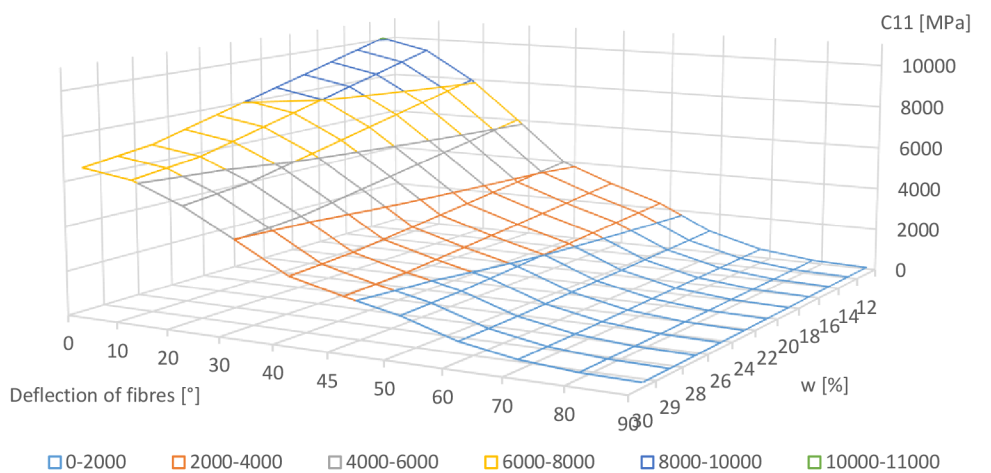
Graph 31 - the dependence of the stiffness parameter C11 on the fiber orientation and moisture content
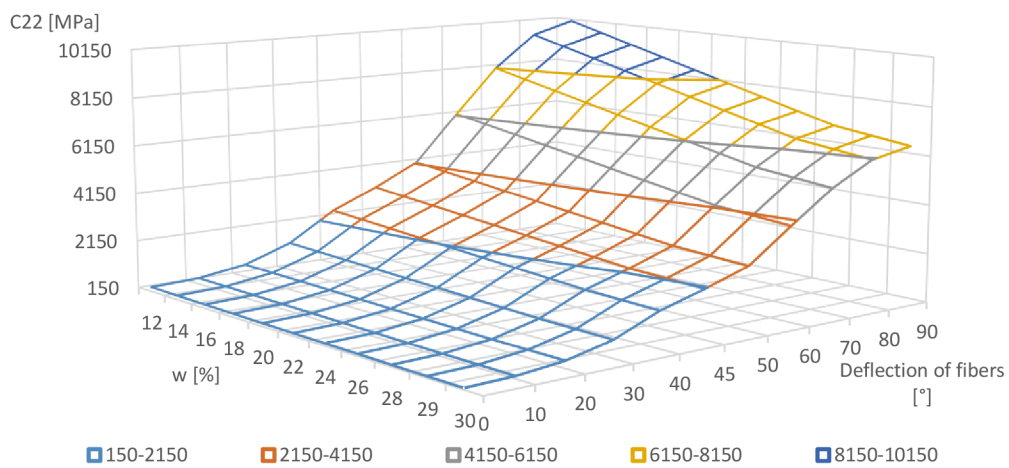
Graph 32 - the dependence of the stiffness parameter C22 on the fiber orientation and moisture content
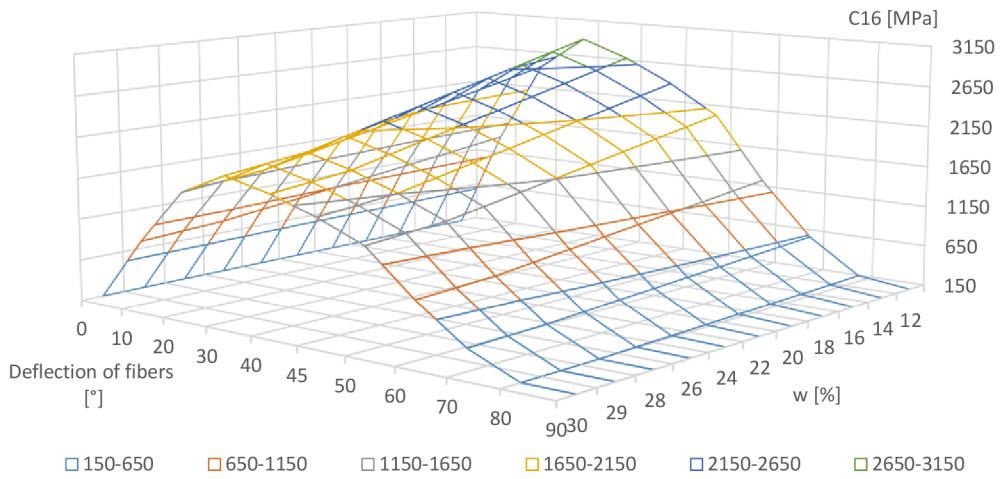
Graph 33 - the dependence of the stiffness parameter C16 on the fibre orientation and moisture content
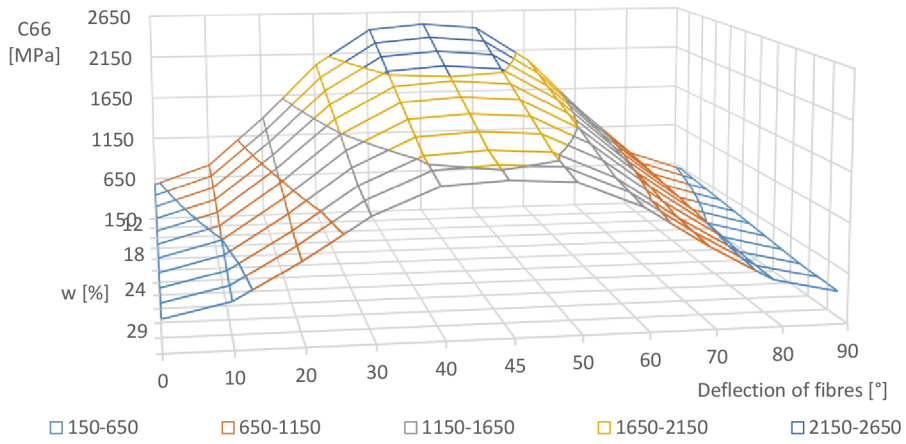
Graph 34 - the dependence of the stiffness parameter C66 on the fiber orientation and moisture content
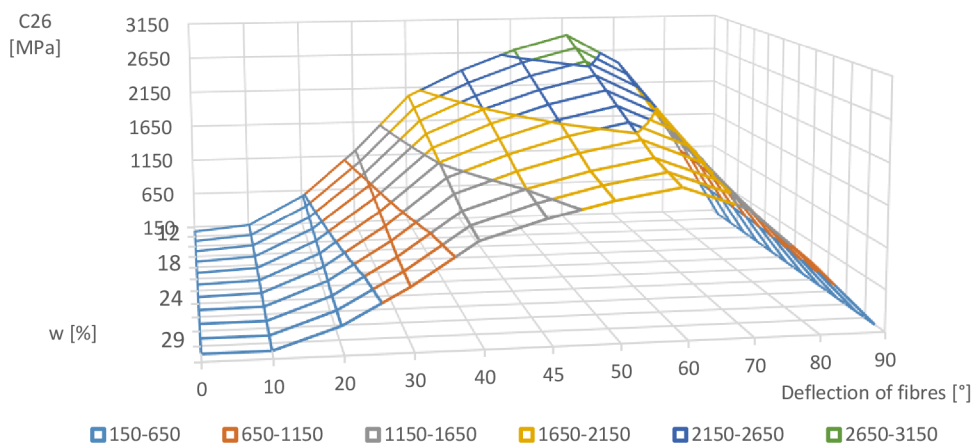
Graph 35 - the dependence of the stiffness parameter C26 on the fiber orientation and moisture content
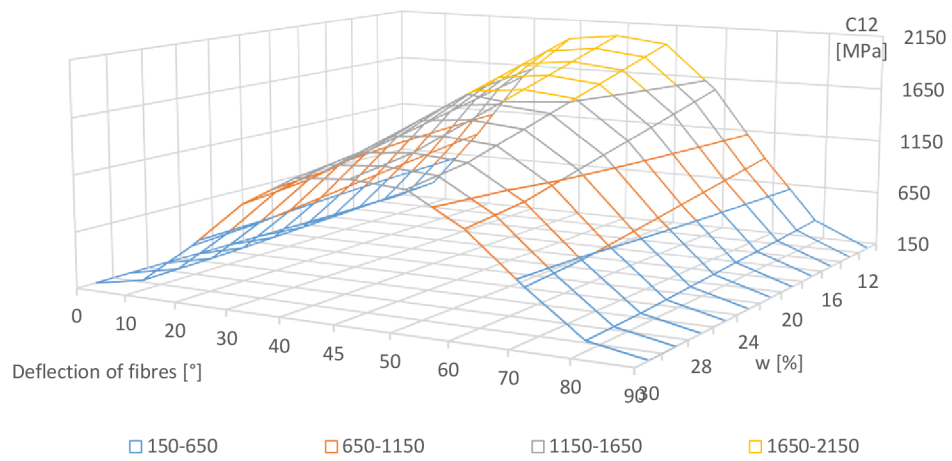
Graph 36 - the dependence of the stiffness parameter C12 on the fiber orientation and moisture content

13.6 Numerical FlexPDE script – Non-stationary 3D moisture diffusion

```
TITLE 'Non-stationary 3D moisture diffusion at 20°C'

SELECT
errlim=1e-5
painted

COORDINATES
cartesian3

VARIABLES
w

DEFINITIONS
vyska = 0.1
delka = 1.0
tp=273.15+20
ro=0.450
w_fin_voda=0.30
w_fin_vzduch=0.16

koeficient1=3.5
koeficient2=1

patm=100000
rvoda=1
R=8.341
rk=ro/(1+0.28*ro)
Pw=1-rk*(0.653+w)
Ea=38500-29000*w
Eo=40600+42.4*(tp-273)
po=1.3*10^(11)*exp(-Eo/(R*tp))
rBS=1.53/(1+1.53*w)
A=7.731706-0.014348*tp
B=0.008746+0.000567*tp
dphidw=100*A*B*exp(-100*B*w)*exp(-A*exp(-100*B*w))

Da=(2.2/patm)*(tp/273.15)^1.75
DBT=7*10^(-6)*exp(-Ea/(R*tp))
DV=Da*0.018*po/(rBS*rvoda*R*tp)*dphidw

DTang=(1/(1-Pw))*(DBT*DV/(DBT+DV*(1-Pw^(1/2))))*koeficient1
DRad=3/2*DTang

DBL=2.5*DBT
DLong=(Pw/(1-Pw))*(DV* DBL/(DBL+0.01*(1-Pw^(1/2))*DV))*koeficient2

hw_voda=1e-6
hw_vzduch=2e-7

INITIAL VALUES
w=0.12
```

```
EQUATIONS
dx(DLong*dx(w))+dy(DRad*dy(w))+dz(DTang*dz(w))-dt(w)=0

EXTRUSION
z = -vyska/2,vyska/2

BOUNDARIES

   surface 1 natural(w)=hw_vzduch*(w_fin_vzduch-w)
   surface 2 natural(w)=hw_voda*(w_fin_voda-w)

    Region 1
         start(-delka/2,-delka/2)
             natural(w)=hw_vzduch*(w_fin_vzduch-w)
         line to (delka/2,-delka/2)
         to (delka/2,delka/2)
         to (-delka/2,delka/2)
         to close

TIME
0 to 30*86400

PLOTS
    for t = 0 by 1*86400 to 30*86400
contour(w) on z=0  as "Moisture distribution in the plane XY [-]"
contour(w) on x=0  as "Moisture distribution in the plane YZ [-]"
contour(w) on y=0  as "Moisture distribution in the plane XZ [-]"
elevation(w) from (-delka/2,0,0) to (delka/2,0,0) as "Moisture content
- X-axis [-]"
elevation(w) from (0,-delka/2,0) to (0,delka/2,0) as "Moisture content
Y-axis [-]"
elevation(w) from (0,0,-vyska/2) to (0,0,vyska/2) as "Moisture content
-Z-axis [-]"

HISTORIES
history(w) at (0,0,-0.045) (0,0,0) (0,0,0.045) fixed range(0.1,0.35) as
"Moisture content change over time [-]"

END
```

13.7 Numerical FlexPDE script – CPT

```
TITLE 'Bending - 3 LAYERS - CPT'

SELECT
ngrid=16      { increase initial gridding }
errlim =1e-4       { increase accuracy to resolve stresses }
painted                 { paint all contour plots }

VARIABLES
u
v
w
wxx
wyy
uxx
```

```
uyy
vxx
vyy

DEFINITIONS     { parameter definitions }
E_11  = 11*10^9
E_22 = 0.37*10^9
G_12 = 0.69*10^9
G_13 = G_12
G_23 = G_12

v12=0.2
v21 = (E_22/E_11)*v12

! LAMINAE LAYERS, GEOMETRY
h1 = 0.03
h2 = 0.03
h3 = 0.03
h=h1 + h2 + h3

rho = 410
g=rho*9.81
L1=1.5
L2=0.3

a1 = 0
a2 = 90
a3 = 0

p= - 12000 - (g*h) {N.m-2}

Q11 = E_11 / (1-v12*v21)
Q12 = (v12 * E_22) / (1-v12*v21)
Q16 = 0
Q26 = 0
Q22 = E_22 / (1-v12*v21)
Q66 = G_12

m1=1 !cos(30 degrees)
n1=0 !sin(30 degrees)
m2=0 !cos(55 degrees)
n2=1 !sin(55 degrees)
m3=1 !cos(83 degrees)
n3=0 !sin(83 degrees)

Q_11_1 = Q11*m1^4+2*(Q12+2*Q66)*m1^2*n1^2+Q22*n1^4
Q_12_1 = (Q11+Q22-4*Q66)*m1^2*n1^2+Q12*(m1^4+n1^4)
Q_22_1 = Q11*n1^4+2*(Q12+2*Q66)*m1^2*n1^2+Q22*m1^4
Q_16_1 = (Q11-Q12-2*Q66)*(m1)^3*n1+(Q12-Q22+2*Q66)*m1*(n1)^3
Q_26_1 = (Q11-Q12-2*Q66)*n1^3*m1+(Q12-Q22+2*Q66)*n1*m1^3
Q_66_1 = (Q11+Q22-2*Q12-2*Q66)*m1^2*n1^2+Q66*(m1^4+n1^4)

Q_11_2 = Q11*m2^4+2*(Q12+2*Q66)*m2^2*n2^2+Q22*n2^4
Q_12_2 = (Q11+Q22-4*Q66)*m2^2*n2^2+Q12*(m2^4+n2^4)
Q_22_2 = Q11*n2^4+2*(Q12+2*Q66)*m2^2*n2^2+Q22*m2^4
Q_16_2 = (Q11-Q12-2*Q66)*m2^3*n2+(Q12-Q22+2*Q66)*m2*n2^3
Q_26_2 = (Q11-Q12-2*Q66)*n2^3*m2+(Q12-Q22+2*Q66)*n2*m2^3
```

```
Q_66_2 = (Q11+Q22-2*Q12-2*Q66)*m2^2*n2^2+Q66*(m2^4+n2^4)


Q_11_3 = Q11*m3^4+2*(Q12+2*Q66)*m3^2*n3^2+Q22*n3^4
Q_12_3 = (Q11+Q22-4*Q66)*m3^2*n3^2+Q12*(m3^4+n3^4)
Q_22_3 = Q11*n3^4+2*(Q12+2*Q66)*m3^2*n3^2+Q22*m3^4
Q_16_3 = (Q11-Q12-2*Q66)*m3^3*n3+(Q12-Q22+2*Q66)*m3*n3^3
Q_26_3 = (Q11-Q12-2*Q66)*n3^3*m3+(Q12-Q22+2*Q66)*n3*m3^3
Q_66_3 = (Q11+Q22-2*Q12-2*Q66)*m3^2*n3^2+Q66*(m3^4+n3^4)

A11 = Q_11_1 * ( (h2/2 + h1) - h2/2) + Q_11_2 * ( (h2/2) - (-h2/2)) +
Q_11_3 * ( (-h2/2) - (-h2/2 - h3))
A12 = Q_12_1 * ( (h2/2 + h1) - h2/2) + Q_12_2 * ( (h2/2) - (-h2/2)) +
Q_12_3 * ( (-h2/2) - (-h2/2 - h3))
A22 = Q_22_1 * ( (h2/2 + h1) - h2/2) + Q_22_2 * ( (h2/2) - (-h2/2)) +
Q_22_3 * ( (-h2/2) - (-h2/2 - h3))
A16 = Q_16_1 * ( (h2/2 + h1) - h2/2) + Q_16_2 * ( (h2/2) - (-h2/2)) +
Q_16_3 * ( (-h2/2) - (-h2/2 - h3))
A26 = Q_26_1 * ( (h2/2 + h1) - h2/2) + Q_26_2 * ( (h2/2) - (-h2/2)) +
Q_26_3 * ( (-h2/2) - (-h2/2 - h3))
A66 = Q_66_1 * ( (h2/2 + h1) - h2/2) + Q_66_2 * ( (h2/2) - (-h2/2)) +
Q_66_3 * ( (-h2/2) - (-h2/2 - h3))

B11 = 1/2 * ( Q_11_1 * ( (h2/2 + h1)^2 - (h2/2)^2) + Q_11_2 * (
(h2/2)^2 - (-h2/2)^2) + Q_11_3 * ( (-h2/2)^2 - (-h2/2 - h3)^2))
B12 = 1/2 * ( Q_12_1 * ( (h2/2 + h1)^2 - (h2/2)^2) + Q_12_2 * (
(h2/2)^2 - (-h2/2)^2) + Q_12_3 * ( (-h2/2)^2 - (-h2/2 - h3)^2))
B22 = 1/2 * ( Q_22_1 * ( (h2/2 + h1)^2 - (h2/2)^2) + Q_22_2 * (
(h2/2)^2 - (-h2/2)^2) + Q_22_3 * ( (-h2/2)^2 - (-h2/2 - h3)^2))
B16 = 1/2 * ( Q_16_1 * ( (h2/2 + h1)^2 - (h2/2)^2) + Q_16_2 * (
(h2/2)^2 - (-h2/2)^2) + Q_16_3 * ( (-h2/2)^2 - (-h2/2 - h3)^2))
B26 = 1/2 * ( Q_26_1 * ( (h2/2 + h1)^2 - (h2/2)^2) + Q_26_2 * (
(h2/2)^2 - (-h2/2)^2) + Q_26_3 * ( (-h2/2)^2 - (-h2/2 - h3)^2))
B66 = 1/2 * ( Q_66_1 * ( (h2/2 + h1)^2 - (h2/2)^2) + Q_66_2 * (
(h2/2)^2 - (-h2/2)^2) + Q_66_3 * ( (-h2/2)^2 - (-h2/2 - h3)^2))

D11 = 1/3 * ( Q_11_1 * ( (h2/2 + h1)^3 - (h2/2)^3) + Q_11_2 * (
(h2/2)^3 - (-h2/2)^3) + Q_11_3 * ( (-h2/2)^3 - (-h2/2 - h3)^3))
D12 = 1/3 * ( Q_12_1 * ( (h2/2 + h1)^3 - (h2/2)^3) + Q_12_2 * (
(h2/2)^3 - (-h2/2)^3) + Q_12_3 * ( (-h2/2)^3 - (-h2/2 - h3)^3))
D22 = 1/3 * ( Q_22_1 * ( (h2/2 + h1)^3 - (h2/2)^3) + Q_22_2 * (
(h2/2)^3 - (-h2/2)^3) + Q_22_3 * ( (-h2/2)^3 - (-h2/2 - h3)^3))
D16 = 1/3 * ( Q_16_1 * ( (h2/2 + h1)^3 - (h2/2)^3) + Q_16_2 * (
(h2/2)^3 - (-h2/2)^3) + Q_16_3 * ( (-h2/2)^3 - (-h2/2 - h3)^3))
D26 = 1/3 * ( Q_26_1 * ( (h2/2 + h1)^3 - (h2/2)^3) + Q_26_2 * (
(h2/2)^3 - (-h2/2)^3) + Q_26_3 * ( (-h2/2)^3 - (-h2/2 - h3)^3))
D66 = 1/3 * ( Q_66_1 * ( (h2/2 + h1)^3 - (h2/2)^3) + Q_66_2 * (
(h2/2)^3 - (-h2/2)^3) + Q_66_3 * ( (-h2/2)^3 - (-h2/2 - h3)^3))

!_____


ex=dx(u)
ey=dy(v)
exy=dx(v)+dy(u)
kx=-dxx(w)
ky=-dyy(w)
kxy=-2*( dxy(w) )
```

```
{1.
TOP_____}

e1_1_top = ex + (h1+h2/2) * kx
e2_1_top = ey + (h1+h2/2) * ky
e6_1_top = exy + (h1+h2/2) * kxy

Sigma_x_1_top = Q_11_1*e1_1_top + Q_12_1*e2_1_top + Q_16_1*e6_1_top
Sigma_y_1_top = Q_12_1*e1_1_top + Q_22_1*e2_1_top + Q_26_1*e6_1_top
Sigma_xy_1_top = Q_16_1*e1_1_top + Q_26_1*e2_1_top + Q_66_1*e6_1_top

{1.
MID_____}

e1_1_mid = ex + (h1/2+h2/2) * kx
e2_1_mid = ey + (h1/2+h2/2) * ky
e6_1_mid = exy + (h1/2+h2/2) * kxy

Sigma_x_1_mid = Q_11_1*e1_1_mid + Q_12_1*e2_1_mid + Q_16_1*e6_1_mid
Sigma_y_1_mid = Q_12_1*e1_1_mid + Q_22_1*e2_1_mid + Q_26_1*e6_1_mid
Sigma_xy_1_mid = Q_16_1*e1_1_mid + Q_26_1*e2_1_mid + Q_66_1*e6_1_mid

{1.
BOT_____}

e1_1_bot = ex + (h2/2) * kx
e2_1_bot = ey + (h2/2) * ky
e6_1_bot = exy + (h2/2) * kxy

Sigma_x_1_bot = Q_11_1*e1_1_bot + Q_12_1*e2_1_bot + Q_16_1*e6_1_bot
Sigma_y_1_bot = Q_12_1*e1_1_bot + Q_22_1*e2_1_bot + Q_26_1*e6_1_bot
Sigma_xy_1_bot = Q_16_1*e1_1_bot + Q_26_1*e2_1_bot + Q_66_1*e6_1_bot

{2.
TOP_____}

e1_2_top = ex + (h2/2) * kx
e2_2_top = ey + (h2/2) * ky
e6_2_top = exy + (h2/2) * kxy

Sigma_x_2_top = Q_11_2*e1_2_top + Q_12_2*e2_2_top + Q_16_2*e6_2_top
Sigma_y_2_top = Q_12_2*e1_2_top + Q_22_2*e2_2_top + Q_26_2*e6_2_top
Sigma_xy_2_top = Q_16_2*e1_2_top + Q_26_2*e2_2_top + Q_66_2*e6_2_top

{2.
MID_____}

e1_2_mid = ex + (0) * kx
e2_2_mid = ey + (0) * ky
e6_2_mid = exy + (0) * kxy

Sigma_x_2_mid = Q_11_2*e1_2_mid + Q_12_2*e2_2_mid + Q_16_2*e6_2_mid
Sigma_y_2_mid = Q_12_2*e1_2_mid + Q_22_2*e2_2_mid + Q_26_2*e6_2_mid
Sigma_xy_2_mid = Q_16_2*e1_2_mid + Q_26_2*e2_2_mid + Q_66_2*e6_2_mid

{2.
BOT_____}
```

```
e1_2_bot = ex + (-h2/2) * kx
e2_2_bot = ey + (-h2/2) * ky
e6_2_bot = exy + (-h2/2) * kxy

Sigma_x_2_bot = Q_11_2*e1_2_bot + Q_12_2*e2_2_bot + Q_16_2*e6_2_bot
Sigma_y_2_bot = Q_12_2*e1_2_bot + Q_22_2*e2_2_bot + Q_26_2*e6_2_bot
Sigma_xy_2_bot = Q_16_2*e1_2_bot + Q_26_2*e2_2_bot + Q_66_2*e6_2_bot
```

{3.
TOP_____}

```
e1_3_top = ex + (-h2/2) * kx
e2_3_top = ey + (-h2/2) * ky
e6_3_top = exy + (-h2/2) * kxy

Sigma_x_3_top = Q_11_3*e1_3_top + Q_12_3*e2_3_top + Q_16_3*e6_3_top
Sigma_y_3_top = Q_12_3*e1_3_top + Q_22_3*e2_3_top + Q_26_3*e6_3_top
Sigma_xy_3_top = Q_16_3*e1_3_top + Q_26_3*e2_3_top + Q_66_3*e6_3_top
```

{3.
MID_____}

```
e1_3_mid = ex + (-h1/2-h2/2) * kx
e2_3_mid = ey + (-h1/2-h2/2) * ky
e6_3_mid = exy + (-h1/2-h2/2) * kxy

Sigma_x_3_mid = Q_11_3*e1_3_mid + Q_12_3*e2_3_mid + Q_16_3*e6_3_mid
Sigma_y_3_mid = Q_12_3*e1_3_mid + Q_22_3*e2_3_mid + Q_26_3*e6_3_mid
Sigma_xy_3_mid = Q_16_3*e1_3_mid + Q_26_3*e2_3_mid + Q_66_3*e6_3_mid
```

{3.
BOT_____}

```
e1_3_bot = ex + (-h1-h2/2) * kx
e2_3_bot = ey + (-h1-h2/2) * ky
e6_3_bot = exy + (-h1-h2/2) * kxy

Sigma_x_3_bot = Q_11_3*e1_3_bot + Q_12_3*e2_3_bot + Q_16_3*e6_3_bot
Sigma_y_3_bot = Q_12_3*e1_3_bot + Q_22_3*e2_3_bot + Q_26_3*e6_3_bot
Sigma_xy_3_bot = Q_16_3*e1_3_bot + Q_26_3*e2_3_bot + Q_66_3*e6_3_bot
```

INITIAL VALUES
```
u = 0
v = 0
w  = 0
wxx = 0
wyy = 0
uxx = 0
uyy = 0
vxx = 0
vyy = 0
!wx = 0
!wy = 0
```

EQUATIONS

```
wxx:    dxx(w)=wxx
wyy:    dyy(w)=wyy
uxx:    dxx(u)=uxx
uyy:    dyy(u)=uyy
vxx:    dxx(v)=vxx
vyy:    dyy(v)=vyy

u:
A11*dxx(u)+A12*dxy(v)+A16*(dxy(u)+dxx(v))-
(B11*dx(wxx)+B12*dx(wyy)+2*B16*dy(wxx)) +
A16*dxy(u)+A26*dyy(v)+A66*(dyy(u)+dxy(v)) -
(B16*dy(wxx)+B26*dy(wyy)+2*B66*dx(wyy))=0

v:
A16*dxx(u)+A26*dxy(v)+A66*(dxy(u)+dxx(v)) -
(B16*dx(wxx)+B26*dx(wyy)+2*B66*dy(wxx)) +
A12*dxy(u)+A22*dyy(v)+A26*(dyy(u)+dxy(v)) -
(B12*dy(wxx)+B22*dy(wyy)+2*B26*dx(wyy)) = 0

w:
B11*dx(uxx)+B12*dy(vxx)+B16*(dy(uxx)+dx(vxx)) -
(D11*dxx(wxx)+D12*dyy(wxx)+2*D16*(dxy(wxx))) +
B16*dy(uxx)+B26*dx(vyy)+B66*(dx(uyy)+dy(vxx)) -
(D16*dxy(wxx)+D26*dxy(wyy)+2*D66*(dxx(wyy))) +
B12*dx(uyy)+B22*dy(vyy)+B26*(dy(uyy)+dx(vyy)) -
(D12*dxx(wyy)+D22*dyy(wyy)+2*D26*(dxy(wyy))) = -p
```

BOUNDARY CONDITIONS

"simply supported y" :
```
            VALUE(w)=0
            VALUE(wxx)=0
            natural(wyy)=0
            VALUE(v)=0
            VALUE(u)=0
            natural(uxx)=0
            natural(uyy)=0
            VALUE(vxx)=0
            VALUE(vyy)=0
```

"free edge x" :
```
            natural(w)=0
            natural(wxx)=0
            VALUE(wyy)=0
            VALUE(v)=0
            natural(u)=0
            natural(uxx)=0
            natural(uyy)=0
            natural(vxx)=0
            natural(vyy)=0
```

BOUNDARIES
```
 region 1
      start (0,0)
            USE BC "free edge x"
      line to (L1,0)
```

```
                USE BC "simply supported y"
        line to (L1,L2)
                USE BC "free edge x"
        line to (0,L2)
                USE BC "simply supported y"
line to close

PLOTS
        contour(w)      { show deformed grid as solution progresses }
          surface(w)
          elevation(w) from (0,L2/2) to (L1/2,L2/2)
          elevation(w) from (L1/2,0) to (L1/2,L2)

END
```

13.8 Numerical FlexPDE script – FOSDT

```
TITLE 'Bending - 3 LAYERS - FOSDT-DE'

SELECT
ngrid=21              { increase initial gridding }
cubic                  { Use Cubic Basis }
errlim =1e-4             { increase accuracy to resolve stresses }
painted                  { paint all contour plots }
!CHANGELIM = 0.1
!STAGES = 36
!autostage = on
!PREFER_STABILITY=on
!NONLINEAR=off

VARIABLES
wxx
wyy
w
u
v
F_x_x
F_x
F_y_y
F_y

DEFINITIONS     { parameter definitions }
    layer_1_w = 30
    layer_2_w = 12
    layer_3_w = 12
      layer11=12                                        {°C}
      layer12= layer_1_w
      layer21=12
      layer22=layer_2_w
      layer31=12
      layer32=layer_3_w
    abs_w_1=(layer11-layer12)
    abs_w_2=(layer21-layer22)
    abs_w_3=(layer31-layer32)

! Layer 1    C22
```

130

```
E_11_1_w12 = 11*10^9
E_22_1_w12 = 0.37*10^9
G_12_1_w12 = 0.69*10^9
G_13_1_w12 = G_12_1_w12
G_23_1_w12 = G_12_1_w12
E_11_1 = E_11_1_w12*(1+0.02*(12-layer_1_w))
E_22_1 = E_22_1_w12*(1+0.02*(12-layer_1_w))
G_12_1 = G_12_1_w12*(1+0.02*(12-layer_1_w))
G_13_1 = G_13_1_w12*(1+0.02*(12-layer_1_w))
G_23_1 = G_23_1_w12*(1+0.02*(12-layer_1_w))

v12_1=0.2
v21_1 = (E_22_1/E_11_1)*v12_1

rho_1 = 420 !kg/m3
rho0_1=rho_1/1000 !g/m3
g_1=rho_1*9.81

Q11_1 = E_11_1 / (1-v12_1*v21_1)
Q12_1 = (v12_1 * E_22_1) / (1-v12_1*v21_1)
Q16_1 = 0
Q26_1 = 0
Q22_1 = E_22_1 / (1-v12_1*v21_1)
Q66_1 = G_12_1
Q44_1 = G_23_1
Q55_1 = G_13_1

! Layer 2    C22
E_11_2_w12 = 11*10^9
E_22_2_w12 = 0.37*10^9
G_12_2_w12 = 0.69*10^9
G_13_2_w12 = G_12_2_w12
G_23_2_w12 = G_12_2_w12

E_11_2 = E_11_2_w12*(1+0.02*(12-layer_2_w))
E_22_2 = E_22_2_w12*(1+0.02*(12-layer_2_w))
G_12_2 = G_12_2_w12*(1+0.02*(12-layer_2_w))
G_13_2 = G_13_2_w12*(1+0.02*(12-layer_2_w))
G_23_2 = G_23_2_w12*(1+0.02*(12-layer_2_w))

v12_2 = 0.2
v21_2 = (E_22_2/E_11_2)*v12_2

rho_2 = 420
rho0_2=rho_2/1000
g_2=rho_2*9.81

Q11_2 = E_11_2 / (1-v12_2*v21_2)
Q12_2 = (v12_2 * E_22_2) / (1-v12_2*v21_2)
Q16_2 = 0
Q26_2 = 0
Q22_2 = E_22_2 / (1-v12_2*v21_2)
Q66_2 = G_12_2
Q44_2 = G_23_2
Q55_2 = G_13_2

! Layer 3    C22
```

```
E_11_3_w12 = 11*10^9
E_22_3_w12 = 0.37*10^9
G_12_3_w12 = 0.69*10^9
G_13_3_w12 = G_12_3_w12
G_23_3_w12 = G_12_3_w12
E_11_3 = E_11_3_w12*(1+0.02*(12-layer_3_w))
E_22_3 = E_22_3_w12*(1+0.02*(12-layer_3_w))
G_12_3 = G_12_3_w12*(1+0.02*(12-layer_3_w))
G_13_3 = G_13_3_w12*(1+0.02*(12-layer_3_w))
G_23_3 = G_23_3_w12*(1+0.02*(12-layer_3_w))

v12_3 = 0.2
v21_3 = (E_22_3/E_11_3)*v12_3

rho_3 = 420
rho0_3=rho_3/1000
g_3=rho_3*9.81

Q11_3 = E_11_3 / (1-v12_3*v21_3)
Q12_3 = (v12_3 * E_22_3) / (1-v12_3*v21_3)
Q16_3 = 0
Q26_3 = 0
Q22_3 = E_22_3 / (1-v12_3*v21_3)
Q66_3 = G_12_3
Q44_3 = G_23_3
Q55_3 = G_13_3

! LAMINAE LAYERS THICKNESS, GEOMETRY
h1 = 0.03
h2 = 0.03
h3 = 0.03
h=h1 + h2 + h3

L1=1.5
L2=0.3

p= - 12000    {N.m-2}

m1=1 !cos(a1 degrees)
n1=0 !sin(a1 degrees)
m2=0 !cos(a2 degrees)
n2=1 !sin(a2 degrees)
m3=1 !cos(a3 degrees)
n3=0 !sin(a3 degrees)

Q_11_1 = Q11_1*m1^4+2*(Q12_1+2*Q66_1)*m1^2*n1^2+Q22_1*n1^4
Q_12_1 = (Q11_1+Q22_1-4*Q66_1)*m1^2*n1^2+Q12_1*(m1^4+n1^4)
Q_22_1 = Q11_1*n1^4+2*(Q12_1+2*Q66_1)*m1^2*n1^2+Q22_1*m1^4
Q_16_1 = (Q11_1-Q12_1-2*Q66_1)*(m1)^3*n1+(Q12_1-Q22_1+2*Q66_1)*m1*(n1)^3
Q_26_1 = (Q11_1-Q12_1-2*Q66_1)*n1^3*m1+(Q12_1-Q22_1+2*Q66_1)*n1*m1^3
Q_66_1 = (Q11_1+Q22_1-2*Q12_1-2*Q66_1)*m1^2*n1^2+Q66_1*(m1^4+n1^4)
Q_44_1 = Q44_1*m1^2+Q55_1*n1^2
Q_45_1 = (Q55_1-Q44_1)*n1*m1
Q_55_1 = Q55_1*m1^2+Q44_1*n1^2

Q_11_2 = Q11_2*m2^4+2*(Q12_2+2*Q66_2)*m2^2*n2^2+Q22_2*n2^4
```

```
Q_12_2 = (Q11_2+Q22_2-4*Q66_2)*m2^2*n2^2+Q12_2*(m2^4+n2^4)
Q_22_2 = Q11_2*n2^4+2*(Q12_2+2*Q66_2)*m2^2*n2^2+Q22_2*m2^4
Q_16_2 = (Q11_2-Q12_2-2*Q66_2)*m2^3*n2+(Q12_2-Q22_2+2*Q66_2)*m2*n2^3
Q_26_2 = (Q11_2-Q12_2-2*Q66_2)*n2^3*m2+(Q12_2-Q22_2+2*Q66_2)*n2*m2^3
Q_66_2 = (Q11_2+Q22_2-2*Q12_2-2*Q66_2)*m2^2*n2^2+Q66_2*(m2^4+n2^4)
Q_44_2 = Q44_2*m2^2+Q55_2*n2^2
Q_45_2 = (Q55_2-Q44_2)*n2*m2
Q_55_2 = Q55_2*m2^2+Q44_2*n2^2


Q_11_3 = Q11_3*m3^4+2*(Q12_3+2*Q66_3)*m3^2*n3^2+Q22_3*n3^4
Q_12_3 = (Q11_3+Q22_3-4*Q66_3)*m3^2*n3^2+Q12_3*(m3^4+n3^4)
Q_22_3 = Q11_3*n3^4+2*(Q12_3+2*Q66_3)*m3^2*n3^2+Q22_3*m3^4
Q_16_3 = (Q11_3-Q12_3-2*Q66_3)*m3^3*n3+(Q12_3-Q22_3+2*Q66_3)*m3*n3^3
Q_26_3 = (Q11_3-Q12_3-2*Q66_3)*n3^3*m3+(Q12_3-Q22_3+2*Q66_3)*n3*m3^3
Q_66_3 = (Q11_3+Q22_3-2*Q12_3-2*Q66_3)*m3^2*n3^2+Q66_3*(m3^4+n3^4)
Q_44_3 = Q44_3*m3^2+Q55_3*n3^2
Q_45_3 = (Q55_3-Q44_3)*n3*m3
Q_55_3 = Q55_3*m3^2+Q44_3*n3^2


A11 = Q_11_1 * ( (h2/2 + h1) - h2/2) + Q_11_2 * ( (h2/2) - (-h2/2)) +
Q_11_3 * ( (-h2/2) - (-h2/2 - h3))
A12 = Q_12_1 * ( (h2/2 + h1) - h2/2) + Q_12_2 * ( (h2/2) - (-h2/2)) +
Q_12_3 * ( (-h2/2) - (-h2/2 - h3))
A22 = Q_22_1 * ( (h2/2 + h1) - h2/2) + Q_22_2 * ( (h2/2) - (-h2/2)) +
Q_22_3 * ( (-h2/2) - (-h2/2 - h3))
A16 = Q_16_1 * ( (h2/2 + h1) - h2/2) + Q_16_2 * ( (h2/2) - (-h2/2)) +
Q_16_3 * ( (-h2/2) - (-h2/2 - h3))
A26 = Q_26_1 * ( (h2/2 + h1) - h2/2) + Q_26_2 * ( (h2/2) - (-h2/2)) +
Q_26_3 * ( (-h2/2) - (-h2/2 - h3))
A66 = Q_66_1 * ( (h2/2 + h1) - h2/2) + Q_66_2 * ( (h2/2) - (-h2/2)) +
Q_66_3 * ( (-h2/2) - (-h2/2 - h3))


A44 = Q_44_1 * ( (h2/2 + h1) - h2/2) + Q_44_2 * ( (h2/2) - (-h2/2)) +
Q_44_3 * ( (-h2/2) - (-h2/2 - h3))
A45 = Q_45_1 * ( (h2/2 + h1) - h2/2) + Q_45_2 * ( (h2/2) - (-h2/2)) +
Q_45_3 * ( (-h2/2) - (-h2/2 - h3))
A55 = Q_55_1 * ( (h2/2 + h1) - h2/2) + Q_55_2 * ( (h2/2) - (-h2/2)) +
Q_55_3 * ( (-h2/2) - (-h2/2 - h3))

    A=matrix((A11,A12,A16),(A12,A22,A26),(A16,A26,A66))

B11 = 1/2 * ( Q_11_1 * ( (h2/2 + h1)^2 - (h2/2)^2) + Q_11_2 * ( (h2/2)^2 -
(-h2/2)^2) + Q_11_3 * ( (-h2/2)^2 - (-h2/2 - h3)^2))
B12 = 1/2 * ( Q_12_1 * ( (h2/2 + h1)^2 - (h2/2)^2) + Q_12_2 * ( (h2/2)^2 -
(-h2/2)^2) + Q_12_3 * ( (-h2/2)^2 - (-h2/2 - h3)^2))
B22 = 1/2 * ( Q_22_1 * ( (h2/2 + h1)^2 - (h2/2)^2) + Q_22_2 * ( (h2/2)^2 -
(-h2/2)^2) + Q_22_3 * ( (-h2/2)^2 - (-h2/2 - h3)^2))
B16 = 1/2 * ( Q_16_1 * ( (h2/2 + h1)^2 - (h2/2)^2) + Q_16_2 * ( (h2/2)^2 -
(-h2/2)^2) + Q_16_3 * ( (-h2/2)^2 - (-h2/2 - h3)^2))
B26 = 1/2 * ( Q_26_1 * ( (h2/2 + h1)^2 - (h2/2)^2) + Q_26_2 * ( (h2/2)^2 -
(-h2/2)^2) + Q_26_3 * ( (-h2/2)^2 - (-h2/2 - h3)^2))
B66 = 1/2 * ( Q_66_1 * ( (h2/2 + h1)^2 - (h2/2)^2) + Q_66_2 * ( (h2/2)^2 -
(-h2/2)^2) + Q_66_3 * ( (-h2/2)^2 - (-h2/2 - h3)^2))


    B=matrix((B11,B12,B16),(B12,B22,B26),(B16,B26,B66))
```

```
D11 = 1/3 * ( Q_11_1 * ( (h2/2 + h1)^3 - (h2/2)^3) + Q_11_2 * ( (h2/2)^3 -
(-h2/2)^3) + Q_11_3 * ( (-h2/2)^3 - (-h2/2 - h3)^3))
D12 = 1/3 * ( Q_12_1 * ( (h2/2 + h1)^3 - (h2/2)^3) + Q_12_2 * ( (h2/2)^3 -
(-h2/2)^3) + Q_12_3 * ( (-h2/2)^3 - (-h2/2 - h3)^3))
D22 = 1/3 * ( Q_22_1 * ( (h2/2 + h1)^3 - (h2/2)^3) + Q_22_2 * ( (h2/2)^3 -
(-h2/2)^3) + Q_22_3 * ( (-h2/2)^3 - (-h2/2 - h3)^3))
D16 = 1/3 * ( Q_16_1 * ( (h2/2 + h1)^3 - (h2/2)^3) + Q_16_2 * ( (h2/2)^3 -
(-h2/2)^3) + Q_16_3 * ( (-h2/2)^3 - (-h2/2 - h3)^3))
D26 = 1/3 * ( Q_26_1 * ( (h2/2 + h1)^3 - (h2/2)^3) + Q_26_2 * ( (h2/2)^3 -
(-h2/2)^3) + Q_26_3 * ( (-h2/2)^3 - (-h2/2 - h3)^3))
D66 = 1/3 * ( Q_66_1 * ( (h2/2 + h1)^3 - (h2/2)^3) + Q_66_2 * ( (h2/2)^3 -
(-h2/2)^3) + Q_66_3 * ( (-h2/2)^3 - (-h2/2 - h3)^3))

    D=matrix((D11,D12,D16),(D12,D22,D26),(D16,D26,D66))



!MOISTURE STRAINS_____

KaT_1=(2/3)*rho0_1
KaR_1=(1/30)*rho0_1
KaL_1=(1/30)*rho0_1
KaT_2=(2/3)*rho0_2
KaR_2=(1/30)*rho0_2
KaL_2=(1/30)*rho0_2
KaT_3=(2/3)*rho0_3
KaR_3=(1/30)*rho0_3
KaL_3=(1/30)*rho0_3

ew11_1=(KaL_1*(abs_w_1))/100
ew22_1=(KaR_1*(abs_w_1))/100

ew11_2=(KaL_2*(abs_w_2))/100
ew22_2=(KaR_2*(abs_w_2))/100

ew11_3=(KaL_3*(abs_w_3))/100
ew22_3=(KaR_3*(abs_w_3))/100

!_____

Ks =  5/6     ! First order shear plate theory coefficient for shear stress

e_x = dx(u)
e_y = dy(v)
e_xy = dy(u)+dx(v)

Kx = dx(F_x)
Ky = dy(F_y)
Kxy = 2*(dy(F_x)+dx(F_y))

eyz = (F_y) +dy(w)
exz = (F_x) + dx(w)

{1. TOP_____}

e1_1_top = e_x + (h1+h2/2)*Kx + ew11_1
e2_1_top = e_y + (h1+h2/2)*Ky + ew22_1
```

```
e6_1_top = e_xy + (h1+h2/2)*Kxy
e4_1_top = eyz
e5_1_top = exz
```

{1. MID

```
Sigma1_1_top = Q_11_1*e1_1_top + Q_12_1*e2_1_top + Q_16_1*e6_1_top
Sigma2_1_top = Q_12_1*e1_1_top + Q_22_1*e2_1_top + Q_26_1*e6_1_top
Sigma6_1_top = Q_16_1*e1_1_top + Q_26_1*e2_1_top + Q_66_1*e6_1_top
Sigma4_1_top = Q_44_1 * e4_1_top + Q_45_1 * e5_1_top
Sigma5_1_top =Q_45_1 * e4_1_top + Q_55_1 * e5_1_top
```

```
e1_1_mid = e_x + (h1/2+h2/2)*Kx + ew11_1
e2_1_mid = e_y + (h1/2+h2/2)*Ky + ew22_1
e6_1_mid = e_xy + (h1/2+h2/2)*Kxy
e4_1_mid = eyz
e5_1_mid = exz
```

```
Sigma1_1_mid = Q_11_1*e1_1_mid + Q_12_1*e2_1_mid + Q_16_1*e6_1_mid
Sigma2_1_mid = Q_12_1*e1_1_mid + Q_22_1*e2_1_mid + Q_26_1*e6_1_mid
Sigma6_1_mid = Q_16_1*e1_1_mid + Q_26_1*e2_1_mid + Q_66_1*e6_1_mid
Sigma4_1_mid = Q_44_1 * e4_1_mid + Q_45_1 * e5_1_mid
Sigma5_1_mid =Q_45_1 * e4_1_mid + Q_55_1 * e5_1_mid
```

}

{1. BOT

```
e1_1_bot = e_x + (h2/2)*Kx + ew11_1
e2_1_bot = e_y + (h2/2)*Ky + ew22_1
e6_1_bot = e_xy + (h2/2)*Kxy
e4_1_bot = eyz
e5_1_bot = exz
```

```
Sigma1_1_bot = Q_11_1*e1_1_bot + Q_12_1*e2_1_bot + Q_16_1*e6_1_bot
Sigma2_1_bot = Q_12_1*e1_1_bot + Q_22_1*e2_1_bot + Q_26_1*e6_1_bot
Sigma6_1_bot = Q_16_1*e1_1_bot + Q_26_1*e2_1_bot + Q_66_1*e6_1_bot
Sigma4_1_bot = Q_44_1 * e4_1_bot + Q_45_1 * e5_1_bot
Sigma5_1_bot =Q_45_1 * e4_1_bot + Q_55_1 * e5_1_bot
```

}

{2. TOP

```
e1_2_top = e_x + (h2/2)*Kx + ew11_2
e2_2_top = e_y + (h2/2)*Ky + ew22_2
e6_2_top = e_xy + (h2/2)*Kxy
e4_2_top = eyz
e5_2_top = exz
```

```
Sigma1_2_top = Q_11_2*e1_2_top + Q_12_2*e2_2_top + Q_16_2*e6_2_top
Sigma2_2_top = Q_12_2*e1_2_top + Q_22_2*e2_2_top + Q_26_2*e6_2_top
Sigma6_2_top = Q_16_2*e1_2_top + Q_26_2*e2_2_top + Q_66_2*e6_2_top
Sigma4_2_top = Q_44_2 * e4_2_top + Q_45_2 * e5_2_top
Sigma5_2_top =Q_45_2 * e4_2_top + Q_55_2 * e5_2_top
```

}

{2. MID

```
e1_2_mid = e_x + (0)*Kx + ew11_2
e2_2_mid = e_y + (0)*Ky + ew22_2
e6_2_mid = e_xy + (0)*Kxy
```

```
e4_2_mid = eyz
e5_2_mid = exz

Sigma1_2_mid = Q_11_2*e1_2_mid + Q_12_2*e2_2_mid + Q_16_2*e6_2_mid
Sigma2_2_mid = Q_12_2*e1_2_mid + Q_22_2*e2_2_mid + Q_26_2*e6_2_mid
Sigma6_2_mid = Q_16_2*e1_2_mid + Q_26_2*e2_2_mid + Q_66_2*e6_2_mid
Sigma4_2_mid = Q_44_2 * e4_2_mid + Q_45_2 * e5_2_mid
Sigma5_2_mid = Q_45_2 * e4_2_mid + Q_55_2 * e5_2_mid

{2. BOT_____}

e1_2_bot = e_x + (-h2/2)*Kx + ew11_2
e2_2_bot = e_y + (-h2/2)*Ky + ew22_2
e6_2_bot = e_xy + (-h2/2)*Kxy
e4_2_bot = eyz
e5_2_bot = exz

Sigma1_2_bot = Q_11_2*e1_2_bot + Q_12_2*e2_2_bot + Q_16_2*e6_2_bot
Sigma2_2_bot = Q_12_2*e1_2_bot + Q_22_2*e2_2_bot + Q_26_2*e6_2_bot
Sigma6_2_bot = Q_16_2*e1_2_bot + Q_26_2*e2_2_bot + Q_66_2*e6_2_bot
Sigma4_2_bot = Q_44_2 * e4_2_bot + Q_45_2 * e5_2_bot
Sigma5_2_bot = Q_45_2 * e4_2_bot + Q_55_2 * e5_2_bot

{3. TOP_____}

e1_3_top = e_x + (-h2/2)*Kx + ew11_3
e2_3_top = e_y + (-h2/2)*Ky + ew22_3
e6_3_top = e_xy + (-h2/2)*Kxy
e4_3_top = eyz
e5_3_top = exz

Sigma1_3_top = Q_11_3*e1_3_top + Q_12_3*e2_3_top + Q_16_3*e6_3_top
Sigma2_3_top = Q_12_3*e1_3_top + Q_22_3*e2_3_top + Q_26_3*e6_3_top
Sigma6_3_top = Q_16_3*e1_3_top + Q_26_3*e2_3_top + Q_66_3*e6_3_top
Sigma4_3_top = Q_44_3 * e4_3_top + Q_45_3 * e5_3_top
Sigma5_3_top = Q_45_3 * e4_3_top + Q_55_3 * e5_3_top

{3. MID_____}

e1_3_mid = e_x + (-h2/2-h3/2)*Kx + ew11_3
e2_3_mid = e_y + (-h2/2-h3/2)*Ky + ew22_3
e6_3_mid = e_xy + (-h2/2-h3/2)*Kxy
e4_3_mid = eyz
e5_3_mid = exz

Sigma1_3_mid = Q_11_3*e1_3_mid + Q_12_3*e2_3_mid + Q_16_3*e6_3_mid
Sigma2_3_mid = Q_12_3*e1_3_mid + Q_22_3*e2_3_mid + Q_26_3*e6_3_mid
Sigma6_3_mid = Q_16_3*e1_3_mid + Q_26_3*e2_3_mid + Q_66_3*e6_3_mid
Sigma4_3_mid = Q_44_3 * e4_3_mid + Q_45_3 * e5_3_mid
Sigma5_3_mid = Q_45_3 * e4_3_mid + Q_55_3 * e5_3_mid

{3. BOT_____}

e1_3_bot = e_x + (-h2/2-h3)*Kx + ew11_3
e2_3_bot = e_y + (-h2/2-h3)*Ky + ew22_3
e6_3_bot = e_xy + (-h2/2-h3)*Kxy
e4_3_bot = eyz
```

```
e5_3_bot = exz

Sigma1_3_bot = Q_11_3*e1_3_bot + Q_12_3*e2_3_bot + Q_16_3*e6_3_bot
Sigma2_3_bot = Q_12_3*e1_3_bot + Q_22_3*e2_3_bot + Q_26_3*e6_3_bot
Sigma6_3_bot = Q_16_3*e1_3_bot + Q_26_3*e2_3_bot + Q_66_3*e6_3_bot
Sigma4_3_bot = Q_44_3 * e4_3_bot + Q_45_3 * e5_3_bot
Sigma5_3_bot = Q_45_3 * e4_3_bot + Q_55_3 * e5_3_bot
```

INITIAL VALUES
```
u = 0
v = 0
wxx = 0
wyy = 0
w = 0
F_x_x = 0
F_y_y = 0
```

EQUATIONS

```
F_x_x: dx(F_x)=F_x_x
F_y_y: dy(F_y)=F_y_y
wxx: dxx(w)=wxx
wyy: dyy(w)=wyy
```

u:
```
A11*dxx(u)+A12*dxy(v)+A16*(dxy(u)+dxx(v))+B11*dxx(F_x)+B12*dxy(F_y)+B16*(dx
y(F_x)+dxx(F_y))+A16*dxy(u)+A26*dyy(v)+A66*(dyy(u)+dxy(v))+B16*dxy(F_x)+B26
*dyy(F_y)+B66*(dyy(F_x)+dxy(F_y))=0
```

v:
```
A16*dxx(u)+A26*dxy(v)+A66*(dxy(u)+dxx(v))+B16*dxx(F_x)+B26*dxy(F_y)+B66*(dx
y(F_x)+dxx(F_y))+A12*dxy(u)+A22*dyy(v)+A26*(dyy(u)+dxy(v))+B12*dxy(F_x)+B22
*dyy(F_y)+B26*(dyy(F_x)+dxy(F_y))=0
```

w:
```
Ks*A45*(dx(F_y)+dxy(w))+Ks*A55*(dx(F_x)+dxx(w))+Ks*A44*(dy(F_y)+dyy(w))+Ks*
A45*(dy(F_x)+dxy(w))=-p
```

F_x:
```
B11*dxx(u)+B12*dxy(v)+B16*(dxy(u)+dxx(v))+D11*dxx(F_x)+D12*dxy(F_y)+D16*(dx
y(F_x)+dxx(F_y))+B16*dxy(u)+B26*dyy(v)+B66*(dyy(u)+dxy(v))+D16*dxy(F_x)+D26
*dyy(F_y)+D66*(dyy(F_x)+dxy(F_y))=Ks*A45*(F_y+dy(w))+Ks*A55*(F_x+dx(w))
```

F_y:
```
B16*dxx(u)+B26*dxy(v)+B66*(dxy(u)+dxx(v))+D16*dxx(F_x)+D26*dxy(F_y)+D66*(dx
y(F_x)+dxx(F_y))+B12*dxy(u)+B22*dyy(v)+B26*(dyy(u)+dxy(v))+D12*dxy(F_x)+D22
*dyy(F_y)+D26*(dyy(F_x)+dxy(F_y))=Ks*A44*(F_y+dy(w))+Ks*A45*(F_x+dx(w))
```

BOUNDARIES
```
 region 1

{---------X----------} start (0,0) {----------X---------}

value(F_x_x)=0
natural(F_y_y)=0
natural(w)=0
value(wyy)=0
```

```
natural(wxx)=0
natural(u)=0
value(v)=0

{---------Y----------} line to (L1,0)  {----------Y---------}

value(F_x_x)=0
value(F_y_y)=0
value(w)=0
natural(wyy)=0
value(wxx)=0
natural(u)=0
natural(v)=0

{---------X----------} line to (L1,L2) {---------X----------}

value(F_x_x)=0
natural(F_y_y)=0
natural(w)=0
value(wyy)=0
natural(wxx)=0
natural(u)=0
value(v)=0

{----------Y---------} line to (0,L2) {----------Y---------}

value(F_x_x)=0
value(F_y_y)=0
value(w)=0
natural(wyy)=0
value(wxx)=0
natural(u)=0
natural(v)=0

line to close


PLOTS
      contour(w)     { show deformed grid as solution progresses }
       surface(w)
        elevation(w) from (0,L2/2) to (L1/2,L2/2)
        elevation(w) from (L1/2,0) to (L1/2,L2)

END
```

13.9 Numerical FlexPDE script – SOSDT

```
TITLE 'Bending - 3 LAYERS-SOSDT'

SELECT
ngrid=31       { increase initial gridding }
cubic            { Use Cubic Basis }
errlim = 1e-4      { increase accuracy to resolve stresses }
```

```
!painted              { paint all contour plots }
!CHANGELIM = 0.1
!STAGES = 36
!autostage = on
!PREFER_STABILITY=on
!NONLINEAR=off

VARIABLES
w
u
v
F_1
F_2
P_1
P_2
!Mx
!My
!Nx
!Ny

DEFINITIONS     { parameter definitions }
layer_1_w = 30
layer_2_w = 12
layer_3_w = 12
layer11=12                                          {°C}
layer12= layer_1_w
layer21=12
layer22=layer_2_w
layer31=12
layer32=layer_3_w

abs_w_1=(layer11-layer12)
abs_w_2=(layer21-layer22)
abs_w_3=(layer31-layer32)

! Layer 1   C22
E_11_1_w12 = 11*10^9
E_22_1_w12 = 0.37*10^9
G_12_1_w12 = 0.69*10^9
G_13_1_w12 = G_12_1_w12
G_23_1_w12 = G_12_1_w12

E_11_1 = E_11_1_w12*(1+0.02*(12-layer_1_w))
E_22_1 = E_22_1_w12*(1+0.02*(12-layer_1_w))
G_12_1 = G_12_1_w12*(1+0.02*(12-layer_1_w))
G_13_1 = G_13_1_w12*(1+0.02*(12-layer_1_w))
G_23_1 = G_23_1_w12*(1+0.02*(12-layer_1_w))

v12_1=0.2
v21_1 = (E_22_1/E_11_1)*v12_1

rho_1 = 420
rho0_1=rho_1/1000
g_1=rho_1*9.81

Q11_1 = E_11_1 / (1-v12_1*v21_1)
Q12_1 = (v12_1 * E_22_1) / (1-v12_1*v21_1)
```

```
Q16_1 = 0
Q26_1 = 0
Q22_1 = E_22_1 / (1-v12_1*v21_1)
Q66_1 = G_12_1
Q44_1 = G_23_1
Q55_1 = G_13_1

! Layer 2    C22

E_11_2_w12 = 11*10^9
E_22_2_w12 = 0.37*10^9
G_12_2_w12 = 0.69*10^9
G_13_2_w12 = G_12_2_w12
G_23_2_w12 = G_12_2_w12

E_11_2 = E_11_2_w12*(1+0.02*(12-layer_2_w))
E_22_2 = E_22_2_w12*(1+0.02*(12-layer_2_w))
G_12_2 = G_12_2_w12*(1+0.02*(12-layer_2_w))
G_13_2 = G_13_2_w12*(1+0.02*(12-layer_2_w))
G_23_2 = G_23_2_w12*(1+0.02*(12-layer_2_w))

v12_2 = 0.2
v21_2 = (E_22_2/E_11_2)*v12_2

rho_2 = 420
rho0_2=rho_2/1000
g_2=rho_2*9.81

Q11_2 = E_11_2 / (1-v12_2*v21_2)
Q12_2 = (v12_2 * E_22_2) / (1-v12_2*v21_2)
Q16_2 = 0
Q26_2 = 0
Q22_2 = E_22_2 / (1-v12_2*v21_2)
Q66_2 = G_12_2
Q44_2 = G_23_2
Q55_2 = G_13_2

! Layer 3    C22

E_11_3_w12 = 11*10^9
E_22_3_w12 = 0.37*10^9
G_12_3_w12 = 0.69*10^9
G_13_3_w12 = G_12_3_w12
G_23_3_w12 = G_12_3_w12

E_11_3 = E_11_3_w12*(1+0.02*(12-layer_3_w))
E_22_3 = E_22_3_w12*(1+0.02*(12-layer_3_w))
G_12_3 = G_12_3_w12*(1+0.02*(12-layer_3_w))
G_13_3 = G_13_3_w12*(1+0.02*(12-layer_3_w))
G_23_3 = G_23_3_w12*(1+0.02*(12-layer_3_w))

v12_3 = 0.2
v21_3 = (E_22_3/E_11_3)*v12_3

rho_3 = 420
rho0_3=rho_3/1000
g_3=rho_3*9.81
```

```
Q11_3 = E_11_3 / (1-v12_3*v21_3)
Q12_3 = (v12_3 * E_22_3) / (1-v12_3*v21_3)
Q16_3 = 0
Q26_3 = 0
Q22_3 = E_22_3 / (1-v12_3*v21_3)
Q66_3 = G_12_3
Q44_3 = G_23_3
Q55_3 = G_13_3

! LAMINAE LAYERS, GEOMETRY
h1 = 0.03
h2 = 0.03
h3 = 0.03
h=h1 + h2 + h3

L1=1.5
L2=0.3

p= - 12000 {N.m-2}

m1=1! cos(30 degrees)      !1 !cos(40 degrees) !cos(a1 degrees)
n1=0! sin(30 degrees)      !0 !sin(40 degrees) !sin(a1 degrees)
m2=0! cos(55 degrees)      !0 !cos (20 degrees)!cos(a2 degrees)
n2=1! sin(55 degrees)      !1 !sin(20 degrees)  !sin(a2 degrees)
m3=1! cos(83 degrees)      !1 !cos(55 degrees) !cos(a3 degrees)
n3=0 !sin(83 degrees)            !0 !sin(55 degrees) !sin(a3 degrees)

Q_11_1 = Q11_1*m1^4+2*(Q12_1+2*Q66_1)*m1^2*n1^2+Q22_1*n1^4
Q_12_1 = (Q11_1+Q22_1-4*Q66_1)*m1^2*n1^2+Q12_1*(m1^4+n1^4)
Q_22_1 = Q11_1*n1^4+2*(Q12_1+2*Q66_1)*m1^2*n1^2+Q22_1*m1^4
Q_16_1 = (Q11_1-Q12_1-2*Q66_1)*(m1)^3*n1+(Q12_1-Q22_1+2*Q66_1)*m1*(n1)^3
Q_26_1 = (Q11_1-Q12_1-2*Q66_1)*n1^3*m1+(Q12_1-Q22_1+2*Q66_1)*n1*m1^3
Q_66_1 = (Q11_1+Q22_1-2*Q12_1-2*Q66_1)*m1^2*n1^2+Q66_1*(m1^4+n1^4)
Q_44_1 = Q44_1*m1^2+Q55_1*n1^2
Q_45_1 = (Q55_1-Q44_1)*n1*m1
Q_55_1 = Q55_1*m1^2+Q44_1*n1^2

Q_11_2 = Q11_2*m2^4+2*(Q12_2+2*Q66_2)*m2^2*n2^2+Q22_2*n2^4
Q_12_2 = (Q11_2+Q22_2-4*Q66_2)*m2^2*n2^2+Q12_2*(m2^4+n2^4)
Q_22_2 = Q11_2*n2^4+2*(Q12_2+2*Q66_2)*m2^2*n2^2+Q22_2*m2^4
Q_16_2 = (Q11_2-Q12_2-2*Q66_2)*m2^3*n2+(Q12_2-Q22_2+2*Q66_2)*m2*n2^3
Q_26_2 = (Q11_2-Q12_2-2*Q66_2)*n2^3*m2+(Q12_2-Q22_2+2*Q66_2)*n2*m2^3
Q_66_2 = (Q11_2+Q22_2-2*Q12_2-2*Q66_2)*m2^2*n2^2+Q66_2*(m2^4+n2^4)
Q_44_2 = Q44_2*m2^2+Q55_2*n2^2
Q_45_2 = (Q55_2-Q44_2)*n2*m2
Q_55_2 = Q55_2*m2^2+Q44_2*n2^2

Q_11_3 = Q11_3*m3^4+2*(Q12_3+2*Q66_3)*m3^2*n3^2+Q22_3*n3^4
Q_12_3 = (Q11_3+Q22_3-4*Q66_3)*m3^2*n3^2+Q12_3*(m3^4+n3^4)
Q_22_3 = Q11_3*n3^4+2*(Q12_3+2*Q66_3)*m3^2*n3^2+Q22_3*m3^4
Q_16_3 = (Q11_3-Q12_3-2*Q66_3)*m3^3*n3+(Q12_3-Q22_3+2*Q66_3)*m3*n3^3
Q_26_3 = (Q11_3-Q12_3-2*Q66_3)*n3^3*m3+(Q12_3-Q22_3+2*Q66_3)*n3*m3^3
Q_66_3 = (Q11_3+Q22_3-2*Q12_3-2*Q66_3)*m3^2*n3^2+Q66_3*(m3^4+n3^4)
Q_44_3 = Q44_3*m3^2+Q55_3*n3^2
Q_45_3 = (Q55_3-Q44_3)*n3*m3
Q_55_3 = Q55_3*m3^2+Q44_3*n3^2
```

```
A11 = Q_11_1 * ( (h2/2 + h1) - (h2/2)) + Q_11_2 * ( (h2/2) - (-h2/2))+
Q_11_3 * ( (-h2/2) - (-h2/2 - h3))
A12 = Q_12_1 * ( (h2/2 + h1) - (h2/2)) + Q_12_2 * ( (h2/2) - (-h2/2))+
Q_12_3 * ( (-h2/2) - (-h2/2 - h3))
A22 = Q_22_1 * ( (h2/2 + h1) - (h2/2)) + Q_22_2 * ( (h2/2) - (-h2/2))+
Q_22_3 * ( (-h2/2) - (-h2/2 - h3))
A16 = Q_16_1 * ( (h2/2 + h1) - (h2/2)) + Q_16_2 * ( (h2/2) - (-h2/2))+
Q_16_3 * ( (-h2/2) - (-h2/2 - h3))
A26 = Q_26_1 * ( (h2/2 + h1) - (h2/2)) + Q_26_2 * ( (h2/2) - (-h2/2))+
Q_26_3 * ( (-h2/2) - (-h2/2 - h3))
A66 = Q_66_1 * ( (h2/2 + h1) - (h2/2)) + Q_66_2 * ( (h2/2) - (-h2/2))+
Q_66_3 * ( (-h2/2) - (-h2/2 - h3))

A44 = Q_44_1 * ( (h2/2 + h1) - (h2/2)) + Q_44_2 * ( (h2/2) - (-h2/2))+
Q_44_3 * ( (-h2/2) - (-h2/2 - h3))
A45 = Q_45_1 * ( (h2/2 + h1) - (h2/2)) + Q_45_2 * ( (h2/2) - (-h2/2))+
Q_45_3 * ( (-h2/2) - (-h2/2 - h3))
A55 = Q_55_1 * ( (h2/2 + h1) - (h2/2)) + Q_55_2 * ( (h2/2) - (-h2/2))+
Q_55_3 * ( (-h2/2) - (-h2/2 - h3))

    A=matrix((A11,A12,A16),(A12,A22,A26),(A16,A26,A66))

B11 = 1/2 *(Q_11_1 * ( (h2/2 + h1)^2 - (h2/2)^2) + Q_11_2 * ( (h2/2)^2 - (-
h2/2)^2) + Q_11_3 * ( (-h2/2)^2 - (-h2/2 - h3)^2))
B12 = 1/2 *(Q_12_1 * ( (h2/2 + h1)^2 - (h2/2)^2) + Q_12_2 * ( (h2/2)^2 - (-
h2/2)^2) + Q_12_3 * ( (-h2/2)^2 - (-h2/2 - h3)^2))
B22 = 1/2 *(Q_22_1 * ( (h2/2 + h1)^2 - (h2/2)^2) + Q_22_2 * ( (h2/2)^2 - (-
h2/2)^2) + Q_22_3 * ( (-h2/2)^2 - (-h2/2 - h3)^2))
B16 = 1/2 *(Q_16_1 * ( (h2/2 + h1)^2 - (h2/2)^2) + Q_16_2 * ( (h2/2)^2 - (-
h2/2)^2) + Q_16_3 * ( (-h2/2)^2 - (-h2/2 - h3)^2))
B26 = 1/2 *(Q_26_1 * ( (h2/2 + h1)^2 - (h2/2)^2) + Q_26_2 * ( (h2/2)^2 - (-
h2/2)^2) + Q_26_3 * ( (-h2/2)^2 - (-h2/2 - h3)^2))
B66 = 1/2 *(Q_66_1 * ( (h2/2 + h1)^2 - (h2/2)^2) + Q_66_2 * ( (h2/2)^2 - (-
h2/2)^2) + Q_66_3 * ( (-h2/2)^2 - (-h2/2 - h3)^2))

B44 = 1/2 *(Q_44_1 * ( (h2/2 + h1)^2 - (h2/2)^2) + Q_44_2 * ( (h2/2)^2 - (-
h2/2)^2) + Q_44_3 * ( (-h2/2)^2 - (-h2/2 - h3)^2))
B45 = 1/2 *(Q_45_1 * ( (h2/2 + h1)^2 - (h2/2)^2) + Q_45_2 * ( (h2/2)^2 - (-
h2/2)^2) + Q_45_3 * ( (-h2/2)^2 - (-h2/2 - h3)^2))
B55 = 1/2 *(Q_55_1 * ( (h2/2 + h1)^2 - (h2/2)^2) + Q_55_2 * ( (h2/2)^2 - (-
h2/2)^2) + Q_55_3 * ( (-h2/2)^2 - (-h2/2 - h3)^2))

    B=matrix((A11,A12,A16),(A12,A22,A26),(A16,A26,A66))

D11 = 1/3 *( Q_11_1 * ( (h2/2 + h1)^3 - (h2/2)^3) + Q_11_2 * ( (h2/2)^3 -
(-h2/2)^3) + Q_11_3 * ( (-h2/2)^3 - (-h2/2 - h3)^3))
D12 = 1/3 *( Q_12_1 * ( (h2/2 + h1)^3 - (h2/2)^3) + Q_12_2 * ( (h2/2)^3 -
(-h2/2)^3) + Q_12_3 * ( (-h2/2)^3 - (-h2/2 - h3)^3))
D22 = 1/3 *( Q_22_1 * ( (h2/2 + h1)^3 - (h2/2)^3) + Q_22_2 * ( (h2/2)^3 -
(-h2/2)^3) + Q_22_3 * ( (-h2/2)^3 - (-h2/2 - h3)^3))
D16 = 1/3 *( Q_16_1 * ( (h2/2 + h1)^3 - (h2/2)^3) + Q_16_2 * ( (h2/2)^3 -
(-h2/2)^3) + Q_16_3 * ( (-h2/2)^3 - (-h2/2 - h3)^3))
D26 = 1/3 *( Q_26_1 * ( (h2/2 + h1)^3 - (h2/2)^3) + Q_26_2 * ( (h2/2)^3 -
(-h2/2)^3) + Q_26_3 * ( (-h2/2)^3 - (-h2/2 - h3)^3))
D66 = 1/3 *( Q_66_1 * ( (h2/2 + h1)^3 - (h2/2)^3) + Q_66_2 * ( (h2/2)^3 -
(-h2/2)^3) + Q_66_3 * ( (-h2/2)^3 - (-h2/2 - h3)^3))
```

```
D44 = 1/3 *( Q_44_1 * ( (h2/2 + h1)^3 - (h2/2)^3) + Q_44_2 * ( (h2/2)^3 -
(-h2/2)^3) + Q_44_3 * ( (-h2/2)^3 - (-h2/2 - h3)^3))
D45 = 1/3 *( Q_45_1 * ( (h2/2 + h1)^3 - (h2/2)^3) + Q_45_2 * ( (h2/2)^3 -
(-h2/2)^3) + Q_45_3 * ( (-h2/2)^3 - (-h2/2 - h3)^3))
D55 = 1/3 *( Q_55_1 * ( (h2/2 + h1)^3 - (h2/2)^3) + Q_55_2 * ( (h2/2)^3 -
(-h2/2)^3) + Q_55_3 * ( (-h2/2)^3 - (-h2/2 - h3)^3))

    D=matrix((B11,B12,B16),(B12,B22,B26),(B16,B26,B66))

E11 = 1/4 *( Q_11_1 * ( (h2/2 + h1)^4 - (h2/2)^4) + Q_11_2 * ( (h2/2)^4 -
(-h2/2)^4) + Q_11_3 * ( (-h2/2)^4 - (-h2/2 - h3)^4))
E12 = 1/4* ( Q_12_1 * ( (h2/2 + h1)^4 - (h2/2)^4) + Q_12_2 * ( (h2/2)^4 -
(-h2/2)^4) + Q_12_3 * ( (-h2/2)^4 - (-h2/2 - h3)^4))
E22 = 1/4* ( Q_22_1 * ( (h2/2 + h1)^4 - (h2/2)^4) + Q_22_2 * ( (h2/2)^4 -
(-h2/2)^4) + Q_22_3 * ( (-h2/2)^4 - (-h2/2 - h3)^4))
E16 = 1/4* ( Q_16_1 * ( (h2/2 + h1)^4 - (h2/2)^4) + Q_16_2 * ( (h2/2)^4 -
(-h2/2)^4) + Q_16_3 * ( (-h2/2)^4 - (-h2/2 - h3)^4))
E26 = 1/4* ( Q_26_1 * ( (h2/2 + h1)^4 - (h2/2)^4) + Q_26_2 * ( (h2/2)^4 -
(-h2/2)^4) + Q_26_3 * ( (-h2/2)^4 - (-h2/2 - h3)^4))
E66 = 1/4* ( Q_66_1 * ( (h2/2 + h1)^4 - (h2/2)^4) + Q_66_2 * ( (h2/2)^4 -
(-h2/2)^4) + Q_66_3 * ( (-h2/2)^4 - (-h2/2 - h3)^4))

E44 = 1/4* ( Q_44_1 * ( (h2/2 + h1)^4 - (h2/2)^4) + Q_44_2 * ( (h2/2)^4 -
(-h2/2)^4) + Q_44_3 * ( (-h2/2)^4 - (-h2/2 - h3)^4))
E45 = 1/4* ( Q_45_1 * ( (h2/2 + h1)^4 - (h2/2)^4) + Q_45_2 * ( (h2/2)^4 -
(-h2/2)^4) + Q_45_3 * ( (-h2/2)^4 - (-h2/2 - h3)^4))
E55 = 1/4* ( Q_55_1 * ( (h2/2 + h1)^4 - (h2/2)^4) + Q_55_2 * ( (h2/2)^4 -
(-h2/2)^4) + Q_55_3 * ( (-h2/2)^4 - (-h2/2 - h3)^4))

    E=matrix((E11,E12,E16),(E12,E22,E26),(E16,E26,E66))

F11 = 1/5* ( Q_11_1 * ( (h2/2 + h1)^5 - (h2/2)^5) + Q_11_2 * ( (h2/2)^5 -
(-h2/2)^5) + Q_11_3 * ( (-h2/2)^5 - (-h2/2 - h3)^5))
F12 = 1/5* ( Q_12_1 * ( (h2/2 + h1)^5 - (h2/2)^5) + Q_12_2 * ( (h2/2)^5 -
(-h2/2)^5) + Q_12_3 * ( (-h2/2)^5 - (-h2/2 - h3)^5))
F22 = 1/5* ( Q_22_1 * ( (h2/2 + h1)^5 - (h2/2)^5) + Q_22_2 * ( (h2/2)^5 -
(-h2/2)^5) + Q_22_3 * ( (-h2/2)^5 - (-h2/2 - h3)^5))
F16 = 1/5* ( Q_16_1 * ( (h2/2 + h1)^5 - (h2/2)^5) + Q_16_2 * ( (h2/2)^5 -
(-h2/2)^5) + Q_16_3 * ( (-h2/2)^5 - (-h2/2 - h3)^5))
F26 = 1/5* ( Q_26_1 * ( (h2/2 + h1)^5 - (h2/2)^5) + Q_26_2 * ( (h2/2)^5 -
(-h2/2)^5) + Q_26_3 * ( (-h2/2)^5 - (-h2/2 - h3)^5))
F66 = 1/5* ( Q_66_1 * ( (h2/2 + h1)^5 - (h2/2)^5) + Q_66_2 * ( (h2/2)^5 -
(-h2/2)^5) + Q_66_3 * ( (-h2/2)^5 - (-h2/2 - h3)^5))

F44 = 1/5* ( Q_44_1 * ( (h2/2 + h1)^5 - (h2/2)^5) + Q_44_2 * ( (h2/2)^5 -
(-h2/2)^5) + Q_44_3 * ( (-h2/2)^5 - (-h2/2 - h3)^5))
F45 = 1/5* ( Q_45_1 * ( (h2/2 + h1)^5 - (h2/2)^5) + Q_45_2 * ( (h2/2)^5 -
(-h2/2)^5) + Q_45_3 * ( (-h2/2)^5 - (-h2/2 - h3)^5))
F55 = 1/5* ( Q_55_1 * ( (h2/2 + h1)^5 - (h2/2)^5) + Q_55_2 * ( (h2/2)^5 -
(-h2/2)^5) + Q_55_3 * ( (-h2/2)^5 - (-h2/2 - h3)^5))

    F=matrix((F11,F12,F16,0,0),(F12,F22,F26,0,0),(F16,F26,F66,0,0))


!MOISTURE STRAINS_____
```

```
KaT_1=(2/3)*rho0_1
KaR_1=(1/30)*rho0_1
KaL_1=(1/30)*rho0_1
KaT_2=(2/3)*rho0_2
KaR_2=(1/30)*rho0_2
KaL_2=(1/30)*rho0_2
KaT_3=(2/3)*rho0_3
KaR_3=(1/30)*rho0_3
KaL_3=(1/30)*rho0_3

ew11_1=(KaL_1*(abs_w_1))/100
ew22_1=(KaR_1*(abs_w_1))/100
ew11_2=(KaL_2*(abs_w_2))/100
ew22_2=(KaR_2*(abs_w_2))/100
ew11_3=(KaL_3*(abs_w_3))/100
ew22_3=(KaR_3*(abs_w_3))/100

!_____

ex=dx(u)
ey=dy(u)
exy=dx(v)+dy(u)
kx=dx(F_1)
ky=dy(P_1)
kxy=dx(P_1)+dy(F_1)
kkx=dx(F_2)
kky=dy(P_2)
kkxy=dx(P_2)+dy(F_2)
eyz=P_1+dy(w)
exz=F_1+dx(w)
eeyz=2*P_2
eexz=2*F_2

{1. TOP_____}

e1_1_top = ex + (h1+h2/2)*kx+((h1+h2/2)^2)*kkx + ew11_1
e2_1_top = ey + (h1+h2/2)*ky+((h1+h2/2)^2)*kky + ew22_1
e6_1_top = exy + (h1+h2/2)*kxy + ((h1+h2/2)^2)*kkxy
e4_1_top = eyz + (h1+h2/2)*eeyz
e5_1_top = exz + (h1+h2/2)*eexz

Sigma1_1_top = Q_11_1*e1_1_top + Q_12_1*e2_1_top + Q_16_1*e6_1_top
Sigma2_1_top = Q_12_1*e1_1_top + Q_22_1*e2_1_top + Q_26_1*e6_1_top
Sigma6_1_top = Q_16_1*e1_1_top + Q_26_1*e2_1_top + Q_66_1*e6_1_top
Sigma4_1_top =+ Q_44_1*e4_1_top + Q_45_1*e5_1_top
Sigma5_1_top =+ Q_45_1*e4_1_top + Q_55_1*e5_1_top

{1. MID_____}

e1_1_mid = ex + (h1/2+h2/2)*kx+((h1/2+h2/2)^2)*kkx  + ew11_1
e2_1_mid = ey + (h1/2+h2/2)*ky+((h1/2+h2/2)^2)*kky + ew22_1
e6_1_mid = exy + (h1/2+h2/2)*kxy + ((h1/2+h2/2)^2)*kkxy
e4_1_mid = eyz + (h1/2+h2/2)*eeyz
e5_1_mid = exz + (h1/2+h2/2)*eexz

Sigma1_1_mid = Q_11_1*e1_1_mid + Q_12_1*e2_1_mid + Q_16_1*e6_1_mid
Sigma2_1_mid = Q_12_1*e1_1_mid + Q_22_1*e2_1_mid + Q_26_1*e6_1_mid
```

```
Sigma6_1_mid = Q_16_1*e1_1_mid + Q_26_1*e2_1_mid + Q_66_1*e6_1_mid
Sigma4_1_mid = + Q_44_1*e4_1_mid + Q_45_1*e5_1_mid
Sigma5_1_mid = + Q_45_1*e4_1_mid + Q_55_1*e5_1_mid
```

{1. BOT_____}

```
e1_1_bot = ex + (h2/2)*kx+((h2/2)^2)*kkx + ew11_1
e2_1_bot = ey + (h2/2)*ky+((h2/2)^2)*kky + ew22_1
e6_1_bot = exy + (h2/2)*kxy + ((h2/2)^2)*kkxy
e4_1_bot = eyz + (h2/2)*eeyz
e5_1_bot = exz + (h2/2)*eexz

Sigma1_1_bot = Q_11_1*e1_1_bot + Q_12_1*e2_1_bot + Q_16_1*e6_1_bot
Sigma2_1_bot = Q_12_1*e1_1_bot + Q_22_1*e2_1_bot + Q_26_1*e6_1_bot
Sigma6_1_bot = Q_16_1*e1_1_bot + Q_26_1*e2_1_bot + Q_66_1*e6_1_bot
Sigma4_1_bot = + Q_44_1*e4_1_bot + Q_45_1*e5_1_bot
Sigma5_1_bot = + Q_45_1*e4_1_bot + Q_55_1*e5_1_bot
```

{2. TOP_____}

```
e1_2_top = ex + (h2/2)*kx+((h2/2)^2)*kkx + ew11_2
e2_2_top = ey + (h2/2)*ky+((h2/2)^2)*kky + ew22_2
e6_2_top = exy + (h2/2)*kxy + ((h2/2)^2)*kkxy
e4_2_top = eyz + (h2/2)*eeyz
e5_2_top = exz + (h2/2)*eexz


Sigma1_2_top = Q_11_2*e1_2_top + Q_12_2*e2_2_top + Q_16_2*e6_2_top
Sigma2_2_top = Q_12_2*e1_2_top + Q_22_2*e2_2_top + Q_26_2*e6_2_top
Sigma6_2_top = Q_16_2*e1_2_top + Q_26_2*e2_2_top + Q_66_2*e6_2_top
Sigma4_2_top = + Q_44_2*e4_2_top + Q_45_2*e5_2_top
Sigma5_2_top = + Q_45_2*e4_2_top + Q_55_2*e5_2_top
```

{2.MID_____}

```
e1_2_MID = ex + (0)*kx+((0)^2)*kkx + ew11_2
e2_2_MID = ey + (0)*ky+((0)^2)*kky + ew22_2
e6_2_MID = exy + (0)*kxy + ((0)^2)*kkxy
e4_2_MID = eyz + (0)*eeyz
e5_2_MID = exz + (0)*eexz


Sigma1_2_MID = Q_11_2*e1_2_MID + Q_12_2*e2_2_MID + Q_16_2*e6_2_MID
Sigma2_2_MID = Q_12_2*e1_2_MID + Q_22_2*e2_2_MID + Q_26_2*e6_2_MID
Sigma6_2_MID = Q_16_2*e1_2_MID + Q_26_2*e2_2_MID + Q_66_2*e6_2_MID
Sigma4_2_MID = + Q_44_2*e4_2_MID + Q_45_2*e5_2_MID
Sigma5_2_MID = + Q_45_2*e4_2_MID + Q_55_2*e5_2_MID
```

{2. BOT_____}

```
e1_2_bot = ex + (-h2/2)*kx+((-h2/2)^2)*kkx + ew11_2
e2_2_bot = ey + (-h2/2)*ky+((-h2/2)^2)*kky + ew22_2
e6_2_bot = exy + (-h2/2)*kxy + ((-h2/2)^2)*kkxy
e4_2_bot = eyz + (-h2/2)*eeyz
e5_2_bot = exz + (-h2/2)*eexz
```

```
Sigma1_2_bot = Q_11_2*e1_2_bot + Q_12_2*e2_2_bot + Q_12_2*e2_2_bot + Q_16_2*e6_2_bot
Sigma2_2_bot = Q_12_2*e1_2_bot + Q_22_2*e2_2_bot + Q_22_2*e2_2_bot + Q_26_2*e6_2_bot
Sigma6_2_bot = Q_16_2*e1_2_bot + Q_26_2*e2_2_bot + Q_26_2*e2_2_bot + Q_66_2*e6_2_bot
Sigma4_2_bot = + Q_44_2*e4_2_bot + Q_45_2*e5_2_bot
Sigma5_2_bot = + Q_45_2*e4_2_bot + Q_55_2*e5_2_bot
```

{3. TOP}

```
e1_3_top = ex + (-h2/2)*kx+((-h2/2)^2)*kkx + ew11_3
e2_3_top = ey + (-h2/2)*ky+((-h2/2)^2)*kky + ew22_3
e6_3_top = exy + (-h2/2)*kxy + ((-h2/2)^2)*kkxy
e4_3_top = eyz + (-h2/2)*eeyz
e5_3_top = exz + (-h2/2)*eexz
```

```
Sigma1_3_top = Q_11_3*e1_3_top + Q_12_3*e2_3_top + Q_16_3*e6_3_top
Sigma2_3_top = Q_12_3*e1_3_top + Q_22_3*e2_3_top + Q_26_3*e6_3_top
Sigma6_3_top = Q_16_3*e1_3_top + Q_26_3*e2_3_top + Q_66_3*e6_3_top
Sigma4_3_top = + Q_44_3*e4_3_top + Q_45_3*e5_3_top
Sigma5_3_top = + Q_45_3*e4_3_top + Q_55_3*e5_3_top
```

{3. MID}

```
e1_3_mid = ex + (-h3/2-h2/2)*kx+((-h3/2-h2/2)^2)*kkx + ew11_3
e2_3_mid = ey + (-h3/2-h2/2)*ky+((-h3/2-h2/2)^2)*kky + ew22_3
e6_3_mid = exy + (-h3/2-h2/2)*kxy + ((-h3/2-h2/2)^2)*kkxy
e4_3_mid = eyz + (-h3/2-h2/2)*eeyz
e5_3_mid = exz + (-h3/2-h2/2)*eexz
```

```
Sigma1_3_mid = Q_11_3*e1_3_mid + Q_12_3*e2_3_mid + Q_16_3*e6_3_mid
Sigma2_3_mid = Q_12_3*e1_3_mid + Q_22_3*e2_3_mid + Q_26_3*e6_3_mid
Sigma6_3_mid = Q_16_3*e1_3_mid + Q_26_3*e2_3_mid + Q_66_3*e6_3_mid
Sigma4_3_mid = + Q_44_3*e4_3_mid + Q_45_3*e5_3_mid
Sigma5_3_mid = + Q_45_3*e4_3_mid + Q_55_3*e5_3_mid
```

{3. BOT}

```
e1_3_bot = ex + (-h2/2-h3)*kx+((-h2/2-h3)^2)*kkx + ew11_3
e2_3_bot = ey + (-h2/2-h3)*ky+((-h2/2-h3)^2)*kky + ew22_3
e6_3_bot = exy + (-h2/2-h3)*kxy + ((-h2/2-h3)^2)*kkxy
e4_3_bot = eyz + (-h2/2-h3)*eeyz
e5_3_bot = exz + (-h2/2-h3)*eexz
```

```
Sigma1_3_bot = Q_11_3*e1_3_bot + Q_12_3*e2_3_bot + Q_16_3*e6_3_bot
Sigma2_3_bot = Q_12_3*e1_3_bot + Q_22_3*e2_3_bot + Q_26_3*e6_3_bot
Sigma6_3_bot = Q_16_3*e1_3_bot + Q_26_3*e2_3_bot + Q_66_3*e6_3_bot
Sigma4_3_bot = + Q_44_3*e4_3_bot + Q_45_3*e5_3_bot
Sigma5_3_bot = + Q_45_3*e4_3_bot + Q_55_3*e5_3_bot
```

INITIAL VALUES

```
w=0
u=0
v=0
F_1=0
F_2=0
P_1=0
P_2=0
```

w:
```
A45*(dx(P_1)+dxy(w))+A55*(dx(F_1)+dxx(w))+B45*dx(2*P_2)+B55*dx(2*F_2)
+A44*(dy(P_1)+dyy(w))+A45*(dy(F_1)+dxy(w))+B44*dy(2*P_2)+B45*dy(2*F_2)= -p


A55*dx(F_1)+A55*dxx(w)+2*B55*dx(F_2)+A44*dy(P_1)+A44*dyy(w)+2*B44*dy(P_2) +
p=0
```

u:
```
A11*dxx(u)+A12*dxy(v)+A16*(dxy(u)+dxx(v))+B11*dxx(F_1)+B12*dxy(P_1)+B16*(dx
y(F_1)+dxx(P_1))+D11*dxx(F_2)+D12*dxy(P_2)+D16*(dxy(F_2)+dxx(P_2))+A16*dxy(
u)+A26*dyy(v)+A66*(dyy(u)+dxy(v))+B16*dxy(F_1)+B26*dyy(P_1)+B66*(dyy(F_1)+d
xy(P_1))+D16*dxy(F_2)+D26*dyy(P_2)+D66*(dyy(F_2)+dxy(P_2)) = 0
```

v:
```
A16*dxx(u)+A26*dxy(v)+A66*(dxy(u)+dxx(v))+B16*dxx(F_1)+B26*dxy(P_1)+B66*(dx
y(F_1)+dxx(P_1))+D16*dxx(F_2)+D26*dxy(P_2)+D66*(dxy(F_2)+dxx(P_2))+A12*dxy(
u)+A22*dyy(v)+A26*(dyy(u)+dxy(v))+B12*dxy(F_1)+B22*dyy(P_1)+B26*(dyy(F_1)+d
xy(P_1))+D12*dxy(F_2)+D22*dyy(P_2)+D26*(dyy(F_2)+dxy(P_2)) = 0
```

F_1:
```
B11*dxx(u)+B12*dxy(v)+B16*(dxy(u)+dxx(v))+D11*dxx(F_1)+D12*dxy(P_1)+D16*(dx
y(F_1)+dxx(P_1))+E11*dxx(F_2)+E12*dxy(P_2)+E16*(dxy(F_2)+dxx(P_2))+B16*dxy(
u)+B26*dyy(v)+B66*(dyy(u)+dxy(v))+D16*dxy(F_1)+D26*dyy(P_1)+D66*(dyy(F_1)+d
xy(P_1))+E16*dxy(F_2)+E26*dyy(P_2)+E66*(dyy(F_2)+dxy(P_2))-
(A45*(P_1+dy(w))+A55*(F_1+dx(w))+B45*2*P_2+B55*2*F_2)= 0
```

F_2:
```
B16*dxx(u)+B26*dxy(v)+B66*(dxy(u)+dxx(v))+D16*dxx(F_1)+D26*dxy(P_1)+D66*(dx
y(F_1)+dxx(P_1))+E16*dxx(F_2)+E26*dxy(P_2)+E66*(dxy(F_2)+dxx(P_2))+B12*dxy(
u)+B22*dyy(v)+B26*(dyy(u)+dxy(v))+D12*dxy(F_1)+D22*dyy(P_1)+D26*(dyy(F_1)+d
xy(P_1))+E12*dxy(F_2)+E22*dyy(P_2)+E26*(dyy(F_2)+dxy(P_2)) -
(A44*(P_1+dy(w))+A45*(F_1+dx(w))+B44*2*P_2+B45*2*F_2)= 0
```

P_1:
```
D11*dxx(u)+D12*dxy(v)+D16*(dxy(u)+dxx(v))+E11*dxx(F_1)+E12*dxy(P_1)+E16*(dx
y(F_1)+dxx(P_1))+F11*dxx(F_2)+F12*dxy(P_2)+F16*(dxy(F_2)+dxx(P_2))+D16*dxy(
u)+D26*dyy(v)+D66*(dyy(u)+dxy(v))+E16*dxy(F_1)+E26*dyy(P_1)+E66*(dyy(F_1)+d
xy(P_1))+F16*dxy(F_2)+F26*dyy(P_2)+F66*(dyy(F_2)+dxy(P_2))-
(B45*(P_1+dy(w))+B55*(F_1+dx(w))+D45*2*P_2+D55*2*F_2)= 0
```

P_2:
```
D16*dxx(u)+D26*dxy(v)+D66*(dxy(u)+dxx(v))+E16*dxx(F_1)+E26*dxy(P_1)+E66*(dx
y(F_1)+dxx(P_1))+F16*dxx(F_2)+F26*dxy(P_2)+F66*(dxy(F_2)+dxx(P_2))+D12*dxy(
u)+D22*dyy(v)+D26*(dyy(u)+dxy(v))+E12*dxy(F_1)+E22*dyy(P_1)+E26*(dyy(F_1)+d
xy(P_1))+F12*dxy(F_2)+F22*dyy(P_2)+F26*(dyy(F_2)+dxy(P_2))-
(B44*(P_1+dy(w))+B45*(F_1+dx(w))+D44*2*P_2+D45*2*F_2)= 0
```

BOUNDARIES
 region 1

  start (0,0)
        natural(v)=0
        natural(w)=0

```
            natural(P_1)=0
            natural(P_2)=0
            natural(u)=0
            natural(F_1)=0
            natural(F_2)=0


line to (L1,0)
            natural(v)=0
            value(w)=0
            natural(P_1)=0
            value(P_2)=0
            natural(u)=0
            natural(F_1)=0
            natural(F_2)=0

line to (L1,L2)
            natural(v)=0
            natural(w)=0
            natural(P_1)=0
            natural(P_2)=0
            natural(u)=0
            natural(F_1)=0
            natural(F_2)=0

line to (0,L2)
            natural(v)=0
            value(w)=0
            natural(P_1)=0
            value(P_2)=0
            natural(u)=0
            natural(F_1)=0
            natural(F_2)=0

line to close

PLOTS
        contour(w)      { show deformed grid as solution progresses }
        surface(w)
         elevation(w) from (0,L2/2) to (L1,L2/2)
         elevation(w) from (L1/2,0) to (L1/2,L2)

END
```

13.10 Numerical FlexPDE script – TOSDT

```
TITLE 'Bending - 3 LAYERS - TOSDT'

SELECT
ngrid=31     { increase initial gridding }
cubic          { Use Cubic Basis }
errlim = 1e-4     { increase accuracy to resolve stresses }
painted              { paint all contour plots }
!CHANGELIM = 0.1
```

```
!STAGES = 36
!autostage = on
!PREFER_STABILITY=on
!NONLINEAR=off

VARIABLES
w
u
v
F_x
F_y
P_x
P_y
L_x
L_y

DEFINITIONS      { parameter definitions }
layer_1_w = 30
layer_2_w = 12
layer_3_w = 12
layer11=12                                                    {°C}
layer12= layer_1_w
layer21=12
layer22=layer_2_w
layer31=12
layer32=layer_3_w

abs_w_1=(layer11-layer12)
abs_w_2=(layer21-layer22)
abs_w_3=(layer31-layer32)

! Layer 1    C22
E_11_1_w12 = 11*10^9
E_22_1_w12 = 0.37*10^9
G_12_1_w12 = 0.69*10^9
G_13_1_w12 = G_12_1_w12
G_23_1_w12 = G_12_1_w12
E_11_1 = E_11_1_w12*(1+0.02*(12-layer_1_w))
E_22_1 = E_22_1_w12*(1+0.02*(12-layer_1_w))
G_12_1 = G_12_1_w12*(1+0.02*(12-layer_1_w))
G_13_1 = G_13_1_w12*(1+0.02*(12-layer_1_w))
G_23_1 = G_23_1_w12*(1+0.02*(12-layer_1_w))

v12_1=0.2
v21_1 = (E_22_1/E_11_1)*v12_1

rho_1 = 420
rho0_1=rho_1/1000
g_1=rho_1*9.81

Q11_1 = E_11_1 / (1-v12_1*v21_1)
Q12_1 = (v12_1 * E_22_1) / (1-v12_1*v21_1)
Q16_1 = 0
Q26_1 = 0
Q22_1 = E_22_1 / (1-v12_1*v21_1)
Q66_1 = G_12_1
Q44_1 = G_23_1
```

```
Q55_1 = G_13_1


! Layer 2    C22
E_11_2_w12 = 11*10^9
E_22_2_w12 = 0.37*10^9
G_12_2_w12 = 0.69*10^9
G_13_2_w12 = G_12_2_w12
G_23_2_w12 = G_12_2_w12
E_11_2 = E_11_2_w12*(1+0.02*(12-layer_2_w))
E_22_2 = E_22_2_w12*(1+0.02*(12-layer_2_w))
G_12_2 = G_12_2_w12*(1+0.02*(12-layer_2_w))
G_13_2 = G_13_2_w12*(1+0.02*(12-layer_2_w))
G_23_2 = G_23_2_w12*(1+0.02*(12-layer_2_w))

v12_2 = 0.2
v21_2 = (E_22_2/E_11_2)*v12_2

rho_2 = 420
rho0_2=rho_2/1000
g_2=rho_2*9.81

Q11_2 = E_11_2 / (1-v12_2*v21_2)
Q12_2 = (v12_2 * E_22_2) / (1-v12_2*v21_2)
Q16_2 = 0
Q26_2 = 0
Q22_2 = E_22_2 / (1-v12_2*v21_2)
Q66_2 = G_12_2
Q44_2 = G_23_2
Q55_2 = G_13_2

! Layer 3    C22
E_11_3_w12 = 11*10^9
E_22_3_w12 = 0.37*10^9
G_12_3_w12 = 0.69*10^9
G_13_3_w12 = G_12_3_w12
G_23_3_w12 = G_12_3_w12
E_11_3 = E_11_3_w12*(1+0.02*(12-layer_3_w))
E_22_3 = E_22_3_w12*(1+0.02*(12-layer_3_w))
G_12_3 = G_12_3_w12*(1+0.02*(12-layer_3_w))
G_13_3 = G_13_3_w12*(1+0.02*(12-layer_3_w))
G_23_3 = G_23_3_w12*(1+0.02*(12-layer_3_w))

v12_3 = 0.2
v21_3 = (E_22_3/E_11_3)*v12_3

rho_3 = 420
rho0_3=rho_3/1000
g_3=rho_3*9.81

Q11_3 = E_11_3 / (1-v12_3*v21_3)
Q12_3 = (v12_3 * E_22_3) / (1-v12_3*v21_3)
Q16_3 = 0
Q26_3 = 0
Q22_3 = E_22_3 / (1-v12_3*v21_3)
Q66_3 = G_12_3
Q44_3 = G_23_3
```

```
Q55_3 = G_13_3


! LAMINAE LAYERS, GEOMETRY
h1 = 0.03
h2 = 0.03
h3 = 0.03
h=h1 + h2 + h3

L1=1.5
L2=0.3

p= -12000     {N.m-2}

m1=1 !cos(a1 degrees)
n1=0 !sin(a1 degrees)
m2=0 !cos(a2 degrees)
n2=1 !sin(a2 degrees)
m3=1 !cos(a3 degrees)
n3=0 !sin(a3 degrees)

Q_11_1 = Q11_1*m1^4+2*(Q12_1+2*Q66_1)*m1^2*n1^2+Q22_1*n1^4
Q_12_1 = (Q11_1+Q22_1-4*Q66_1)*m1^2*n1^2+Q12_1*(m1^4+n1^4)
Q_22_1 = Q11_1*n1^4+2*(Q12_1+2*Q66_1)*m1^2*n1^2+Q22_1*m1^4
Q_16_1 = (Q11_1-Q12_1-2*Q66_1)*(m1)^3*n1+(Q12_1-Q22_1+2*Q66_1)*m1*(n1)^3
Q_26_1 = (Q11_1-Q12_1-2*Q66_1)*n1^3*m1+(Q12_1-Q22_1+2*Q66_1)*n1*m1^3
Q_66_1 = (Q11_1+Q22_1-2*Q12_1-2*Q66_1)*m1^2*n1^2+Q66_1*(m1^4+n1^4)
Q_44_1 = Q44_1*m1^2+Q55_1*n1^2
Q_45_1 = (Q55_1-Q44_1)*n1*m1
Q_55_1 = Q55_1*m1^2+Q44_1*n1^2

Q_11_2 = Q11_2*m2^4+2*(Q12_2+2*Q66_2)*m2^2*n2^2+Q22_2*n2^4
Q_12_2 = (Q11_2+Q22_2-4*Q66_2)*m2^2*n2^2+Q12_2*(m2^4+n2^4)
Q_22_2 = Q11_2*n2^4+2*(Q12_2+2*Q66_2)*m2^2*n2^2+Q22_2*m2^4
Q_16_2 = (Q11_2-Q12_2-2*Q66_2)*m2^3*n2+(Q12_2-Q22_2+2*Q66_2)*m2*n2^3
Q_26_2 = (Q11_2-Q12_2-2*Q66_2)*n2^3*m2+(Q12_2-Q22_2+2*Q66_2)*n2*m2^3
Q_66_2 = (Q11_2+Q22_2-2*Q12_2-2*Q66_2)*m2^2*n2^2+Q66_2*(m2^4+n2^4)
Q_44_2 = Q44_2*m2^2+Q55_2*n2^2
Q_45_2 = (Q55_2-Q44_2)*n2*m2
Q_55_2 = Q55_2*m2^2+Q44_2*n2^2

Q_11_3 = Q11_3*m3^4+2*(Q12_3+2*Q66_3)*m3^2*n3^2+Q22_3*n3^4
Q_12_3 = (Q11_3+Q22_3-4*Q66_3)*m3^2*n3^2+Q12_3*(m3^4+n3^4)
Q_22_3 = Q11_3*n3^4+2*(Q12_3+2*Q66_3)*m3^2*n3^2+Q22_3*m3^4
Q_16_3 = (Q11_3-Q12_3-2*Q66_3)*m3^3*n3+(Q12_3-Q22_3+2*Q66_3)*m3*n3^3
Q_26_3 = (Q11_3-Q12_3-2*Q66_3)*n3^3*m3+(Q12_3-Q22_3+2*Q66_3)*n3*m3^3
Q_66_3 = (Q11_3+Q22_3-2*Q12_3-2*Q66_3)*m3^2*n3^2+Q66_3*(m3^4+n3^4)
Q_44_3 = Q44_3*m3^2+Q55_3*n3^2
Q_45_3 = (Q55_3-Q44_3)*n3*m3
Q_55_3 = Q55_3*m3^2+Q44_3*n3^2

A11 = Q_11_1 * ( (h2/2 + h1) - (h2/2)) + Q_11_2 * ( (h2/2) - (-h2/2))+
Q_11_3 * ( (-h2/2) - (-h2/2 - h3))
A12 = Q_12_1 * ( (h2/2 + h1) - (h2/2)) + Q_12_2 * ( (h2/2) - (-h2/2))+
Q_12_3 * ( (-h2/2) - (-h2/2 - h3))
A22 = Q_22_1 * ( (h2/2 + h1) - (h2/2)) + Q_22_2 * ( (h2/2) - (-h2/2))+
Q_22_3 * ( (-h2/2) - (-h2/2 - h3))
```

A16 = Q_16_1 * ((h2/2 + h1) - (h2/2)) + Q_16_2 * ((h2/2) - (-h2/2))+
Q_16_3 * ((-h2/2) - (-h2/2 - h3))
A26 = Q_26_1 * ((h2/2 + h1) - (h2/2)) + Q_26_2 * ((h2/2) - (-h2/2))+
Q_26_3 * ((-h2/2) - (-h2/2 - h3))
A66 = Q_66_1 * ((h2/2 + h1) - (h2/2)) + Q_66_2 * ((h2/2) - (-h2/2))+
Q_66_3 * ((-h2/2) - (-h2/2 - h3))
A44 = Q_44_1 * ((h2/2 + h1) - (h2/2)) + Q_44_2 * ((h2/2) - (-h2/2))+
Q_44_3 * ((-h2/2) - (-h2/2 - h3))
A45 = Q_45_1 * ((h2/2 + h1) - (h2/2)) + Q_45_2 * ((h2/2) - (-h2/2))+
Q_45_3 * ((-h2/2) - (-h2/2 - h3))
A55 = Q_55_1 * ((h2/2 + h1) - (h2/2)) + Q_55_2 * ((h2/2) - (-h2/2))+
Q_55_3 * ((-h2/2) - (-h2/2 - h3))

    A=matrix((A11,A12,A16),(A12,A22,A26),(A16,A26,A66))

B11 = 1/2 *(Q_11_1 * ((h2/2 + h1)^2 - (h2/2)^2) + Q_11_2 * ((h2/2)^2 - (-
h2/2)^2) + Q_11_3 * ((-h2/2)^2 - (-h2/2 - h3)^2))
B12 = 1/2 *(Q_12_1 * ((h2/2 + h1)^2 - (h2/2)^2) + Q_12_2 * ((h2/2)^2 - (-
h2/2)^2) + Q_12_3 * ((-h2/2)^2 - (-h2/2 - h3)^2))
B22 = 1/2 *(Q_22_1 * ((h2/2 + h1)^2 - (h2/2)^2) + Q_22_2 * ((h2/2)^2 - (-
h2/2)^2) + Q_22_3 * ((-h2/2)^2 - (-h2/2 - h3)^2))
B16 = 1/2 *(Q_16_1 * ((h2/2 + h1)^2 - (h2/2)^2) + Q_16_2 * ((h2/2)^2 - (-
h2/2)^2) + Q_16_3 * ((-h2/2)^2 - (-h2/2 - h3)^2))
B26 = 1/2 *(Q_26_1 * ((h2/2 + h1)^2 - (h2/2)^2) + Q_26_2 * ((h2/2)^2 - (-
h2/2)^2) + Q_26_3 * ((-h2/2)^2 - (-h2/2 - h3)^2))
B66 = 1/2 *(Q_66_1 * ((h2/2 + h1)^2 - (h2/2)^2) + Q_66_2 * ((h2/2)^2 - (-
h2/2)^2) + Q_66_3 * ((-h2/2)^2 - (-h2/2 - h3)^2))
B44 = 1/2 *(Q_44_1 * ((h2/2 + h1)^2 - (h2/2)^2) + Q_44_2 * ((h2/2)^2 - (-
h2/2)^2) + Q_44_3 * ((-h2/2)^2 - (-h2/2 - h3)^2))
B45 = 1/2 *(Q_45_1 * ((h2/2 + h1)^2 - (h2/2)^2) + Q_45_2 * ((h2/2)^2 - (-
h2/2)^2) + Q_45_3 * ((-h2/2)^2 - (-h2/2 - h3)^2))
B55 = 1/2 *(Q_55_1 * ((h2/2 + h1)^2 - (h2/2)^2) + Q_55_2 * ((h2/2)^2 - (-
h2/2)^2) + Q_55_3 * ((-h2/2)^2 - (-h2/2 - h3)^2))

    B=matrix((A11,A12,A16),(A12,A22,A26),(A16,A26,A66))

D11 = 1/3 *(Q_11_1 * ((h2/2 + h1)^3 - (h2/2)^3) + Q_11_2 * ((h2/2)^3 -
(-h2/2)^3) + Q_11_3 * ((-h2/2)^3 - (-h2/2 - h3)^3))
D12 = 1/3 *(Q_12_1 * ((h2/2 + h1)^3 - (h2/2)^3) + Q_12_2 * ((h2/2)^3 -
(-h2/2)^3) + Q_12_3 * ((-h2/2)^3 - (-h2/2 - h3)^3))
D22 = 1/3 *(Q_22_1 * ((h2/2 + h1)^3 - (h2/2)^3) + Q_22_2 * ((h2/2)^3 -
(-h2/2)^3) + Q_22_3 * ((-h2/2)^3 - (-h2/2 - h3)^3))
D16 = 1/3 *(Q_16_1 * ((h2/2 + h1)^3 - (h2/2)^3) + Q_16_2 * ((h2/2)^3 -
(-h2/2)^3) + Q_16_3 * ((-h2/2)^3 - (-h2/2 - h3)^3))
D26 = 1/3 *(Q_26_1 * ((h2/2 + h1)^3 - (h2/2)^3) + Q_26_2 * ((h2/2)^3 -
(-h2/2)^3) + Q_26_3 * ((-h2/2)^3 - (-h2/2 - h3)^3))
D66 = 1/3 *(Q_66_1 * ((h2/2 + h1)^3 - (h2/2)^3) + Q_66_2 * ((h2/2)^3 -
(-h2/2)^3) + Q_66_3 * ((-h2/2)^3 - (-h2/2 - h3)^3))
D44 = 1/3 *(Q_44_1 * ((h2/2 + h1)^3 - (h2/2)^3) + Q_44_2 * ((h2/2)^3 -
(-h2/2)^3) + Q_44_3 * ((-h2/2)^3 - (-h2/2 - h3)^3))
D45 = 1/3 *(Q_45_1 * ((h2/2 + h1)^3 - (h2/2)^3) + Q_45_2 * ((h2/2)^3 -
(-h2/2)^3) + Q_45_3 * ((-h2/2)^3 - (-h2/2 - h3)^3))
D55 = 1/3 *(Q_55_1 * ((h2/2 + h1)^3 - (h2/2)^3) + Q_55_2 * ((h2/2)^3 -
(-h2/2)^3) + Q_55_3 * ((-h2/2)^3 - (-h2/2 - h3)^3))

    D=matrix((B11,B12,B16),(B12,B22,B26),(B16,B26,B66))

```
E11 = 1/4 *( Q_11_1 * ( (h2/2 + h1)^4 - (h2/2)^4) + Q_11_2 * ( (h2/2)^4 -
(-h2/2)^4) + Q_11_3 * ( (-h2/2)^4 - (-h2/2 - h3)^4))
E12 = 1/4* ( Q_12_1 * ( (h2/2 + h1)^4 - (h2/2)^4) + Q_12_2 * ( (h2/2)^4 -
(-h2/2)^4) + Q_12_3 * ( (-h2/2)^4 - (-h2/2 - h3)^4))
E22 = 1/4* ( Q_22_1 * ( (h2/2 + h1)^4 - (h2/2)^4) + Q_22_2 * ( (h2/2)^4 -
(-h2/2)^4) + Q_22_3 * ( (-h2/2)^4 - (-h2/2 - h3)^4))
E16 = 1/4* ( Q_16_1 * ( (h2/2 + h1)^4 - (h2/2)^4) + Q_16_2 * ( (h2/2)^4 -
(-h2/2)^4) + Q_16_3 * ( (-h2/2)^4 - (-h2/2 - h3)^4))
E26 = 1/4* ( Q_26_1 * ( (h2/2 + h1)^4 - (h2/2)^4) + Q_26_2 * ( (h2/2)^4 -
(-h2/2)^4) + Q_26_3 * ( (-h2/2)^4 - (-h2/2 - h3)^4))
E66 = 1/4* ( Q_66_1 * ( (h2/2 + h1)^4 - (h2/2)^4) + Q_66_2 * ( (h2/2)^4 -
(-h2/2)^4) + Q_66_3 * ( (-h2/2)^4 - (-h2/2 - h3)^4))
E44 = 1/4* ( Q_44_1 * ( (h2/2 + h1)^4 - (h2/2)^4) + Q_44_2 * ( (h2/2)^4 -
(-h2/2)^4) + Q_44_3 * ( (-h2/2)^4 - (-h2/2 - h3)^4))
E45 = 1/4* ( Q_45_1 * ( (h2/2 + h1)^4 - (h2/2)^4) + Q_45_2 * ( (h2/2)^4 -
(-h2/2)^4) + Q_45_3 * ( (-h2/2)^4 - (-h2/2 - h3)^4))
E55 = 1/4* ( Q_55_1 * ( (h2/2 + h1)^4 - (h2/2)^4) + Q_55_2 * ( (h2/2)^4 -
(-h2/2)^4) + Q_55_3 * ( (-h2/2)^4 - (-h2/2 - h3)^4))

    E=matrix((E11,E12,E16),(E12,E22,E26),(E16,E26,E66))

F11 = 1/5* ( Q_11_1 * ( (h2/2 + h1)^5 - (h2/2)^5) + Q_11_2 * ( (h2/2)^5 -
(-h2/2)^5) + Q_11_3 * ( (-h2/2)^5 - (-h2/2 - h3)^5))
F12 = 1/5* ( Q_12_1 * ( (h2/2 + h1)^5 - (h2/2)^5) + Q_12_2 * ( (h2/2)^5 -
(-h2/2)^5) + Q_12_3 * ( (-h2/2)^5 - (-h2/2 - h3)^5))
F22 = 1/5* ( Q_22_1 * ( (h2/2 + h1)^5 - (h2/2)^5) + Q_22_2 * ( (h2/2)^5 -
(-h2/2)^5) + Q_22_3 * ( (-h2/2)^5 - (-h2/2 - h3)^5))
F16 = 1/5* ( Q_16_1 * ( (h2/2 + h1)^5 - (h2/2)^5) + Q_16_2 * ( (h2/2)^5 -
(-h2/2)^5) + Q_16_3 * ( (-h2/2)^5 - (-h2/2 - h3)^5))
F26 = 1/5* ( Q_26_1 * ( (h2/2 + h1)^5 - (h2/2)^5) + Q_26_2 * ( (h2/2)^5 -
(-h2/2)^5) + Q_26_3 * ( (-h2/2)^5 - (-h2/2 - h3)^5))
F66 = 1/5* ( Q_66_1 * ( (h2/2 + h1)^5 - (h2/2)^5) + Q_66_2 * ( (h2/2)^5 -
(-h2/2)^5) + Q_66_3 * ( (-h2/2)^5 - (-h2/2 - h3)^5))
F44 = 1/5* ( Q_44_1 * ( (h2/2 + h1)^5 - (h2/2)^5) + Q_44_2 * ( (h2/2)^5 -
(-h2/2)^5) + Q_44_3 * ( (-h2/2)^5 - (-h2/2 - h3)^5))
F45 = 1/5* ( Q_45_1 * ( (h2/2 + h1)^5 - (h2/2)^5) + Q_45_2 * ( (h2/2)^5 -
(-h2/2)^5) + Q_45_3 * ( (-h2/2)^5 - (-h2/2 - h3)^5))
F55 = 1/5* ( Q_55_1 * ( (h2/2 + h1)^5 - (h2/2)^5) + Q_55_2 * ( (h2/2)^5 -
(-h2/2)^5) + Q_55_3 * ( (-h2/2)^5 - (-h2/2 - h3)^5))

    F=matrix((F11,F12,F16,0,0),(F12,F22,F26,0,0),(F16,F26,F66,0,0))

G11 = 1/6* ( Q_11_1 * ( (h2/2 + h1)^6 - (h2/2)^6) + Q_11_2 * ( (h2/2)^6 -
(-h2/2)^6) + Q_11_3 * ( (-h2/2)^6 - (-h2/2 - h3)^6))
G12 = 1/6* ( Q_12_1 * ( (h2/2 + h1)^6 - (h2/2)^6) + Q_12_2 * ( (h2/2)^6 -
(-h2/2)^6) + Q_12_3 * ( (-h2/2)^6 - (-h2/2 - h3)^6))
G22 = 1/6* ( Q_22_1 * ( (h2/2 + h1)^6 - (h2/2)^6) + Q_22_2 * ( (h2/2)^6 -
(-h2/2)^6) + Q_22_3 * ( (-h2/2)^6 - (-h2/2 - h3)^6))
G16 = 1/6* ( Q_16_1 * ( (h2/2 + h1)^6 - (h2/2)^6) + Q_16_2 * ( (h2/2)^6 -
(-h2/2)^6) + Q_16_3 * ( (-h2/2)^6 - (-h2/2 - h3)^6))
G26 = 1/6* ( Q_26_1 * ( (h2/2 + h1)^6 - (h2/2)^6) + Q_26_2 * ( (h2/2)^6 -
(-h2/2)^6) + Q_26_3 * ( (-h2/2)^6 - (-h2/2 - h3)^6))
G66 = 1/6* ( Q_66_1 * ( (h2/2 + h1)^6 - (h2/2)^6) + Q_66_2 * ( (h2/2)^6 -
(-h2/2)^6) + Q_66_3 * ( (-h2/2)^6 - (-h2/2 - h3)^6))
G44 = 1/6* ( Q_44_1 * ( (h2/2 + h1)^6 - (h2/2)^6) + Q_44_2 * ( (h2/2)^6 -
(-h2/2)^6) + Q_44_3 * ( (-h2/2)^6 - (-h2/2 - h3)^6))
```

```
G45 = 1/6* ( Q_45_1 * ( (h2/2 + h1)^6 - (h2/2)^6) + Q_45_2 * ( (h2/2)^6 -
(-h2/2)^6) + Q_45_3 * ( (-h2/2)^6 - (-h2/2 - h3)^6))
G55 = 1/6* ( Q_55_1 * ( (h2/2 + h1)^6 - (h2/2)^6) + Q_55_2 * ( (h2/2)^6 -
(-h2/2)^6) + Q_55_3 * ( (-h2/2)^6 - (-h2/2 - h3)^6))

    G=matrix((G11,G12,G16,0,0),(G12,G22,G26,0,0),(G16,G26,G66,0,0))

H11 = 1/7* ( Q_11_1 * ( (h2/2 + h1)^7 - (h2/2)^7) + Q_11_2 * ( (h2/2)^7 -
(-h2/2)^7) + Q_11_3 * ( (-h2/2)^7 - (-h2/2 - h3)^7))
H12 = 1/7* ( Q_12_1 * ( (h2/2 + h1)^7 - (h2/2)^7) + Q_12_2 * ( (h2/2)^7 -
(-h2/2)^7) + Q_12_3 * ( (-h2/2)^7 - (-h2/2 - h3)^7))
H22 = 1/7* ( Q_22_1 * ( (h2/2 + h1)^7 - (h2/2)^7) + Q_22_2 * ( (h2/2)^7 -
(-h2/2)^7) + Q_22_3 * ( (-h2/2)^7 - (-h2/2 - h3)^7))
H16 = 1/7* ( Q_16_1 * ( (h2/2 + h1)^7 - (h2/2)^7) + Q_16_2 * ( (h2/2)^7 -
(-h2/2)^7) + Q_16_3 * ( (-h2/2)^7 - (-h2/2 - h3)^7))
H26 = 1/7* ( Q_26_1 * ( (h2/2 + h1)^7 - (h2/2)^7) + Q_26_2 * ( (h2/2)^7 -
(-h2/2)^7) + Q_26_3 * ( (-h2/2)^7 - (-h2/2 - h3)^7))
H66 = 1/7* ( Q_66_1 * ( (h2/2 + h1)^7 - (h2/2)^7) + Q_66_2 * ( (h2/2)^7 -
(-h2/2)^7) + Q_66_3 * ( (-h2/2)^7 - (-h2/2 - h3)^7))
H44 = 1/7* ( Q_44_1 * ( (h2/2 + h1)^7 - (h2/2)^7) + Q_44_2 * ( (h2/2)^7 -
(-h2/2)^7) + Q_44_3 * ( (-h2/2)^7 - (-h2/2 - h3)^7))
H45 = 1/7* ( Q_45_1 * ( (h2/2 + h1)^7 - (h2/2)^7) + Q_45_2 * ( (h2/2)^7 -
(-h2/2)^7) + Q_45_3 * ( (-h2/2)^7 - (-h2/2 - h3)^7))
H55 = 1/7* ( Q_55_1 * ( (h2/2 + h1)^7 - (h2/2)^7) + Q_55_2 * ( (h2/2)^7 -
(-h2/2)^7) + Q_55_3 * ( (-h2/2)^7 - (-h2/2 - h3)^7))

    HH=matrix((H11,H12,H16,0,0),(H12,H22,H26,0,0),(H16,H26,H66,0,0))

!MOISTURE STRAINS_____

KaT_1=(2/3)*rho0_1
KaR_1=(1/30)*rho0_1
KaL_1=(1/30)*rho0_1
KaT_2=(2/3)*rho0_2
KaR_2=(1/30)*rho0_2
KaL_2=(1/30)*rho0_2
KaT_3=(2/3)*rho0_3
KaR_3=(1/30)*rho0_3
KaL_3=(1/30)*rho0_3

ew11_1=(KaL_1*(abs_w_1))/100
ew22_1=(KaR_1*(abs_w_1))/100
ew11_2=(KaL_2*(abs_w_2))/100
ew22_2=(KaR_2*(abs_w_2))/100
ew11_3=(KaL_3*(abs_w_3))/100
ew22_3=(KaR_3*(abs_w_3))/100

ex_0=dx(u)
ey_0=dy(u)
exy_0=(dx(v)+dy(u))
ex_1=dx(P_x)
ey_1=dy(P_y)
exy_1=2*(dx(P_y)+dy(P_x))

ex_2=dx(F_x)
ey_2=dy(F_y)
exy_2=3*(dx(F_y)+dy(F_x))
```

```
ex_3=dx(L_x)
ey_3=dy(L_y)
exy_3= 4*(dx(L_y)+dy(L_x))
exz_0=(P_x +dx(w))
eyz_0=(P_y +dy(w))
exz_1= 2*F_x
eyz_1= 2*F_y
exz_2= 3*L_x
eyz_2= 3*L_y
```

{1. TOP_____}

```
e1_1_top = ex_0    + ex_1 * (h1+h2/2) + ex_2 * (( h1+h2/2)^2) + ex_3 * ((
h1+h2/2)^3)    + ew11_1
e2_1_top = ey_0    + ey_1 * (h1+h2/2) + ey_2 * (( h1+h2/2)^2) + ey_3 * ((
h1+h2/2)^3)    + ew22_1
e6_1_top = exy_0   + exy_1 * (h1+h2/2) + exy_2 * (( h1+h2/2)^2) + exy_3 *
(( h1+h2/2)^3)
e4_1_top = eyz_0 + eyz_1 * (h1+h2/2) + eyz_2 * ((h1+h2/2)^2)
e5_1_top = exz_0 + exz_1 * (h1+h2/2) +  exz_2 * ((h1+h2/2)^2)

Sigma1_1_top = Q_11_1*e1_1_top + Q_12_1*e2_1_top + Q_16_1*e6_1_top
Sigma2_1_top = Q_12_1*e1_1_top + Q_22_1*e2_1_top + Q_26_1*e6_1_top
Sigma6_1_top = Q_16_1*e1_1_top + Q_26_1*e2_1_top + Q_66_1*e6_1_top
Sigma4_1_top = + Q_44_1*e4_1_top + Q_45_1*e5_1_top
Sigma5_1_top = + Q_45_1*e4_1_top + Q_55_1*e5_1_top
```

{1. MID_____}

```
e1_1_mid = ex_0    + ex_1 * (h1/2+h2/2) + ex_2 * (( h1/2+h2/2)^2) + ex_3 *
(( h1/2+h2/2)^3)    + ew11_1
e2_1_mid = ey_0    + ey_1 * (h1/2+h2/2) + ey_2 * (( h1/2+h2/2)^2) + ey_3 *
(( h1/2+h2/2)^3)    + ew22_1
e6_1_mid = exy_0   + exy_1 * (h1/2+h2/2) + exy_2 * (( h1/2+h2/2)^2) +
exy_3 * (( h1/2+h2/2)^3)
e4_1_mid = eyz_0 + eyz_1 * (h1/2+h2/2) + eyz_2 * ((h1/2+h2/2)^2)
e5_1_mid = exz_0 + exz_1 * (h1/2+h2/2) + exz_2 * ((h1/2+h2/2)^2)

Sigma1_1_mid = Q_11_1*e1_1_mid + Q_12_1*e2_1_mid + Q_16_1*e6_1_mid
Sigma2_1_mid = Q_12_1*e1_1_mid + Q_22_1*e2_1_mid + Q_26_1*e6_1_mid
Sigma6_1_mid = Q_16_1*e1_1_mid + Q_26_1*e2_1_mid + Q_66_1*e6_1_mid
Sigma4_1_mid = + Q_44_1*e4_1_mid + Q_45_1*e5_1_mid
Sigma5_1_mid = + Q_45_1*e4_1_mid + Q_55_1*e5_1_mid
```

{1. BOT_____}

```
e1_1_bot = ex_0 + ex_1 * (h2/2) + ex_2 * ((h2/2)^2) + ex_3 * ((h2/2)^3)
+ ew11_1
e2_1_bot = ey_0 + ey_1 * (h2/2) + ey_2 * ((h2/2)^2) + ey_3 * ((h2/2)^3)
+ ew22_1
e6_1_bot = exy_0+ exy_1 * (h2/2) + exy_2 * ((h2/2)^2) + exy_3 * ((h2/2)^3)
e4_1_bot = eyz_0 + eyz_1 * (h2/2) + eyz_2 * ((h2/2)^2)
e5_1_bot = exz_0 + exz_1 * (h2/2) + exz_2 * ((h2/2)^2)

Sigma1_1_bot = Q_11_1*e1_1_bot + Q_12_1*e2_1_bot + Q_16_1*e6_1_bot
Sigma2_1_bot = Q_12_1*e1_1_bot + Q_22_1*e2_1_bot + Q_26_1*e6_1_bot
Sigma6_1_bot = Q_16_1*e1_1_bot + Q_26_1*e2_1_bot + Q_66_1*e6_1_bot
```

```
Sigma4_1_bot = + Q_44_1*e4_1_bot + Q_45_1*e5_1_bot
Sigma5_1_bot = + Q_45_1*e4_1_bot + Q_55_1*e5_1_bot
```

{2. TOP_____}

```
e1_2_top = ex_0 + ex_1 * (h2/2)+ex_2 * (( h2/2)^2) + ex_3 * (( h2/2)^3)
+ ew11_2
e2_2_top = ey_0 + ey_1 * (h2/2)+ey_2 * (( h2/2)^2) + ey_3 * (( h2/2)^3)
+ ew22_2
e6_2_top = exy_0   + exy_1 * (h2/2) + exy_2 * (( h2/2)^2) + exy_3 * ((
h2/2)^3)
e4_2_top = eyz_0 + eyz_1 * (h2/2) + eyz_2 * ((h2/2)^2)
e5_2_top = exz_0 + exz_1 * (h2/2) + exz_2 * ((h2/2)^2)

Sigma1_2_top = Q_11_2*e1_2_top + Q_12_2*e2_2_top + Q_16_2*e6_2_top
Sigma2_2_top = Q_12_2*e1_2_top + Q_22_2*e2_2_top + Q_26_2*e6_2_top
Sigma6_2_top = Q_16_2*e1_2_top + Q_26_2*e2_2_top + Q_66_2*e6_2_top
Sigma4_2_top = + Q_44_2*e4_2_top + Q_45_2*e5_2_top
Sigma5_2_top = + Q_45_2*e4_2_top + Q_55_2*e5_2_top
```

{2. MID_____}

```
e1_2_mid = ex_0 + ex_1 * (0) + ex_2 * (( 0)^2) + ex_3 * (( 0)^3)         +
ew11_2
e2_2_mid = ey_0 + ey_1 * (0) + ey_2 * (( 0)^2) + ey_3 * (( 0)^3)         +
ew22_2
e6_2_mid = exy_0   + exy_1 * (0) + exy_2 * (( 0)^2) + exy_3 * (( 0)^3)
e4_2_mid = eyz_0 + eyz_1 * (0) + eyz_2 * ((0)^2)
e5_2_mid = exz_0 + exz_1 * (0) + exz_2 * ((0)^2)

Sigma1_2_mid = Q_11_2*e1_2_mid + Q_12_2*e2_2_mid + Q_16_2*e6_2_mid
Sigma2_2_mid = Q_12_2*e1_2_mid + Q_22_2*e2_2_mid + Q_26_2*e6_2_mid
Sigma6_2_mid = Q_16_2*e1_2_mid + Q_26_2*e2_2_mid + Q_66_2*e6_2_mid
Sigma4_2_mid = + Q_44_2*e4_2_mid + Q_45_2*e5_2_mid
Sigma5_2_mid = + Q_45_2*e4_2_mid + Q_55_2*e5_2_mid
```

{2. BOT_____}

```
e1_2_bot = ex_0     + ex_1 * (-h2/2) + ex_2 * (( -h2/2)^2) + ex_3 * (( -
h2/2)^3)          + ew11_2
e2_2_bot = ey_0     + ey_1 * (-h2/2) + ey_2 * (( -h2/2)^2) + ey_3 * (( -
h2/2)^3)         + ew22_2
e6_2_bot = exy_0    + exy_1 * (-h2/2) + exy_2 * (( -h2/2)^2) + exy_3 * (( -
h2/2)^3)
e4_2_bot = eyz_0 + eyz_1 * (-h2/2) + eyz_2 * ((-h2/2)^2)
e5_2_bot = exz_0 + exz_1 * (-h2/2) + exz_2 * ((-h2/2)^2)

Sigma1_2_bot = Q_11_2*e1_2_bot + Q_12_2*e2_2_bot + Q_16_2*e6_2_bot
Sigma2_2_bot = Q_12_2*e1_2_bot + Q_22_2*e2_2_bot + Q_26_2*e6_2_bot
Sigma6_2_bot = Q_16_2*e1_2_bot + Q_26_2*e2_2_bot + Q_66_2*e6_2_bot
Sigma4_2_bot = + Q_44_2*e4_2_bot + Q_45_2*e5_2_bot
Sigma5_2_bot = + Q_45_2*e4_2_bot + Q_55_2*e5_2_bot
```

{3. TOP_____}

```
e1_3_top = ex_0     + ex_1 * (-h2/2) + ex_2 * (( -h2/2)^2) + ex_3 * (( -
h2/2)^3)            + ew11_3
```

```
e2_3_top = ey_0    + ey_1 * (-h2/2) + ey_2 * (( -h2/2)^2) + ey_3 * (( -
h2/2)^3)        + ew22_3
e6_3_top = exy_0   + exy_1 * (-h2/2) + exy_2 * (( -h2/2)^2) + exy_3 * (( -
h2/2)^3)
e4_3_top = eyz_0 + eyz_1 * (-h2/2) + eyz_2 * ((-h2/2)^2)
e5_3_top = exz_0 + exz_1 * (-h2/2) + exz_2 * ((-h2/2)^2)

Sigma1_3_top = Q_11_3*e1_3_top + Q_12_3*e2_3_top + Q_16_3*e6_3_top
Sigma2_3_top = Q_12_3*e1_3_top + Q_22_3*e2_3_top + Q_26_3*e6_3_top
Sigma6_3_top = Q_16_3*e1_3_top + Q_26_3*e2_3_top + Q_66_3*e6_3_top
Sigma4_3_top = + Q_44_3*e4_3_top + Q_45_3*e5_3_top
Sigma5_3_top = + Q_45_3*e4_3_top + Q_55_3*e5_3_top

{3. MID_____}

e1_3_mid = ex_0    + ex_1 * (-h2/2-h3/2) + ex_2 * (( -h2/2-h3/2)^2) + ex_3
* (( -h2/2-h3/2)^3)        + ew11_3
e2_3_mid = ey_0    + ey_1 * (-h2/2-h3/2) + ey_2 * (( -h2/2-h3/2)^2) + ey_3
* (( -h2/2-h3/2)^3)        + ew22_3
e6_3_mid = exy_0   + exy_1 * (-h2/2-h3/2) + exy_2 * (( -h2/2-h3/2)^2) +
exy_3 * (( -h2/2-h3/2)^3)
e4_3_mid = eyz_0 + eyz_1 * (-h2/2-h3/2) + eyz_2 * ((-h2/2-h3/2)^2)
e5_3_mid = exz_0 + exz_1 * (-h2/2-h3/2) + exz_2 * ((-h2/2-h3/2)^2)

Sigma1_3_mid = Q_11_3*e1_3_mid + Q_12_3*e2_3_mid + Q_16_3*e6_3_mid
Sigma2_3_mid = Q_12_3*e1_3_mid + Q_22_3*e2_3_mid + Q_26_3*e6_3_mid
Sigma6_3_mid = Q_16_3*e1_3_mid + Q_26_3*e2_3_mid + Q_66_3*e6_3_mid
Sigma4_3_mid = + Q_44_3*e4_3_mid + Q_45_3*e5_3_mid
Sigma5_3_mid = + Q_45_3*e4_3_mid + Q_55_3*e5_3_mid

{3. BOT_____}

e1_3_bot = ex_0    + ex_1 * (-h2/2-h3) + ex_2 * (( -h2/2-h3)^2) + ex_3 *
(( -h2/2-h3)^3)        + ew11_3
e2_3_bot = ey_0    + ey_1 * (-h2/2-h3) + ey_2 * (( -h2/2-h3)^2) + ey_3 *
(( -h2/2-h3)^3)        + ew22_3
e6_3_bot = exy_0   + exy_1 * (-h2/2-h3) + exy_2 * (( -h2/2-h3)^2) + exy_3
* (( -h2/2-h3)^3)
e4_3_bot = eyz_0 + eyz_1 * (-h2/2-h3) + eyz_2 * ((-h2/2-h3)^2)
e5_3_bot = exz_0 + exz_1 * (-h2/2-h3) + exz_2 * ((-h2/2-h3)^2)

Sigma1_3_bot = Q_11_3*e1_3_bot + Q_12_3*e2_3_bot + Q_16_3*e6_3_bot
Sigma2_3_bot = Q_12_3*e1_3_bot + Q_22_3*e2_3_bot + Q_26_3*e6_3_bot
Sigma6_3_bot = Q_16_3*e1_3_bot + Q_26_3*e2_3_bot + Q_66_3*e6_3_bot
Sigma4_3_bot =  + Q_44_3*e4_3_bot + Q_45_3*e5_3_bot
Sigma5_3_bot =  + Q_45_3*e4_3_bot + Q_55_3*e5_3_bot

INITIAL VALUES
w=0
u=0
v=0
F_x=0
F_y=0
P_x=0
P_y=0
L_x=0
L_y=0
```

EQUATIONS

w:

```
A45*(dx(P_y)+dxy(w))+A55*(dx(P_x)+dxx(w))+2*B45*dx(F_y)+2*B55*dx(F_x)+3*D45
*dx(L_y)+3*D55*dx(L_x)+A44*(dy(P_y)+dyy(w))+A45*(dy(P_x)+dxy(w))+2*B44*dy(F
_y)+2*B45*dy(F_x)+3*D44*dy(L_y)+3*D45*dy(L_x)= -p
```

u:

```
A11*dxx(u)+A12*dxy(v)+A16*(dxy(u)+dxx(v))+B11*dxx(P_x)+B12*dxy(P_y)+B16*(dx
y(P_x)+dxx(P_y))+D11*dxx(F_x)+D12*dxy(F_y)+D16*(dxy(F_x)+dxx(F_y))+E11*dxx(
L_x)+E12*dxy(L_y)+E16*(dxy(L_x)+dxx(L_y))+A16*dxy(u)+A26*dyy(v)+A66*(dyy(u)
+dxy(v))+B16*dxy(P_x)+B26*dyy(P_y)+B66*(dyy(P_x)+dxy(P_y))+D16*dxy(F_x)+D26
*dyy(F_y)+D66*(dyy(F_x)+dxy(F_y))+E16*dxy(L_x)+E26*dyy(L_y)+E66*(dyy(L_x)+d
xy(L_y))=0
```

v:

```
A16*dxx(u)+A26*dxy(v)+A66*(dxy(u)+dxx(v))+B16*dxx(P_x)+B26*dxy(P_y)+B66*(dy
x(P_x)+dxx(P_y))+D16*dxx(F_x)+D26*dxy(F_y)+D66*(dxy(F_x)+dxx(F_y))+E16*dxx(
L_x)+E26*dxy(L_y)+E66*(dxy(L_x)+dxx(L_y))+A12*dxy(u)+A22*dyy(v)+A26*(dyy(u)
+dxy(v))+B12*dxy(P_x)+B22*dyy(P_y)+B26*(dyy(P_x)+dxy(P_y))+D12*dxy(F_x)+D22
*dyy(F_y)+D26*(dyy(F_x)+dxy(F_y))+E12*dxy(L_x)+E22*dyy(L_y)+E26*(dyy(L_x)+d
xy(L_y))=0
```

F_x:

```
B11*dxx(u)+B12*dxy(v)+B16*(dxy(u)+dxx(v))+D11*dxx(P_x)+D12*dxy(P_y)+D16*(dx
y(P_x)+dxx(P_y))+E11*dxx(F_x)+E12*dxy(F_y)+E16*(dxy(F_x)+dxx(F_y))+F11*dxx(
L_x)+F12*dxy(L_y)+F16*(dxy(L_x)+dxx(L_y))+B16*dxy(u)+B26*dyy(v)+B66*(dyy(u)
+dxy(v))+D16*dxy(P_x)+D26*dyy(P_y)+D66*(dyy(P_x)+dxy(P_y))+E16*dxy(F_x)+E26
*dyy(F_y)+E66*(dyy(F_x)+dxy(F_y))+F16*dxy(L_x)+F26*dyy(L_y)+F66*(dyy(L_x)+d
xy(L_y))-
(A45*(P_y+dy(w))+A55*(P_x+dx(w))+2*B45*F_y+2*B55*F_x+3*D45*L_y+3*D55*L_x)-
(D45*(P_y+dy(w))+D55*(P_x+dx(w))+2*E45*F_y+2*E55*F_x+3*F45*L_y+3*F55*L_x)=0
```

F_y:

```
B16*dxx(u)+B26*dxy(v)+B66*(dxy(u)+dxx(v))+D16*dxx(P_x)+D26*dxy(P_y)+D66*(dx
y(P_x)+dxx(P_y))+E16*dxx(F_x)+E26*dxy(F_y)+E66*(dxy(F_x)+dxx(F_y))+F16*dxx(
L_x)+F26*dxy(L_y)+F66*(dxy(L_x)+dxx(L_y))+B12*dxy(u)+B22*dyy(v)+B26*(dyy(u)
+dxy(v))+D12*dxy(P_x)+D22*dyy(P_y)+D26*(dyy(P_x)+dxy(P_y))+E12*dxy(F_x)+E22
*dyy(F_y)+E26*(dyy(F_x)+dxy(F_y))+F12*dxy(L_x)+F22*dyy(L_y)+F26*(dyy(L_x)+d
xy(L_y))-
(A44*(P_y+dy(w))+A45*(P_x+dx(w))+2*B44*F_y+2*B45*F_x+3*D44*L_y+3*D45*L_x)-
(D44*(P_y+dy(w))+D45*(P_x+dx(w))+2*E44*F_y+2*E45*F_x+3*F44*L_y+3*F45*L_x)=0
```

P_x:

```
E11*dxx(u)+E12*dxy(v)+E16*(dxy(u)+dxx(v))+F11*dxx(P_x)+F12*dxy(P_y)+F16*(dx
y(P_x)+dxx(P_y))+G11*dxx(F_x)+G12*dxy(F_y)+G16*(dxy(F_x)+dxx(F_y))+H11*dxx(
L_x)+H12*dxy(L_y)+H16*(dxy(L_x)+dxx(L_y))+E16*dxy(u)+E26*dyy(v)+E66*(dyy(u)
+dxy(v))+F16*dxy(P_x)+F26*dyy(P_y)+F66*(dyy(P_x)+dxy(P_y))+G16*dxy(F_x)+G26
*dyy(F_y)+G66*(dyy(F_x)+dxy(F_y))+H16*dxy(L_x)+H26*dyy(L_y)+H66*(dyy(L_x)+d
xy(L_y))-
3*(D45*(P_y+dy(w))+D55*(P_x+dx(w))+2*E45*F_y+2*E55*F_x+3*F45*L_y+3*F55*L_x)
=0
```

P_y:

```
E16*dxx(u)+E26*dxy(v)+E66*(dxy(u)+dxx(v))+F16*dxx(P_x)+F26*dxy(P_y)+F66*(dx
y(P_x)+dxx(P_y))+G16*dxx(F_x)+G26*dxy(F_y)+G66*(dxy(F_x)+dxx(F_y))+H16*dxx(
L_x)+H26*dxy(L_y)+H66*(dxy(L_x)+dxx(L_y))+E12*dxy(u)+E22*dyy(v)+E26*(dyy(u)
+dxy(v))+F12*dxy(P_x)+F22*dyy(P_y)+F26*(dyy(P_x)+dxy(P_y))+G12*dxy(F_x)+G22
*dyy(F_y)+G26*(dyy(F_x)+dxy(F_y))+H12*dxy(L_x)+H22*dyy(L_y)+H26*(dyy(L_x)+d
xy(L_y))-
3*(D44*(P_y+dy(w))+D45*(P_x+dx(w))+2*E44*F_y+2*E45*F_x+3*F44*L_y+3*F45*L_x)
=0


L_x:
D11*dxx(u)+D12*dxy(v)+D16*(dxy(u)+dxx(v))+E11*dxx(P_x)+E12*dxy(P_y)+E16*(dx
y(P_x)+dxx(P_y))+F11*dxx(F_x)+F12*dxy(F_y)+F16*(dxy(F_x)+dxx(F_y))+G11*dxx(
L_x)+G12*dxy(L_y)+G16*(dxy(L_x)+dxx(L_y))+D16*dxy(u)+D26*dyy(v)+D66*(dyy(u)
+dxy(v))+E16*dxy(P_x)+E26*dyy(P_y)+E66*(dyy(P_x)+dxy(P_y))+F16*dxy(F_x)+F26
*dyy(F_y)+F66*(dyy(F_x)+dxy(F_y))+G16*dxy(L_x)+G26*dyy(L_y)+G66*(dyy(L_x)+d
xy(L_y))-
2*(B45*(P_y+dy(w))+B55*(P_x+dx(w))+2*D45*F_y+2*D55*F_x+3*E45*L_y+3*E55*L_x)
=0


L_y:
D16*dxx(u)+D26*dxy(v)+D66*(dxy(u)+dxx(v))+E16*dxx(P_x)+E26*dxy(P_y)+E66*(dx
y(P_x)+dxx(P_y))+F16*dxx(F_x)+F26*dxy(F_y)+F66*(dxy(F_x)+dxx(F_y))+G16*dxx(
L_x)+G26*dxy(L_y)+G66*(dxy(L_x)+dxx(L_y))+D12*dxy(u)+D22*dyy(v)+D26*(dyy(u)
+dxy(v))+E12*dxy(P_x)+E22*dyy(P_y)+E26*(dyy(P_x)+dxy(P_y))+F12*dxy(F_x)+F22
*dyy(F_y)+F26*(dyy(F_x)+dxy(F_y))+G12*dxy(L_x)+G22*dyy(L_y)+G26*(dyy(L_x)+d
xy(L_y))-
2*(B44*(P_y+dy(w))+B45*(P_x+dx(w))+2*D44*F_y+2*D45*F_x+3*E44*L_y+3*E45*L_x)
=0

BOUNDARIES
 region 1
  start (0,0)
        natural(v)=0
        natural(w)=0
        natural(P_x)=0
        natural(P_y)=0
        natural(L_x)=0
        natural(L_y)=0
        natural(u)=0
        natural(F_x)=0
        natural(F_y)=0
line to (L1,0)
        natural(v)=0
        value(w)=0
        natural(P_x)=0
        natural(P_y)=0
        natural(L_x)=0
        natural(L_y)=0
        natural(u)=0
        natural(F_x)=0
        natural(F_y)=0
line to (L1,L2)
        natural(v)=0
        natural(w)=0
        natural(P_x)=0
        natural(P_y)=0
        natural(L_x)=0
```

```
        natural(L_y)=0
        natural(u)=0
        natural(F_x)=0
        natural(F_y)=0
line to (0,L2)
        natural(v)=0
        value(w)=0
        natural(P_x)=0
        natural(P_y)=0
        natural(L_x)=0
        natural(L_y)=0
        natural(u)=0
        natural(F_x)=0
        natural(F_y)=0
line to close

PLOTS
     contour(w)      { show deformed grid as solution progresses }
      surface(w)
       elevation(w) from (0,L2/2) to (L1,L2/2)
       elevation(w) from (L1/2,0) to (L1/2,L2)

END
```